Microstructural Analysis of Edible Plants:

The Possibility of Designing Low Glycaemic

Biomimetic Plant Foods

A dissertation presented in partial fulfilment

of the requirements for the degree of

Doctor of Philosophy in Food Technology

at Massey University, Palmerston North, Manawatū, New Zealand

Duc Toan Do

2020

MASSEY UNIVERSITY
TE KUNENGA KI PŪREHUROA
UNIVERSITY OF NEW ZEALAND

Abstract

In the past decades, there has been an increasing interest in quantifying the relationship between structures inherent in plant-based foods and health-benefiting functionality, in particular the dynamic release of nutrients and bioactive compounds during food assimilation in the human gastrointestinal tract. This structure-function relationship can inspire the design of novel biomimetic food structures for nutrient delivery. The major objectives of research studies presented in this dissertation were (1) to investigate the role of plant-based food structures in slowing down *in vitro* starch digestion and (2) to contemplate the possibility of designing biomimetic plant foods for reduced glycaemic impact.

Starch granules are physically trapped in plant cell walls. In order to gain a clear understanding of the cell wall encapsulation of starch, raw intact cotyledon cells and starch granules were isolated from various legumes. The gelatinisation and digestion properties of intracellular starch were quantified and compared with those of isolated starch. Cotyledon cells (mean diameter, D50~98–118μm) contain numerous starch granules that are tightly embedded in the cytoplasmic protein matrix and enclosed within cell walls. Results showed that starch inside cells exhibited restricted swelling and delay in gelatinisation as well as a substantial reduction in the rate and extent of α-amylase hydrolysis compared with isolated starch. Scanning electron microscopy of cells revealed that the cell walls remained intact throughout cooking and digestion.

In another study, raw intact parenchyma cells and starch granules were isolated from Agria and Sunlite potato cultivars. These cells (D50~223–227μm) contain

numerous starch granules of varying sizes and shapes that are trapped in cell walls. This entrapment of starch resulted in higher gelatinisation temperatures in Agria cultivar as well as lower peak and breakdown paste viscosities observed in both cultivars. However, no measurable differences in *in vitro* amylolysis kinetics were found between parenchyma cells and isolated starch.

The results from these two studies showed that the entrapment of starch within the robust thick cotyledon cell wall and protein matrix restricts water and space inside the cell for gelatinisation and limits enzyme access, therefore slowing down starch digestion in legumes. However, the entrapment of starch within the thin parenchyma cell wall doesn't inhibit starch gelatinisation and digestion in potatoes. It was suggested that the presence of the compact protein matrix encapsulating starch granules in the legume cell, which is absent in the potato cell, could explain the observed difference in digestive behaviours of entrapped starch.

To investigate this, isolated navy bean cells were treated with pepsin for 1, 4, or 24 h to degrade the protein matrix to different degrees prior to *in vitro* digestion. It was found that increase in the treatment time generally resulted in lower protein content of cells and higher initial rate and extent of amylolysis. It was speculated that the protein matrix, aside from the cell wall, could act as an additional physical barrier limiting starch-amylase interactions. Consequently, the pepsin cleavage of intracellular proteins may promote access/binding of α-amylase to starch.

To delve into how starch inside plant cells is digested, a novel apparatus was developed for time-lapse optical microscopy of a cohort of individual navy bean cells through each stage of simulated cooking followed by *in vitro* gastric and small

intestinal digestion. The apparatus enabled direct observations of cell wall intactness and small intestinal digestion of starch that progressed inwardly from the periphery towards the centre of each cell. The new technique also allowed quantitative characterisation of the kinetics of amylolysis at the single-cell scale.

The knowledge gained from previous studies enabled the biomimetic creation of novel food structures. Calcium-induced gelation of pectin in the presence of corn starch led to the formation of starch-entrapped particles. Entrapped starch exhibited a marked reduction in the rate and extent of α-amylase hydrolysis compared with free starch. It was suggested that the pectin matrix hinders α-amylase access to starch in a similar manner to the legume cotyledon cell wall.

The final study was conducted to explore the effect of sorghum protein in liming *in vitro* starch digestion in two flour systems: (i) natural whole grain sorghum flour and (ii) binary blends of sorghum starch and kafirin protein isolate (biomimetic flour). Proteins in both systems greatly decreased the rate and extent of starch hydrolysis, possibly due to the formation upon wet cooking of disulphide-bonded kafirin network impeding α-amylase access to starch.

In conclusion, the relationship between natural plant-based food structures and functionality can help to guide rational design and engineering of novel biomimetic foods. The present work demonstrated that starch-entrapped particles can be fabricated from isolated food-grade ingredients using processing technologies for the delivery of nature-like functionality in food systems (i.e. modulation of starch digestion for slow glucose release).

Acknowledgement

First and foremost, I would like to express my sincere gratitude to my Chief Supervisor, Associate Professor Jaspreet Singh (Riddet Institute), and Co-supervisors, Distinguished Professor Harjinder Singh (Riddet Institute), Professor Indrawati Oey (University of Otago), and Associate Professor Stuart Johnson (Curtin University), for their supervision, guidance, and continuous support throughout my PhD journey. I am thankful to my supervisor, A/Prof Jaspreet for providing me the opportunity to pursue my doctoral study under his supervision. I also thank him for his encouragement and his advice on post-PhD career options.

I am grateful to Riddet Institute of Massey University for providing full PhD scholarship to support my study financially as well as providing research and travel grants for allowing me to conduct my research in Canada and attend local and overseas conferences.

I would like to thank Professor Rickey Yada and Dr. John Frostad (Faculty of Land and Food Systems, University of British Columbia, BC, Canada) for giving me the opportunity to work in their laboratory. It was a wonderful experience collaborating with Dr. Frostad on the novel apparatus for time-lapse microscopy of food digestion. His help with microscope chamber design and kinetic modelling of digestion as well as his constructive feedback on the draft research paper were valuable contributions to my thesis.

I would like to thank laboratory managers, Mrs. Maggie Zou (Riddet Institute), Ms. Michelle Tamehana, and Mr. John Edwards (School of Food and Advanced

Technology) for providing me training in the use of laboratory equipment and ordering materials for the project. I also would like to acknowledge Ms. Jordan Taylor and Ms. Niki Minards (Manawatū Microscopy and Imaging Centre) for their help with sample preparation for light and scanning electron microscopy.

Special thanks go to Mr. Abner Bogan and Mrs. Dianne Nguyen (University of British Columbia) for helping me with some of experimental work.

Finally, I would like to thank Mr. Gary Mitchell for treating me like part of his family during my time in Palmerston North. I will always remember his kindness, generosity, and support. My deepest gratitude goes to my dad, mom, and sister for their unconditional love. Thank you for being the best family I could ever ask for and always being there for me through my ups and downs. The completion of this thesis would not have been at all possible without their encouragement and continuous support.

Table of Contents

List of Tables

List of Figures

List of Abbreviations

%	Percent
µg	Micro gram
µL	Micro litre
µm	Micro metre
AMG	Amyloglucosidase
ANOVA	Analysis of Variance
AOAC	Association of Official Analytical Chemists
BC	Bacterial cellulose
BF	Brightfield
BPF	Biomimetic Plant Food
C	Circularity
C_∞	Total starch digested at the end of reaction
$CaCl_2$	Calcium chloride
CLSM	Confocal laser scanning microscope
Con A	Lectin concanavalin A
cP	Centipoise
CS	Corn starch
D50	Mean particle diameter
DDT	Dithiothreitol
DIC	Differential interference contrast
DSC	Differential scanning calorimeter
dwb	Dry weight basis
ENS	Encapsulated starch
ES	Extracellular starch
g	Gram
GAE	Gallic acid equivalent
GI	Gastrointestinal
GP	Gastric pepsin

h	Hour
HCl	Hydrochloric acid
ICC	Isolated cotyledon cell
ID	Inner diameter
ILS	Isolated legume starch
in (”)	Inch
INC	Isolated navy bean cotyledon cell
INS	Isolated navy bean starch
IPC	Isolated potato parenchyma cell
IS	Intracellular starch
IPS	Isolated potato starch
IVT	Invertase
$J.g^{-1}$	Joule per gram
k	Fist-order digestion rate constant
kDa	Kilodalton
KPI	Kafirin protein isolate
kV	Kilo volt
L	Litre
LB	Lipid body
LM	Light microscope
M	Molar
mg	Milli gram
min	Minute
mL	Milli litre
mM	Milli molar
N	Normality
$Na_2S_2O_5$	Sodium metabisulfite
NaOH	Sodium hydroxide
nm	Nanometre
^oC	Degree centigrade

OD	Outer diameter
ParCS	Particle Cohort Study
PB	Protein body
PL	Phospholipid
PP	Pancreatin proteases
R^2	Coefficient of determination
RA	Relative area
R_g	Radius of gyration
RG-I	Rhamnogalacturonan I
RO	Reverse osmosis
rpm	Revolutions per minute
RS	Resistant starch
RVA	Rapid visco analyser
SCFA	Short-chain fatty acid
SDS	Slowly digestible starch
SEM	Scanning electron microscope
SG	Starch granule
SGF	Simulated gastric fluid
SIF	Simulated small intestinal fluid
SM	Starch-entrapped microspheres
TAG	Triacylglycerol
T_c	Conclusion temperature of gelatinisation
T_{gel}	Gelatinisation temperature
T_o	Onset temperature of gelatinisation
T_p	Peak temperature of gelatinisation
U	Unit
USP	Unit of enzyme activity
v/v	Volume by volume
w/v	Weight by volume
w/w	Weight by weight

WGF	Whole grain sorghum flour
α	Alpha
β	Beta
γ	Gamma
ΔH_{gel}	Enthalpy of gelatinisation

List of Publications & Conference Proceedings

Some of the chapters in this thesis have been presented in the following communications:

Publications

Do, D. T., & Singh, J. (2018). Legume Microstructure. In *Reference Module in Food Science*. https://doi.org/10.1016/B978-0-08-100596-5.21683-1

Do, D. T., Singh, J., Oey, I., & Singh, H. (2018). Biomimetic Plant Foods: Structural design and functionality. *Trends in Food Science & Technology*, *82*, 46-59.

Do, D. T., Singh, J., Oey, I., & Singh, H. (2019). Modulating effect of cotyledon cell microstructure on *in vitro* digestion of starch in legumes. *Food Hydrocolloids*, *96*, 112-122.

Do, D. T., Singh, J., Oey, I., Singh, H., Yada, R. Y., & Frostad, J. (2020). A novel apparatus for time-lapse optical microscopy of gelatinisation and digestion of starch inside plant cells. *Food Hydrocolloids*, *104*.

Conference Proceedings

Do, D. T., Singh, J., Oey, I., & Singh, H. (2017, 24-27 October). *Microstructure and* in vitro *starch digestibility of legume cotyledon cells*. Poster session presented at the 4th International Conference on Food Structures, Digestion and Health, Sydney, Australia.

Do, D. T., Singh, J., Oey, I., & Singh, H. (2017, 5-8 November). *Food legume structure regulates* in vitro *starch digestion at the cellular level*. Poster session presented at the 7th International Symposium on Delivery of Functionality in Complex Food Systems, Auckland, New Zealand.

Do, D. T., Singh, J., Oey, I., Singh, H., Yada, R. Y., & Frostad, J. (2019, 2-4 July). *Chamber design for time-lapse optical microscopy of gelatinisation and digestion of starch inside plant cells*. 3MT Oral presentation at NZIFST Annual Conference, Christchurch, New Zealand.

Do, D. T., Singh, J., Oey, I., Singh, H., Yada, R. Y., & Frostad, J. (2019, 7-10 July). *Chamber design for time-lapse optical microscopy of gelatinisation and digestion of starch inside plant cells*. Paper presented at the 8th International Symposium on Delivery of Functionality in Complex Food Systems, Porto, Portugal.

Attendance at the 5th International Conference on Food Structures, Digestion and Health, 30 September-3 October, Rotorua, New Zealand.

CHAPTER ONE: Introduction

1.1. General Introduction

"Let food be thy medicine, and let medicine be thy food". This quote, often attributed to Hippocrates, refers to the fact that foods when consumed in a healthy balanced diet can serve as medicine for the body that helps fight diseases and improves overall health. Unfortunately, the excessive consumption of energy-dense foods among the population defeats the medicinal purpose of foods and is causing diet-related health issues globally. Therefore, one of the major challenges faced by the food industry in modern times is the development of tasty, nutritious, and healthy food products for feeding the fast-growing world population.

Recent decades have witnessed a major shift in the scientific approach towards nutrition. There has been a realisation that the nutritional assessment of a food is not solely based on individual nutrients, but also on the critical effect of food structure on nutrient digestion and health-related implications. Food research especially in this decade has firmly established links between food microstructure and functionality (Capuano & Pellegrini, 2019; Do, Singh, Oey, & Singh, 2018). The physical and sensory attributes (e.g. texture, stability) and functional properties (controlled release and delivery of nutrients and bioactive compounds) are largely dependent on the microstructure of the complex food matrix, and also on a multitude of molecular interactions among food matrix constituents that occur during processing and digestion (Parada & Aguilera, 2007). The knowledge of structure-function relationships can help guide rational design and engineering of

food structures and smart food-grade delivery systems for optimal nutrition and health (Scholten, Moschakis, & Biliaderis, 2014; Lesmes & McClements, 2009; McClements, Decker, Park & Weiss, 2009).

Plant-based foods is an essential part of a healthy human diet. There is a growing scientific consensus that frequent consumption of vegetables, fruits, and grains lowers risks of developing chronic diseases and promotes overall health and well-being (Nestle, 1999). Emerging evidence has suggested that plant food structure at different length scales (i.e. molecule, cell, tissue, and organ) controls digestion and bioaccessibility of nutrients and bioactive molecules (Ogawa *et al.*, 2018; Do *et al.*; 2018). Thus, plant materials can serve as inspiration for the innovative design and fabrication of nature-like food structures or so-called "biomimetic plant foods" (BPFs) for nutrient delivery.

Plant-based foods in nature provide many examples of fascinating structures for biomimetic design. Numerous attempts have been made to unlock the secrets of plant structures. Recent studies have shown that the entrapment of starch granules and proteins in cell walls of legume cotyledons and cereal endosperms limits *in vitro* digestion of starch and protein (Berg, Singh, Hardacre, & Boland, 2012; Bhattarai, Dhital, Mense, Gidley, & Shi, 2018). Particularly, the role of the cotyledon cell structure in modulating starch digestion has lately been a subject of intense research (Dhital, Bhattarai, Gorham, & Gidley, 2016; Do, Singh, Oey, & Singh, 2019). It has also been shown that the formation of disulphide-bonded protein network entrapping starch granules in sorghum flour upon cooking impedes starch digestibility *in vitro* (Zhang & Hamaker, 1998). These natural

structures inspire the design of functional BPFs having slow and/or low starch digestion properties, i.e. sustained and controlled release of glucose with the potential for improved glycaemic control in diabetes and for delivery of resistant starch to the large intestine. Researchers have adopted this nature-inspired design strategy for entrapping starch granules within a polysaccharide matrix (Venkatachalam, Kushnick, Zhang, & Hamaker, 2009) or in a protein network (Lavoisier & Aguilera, 2019) in order to create novel food-grade particles for reduced glycaemic impact.

The research presented in this thesis uses two models of the single plant cell and starch-protein matrix to dissect the role of the cell wall, cytoplasmic protein, and starch granule factors limiting starch susceptibility to *in vitro* amylase digestion at the cellular and subcellular level. This provides an ample opportunity to explore the possibility of designing novel starch-based BPFs having nature-like structures for biomimetic inhibition of starch digestion.

1.2. Overview of Thesis

Chapter 1 describes the rationale for mimicking natural plant structures as a novel approach to engineering foods to control digestion, release, and delivery of macro- and micro-nutrients. The concept of BPFs is introduced for the first time in Chapter 2 (Review of Literature). This chapter provides a brief overview of the microstructure of plant-based foods and their structural disassembly during processing and human gastrointestinal (GI) digestion. We then elucidate the role of plant structure in controlling nutrient digestion and bioaccessibility at different hierarchical levels and length scales, including molecular, cellular, tissue, and

organ levels. Taking inspirations from the inherent structures in natural foods, there is an emerging interest in developing BPFs with nature-like functionality to modulate macronutrient digestion and physiological response.

Following the review of literature, the thesis examines the entrapment of starch granules in plant cells. Intact cells isolated from legume cotyledon (Chapter 3) and potato tuber parenchyma (Chapter 4) are used as a model of starch-entrapped plant cells for studying the effect of cellular microstructure on gelatinisation and *in vitro* digestion of starch.

Despite recent advances in the understanding of isolated legume cells, the cellular structure and mechanism of slow starch digestion are not yet fully understood. Chapter 5 investigates the protein matrix that entraps starch granules inside cotyledon cells and its role as a structural barrier to starch digestion. Chapter 6 presents a novel apparatus for time-lapse optical microscopy of simulated cooking and digestion of navy bean cells. The microscopic information provides new insights into mechanisms involved in slow digestion of intracellular starch, and can be used for kinetic modelling of this process.

The new knowledge obtained from the four previous research chapters with regard to the role of the cotyledon cell wall and protein in inhibition of starch digestion can be utilised by food scientists for development of BPFs. Chapter 7 explores the possibility of designing food-grade starch-entrapped particles using corn starch and pectin, and examines biomimetic factors affecting *in vitro* starch digestion kinetics including pectin encapsulation and particle size.

Chapter 8 investigates the effect of kafirin protein on *in vitro* starch digestion in two model systems: (i) whole sorghum flour and (ii) a two-component mixture of sorghum starch and isolated kafirin. This chapter proposes the concept of biomimetic low-glycaemic-index flour that can be formulated by combining isolated food-grade ingredients, including starch granules, kafirin protein, and cell wall polysaccharides.

Finally, general discussion of experimental work, conclusions, and directions for future research on BPFs are presented in Chapter 9.

CHAPTER TWO: Review of Literature

2.1. Abstract

Background: The increasing number of people living with chronic conditions, such as diabetes and cardiovascular disease, along with the widespread demand for healthier foods have posed significant challenges to the food industry. Plant-based foods, beyond simple nutrition, can provide health-benefiting functionalities within the complex environment of the human GI tract. Biomimetics is defined as taking inspirations from nature to solve human problems. Biomimetic Plant Foods (BPFs) can offer solutions for the future via the design of nature-inspired food structures for improved health and well-being.

Scope and Approach: This review provides new insight into plant food structures in nature, their disassembly in the human GI tract, and their role in controlling the digestive fate of nutrients. Recent developments and future perspectives on designing BPFs are also discussed.

Key Findings and Conclusions: Plant foods in nature possess hierarchically self-assembled structures. During processing and GI digestion, these structures are disassembled to enable liberation and assimilation of nutrients and bioactive molecules contained within the food matrix. The assembly and disassembly are linked to a hierarchy of plant structure within which different levels (molecule, polymer, cell wall, cell, tissue, and organ) and their interactions can modulate nutrient bioaccessibility and digestion. Inspired by nature, BPFs can be engineered

to deliver in-body functionality. The emerging trend of biomimetics may potentially pave the way for the future of foods.

2.2. Introduction

Spanning millions of years of trial and error, natural structures have evolved to well-adapted forms with optimal efficiency via the process of natural selection. The great diversity of structures and functions in nature has always been a source of inspiration for the design and making of various man-made materials, which underlies the concept of biomimetics. Biomimetics is defined as the imitation of biological models, systems, processes, and structures found in nature for the purpose of solving complex human problems (Bhushan, 2009; Fratzl, 2007). Biomimetic materials science is not a new research field. However, we have recently begun to see a growing interest in research and innovation in this area thanks to the expanding interface between biological and material sciences (Fratzl, 2007).

Recent years have witnessed pioneering work on the development of biomimetic foods such as cultured meat and plant-based burgers. This serves as a starting point to introduce the novel concept of Biomimetic Plant Foods (BPFs). BPFs is an emerging platform of research that examines fundamentals of structure-functionality relationships in plant foods of natural origin, which then informs creative design of innovative nature-inspired food materials for delivery of targeted in-body functionality. Such foods have potential health benefits for the management and prevention of chronic diseases.

Natural and biomimetic food systems are vastly different in design strategies to achieve the desired functionality (Table 2.1). Indeed, nature uses a limited range of small molecules and self-assembly principles to build a vast array of larger, more complex plant structures with remarkable functional properties. Unlike nature, humans utilise a large variety of base elements to fabricate structures following an exact design. In addition, the functionality of natural foods, such as fruits and vegetables, is largely imparted by their hierarchical structures. On the contrary, biomimetic foods rely on the choice of raw materials and the selection of processing technologies to acquire specific functions (Fratzl, 2007).

Table 2.1. Natural versus biomimetic food systems, adapted with permission from Fratzl (2007).

Characteristics	Natural food system	Biomimetic food system
Choice of base elements	Limited types of molecules available: C, O, H, N, S, etc.	Large variety of elements (isolated ingredients): starch, protein isolate, refined oil, soluble fibers, etc.
Mode of assembly	Growth by biologically controlled self-assembly (approximate design)	Fabrication from colloidal dispersions, emulsions, amorphous and crystalline phases, gel networks, etc. (exact design)
Structuring for functionality	Hierarchical structuring over multiple length scales, functions imparted by natural forms	Formulation and re-assembling, choice of materials and selection of processing technologies according to functions

The review of literature provides a brief overview of the hierarchical assembly of plant foods and their disassembly during processing and various stages of human digestion. This provides a basis for understanding the multi-scale plant structure and its impact on the digestive fate of nutrients with special emphasis on

macronutrients (i.e. carbohydrate, protein, and lipid). The review will be concluded by presenting recent trends and future outlook in designing BPFs.

2.3. Assembly of plant foods in nature

Plant foods in nature have complex and diverse structures. Interestingly, most plants have not evolved to serve the primary purpose of being foods eaten by humans and animals to sustain life. It turns out that plants have formed intricate structures for other reasons. Fruits are eaten by animals as a way to scatter seeds around (for the spreading of plants and trees). Starches contained in tubers, grain seeds, and bulbs provide reproductive functions for the plants (Ubbink, Burbidge & Mezzenga, 2008). According to Parada and Aguilera (2007), the classification of most plant foods cultivated for human consumption mainly falls into two broad categories, namely fleshy structures and encapsulated embryos (Table 2.2).

Table 2.2. Classification of plant foods in nature.

Classification	Fleshy structures	Encapsulated embryos
Description [1]	Hierarchical composites of hydrated cells (spherical or polyhedral) that are bound together at the cell wall/middle lamella and exhibit turgor pressure	Assembly of dispersed starch granules, proteins, and lipids into discrete pockets
Microstructure [2]	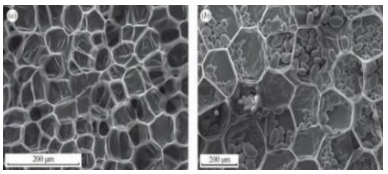 Carrot Potato	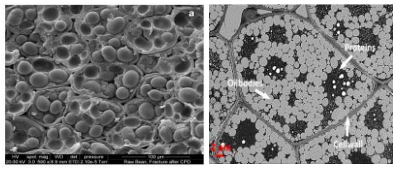 Navy bean Almond
Examples of plant foods	 Tubers Fruits Vegetables	 Cereals Legumes Tree nuts

[1] The description by Parada and Aguilera (2007).

[2] The microstructural images reprinted for carrot and potato from Gibson, Ashby, and Harley (2010) with permission from Cambridge University Press; navy bean from Berg, Singh, Hardacre, and Boland (2012) with permission from Elsevier; and almond from Grundy, Lapsley, and Ellis (2016b).

It is generally accepted that edible plants possess hierarchical structures; i.e. structures of increasingly higher organisation are progressively self-assembled from the molecular to macro scale until achieving desired functions and properties. Nature utilises a limited number of available molecules as building blocks to synthesize numerous polymers and organelles, and then compartmentalises them into cells and tissues at multiple length scales (Aguilera & Stanley, 1999). The hierarchical structure of plant foods is schematically illustrated in Figure 2.1 from the molecular to the macroscopic scale.

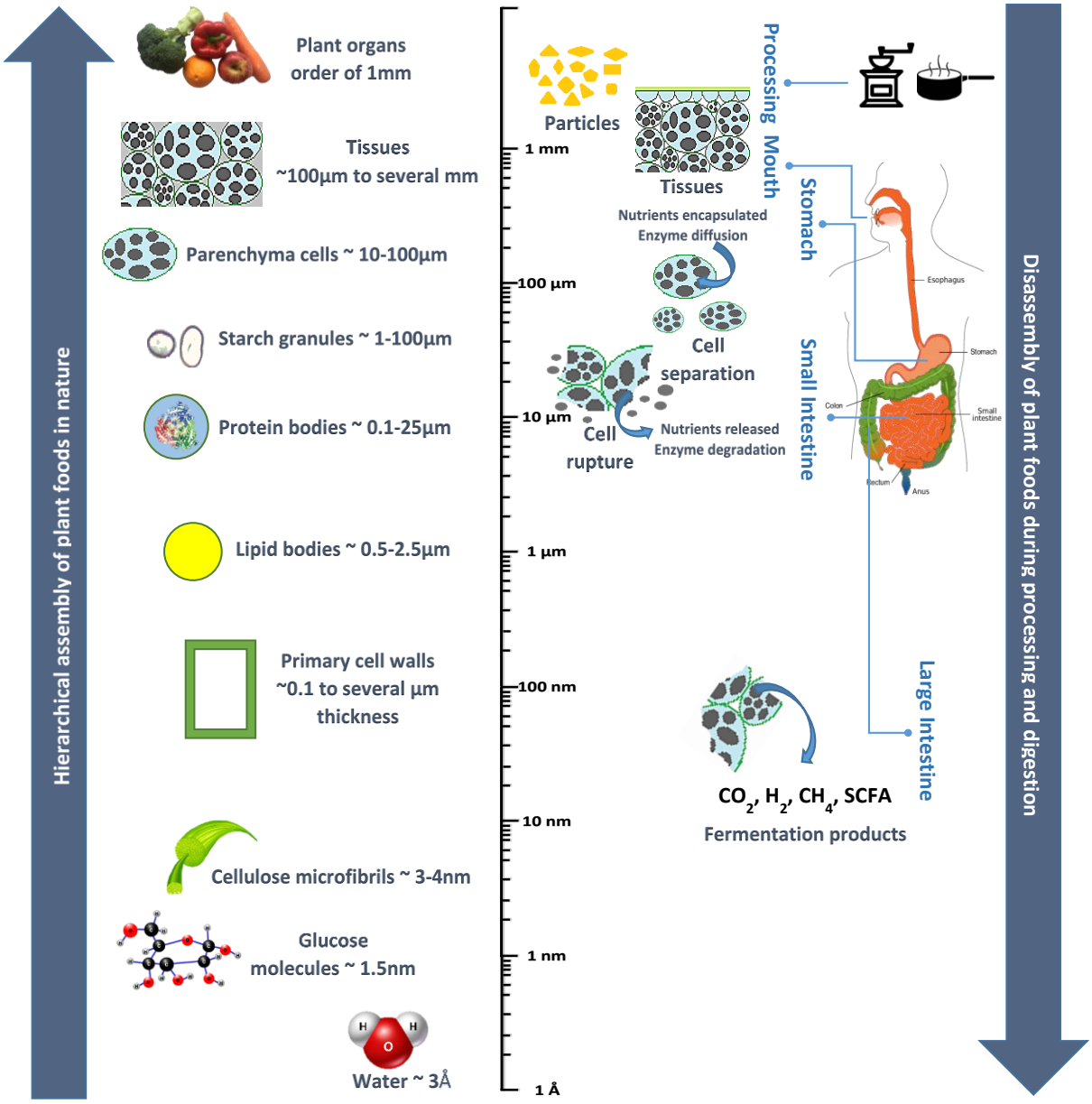

Fig. 2.1. Schematic representation of the hierarchical structure of plant foods in nature and their disassembly during processing and GI digestion. The disassembly process was adapted with permission from Grundy *et al.* (2016a). Picture of the human GI tract was reproduced from https://en.wikipedia.org/wiki/Gastrointestinal_tract (Copyright free).

There is still a long way to go towards fully understanding the assembly of such complex structures in natural foods. With the aid of sophisticated microscopy techniques, considerable progress has been made in gaining insights into the food structure that can be defined as spatial arrangement of various elements and their interactions at different length scales (Aguilera & Stanley, 1999). Principal

structural assemblies present in plant foods include cell walls, starch granules, protein bodies, lipid bodies, cells, and tissues. These structural elements determine the physicochemical and sensory properties along with nutritional quality of foods.

2.3.1. Plant cell walls

Plant cell walls are highly organised composite structures surrounding and protecting plant cells. There are four hierarchical levels of organisation in the cell wall: (1) cellulose molecules, (2) cellulose microfibrils, (3) macrofibrils of primary cell walls, and (4) plant cell walls made up of primary and secondary walls (Gibson, 2012). The primary wall, a major source of dietary fiber, is essentially a three-dimensional interacting network consisting of highly ordered, crystalline cellulose microfibrils (organised phase) embedded in a continuous, non-cellulosic matrix (amorphous phase). The matrix phase is composed of pectins, hemicelluloses, and some minor structural proteins. Cellulose microfibrils are bound together via hemicellulosic tethers providing a load-bearing framework, while pectins function as a plasticiser and control wall porosity (Gibson, 2012; Cosgrove, 1997).

2.3.2. Starch granules

Starch is a principal energy reserve in edible plants and forms the bulk of carbohydrates in the human diet (Singh, Dartois, & Kaur, 2010). Native starch granules (SGs) are made up of two different types of anhydroglucose polymers – amylose and amylopectin. They exhibit a hierarchical architecture with four different levels of granule organisation: (1) individual linear branches – consisting of glucosyl links, (2) whole starch molecules – slightly branched amylose and

highly branched amylopectin, (3) lamella – double helices of short chains of amylopectin in crystalline regions and possible entanglement between amylose and amylopectin chains in amorphous regions, and (4) granules – made up of concentric growth ring shells of radially alternating semi-crystalline and amorphous lamella (Dona, Pages, Gilbert, & Kuchel, 2010).

2.3.3. Protein bodies

Proteins are accumulated in storage tissues of seeds and deposited within specialised subcellular organelles commonly known as protein bodies (PBs). These are typically spherical and small with a size range from 0.1 to 25 μm in diameter. A PB contains an amorphous protein matrix enveloped by an external single membrane (Weber & Neumann, 1980). In sorghum endosperms, three major classes of storage proteins (prolamins), namely α-, β-, and γ- kafirins, are not homogenously distributed within PBs. Specifically, α-kafirin appears to occupy the central region, while β- and γ- kafirins are localised at the periphery (Mesa-Stonestreet, Jhoe, Alavi, & Bean, 2010). Likewise, a typical maize PB consists of an outer shell of primarily β- and γ- zeins and an interior of mainly α-zein. The interactions between these proteins have been postulated to play a role in PB assembly (Lending, Kriz, Larkins, & Bracker, 1988).

2.3.4. Lipid bodies

Seed tissues, including cotyledons and endosperms, store lipids in small discrete subcellular organelles called lipid bodies (LBs). These are usually spherical in shape and have diameters ranging between 0.5 and 2.5 μm. Triacylglycerol (TAG) is a

predominant form of storage lipids. LBs generally consist of a central core of hydrophobic TAG molecules that are stabilised by a phospholipid (PL) monolayer embedded with integral proteins. These proteins include a major structural protein (oleosin) and at least two minor proteins (caleosin and steroleosin). The specific interactions among surface proteins, PLs, and TAGs impart remarkable structural stability to LBs against destabilisation (coalescence and aggregation), regardless of whether they are inside cells or in isolated intact forms (Tzen, 2012).

2.3.5. Cells and tissues

Parenchyma is the most common edible plant tissue and constitutes the cotyledon of legumes and tree nuts, the endosperm of cereals, the cortex and pith of tubers, the pulp of fruits, and the mesophyll of leaf vegetables. Parenchyma tissues are made up of cells that usually have thin and non-lignified walls. The middle lamella, which is rich in pectic substances, glues primary walls of adjacent cells together (Brooker, Widmaier, Graham, & Stiling, 2017).

2.4. Disassembly of plant foods during processing and digestion

During processing and GI digestion, plant foods undergo extensive structural transformations from storage organ – the highest level of structure, through intermediate-level structures (particle, tissue, and cell), to molecular-level constituents. The breakdown of food structures in the GI tract facilitates enzymatic digestion and absorption of nutrients (Fig. 2.1).

2.4.1. Structural disassembly during processing

Processing causes irreversible structural alterations in plant foods. One of the primary consequences of processing is particle size reduction involving the break-up of organs into smaller particles of various sizes and an accompanying increase in surface area available for enzymatic action (Al-Rabadi, Gilbert, & Gidley, 2009). Processing can further reduce food particles to tissues and cells. Depending upon processing conditions and tissue characteristics (e.g. cell-cell adhesion strength), cells can either separate along the middle lamella or rupture across cell walls. High pressure processing or mechanical grinding of intact plant tissues (e.g. legume cotyledons and almond kernels) fractures cell walls and liberates nutrients enclosed within cells (Grundy *et al.*, 2016b; Berg *et al.*, 2012). On the other hand, hydrothermal processing of plant foods (e.g. legumes, potatoes, and carrots) and subsequent application of mechanical shear within the resulting puree induce separation of intact cells without breaking them open (Berg *et al.*, 2012; Tydeman *et al.*, 2010a). Processing can also modify cell walls (e.g. swelling, increased solubility and porosity, etc.) and alter structures and physicochemical properties of subcellular nutrients (e.g. starch gelatinisation/retrogradation, protein denaturation/aggregation, lipid emulsification/coalescence, etc.) (Grundy *et al.*, 2016a). These processing-induced structural modifications cause significant changes in food properties (e.g. colour, texture, rheology, etc.), thereby affecting the quality of final products.

2.4.2. Structural disassembly during human digestion

Digestion is characterised by a series of mechanical and enzymatic processes whereby ingested plant foods are physically and chemically disintegrated to facilitate the reduction of food particle size (mainly in the mouth and stomach), followed by the enzymatic hydrolysis and absorption of nutrients (mainly in the small and large intestine) (Guerra *et al.*, 2012).

The digestion process begins with mastication of foods in the mouth to form a mass bolus and partial starch hydrolysis of starchy foods by salivary α-amylase, followed by the transport of bolus via the esophagus into the stomach (Bornhorst & Singh, 2014; Guerra *et al.*, 2012). During mastication, cells of hard raw nuts and unripe fruits (e.g. almonds and apples) tend to rupture and liberate intracellular contents as a consequence of cell wall disruption at the surface of chewed particles (Ellis *et al.*, 2004). In contrast, cells or cell clusters of hydrothermally processed plant foods (e.g. legumes and tubers) tend to separate rather than rupturing (Grundy *et al.*, 2016a).

During gastric digestion, the swallowed boluses are further softened and physically broken down with the aid of secreted gastric juice and peristalsis contractions in the stomach along with nutrient hydrolysis by digestive enzymes (i.e. pepsin and lipase) (Bornhorst & Singh, 2014; Guerra *et al.*, 2012). The disintegration of solid particles in the stomach is governed primarily by either surface erosion or fragmentation (Kong & Singh, 2009b). Kong and Singh (2009a) studied the simulated gastric digestion of raw almond particles and observed cell separation due to weakening of cell-cell adhesion caused by acidic hydrolysis of the middle

lamella. Acid-induced breakage in cell walls was also detected in most internal cells within the almond tissue and could facilitate the release and hydrolysis of intracellular LBs and PBs.

Partially digested foods expelled from the stomach (chyme) are further broken down into smaller molecules by enzymes in the small intestine. Segmentation and peristaltic contractions assist the transport and mixing of chyme as well as nutrient absorption into the bloodstream through intestinal epithelial cells (Bornhorst & Singh, 2014; Guerra *et al.*, 2012). During this stage, intact plant cells retain structural integrity and enzymes diffuse through cell walls to gain access to intracellular nutrients, whereas rupture of cell walls exposes cellular contents to enzymatic hydrolysis (Berg *et al.*, 2012).

The digestion process terminates in the large intestine inhabited by a community of various species of microorganisms. Their role is to perform fermentation of incompletely digested food particles consisting of mainly carbohydrates (resistant starch (RS) and cell wall polysaccharides), proteins, and peptides. The colonic fermentation generates primary products of short-chain fatty acids (SCFAs), being mainly acetate, propionate, and butyrate with other by-products. These SCFAs are considered to have positive physiological effects on colonic epithelial cells, particularly the protective effects of butyrate against colorectal cancer (Macfarlane & Macfarlane, 2012). Intact cells, as previously observed in hydrothermally processed legumes and carrots, can survive gastric and small intestinal digestion. These cells carrying entrapped nutrients (e.g. starch and carotenoids) remain

undigested and pass on to the colon where they serve as a substrate for microbial fermentation (Tydeman *et al.*, 2010b; Noah *et al.*, 1998).

2.5. Complex structure and functionality of plant foods

Figure 2.2 depicts the hierarchical organisation of plant foods in conjunction with the two processes: (1) assembly (developmental change) and (2) disassembly during processing and GI digestion (processing/physiological change). Six levels make up the organisational hierarchy within which molecules at the lowest level are essential building blocks for the assembly of higher-order structures such as polymers. Cell walls consist of an intricate network of polymers. Cell walls and cellular components (e.g. SGs, PBs, and LBs) are assembled in plant cells. Tissues, which are composed of numerous cells, constitute plant organs. The characteristics of different structural levels contribute to a range of food functionalities: (i) techno-functionality pertaining to organoleptic and stability properties (e.g. texture, colour, taste, aroma release, shelf-life, etc.) and (ii) bio-functionality pertaining to nutritional value and health (i.e. controlling bioaccessibility and GI digestion of nutrients contained within the food matrix); we will focus on the latter aspect in this review.

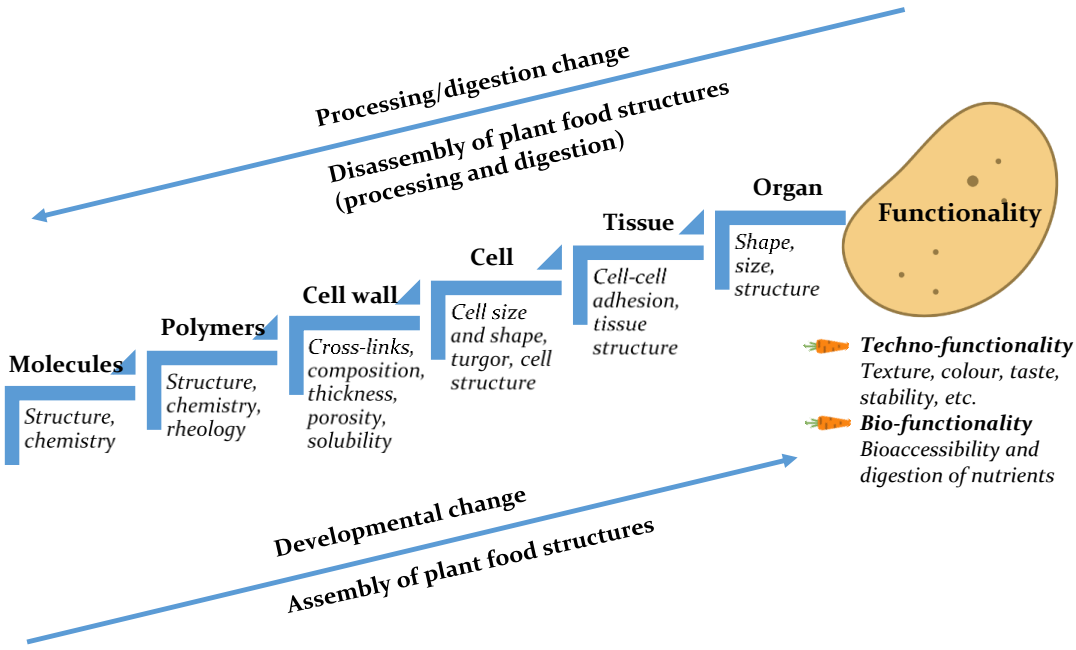

Fig. 2.2. Schematic representation of different hierarchical levels of structure that contribute to the functionality of plant-based foods, adapted with permission from Parker, Parker, Smith, and Waldron (2001).

During digestion, foods are exposed to certain physiological conditions in the human GI tract, such as oral mastication, pH, digestive enzymes, and peristalsis contractions. The natural food matrix provides protection for nutrients from degradation in the gut environment. An all-encompassing body of research has provided compelling evidence that the plant food structure affects GI fate of nutrients (Ellis *et al.*, 2004; Berg *et al.*, 2012; Tydeman *et al.*, 2010a; Parada & Aguilera, 2007). For instance, the entrapment of nutrients within plant matrices limits their digestion and absorption in the body. This is because the protection by the plant matrix and/or interactions with other matrix constituents tends to lower nutrient bioaccessibility (i.e. nutrient release from the food matrix) (Tydeman *et al.*, 2010b; Parada & Aguilera, 2007). However, such protection can be beneficial for controlled macronutrient release (Dhital *et al.*, 2016; Noah *et al.*, 1998).

Plant foods possess structural features at different hierarchical levels and length scales that can play a role in modulating nutrient bioaccessibility and digestion (Fig. 2.3). For example, the encapsulation of SGs in the cotyledon cell wall of navy beans is the main limiting factor of *in vitro* starch digestion. However, when the cell wall barrier is disrupted by processing (e.g. flour milling), intrinsic properties of starch and/or interactions of starch with proteins/lipids are key determinants for starch digestion (Berg *et al.*, 2012).

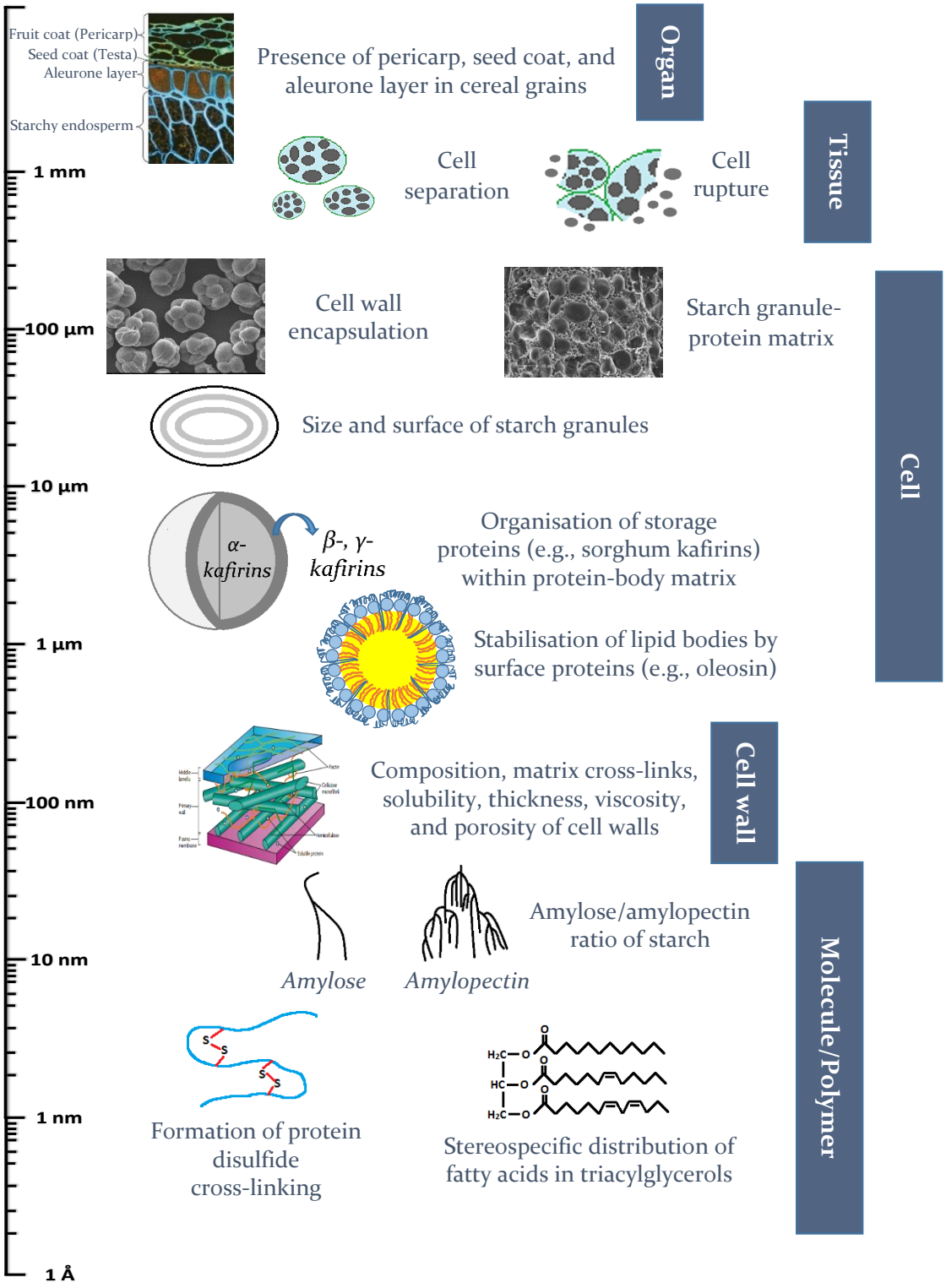

Fig. 2.3. Examples of structural features affecting nutrient bioaccessibility and digestion at different hierarchical levels of plant foods. Permission given for the image reproduction of cell wall from Sticklen (2008); cell wall encapsulation from Do *et al.* (2019); starch granule-protein matrix from Black (2001); and wheat microstructure from Kamal-Eldin *et al.* (2009).

2.6. Structural basis for bioaccessibility and digestion of nutrients in plant foods

2.6.1. Molecular and polymer level

The molecular and polymer structures greatly influence the digestion of plant food nutrients. Indeed, structure and composition of starch can affect its digestibility. Starches with lower proportions of short branch chains and higher proportions of intermediate and long branch chains and/or higher amylose content have been reported to have lower digestibility (Singh *et al.*, 2010). In addition, digestibility of plant proteins is influenced by structural conformations, amino acid sequences, and cross-linking (Duodu *et al.*, 2002; Duodu, Taylor, Belton, & Hamaker, 2003). For example, the formation upon heating of inter- and intra-molecular disulphide bonds in chickpea albumins that are resistant to proteolytic attack reduces protein digestibility (Clemente *et al.*, 2000). Furthermore, previous studies have demonstrated that the molecular weight, positional distribution, and unsaturation degree of fatty acid chains on the glycerol backbone of TAG can have a considerable impact on lipid digestion. In fact, the presence of long-chain saturated fatty acids in tropical plant oils, particularly at sn-1 and sn-3 esterified positions of TAG, has been found to exert negative effects on lipid digestion and absorption (Gallier & Singh, 2012b; McClements, Decker, & Park, 2008).

2.6.2. Cell wall level

Primary cell walls constitute the bulk of dietary fiber intake from plant foods. The health consequences of dietary fiber are strongly linked to mechanisms whereby

they directly influence the physiology of human digestion and the gut function (Capuano, 2017; Grundy *et al.*, 2016a; Padayachee, Day, Howell, & Gidley, 2017). The primary cell wall is viewed as a supramolecular assembly consisting of a mixture of polysaccharides with broad variations in structural and functional characteristics. Its physicochemical properties are determined by the constituent polysaccharides, but perhaps more so, by organisation of these polysaccharides via ionic, covalent, or hydrogen bonding within the three-dimensional wall architecture (Jarvis, 2011). The cell-wall properties are believed to affect the digestive fate of nutrients, including the rate and location of nutrient release in the stomach and the small intestine, and the delivery of indigestible substances (e.g. RS) to the colon.

Solubility. During cooking and GI digestion, the plant cell wall undergoes structural and chemical modifications that affect its solubility. Indeed, solubilisation of pectins in the cell wall/middle lamella upon thermal treatments enhances wall permeability, which facilitates the passage of digestive enzymes through the cell wall for hydrolysis of intracellular nutrients (Capuano, 2017). Crosslinking of cell wall polymers may impart wall strength that resists solubilisation. Frost *et al.* (2016) have recently identified the unique presence in abundance of RG-I galactan firmly attached to cellulose in cell walls of three potato cultivars that have low levels of pectin loss during cooking and low *in vitro* starch digestibility. It is suggested that the ability of the potato cell wall to withstand pectin solubilisation and suppress access of amylase for starch hydrolysis may be associated with the strong interactions between cellulose and RG-I galactan.

Thickness. Variations in cell wall thickness among starchy tissues, such as cereal endosperms and legume cotyledons, can affect the rate and extent of starch digestion. Thicker cell walls are likely to impose greater restrictions on gelatinisation degree of starch trapped in parenchyma cells during cooking and are also degraded to a lower extent during *in vitro* digestion, therefore reducing starch susceptibility to amylolysis (Alminger, Eklund-Jonsson, Kidman, & Langton, 2012; Edwards *et al.*, 2015).

Viscosity. The soluble fiber of mixed-linkage β-glucans present in cell walls of cereals (e.g. oats and barley) has been known to swell and increase the viscosity of foods. The high viscosity of β-glucans can result in reduced rate of starch digestion and lowered postprandial glycaemic responses in humans (Tosh, 2013).

Porosity. Living plant cells communicate with the extracellular environment through the porous cell-wall matrix that is selectively permeable to certain molecules (Burton, Gidley & Fincher, 2010). To facilitate the enzymatic hydrolysis of nutrient molecules inside plant cells during digestion, enzymes penetrate into cells by crossing the cell wall barrier and/or intracellular molecules diffuse out. Berg *et al.* (2012) suggested that the *in vitro* digestion of starch in cotyledon cells of navy beans could partly take place inside cells as a result of enzymatic diffusion through intact cell walls.

The transport of molecules in and out of the cell is controlled by pores in the cell wall. The pores impose restrictions on molecules that the cell allows to pass through. From a nutritional point of view, the pore size controls diffusion of enzyme molecules and thus affects nutrient bioaccessibility (Jarvis, 2011). Grundy

et al. (2016c) reported the estimated pore size of the almond cell wall between 3.4 and 5.0 nm. Despite the relatively smaller radius of gyration of pancreatic lipases (50 kDa, R_g ~ 1.9 nm), the enzymes were observed to permeate only into damaged almond cells, but not into intact cells. It was suggested that the digestion of intracellular lipids could be facilitated by a slow mechanism whereby lipases diffuse slowly through the cell wall and lipolytic products diffuse out. Therefore, cell wall porosity is a critical factor responsible for limiting the bioaccessibility and digestibility of almond lipids.

Binding interactions. In a starch-cellulose system, α-amylase non-specifically binds on cellulose surface, which in turn inhibits α-amylase activity on starch and decreases the initial rate of starch hydrolysis (Dhital, Gidley, & Warren, 2015). This has nutritional implications for the digestion of starch trapped in plant tissues. It has been found that the non-specific binding of α-amylase to cell wall components can limit enzymatic hydrolysis of starch in isolated legume cells (Bhattarai, Dhital, Wu, Chen, & Gidley, 2017; Dhital *et al.*, 2016). Food micronutrients such as polyphenols can also bind to polysaccharide constituents in cell walls of fruits and vegetables. This prevents liberation of nutrients from the food matrix and lowers nutrient bioaccessibility (Padayachee *et al.*, 2017).

2.6.3. Cellular level

2.6.3.1. Starch granules

Native SGs vary in morphology, composition, structure, and digestibility according to different botanical sources of plant foods. In general, starches in cereals are more digestible than those in tubers and legumes (Liu, Donner, Yin, Huang, & Fan,

2006). This can be attributed to several microstructural characteristics of cereal starches at the granular level: (i) smaller granule size and larger granule surface area, (ii) A-type crystallinity in cereal starches is more prone to amylolysis than B-type (tubers) and C-type (legumes) crystallinity, and (iii) the presence of pores and channels on granule surfaces (Singh *et al.*, 2010). Processing of plant foods at both industrial and household scales (e.g. cooking, extrusion, roasting, refrigeration, etc.) causes permanent changes in starch structure, e.g. gelatinisation/ retrogradation, and leads to increase/decrease in starch digestibility (Singh *et al.*, 2010).

2.6.3.2. Protein bodies

Certain plant proteins may not be made easily accessible to enzymes and readily bioavailable for uptake in the human upper gut due to the nature of protein assembly into PB organelles (Teuber, 2002). Studies on sorghum have revealed the effect of PB structure on susceptibility of α-, β-, and γ- kafirins to pepsin digestion. Oria, Hamaker, and Shull (1995) showed a kafirin degradation pattern of native PBs in uncooked sorghum flour during *in vitro* pepsin digestion. Specifically, PB digestion progressed radially inwards from the periphery containing β- and γ-kafirins to the α-kafirin-localised core. Further, α-kafirin was digested more slowly and to a lesser extent compared to the other two kafirins, suggesting that the interior location of α-kafirin limits its exposure to enzymatic attack. Upon cooking, the formation of enzyme-resistant disulphide-bonded polymers of β- and γ-kafirins further impaired access of pepsin to inner α-kafirin, therefore reducing the digestibility of all three kafirins (Oria *et al.*, 1995).

2.6.3.3. Lipid bodies

The "oil-in-water-emulsion-like" structure of plant LBs stabilised by coating layers of PLs and integral proteins is a natural vehicle for the delivery of pre-emulsified lipids in a digestible form similar in nature to milk fat globules and processed lipid foods (Golding & Wooster, 2010). During GI digestion, oleosin plays a key role in maintaining LB stability against lipolysis and coalescence. As such, a loss of emulsifying properties of oleosin at the oil-water interface under GI conditions (i.e. low gastric pH and pepsin action) causes aggregation/flocculation of isolated LBs and facilitates lipid digestion (Gallier & Singh, 2012a; Maurer *et al.*, 2013). In addition, the PL/protein coat could delay TAG hydrolysis by reducing lipase specific activities on the LB. The specific activity of lipases measured on almond LBs has been found to be much lower compared to that measured on almond lipid emulsions stabilised by gum arabic (Beisson *et al.*, 2001). This is consistent with the finding of White, Fisk, Makkhun, and Gray (2009), who showed that the rate of lipase-catalysed hydrolysis and bioaccessibility of α-tocopherol and fatty acids were lower for sunflower LBs than for artificial lipid emulsions stabilised by Tween 20 or whey protein isolate. Therefore, native LBs can act as natural food emulsion with slow digestion properties, providing beneficial physiological consequences such as reduced energy intake and increased satiety.

2.6.3.4. Cell wall encapsulation

Most plants at the cellular level are examples of microencapsulation in nature with each living cell representing a microcapsule (Shahidi & Han, 1993). The plant cell wall acts as a "shell" that not only fulfils functional biology, such as conferring

structural support for the cell membrane against its bursting under the influence of turgor pressure (Jarvis, 2011), but also provides protection for a "core" of subcellular nutrients. One of the most important functions of food encapsulation is the controlled release rate of active "core" ingredients (Shahidi & Han, 1993). This is analogous to the role of cell wall encapsulation in modulating the rate of nutrient release from the plant food matrix during GI digestion (Berg *et al.*, 2012; Ellis *et al.*, 2004; Melito & Tovar, 1995; Tydeman *et al.*, 2010a).

Cotyledon tissue of starchy legumes (e.g. beans, peas and chickpeas) is composed of numerous cells that naturally encapsulate starch. Within each cell, SGs are tightly packed in a cytoplasmic protein matrix and enveloped by a thick outer cell wall (Berg *et al.*, 2012; Brummer, Kaviani, & Tosh, 2015). During hydrothermal cooking of cotyledon tissue (e.g. boiling and steaming), cell walls impose restrictions on water availability, heat transfer and space inside cells, resulting in incomplete swelling and gelatinisation of SGs (Edwards *et al.*, 2015). Cooking also facilitates dissolution of pectic polymers that are involved in cell-cell adhesion, resulting in separation of intact cells instead of cell rupture. During subsequent enzymatic digestion *in vitro*, the partially gelatinised starch is of too high molecular mass to escape via cell wall pores and remains trapped by cell walls, thus limiting amylase accessibility to starch. The combined effects of the incomplete starch gelatinisation and enzyme barrier properties of the cell wall lead to a decrease in the *in vitro* rate and extent of starch hydrolysis (Berg *et al.*, 2012; Brummer *et al.*, 2015). Furthermore, an *in vivo* study on starch digestion in healthy humans found a significant proportion of RS in physically inaccessible form (trapped in intact cells) that was recovered in ileal digesta samples (i.e. the effluent collected at the

end of the small intestine) after 3 h following ingestion of cooked white beans. The formation of RS was largely attributed to partially degraded starch molecules escaping small intestinal digestion due to cell wall encapsulation (Noah *et al.*, 1998). Drastic food processing (e.g. milling and high pressure) can disrupt cell wall integrity and liberate starch, leading to a marked increase in the rate and extent of starch hydrolysis (Berg *et al.*, 2012). Therefore, minimal processing for preservation of cellular intactness is essential for maintaining the low glycaemic properties of food legumes.

Cotyledon tissue can be reduced to a suspension of intact cells following heat or chemical maceration. Studies of these isolated cells have revealed interesting insights about the gelatinisation and digestive behaviours of entrapped starch. It has been reported that a single intact cell wall has sufficient capacity to limit *in vitro* starch digestion by restricting starch gelatinisation and hindering enzyme accessibility to starch (Dhital *et al.*, 2016; Do *et al.*, 2019; Fujimura & Kugimiya, 1994). Other mechanisms have also been postulated to explain the reduced amylolytic susceptibility of intracellular starch, i.e. non-specific binding of amylase to cell wall components (Bhattarai *et al.*, 2017), and the cytoplasmic protein matrix providing an additional barrier against starch-amylase interactions (Rovalino-Córdova, Fogliano, & Capuano, 2018).

Apart from starch, plant cell walls naturally encapsulate other subcellular nutrients including proteins, lipids, and micronutrients. According to Melito and Tovar (1995), cell walls play a pivotal role in limiting *in vitro* protein digestibility in processed legumes. In addition, previous studies have identified cell wall

encapsulation as a major determinant for modulating bioaccessibility and digestibility of lipids in almond seeds (Ellis *et al.*, 2004; Grundy *et al.*, 2016c; Grundy, Wilde, Butterworth, Gray, & Ellis, 2015; Mandalari *et al.*, 2014). It has been demonstrated that a significant proportion of almond cells remains intact and contains undigested lipids at the end of *in vitro* upper gastric and duodenal digestion (Grundy *et al.*, 2015, 2016c). A fraction of cells even endures *in vivo* bacterial fermentation in the large intestine and is found intact in human faecal samples (Ellis *et al.*, 2004). Therefore, though it may seem paradoxical, the regular consumption of almond nuts (high in lipid contents) has been associated with lowered energy intake and decreased risk of cardiovascular diseases (Berry *et al.*, 2008). Food processing and oral mastication induce varying degrees of cellular rupture in the almond tissue, which in turn improves lipid bioaccessibility (Grundy *et al.*, 2016b). Finally, there has been a rapid growth of research into the role of cell wall encapsulation in reducing bioaccessibility of micronutrients, e.g. carotene in carrots (Tydeman *et al.*, 2010a, 2010b), iron in common beans (Glahn, Tako, Cichy, & Wiesinger, 2016), and the effect of processing in breaking down cell walls and making micronutrients more bioaccessible for gut uptake (Bengtsson, Brackmann, Enejder, Alminger, & Svanberg, 2010).

2.6.3.5. Starch-protein matrices

Parenchyma cells in starchy endosperms of cereals (e.g. maize, sorghum, barley, and wheat) contain SGs and PBs that are densely packed in protein matrices. PBs are firmly cemented to surrounding SGs or sometimes indented onto starch surfaces (Black, 2001; Mesa-Stonestreet *et al.*, 2010). The compactness of the

protein matrix and the tight association between SGs and PBs have been known to attenuate starch digestion in raw cereal grains due to the hindering effect of the protein matrix on enzyme accessibility and the weak binding of α-amylase to proteins (Choct, Bird, Littlefield, Balogun, & Rowe, 2001; Yu *et al.*, 2017).

Sorghum serves as an example to further illustrate the effect of the starch-protein matrix on nutrient digestion. Sorghum kafirin proteins affect the nutritional functionality of processed sorghum foods. Since kafirins are buried within the PB structure, they must be released to enhance their functional capacity via physical disruption of PBs by the application of shear forces in food processing (Hamaker & Bugusu, 2003). Kafirins are rich in sulphur-containing amino acids (i.e. cysteine and methionine) and are prone to network formation of intra- and inter-molecular disulphide bonds (Mesa-Stonestreet *et al.*, 2010). Upon cooking sorghum flour, kafirins form extended web-like and rigid sheet-like structures (i.e. disulphide-bonded kafirin oligomers and polymers) surrounding starch. This protein network restricts starch granule expansion/gelatinisation and hinders amylase accessibility during *in vitro* digestion, thus reducing starch digestibility (Ezeogu, Duodu, Emmambux, & Taylor, 2008; Ezeogu, Duodu, & Taylor, 2005). To improve the starch digestibility of sorghum, the protein network must be broken down to enable amylolytic enzymes to gain entry to starch reserves in endosperms. Processing techniques (e.g. germination and high-pressure cooking) disrupt the protein matrix and increase starch susceptibility to amylolysis (Choct *et al.*, 2001; Ezeogu *et al.*, 2005).

The structure and physicochemical properties of cereal proteins vary within and between grain species, leading to varying inhibitory effects of proteins on starch digestion. Kafirins and zeins are both classified as alcohol-soluble prolamins (Mesa-Stonestreet *et al.*, 2010). Despite sharing high homology of amino acid sequence, kafirins contain more cross-linked protein fractions than zeins. As a result, the formation of disulphide cross-linkages and high-molecular-weight protein aggregates is by far more extensive in cooked sorghum flour than in cooked maize flour. The protein matrix and starch in cooked sorghum flour are thus less susceptible to enzymatic attack and less digestible than their maize counterparts (Duodu *et al.*, 2003; Ezeogu *et al.*, 2005, 2008). Besides, Yu *et al.* (2017) reported variations in protein content and composition (notably in hordein fractions) across different barley cultivars, resulting in different levels of inhibitory activity of proteins against amylase and a range of starch digestibility characteristics. Therefore, different barley varieties could potentially be used to develop human foods containing slowly digestible starch (SDS) and animal feeds containing easily digestible starch.

2.6.4. Tissue level

Al-Rabadi *et al.* (2009) and Roman, Gomez, Li, Hamaker, and Martinez (2017) observed an inverse correlation between particle size of milled plant tissues and rate coefficient for *in vitro* starch hydrolysis. One possible explanation for this is that coarse flours appear to possess a lower amount of peripheral damaged starch and a smaller surface area for amylase binding compared with fine flours. Coarse flour particles also have a higher level of structural intactness (e.g. cell wall and

protein matrix), and thus can be more effective in restricting water ingress for starch gelatinisation and limiting diffusion of amylase through the flour matrix.

Previous studies have also provided evidence supporting that at the tissue level of the plant food structure, cell adhesion and cell separation/rupture control the rate and location of nutrient release during GI digestion (Berg *et al.*, 2012; Tydeman *et al.*, 2010a). Developing plants use adhesion between adjacent cells, a central characteristic of multicellular organisms, as a strategy to acquire mechanical strength. The pectin-rich middle lamella is thought to play a crucial role in maintaining cell-cell adhesion and protecting tissue integrity (Jarvis, Briggs, & Knox, 2003). Tissue failure affects organoleptic quality attributes (texture and aroma release) and often occurs in the form of cell separation or cell rupture or a combination of both. The type of failure is determined by relative strength of the cell wall and the cell adhesion force (Waldron, Parker, & Smith, 2003). For example, hydrothermal cooking of starchy foods (e.g. potatoes) results in cell separation and a mealy texture, which can be attributed to loss of turgor pressure and a dual effect of cell wall/middle lamella disassociation and starch swelling pressure (Jarvis, Mackenzie, & Duncan, 1992). Cell separation also occurs during fruit ripening and is facilitated by pectin dissolution in the primary wall/middle lamella by active pectin-degrading enzymes (Jarvis *et al.*, 2003). Once there has been a substantial level of cell separation, it becomes rather difficult to fracture individual cells by any mechanical means (Jarvis, 2011). On the other hand, mechanical or oral processing of unripe fruits causes breakage across cell walls and release of cellular contents, resulting in a soft and juicy texture (Waldron *et al.*, 2003). Intact separated cells preserve structural integrity and protect entrapped

nutrients against enzymatic degradation. Hence, they endure digestion for a longer way down the GI tract as opposed to ruptured cells, but the ability to retain any of the cellular content may depend on the degree to which the cell wall porosity is altered (Jarvis, 2011). From the evidence presented here, it is essential to select suitable processing methods/conditions for achieving efficient separation and minimal fracture of plant cells or vice versa for targeted nutrient delivery (Tydeman *et al.*, 2010a; Grundy, 2016b).

2.6.5. Organ level

Edible plant foods possess structural features affecting nutrient digestion at the organ level. For instance, outer layers present in sorghum grains (i.e. pericarp and polyphenols, gem and lipids) cause lower *in vitro* protein digestibility of whole flours when compared to endosperm flours devoid of these structural layers (Duodu *et al.*, 2002). In addition, Tamura, Singh, Kaur, and Ogawa (2016) found that the aleurone layer in the rice endosperm could inhibit penetration of digestive fluids containing starch-hydrolysing enzymes into the core of intact rice grains. As a result, the *in vitro* starch hydrolysis rate of cooked homogenised rice was found to be eight times higher than that of cooked intact rice. Moreover, Bornhorst, Chang, Rutherfurd, Moughan, and Singh (2013) examined the *in vivo* gastric digestion of cooked rice meals using growing pigs as a model for adult humans. These authors found an accumulation of the bran layer from brown rice in the pig gastric antrum after meal consumption, which could explain a lower gastric emptying rate for protein in brown rice than in white rice (the bran layer had been removed by processing).

2.7. Recent trends in designing biomimetic plant foods (BPFs)

There has been a shift in recent decades from the traditional view of examining nutritional benefits of foods simply based on composition to the recognition of the critical importance of food structure in influencing nutrient digestion and nutritionally related health (Wahlqvist, 2016). The topic of designing foods to control the GI fate of nutrients for improved health and wellness is a rapidly expanding area of research. Within the context of the current understanding of food digestion for health, BPFs emerge as a novel approach for the future of food structure design. However, public opinion has been divided over the notion of biomimetic foods. Dietary guidelines frequently recommend natural foods being an essential basis of a healthy diet as well as avoidance of ultra-processed foods (Wahlqvist, 2016). Needless to say, the consumption of unrefined or minimally processed plant foods provide us with full benefits, and if so, why should we create biomimetic foods? This is a reasoning often given by health-conscious consumers favouring wholesome foods of natural origin over processed or fabricated products. To address this point, the concept of BPFs should be fully realised. In fact, the ultimate vision is not to make an exact replica of natural foods, but rather being inspired by the structure-function relationships to enable the design of nature-like foods with similar or enhanced functionality. Also, it is important to mention that the major advantage of BPFs lies in the design versatility with a wide range of shape, size, structure, and composition for specific and optimal functionality in various food systems.

In this review, we have described plant foods as naturally occurring delivery systems for nutrients and bioactive compounds. Moreover, we have shown that all hierarchical levels of the food structure are involved in controlling the bioaccessibility and digestion of nutrients. Therefore, we propose that structural design principles derived from plants may inspire the creation of high-value healthy BPFs. As illustrated in Fig. 2.4, the plant cell and lipid body are examples of natural templates for designing BPFs with desirable functionalities such as delayed digestion of starch/lipids for reduced postprandial glycemia/lipemia. We also envisage a new category of BPF products that can be tailored for health-promoting applications in helping prevent and combat chronic diseases. Recent studies have shed light on many possibilities of engineering BPFs from food-grade ingredients using processing technologies, and some examples of BPFs are given below.

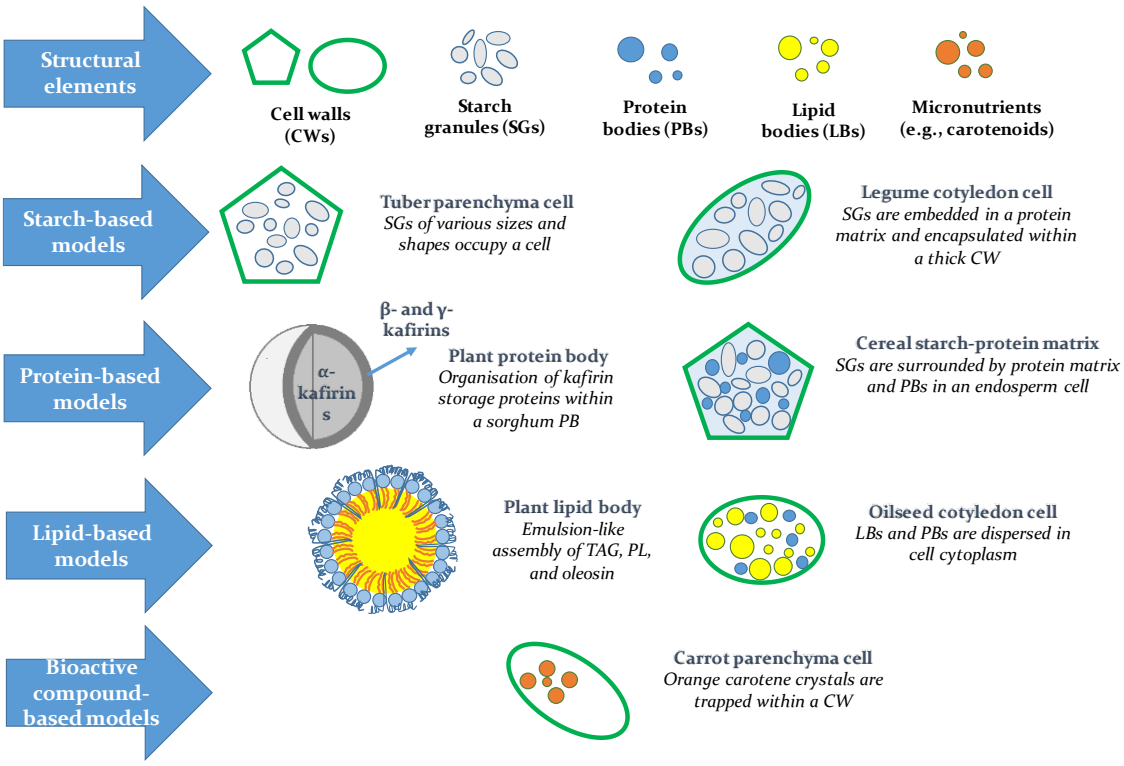

Fig. 2.4. Structural design of plant foods in nature serves as a template for biomimetics. The illustrations do not necessarily represent exact replication of natural structures.

2.7.1. Artificial plant cell walls

Artificial plant cell walls can be reassembled from three basic building blocks of cellulose, xyloglucan, and pectin. In a biotic (living) system, the *in vivo* assembly of the cell wall occurs during the deposition of bacterial cellulose (BC) synthesized extracellularly by the bacterium *Gluconacetobacter xylinus* into a culture medium containing xyloglucan and pectin (Fig. 2.5A) (Cybulska *et al.*, 2010; Gu & Catchmark, 2012). On the other hand, the *in vitro* assembly of the cell wall occurs in an abiotic (non-living) system in which a mixture of isolated polymers (i.e. extracted cellulose fibers and xyloglucan) is incubated with constant mixing (Hayashi, Marsden, & Delmer, 1987; Whitney, Brigham, Darke, Reid, & Gidley, 1995). The BC cell wall shares many similarities to the native wall in terms of chemical composition and microstructure (Cybulska *et al.*, 2010). Whitney and

colleagues have demonstrated that the level of xyloglucan incorporation into the cellulose network in an actively growing BC system is comparable with that in the native wall, but is considerably higher (approximately an order of magnitude) than that in the isolated polymer mixture. Additionally, xyloglucan is capable of penetrating BC fibrils and altering their structures and properties, whereas xyloglucan only adsorbs onto the surface of cellulose particles under *in vitro* conditions (Whitney *et al.*, 1995). Therefore, it is evident that the biosynthesis of BC in the presence of xyloglucan and pectin bio-mimics the assembly of the primary cell wall in nature. In practice, BC-based composites are used as a model system for studying the permeability, porosity, and mechanical characteristics of the plant cell wall as well as fermentation of dietary fiber. The hydrophobic and enzyme-resistant nature of the cell wall is also a source of inspiration for structuring novel encapsulating materials using cell wall polysaccharides to be used in food delivery systems for nutrients and probiotics. For instance, encapsulation of probiotic bacteria (*Bacillus coagulans*) in a composite matrix consisting of bacterial nanocellulose and pectin could protect them against GI conditions. This could be attributed to intermolecular interactions between functional groups of bacterial nanocellulose and pectin, resulting in a compact surface morphology that could limit diffusion of acids and digestive enzymes into the composite matrix (Khorasani & Shojaosadati, 2016).

2.7.2. Artificial lipid bodies

To mimic the unique structure of lipid storage organelles within oilseeds, artificial LBs (Fig. 2.5B) are reconstituted from three principal isolated components

including TAGs, PLs, and integral proteins under the same weight proportions as found in nature. Artificial LBs could be stabilised by oleosin or caleosin but not by steroleosin, and the average size could be controlled by varying the ratio of TAG to protein (Peng, Lin, Lin, & Tzen, 2003). Oleosin-stabilised LBs are similar in size (0.5–2 μm), whereas caleosin-stabilised LBs are 10 times smaller (50-200 nm) in comparison with native LBs (Chen, Chyan, Lee, Huang, & Tzen, 2004). Interestingly, artificial LBs display excellent stability against heat, oxidation, and flocculation/coalescence during storage that resembles the stability of native LBs both inside and outside the environment of the plant cell (Wijesundera & Shen, 2014). Wijesundera *et al.* (2013) prepared artificial LBs from tuna fish oil, PL, and oleosin extracted from canola meal. These were found to readily disperse in water to produce physically stable oil-in-water emulsions which showed no evidence of coalescence during storage at 4 and 40°C. No creaming was detected when these emulsions were subjected to standard conditions of commercial pasteurisation (low temperature long time or high temperature short time). In addition, accelerated oxidation tests demonstrated that these emulsions were significantly more resistant to lipid oxidation when compared with oil-in-water emulsions prepared from tuna fish oil and stabilised with various emulsifiers (i.e. Tween 40, sodium caseinate, and commercial canola protein isolate). Examples of food applications of artificial LBs include development of novel flavouring and emulsifying agents, structuring of food emulsions to control lipid oxidation and digestion, encapsulation of probiotics in dairy products, and being a carrier for delivery of lipid-soluble bioactive compounds (Tzen, 2012).

2.7.3. Bio-mimicking of plant cells

Plant cell wall encapsulation modulates nutrient release and assimilation in the GI tract (refer to Section 2.6.3.4), which can inspire the design of BPFs for nutrient delivery applications. Venkatachalam *et al.* (2009) first reported the development of a novel carbohydrate ingredient called starch-entrapped microspheres (SM) for controlled delivery of glucose. SM were fabricated by entrapping SGs in calcium alginate gel beads. They bear some structural resemblance to starch-entrapped plant cells, but their biopolymer matrix is much less complex than the plant cellular matrix. *In vitro* starch digestion assays combined with scanning electron microscopy techniques demonstrated that gelatinised starch in cooked SM was gradually digested in a layer-by-layer fashion from the outer towards the centre of the microsphere over time. It was therefore suggested that the dense biopolymer matrix could hinder free access of amylolytic enzymes to entrapped starch in a similar manner to the plant cell wall, providing a slow and extended release of glucose during *in vitro* digestion (Venkatachalam *et al.*, 2009). In addition, *in vivo* human studies have shown that incorporation of slowly digestible SM into meals results in delayed gastric emptying (Cisse *et al.*, 2017) and decreased postprandial glycaemic and insulinemic responses (Venkatachalam *et al.*, 2009). Furthermore, a recent clinical trial conducted on human subjects has provided strong evidence that consumption of SM supplementation as a novel source of dietary fiber with slow fermentation properties could improve bowel habits in those with constipation (Rasmussen *et al.*, 2017).

2.7.4. Bio-mimicking of starch-protein matrices

Protein matrices of natural origin modulate starch digestion (refer to Section 2.6.3.5), which can inspire research and development of biomimetic foods with low and slow glycaemic features. Xu and Zhang (2014) reported the microencapsulation of corn starch by zein protein via spray drying for the imitation of natural starch-protein matrices in corn grains. The alcohol-soluble and film-forming properties make zeins an ideal shell material for encapsulation of corn starch. Following a low-temperature spray drying process, spherical particles of encapsulated starch (ENS) were formed and contained native corn starch (CS) enveloped by zein-coating layers (Fig. 2.5C). *In vitro* digestion of raw ENS of various compositions showed that a zein to starch ratio of 1 to 6 yielded materials with the lowest level of rapidly digestible starch and the highest levels of SDS and RS. This ratio was likely the optimal level for maximum encapsulation of SGs with minimal hydrophobic-interaction-induced aggregation of zein molecules. After high-temperature cooking, ENS and CS exhibited different *in vitro* digestion profiles. Specifically when starch samples were treated at 50°C (below CS gelatinisation temperature), ENS had much lower digestibility than CS. After the cooking temperature were raised to 80, 90, or 100°C (above the CS gelatinisation temperature), ENS showed higher levels of SDS and RS than CS. Based on these results, it was speculated that the zein matrix plays a key role in the slow digestion of ENS by forming a physical barrier limiting free access of amylase to starch. During cooking, the hydrophobic zein barrier could be highly effective in resisting water adsorption for swelling and gelatinisation of starch, hence limiting starch

susceptibility to amylolytic attack. Furthermore, incorporation of plasticizers (glycerol and oleic acid) during microencapsulation substantially improved resistance of ENS to thermal treatments and amylolysis. One possible explanation for this is that, apart from forming amylose-lipid complexes, these two plasticizers could act synergistically to improve tensile strength of the zein film. This in turn could decrease heat-induced swelling of entrapped SGs and prevent mechanical breakdown of the zein matrix during digestion. Finally, the study showed promising food application of ENS that can be directly incorporated into beverages for improved postprandial glycaemic control with acceptable sensory quality (Xu & Zhang, 2014).

2.7.5. Bio-mimicking of whole grain tissues

Luo and Zhang (2018) recently attempted to mimic the microstructure of cereal-grain endosperm tissue as found in oat and barley. Whole-grain-like matrices could be constructed by entrapping native CS in calcium cross-linked gel networks of alginate and β-glucan. These polysaccharides act as pectin and hemicellulose constituents of the plant cell wall, respectively. The artificial grain tissue contains cell-like compartments that are morphologically similar to starch-containing endosperm cells of cereal grains (Fig. 2.5D). *In vitro* starch digestion data of cooked artificial grains showed that their SDS content was comparable to that of raw CS but was significantly higher than that of cooked gelatinised CS. It was thus suggested that the co-formed alginate-β-glucan gel matrix in artificial grains could act as a physical barrier impeding amylase access to starch in a manner similar to that seen with cell walls in whole grains. For comparison with artificial grains, a

physical mixture was prepared by combining the same amounts of isolated ingredients including CS, alginate, and β-glucan. Interestingly, the SDS content of the physical mixture was markedly lower than that of the artificial grain. This finding is indicative of the important role of physical intactness of the whole-grain structural form in limiting starch digestion. The whole-grain-like structure can serve as a model to study interactions between starch and other co-existing components within the natural grain matrix. Regarding food application, the artificial grain can potentially be used as a functional ingredient for the development of low-glycaemic-index foods (Luo & Zhang, 2018).

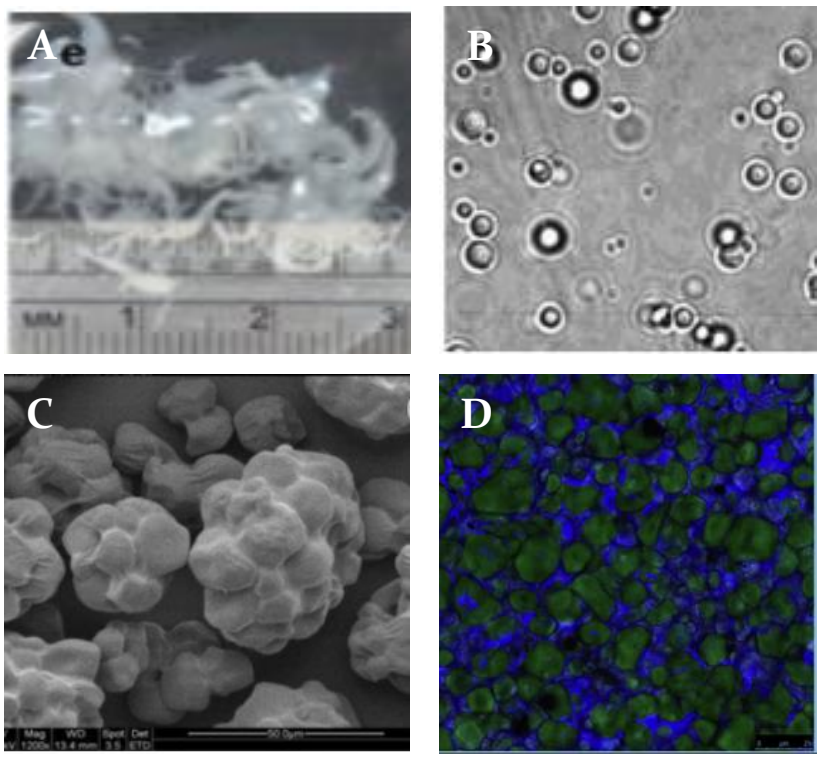

Fig. 2.5. Examples of BPFs. (A) Assembly of primary cell walls from a blend of BC, xyloglucan and pectin after 7 days of incubation, reprinted from Gu and Catchmark (2012) with permission from Elsevier, (B) Stable LBs reconstituted from TAG, PL and oleosin, reprinted with permission from Chen *et al.* (2004), (C) Encapsulation of corn SGs within the zein protein matrix, reprinted from Xu and Zhang (2014) with permission from Elsevier, (D) Entrapment of corn SGs (green) within the alginate-β-glucan gel network (blue), reprinted from Luo and Zhang (2018) with permission from Elsevier.

2.8. Conclusions and future perspectives

The increase in prevalence, incidence and mortality associated with modern chronic diseases has placed substantial health and economic burden on global societies. This situation has accentuated the already growing demand for foods that can help curb the risks or ameliorate the effect of these debilitating conditions. The design and manufacturing of such foods is a challenging task and has attracted considerable interest from the food industry and academics in recent years. Throughout history, solutions for many practical problems facing humanity have come from emulating nature via lessons learned through observations. As we have finally come to understand the complexity behind the process-structure-function relations in plant foods, we can begin to explore opportunities to develop BPFs for optimal nutrition and health.

Designing BPFs presents some technical difficulties. Firstly, it is extremely challenging to mimic the self-assembly process and hierarchical structuring that are inherent in natural foods. Scientific evidence has suggested that intact, minimally processed natural foods seem to have more compact, cohesive matrices and stronger interactions between nutrients. This means they are disassembled and release nutrients in the digestive tract at a slower rate for greater satiety as opposed to artificially reconstructed foods (Fardet, 2015). Furthermore, drastic processing conditions may cause undesirable changes in structures and properties of food elements during isolation or reassembly. Finally, the incorporation of BPFs into food systems can be challenging, especially without adversely influencing the physicochemical or sensory properties of the food. Despite these technical

challenges, the prospects are very exciting. Ongoing and future research initiatives should be directed towards exploring the possibility of designing BPFs for desirable nutritional and health benefits. An interdisciplinary approach should be adopted for conducting research at the dynamic interface of a wide range of disciplines in food science and technology, including structure-digestion, chemistry, engineering, physiology, microbiology and human nutrition.

2.9. Research gaps, questions, and hypotheses

Despite recent advances in the research area of the thesis – microstructural and biomimetic constraints on starch digestion in plant foods – as shown in the literature review, the role of individual cellular and subcellular components present in edible plants (i.e., the cell wall, cytoplasmic protein, and starch granule) and their interactions limiting starch susceptibility to amylase digestion remains unclear and warrants further investigation. In addition, so far, there has been very limited scientific evidence showing how understanding of the inhibitory effects of these components on starch digestion could serve as a platform to explore the possibility of designing low glycaemic foods. As such, within the confines of the thesis topic, the research studies were aimed at examining two specific starch-based food systems – (1) starch-containing plant cells in legumes and (2) starch-protein matrix in sorghum flour – as models for biomimetic inhibition of starch digestion. These food systems were appropriately chosen because they exhibited slow starch digestion properties and allowed ample opportunity to study the microstructural factors affecting amylase digestion of starch at the cellular and subcellular level.

Following the identification of research gaps, research questions and hypotheses were stated. The research chapters presented in this thesis were laid out in a logical sequence to address a series of research questions as summarised in Figure 2.6.

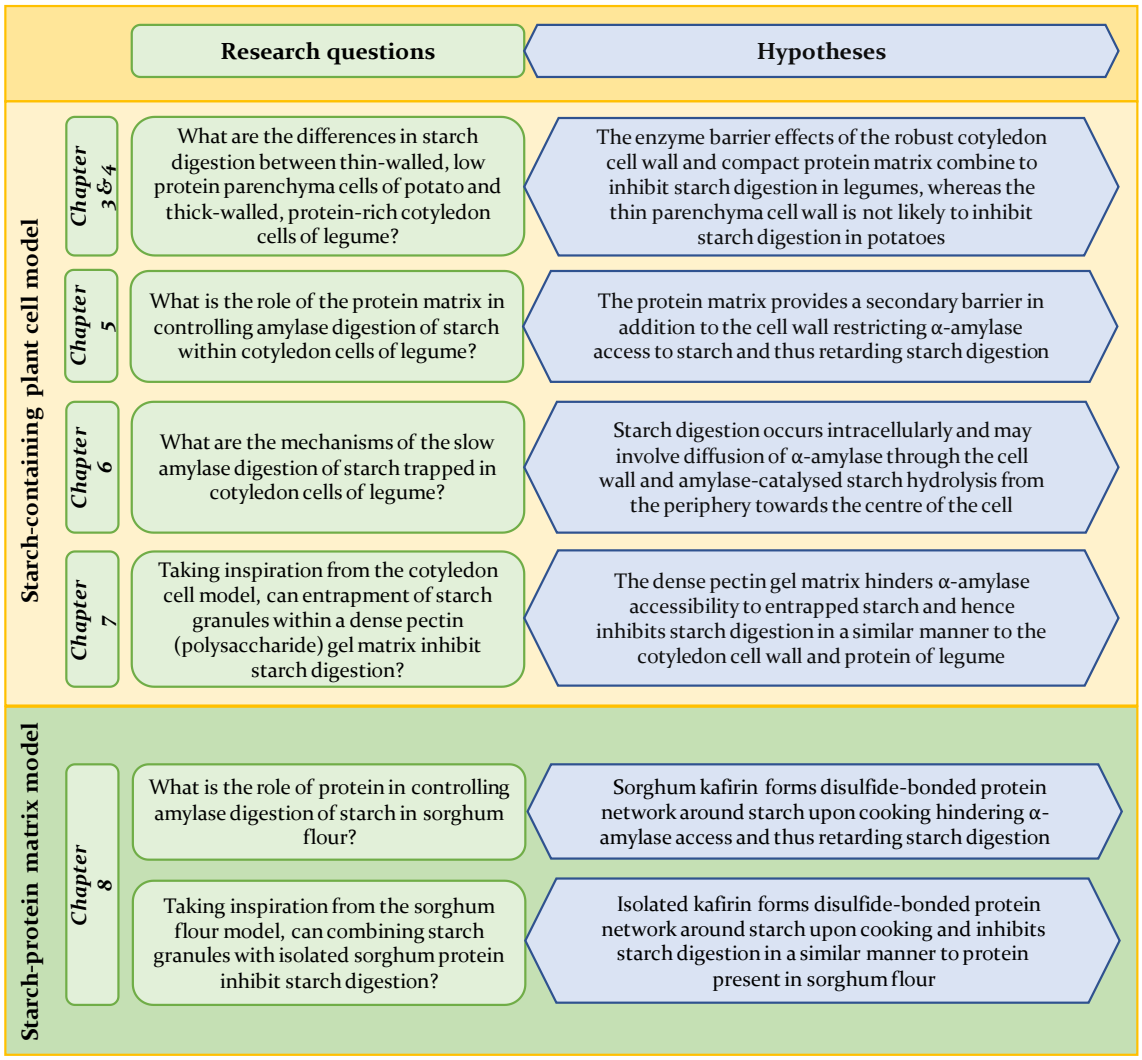

Fig. 2.6. Research questions and hypotheses.

CHAPTER THREE: Modulating effect of cotyledon cell microstructure on *in vitro* digestion of starch in legumes

3.1. Abstract

The cotyledon of legumes consists primarily of numerous starch granule-containing cells bound together by the pectin-rich middle lamella. In this study, we provided detailed characterisation of the microstructure, physicochemical properties, and *in vitro* starch digestion of cotyledon cells. Raw intact cells were obtained from adzuki bean, chickpea, lentil, and lima bean using a sequential acid-alkali isolation method. These cells were then cooked and subjected to *in vitro* gastric and small intestinal digestion. Light micrographs of cells showed various cell shape (ellipsoid or spherical) and size (D50 ~ 98 – 118μm). Cells contained starch granules (D50 ~ 19 – 40μm) that were tightly packed in the cytoplasmic protein matrix and enclosed within cell walls. Upon heating in excess water, starch inside cells exhibited considerably lower swelling, solubility, and paste viscosities, as well as higher gelatinisation transition temperatures than isolated starch. After cooking under similar conditions, starch inside cells exhibited significantly lower rate and extent of hydrolysis than isolated starch during subsequent *in vitro* digestion. Scanning electron microscopic study of representative cells showed preservation of cell wall intactness throughout cooking and digestion. The results indicate that the cotyledon cell structure restricts starch gelatinisation and impedes enzyme accessibility to intracellular starch, thus limiting starch digestion *in vitro*.

3.2. Introduction

Legumes are widely cultivated for human consumption in many regions of the world. Nutritionally, they provide a rich source of complex carbohydrates, proteins, lipids, and dietary fibers along with micronutrients and phytochemicals (antinutrients) (Messina, 1999). Starchy legumes (e.g. beans, peas, chickpeas, and lentils) contain a substantial proportion of SDS that elicits low postprandial glucose and insulin responses and induces prolonged satiety. Such physiological effects make legumes a recommended dietary choice for prevention and management of type 2 diabetes mellitus and obesity (Rizkalla, Bellisle, & Slama, 2002; Tovar, 1996). There are a number of contributing factors to the slow digestion of starch in legumes. These include intrinsic properties of starch (e.g. amylose content and retrograded amylose), interactions of starch with dietary fibers/proteins, and the presence of anti-nutrients (e.g. phytic acid) (Thompson, Button, & Jenkins, 1987; Thorne, Thompson, & Jenkins, 1983; Würsch, Del Vedovo, & Koellreutter, 1986). Emerging evidence has indicated that cotyledon cell structure is also a predominant factor (Berg *et al.*, 2012; Xiong *et al.*, 2018).

Cotyledons of starchy legumes consist of numerous cells. The middle lamella, a pectin-rich substance, helps cement adjacent cells together. Each cell contains starch granules that are tightly embedded in a protein matrix, both surrounded by a cell membrane and a thick, mechanically strong outer cell wall (Berg *et al.*, 2012). The unique structure of cotyledon cells provides effective encapsulation for starch against the extracellular environment. During cooking (e.g. boiling and steaming) of cotyledon tissue, the strong cell wall imposes restrictions on water availability,

heat transfer, and intracellular space that are required for swelling and gelatinisation of entrapped starch granules. This consequently produces a delay in progression of granule expansion and deformation. As a result, starch in cooked tissue exhibits a swollen distorted shape and retains in part granular structure as evidenced by residual birefringence under polarised light (Berg *et al.*, 2012; Edwards *et al.*, 2015; Hahn, Jones, Akha Van, & Rockland, 1977). Cooking also facilitates separation of intact cells containing partially gelatinised starch rather than cell rupture. Cell walls remain mostly intact and effectively hinder accessibility of amylolytic enzymes to starch throughout subsequent *in vitro* digestion. The combined effects of the incomplete starch gelatinisation and the enzyme barrier properties of the cell wall lead to a pronounced reduction in the rate and extent of starch hydrolysis under simulated gastric and small intestinal conditions (Berg *et al.*, 2012). In addition, a significant amount of RS trapped inside intact cells has been recovered in samples of ileal digesta from healthy human subjects after ingestion of meals containing cooked white beans (Noah *et al.*, 1998).

Intact cells can be isolated without gelatinising starch by maceration of cotyledon tissue in acid and then alkali (Kugimiya, 1990). Previous studies have suggested that the swelling and gelatinisation of starch during heating in excess water is suppressed by limited water availability and constrained space inside cells (Fujimura & Kugimiya, 1993, 1994; Fujimura, Liu, & Kugimiya, 1995; Fujimura, Tanaka, Narita, & Isobe, 2007). Despite the detailed knowledge of cotyledon cells regarding the starch gelatinisation behaviour, their enzymatic digestion has not been explored until very recently. It has been reported that a single cell wall can provide an efficient barrier against starch-amylase interactions, which in turn leads

to a lower *in vitro* starch hydrolysis rate of intact cells compared with that of isolated starch or damaged cells devoid of intact structures (Bhattarai *et al.*, 2017; Dhital *et al.*, 2016; Rovalino-Córdova *et al.*, 2018).

The aim of this work was to understand the effect of cotyledon cell microstructure on gelatinisation properties and *in vitro* digestion of starch in legumes. Microscopic techniques were used to observe changes in the external surface and internal structure of cells after cooking and during digestion. The knowledge from this research will provide a better understanding of the role of cotyledon cell microstructure in controlling starch digestion and support the possibility of utilising cotyledon cells as a new functional ingredient by the food industry.

3.3. Materials and Methods

3.3.1. Materials

One batch of whole dry legumes of adzuki bean (*Vigna angularis*), chickpea (*Cicer arietinum* L.), lentil (*Lens culinaris*), and lima bean (*Phaseolus lunatus*) was purchased from a local retail store in Palmerston North, New Zealand. These legumes were kept in sealed plastic bags and stored in an airtight container at 4°C throughout the course of the study. Pepsin (porcine gastric mucosa; ≥ 250 units/mg solid), pancreatin (porcine pancreas, 4x USP), and invertase (from baker's yeast (*S. cerevisiase*), Grade VII, ≥ 300 units/mg solid) were purchased from Sigma – Aldrich Ltd, St Louis, USA. Amyloglucosidase (for Total Dietary Fiber and Starch Assays, 3260U/mL) was supplied by Megazyme International Ireland Ltd.,

Ireland. All other chemicals and reagents were of analytical grade. Reverse osmosis (RO) water was used for all experiments.

3.3.2. Isolation of raw cotyledon cells

Raw intact cotyledon cells were isolated without gelatinising starch by successive treatments of legumes with acid and alkali solutions according to a slight modification of the method described by Kugimiya (1990). Dry legumes were soaked in a 0.1M hydrochloric acid (HCl) solution (pH ~ 1.3) at room temperature (~20°C) for 24 h. The outer seed coats and hypocotyls were then manually removed, and each legume grain was split into two cotyledons. After rinsing with RO water to remove the remaining acids, the cotyledons were soaked in a 0.06M sodium hydroxide (NaOH) solution (pH ~ 12.5) in 1L Schott bottles. These bottles were shaken in a shaking incubator at 20°C and 150 rpm for 24 h. The softened alkali-treated cotyledons were gently mashed by a pestle and mortar to a consistent paste. The resultant paste was successively passed through 150 and 53 µm sieves by repeated washing with RO water. The cell extract was collected on the 53 µm sieve, dehydrated with a graded ethanol series (25%, 50%, 75%, 95%, 100% for 10 min each), and freeze-dried. The dried powder was bottled and stored at room temperature until further analysis.

3.3.3. Isolation of free starch granules

Free starch granules were isolated following the method described by Berg *et al.* (2012) with some modifications. Dry legumes (200 g) were soaked in 400 mL sodium metabisulfite solution (0.5%, w/w) for 18 h at 4°C. After the soaking water

was discarded, the hydrated legumes were washed and wet ground with 500 mL of water at room temperature using a laboratory blender (Breville Pty Ltd, Sydney, Australia). The resultant milky suspension was successively filtered through 150 and 100 µm sieves. The residue left on the sieves was washed 3 – 4 times with abundant water until virtually no more starch passing through. The starch was allowed to settle by sedimentation for 4 h in a beaker. The supernatant was then decanted, and the grey-coloured protein-rich top layer was scraped off using a spatula. The starch deposit was reslurried in excess water and allowed to sediment again. The starch was obtained by repeated washing with water and resettling by sedimentation several times until the supernatant became transparent. The isolated legume starch (ILS) was regularly examined under a light microscope for the presence of impurities (e.g. cell wall fragments). The starch cake was spread onto a tray in a thin layer and dried at 40°C in an oven for 18 h.

3.3.4. Determination of morphological properties

3.3.4.1. Light microscopy

Samples of raw isolated cotyledon cells (ICC) were mounted onto glass microscope slides, suspended in water, sealed with cover slips, and then viewed under an Axiophot light microscope (LM) (Carl Zeiss, Germany) operating in Differential Interference Contrast (DIC) mode using the objective of 20x magnification. Representative light micrographs of cell samples were captured using a Leica DFC320 camera equipped with the Leica software application suite LAS V3.8 (Leica Microsystems).

3.3.4.2. Particle size distribution

Particle size distribution was measured with a laser diffraction particle size analyser (Malvern Mastersizer 2000, Malvern Instruments Ltd., UK). Test samples were mixed with water to obtain homogeneous suspensions that were then added into a small volume sample dispersion unit (Hydro 2000S) until an obscuration level of ~15±1% was obtained. Refractive indices of 1.530 and 1.330 were used for starch/cell and water phases respectively, and particle absorption was set at 0.1.

3.3.5. Determination of chemical composition

Moisture content was determined gravimetrically by drying the legume samples in an oven at 105°C to a constant weight. Samples of ICC were analysed for crude protein (Dumas method, AOAC 968.06, with a conversion factor of 6.25 from nitrogen to protein), lipid (Soxtec method, AOAC 2003.06), and ash (AOAC 930.15). Carbohydrate content was calculated by subtracting from 100% the sum of moisture, ash, protein, and lipid. Chemical composition of ICC was expressed on a dry weight basis (dwb).

Total starch content was analysed using a total starch assay kit (K-TSTA, Megazyme International Ireland Ltd., Ireland) following the instructions given by the manufacturer. To avoid underestimation of the starch content, the cell samples were mechanically broken by crushing the cells with a pestle in mortar prior to analysis. Total amylose content of ILS was determined by an amylose/amylopectin assay kit (K-AMYL, Megazyme International Ireland Ltd., Ireland), based on the

specific complex formation between the amylopectin component of starch with the lectin concanavalin A (Con A).

3.3.6. Determination of swelling power and solubility

Swelling power and solubility were determined using the method of Fujimura and Kugimiya (1994) with some modifications. Samples equivalent to ~200 mg of starch (dwb) were mixed with 10 mL water to yield 2% (w/v) aqueous starch suspensions in 15 mL pre-weighed centrifuge tubes. The suspensions were then heated in a water bath at 90°C for 30 min and afterwards cooled down to room temperature and centrifuged at 3000 rpm for 15 min. Supernatants were subsequently separated from precipitated pastes. The swelling power and solubility were calculated using equations (1) and (2):

$$\text{Solubility (\%)} = \frac{V \times S}{W_s} \times 100\% \quad (3.1)$$

$$\text{Swelling power (g/g)} = \frac{W_p}{W_o - V \times S} \quad (3.2)$$

Where V is the volume of supernatant (mL) measured with a 10 mL graduated cylinder, S is the soluble starch content of supernatant (mg/mL) determined by the total starch assay kit, W_s is the dry mass of starch (mg), W_p is the weight of precipitated paste (mg), W_o is the dry mass of sample (mg).

3.3.7. Determination of thermal properties

Thermal properties were evaluated using a Differential Scanning Calorimeter (TA Q100, TA Instruments, Newcastle, DE) equipped with a thermal data analysis station. Following the method described by Singh, McCarthy, and Singh (2006), a

sample equivalent to ~3.5 mg dry weight starch (calculated based on the starch content in the sample) was accurately weighed into a 40-µL aluminium pan. A predetermined amount of water was then added into the pan using a Hamilton micro-syringe to obtain a starch-water mixture containing 80% water (w/w) to ensure excess water for starch gelatinisation. The pan was hermetically sealed and allowed to stand for 4 h at room temperature to equilibrate the moisture content prior to heating scan in the DSC. The sample pan was heated from 20 to 100°C at a rate of 10°C/min. An empty aluminium pan was included as the reference. Onset temperature (T_o), peak temperature (T_p), conclusion temperature (T_c), and gelatinisation enthalpy (ΔH_{gel}) were calculated using Universal Analysis Software (version 4.5A, TA Instruments).

3.3.8. Determination of pasting properties

Pasting properties were evaluated using a Rapid Visco Analyzer (RVA-4, Newport Scientific Ply Ltd, Warriewood, Australia). Following the method of Singh *et al.* (2006), a sample equivalent to ~2 g dry weight starch (calculated based on the starch content in the sample) was weighed directly into a cylindrical aluminium canister and mixed with 25 g water (corrected for the moisture content in the sample). The starch-water mixture was stirred gently using a plastic rotational paddle before being inserted into the instrument. The starch slurry was subjected to a programmed heating and cooling cycle in which the slurry was equilibrated at 50°C for 1 min, heated to 95°C at the rate of 12.2°C/min, held at 95°C for 2.5 min, cooled to 50°C at the rate of 11.8°C/min, and held at 50°C for 2 min. The rotating speed of the paddle was 960 rpm for the first 10 seconds to facilitate sample

dispersion, and then maintained at constant 160 rpm throughout the analysis. Peak, trough, final, breakdown, and setback viscosities were calculated using Thermocline Software (Newport Scientific) and reported in centipoise (cP).

3.3.9. In vitro *starch digestion*

3.3.9.1. Cooking of samples for *in vitro* digestion

Samples were mixed with water in 400 mL glass beakers to obtain aqueous dispersions containing approximately 4% starch (w/w). The beakers were covered with aluminium foil to avoid water evaporation before being placed in a water bath at ~95°C for 20 min with gentle magnetic stirring to fully gelatinise starch. After cooking the beaker contents were allowed to cool to 37°C in a water bath.

3.3.9.2. Static *in vitro* starch digestion procedure

The *in vitro* digestion was performed following the method described by Dartois, Singh, Kaur, and Singh (2010). A two-stage model system was used to simulate the gastric and small intestinal digestion of starch. The simulated gastric and intestinal fluids (SGF and SIF) were freshly prepared prior to analysis in accordance with the US Pharmacopeia (Pharmacopeia, 2000).

Cooked samples (~ 170 g), prepared as described in section 3.3.9.1, were introduced into 500 mL jacketed glass reactors. Temperature was controlled at 37±1°C by circulating water through the reactor jackets. Contents of each reactor were mechanically stirred by a magnetic stirrer bar at 300 rpm throughout digestion. The reactor contents were stirred for 10 min to allow the temperature to equilibrate to 37±1°C prior to *in vitro* digestion. The pH was initially adjusted to 2.0. The SGF

(17 mL) containing pepsin (enzyme/starch ratio, 1.765:100, w/w) was then added to start the gastric digestion, and the pH was maintained at 1.2. After 30 min, the pH was adjusted to 6.8 in order to inactivate the pepsin enzyme. Subsequently, the SIF (22 mL) containing pancreatin (enzyme/starch ratio, 1.3:100, w/w), amyloglucosidase (enzyme/starch ratio, 0.26:1, v/w), and invertase (enzyme/starch ratio, 1:1,000, w/w) was added to start the 120 min small intestinal digestion, and the pH was maintained at 6.8. The pH of the reactor contents was adjusted throughout digestion using appropriate concentrations of HCl (3 M and 0.5 M) and NaOH (3 M and 0.5 M).

Duplicate aliquots (0.5 mL) were withdrawn from the reactors after 0, 15, and 30 min of the gastric digestion (thereafter referred to as G0, G15, G30), and after 0, 5, 10, 15, 30, 60, 90, and 120 min of the small intestinal digestion (thereafter referred to as I0, I5, I10, I15, I30, I60, I90, I120). The aliquots were immediately transferred to 15 mL centrifuge tubes containing 2 mL of absolute ethanol in order to stop enzymatic activities. The resultant mixtures were vortex-mixed and centrifuged at 1800 *x g* for 10 min. Ethanolic supernatants (0.1 mL) were incubated with 0.5 mL amyloglucosidase and invertase in acetate buffer (0.1 mL amyloglucosidase and 3.75 mg invertase per 10 mL acetate buffer) at pH 5.2 and 37°C for 10 min to completely digest soluble dextrins in the supernatants to glucose. Quantification of glucose was then carried out using a D-glucose assay kit (GOPOD-FORMAT, K-GLUC, Megazyme International Ireland Ltd., Ireland).

The percentage of starch hydrolysis at each sampling time point was used to construct hydrolysis curves and calculated using equation (3):

$$\%S_H = \frac{S_h}{S_i} x100 = 0.9x\frac{G_p}{S_i} x100 \quad (3.3)$$

Where $\%S_H$ is the percentage of starch hydrolysis (%); S_h is the amount of hydrolysed starch (g), S_i is the initial amount of starch (g), and G_p is the amount of glucose produced (g). A conversion factor of 0.9 from starch to glucose is based on the molecular mass ratio of starch monomer to glucose (162/180=0.9).

3.3.9.3. Microstructural characteristics of cotyledon cells

In a separate experiment, samples of ICC were cooked and subjected to *in vitro* starch digestion. Individual 1 mL aliquots were withdrawn from the digestion reactor at predetermined time points as follows: before gastric digestion (cooked cells), at the end of gastric digestion, after 10 and 120 min small intestinal digestion. The aliquots were transferred to 2 mL Eppendorf microcentrifuge tubes, immediately frozen by immersing in liquid nitrogen, and stored at -80°C prior to freeze-drying. The freeze-dried powder was directly mounted on double-sided adhesive tapes on aluminium stubs, sputter coated with gold (SCD 050, Balzers, Liechtenstein), and viewed under a scanning electron microscope (SEM) (FEI Quanta 200 FEI Electron Optics, Eindhoven, The Netherlands). Representative electron micrographs of cell samples were captured with accelerating voltage of 20 kV using the xT microscope software version 3.0.7 (FEI Quanta, Eindhoven, the Netherlands). The freeze-dried cells after 120 min small intestinal digestion were stained with 1% (v/v) Lugol's iodine solution for starch and 0.1% (w/v) Fast Green FCF for cytoplasm and then viewed under the LM operating in Brightfield (BF) mode using the objective of 20x magnification.

3.3.10. Statistical analysis

Reported values were calculated as means of triplicate observations, unless otherwise specified. Tukey's test and analysis of variance (ANOVA) were used to analyse the significance of differences ($p \leq 0.05$) between means using the Minitab 18 software (Minitab Inc., State College, PA).

3.4. Results and Discussion

3.4.1. Isolation of cotyledon cells

Cotyledon cells must be isolated with great care to maintain cellular integrity and minimise starch gelatinisation. Among previously published methods (Kim & Kim, 2015; Dhital *et al.*, 2016) that were attempted in order to establish optimal conditions for cell isolation (results not shown), the successive treatment of cotyledons with acid and alkali (Kugimiya, 1990) resulted in the most effective separation of intact cells without gelatinising starch, along with sufficient quantity of cell materials for experimentation. The sequential acid/alkali treatment could facilitate breakdown of pectic polymers in the middle lamella that are involved in cell-cell adhesion, leading to subsequent cell separation. This isolation method was thus employed to prepare pure ICC for analysis. During isolation, cell extracts were regularly examined under LM to check the purity of samples. We noted the presence of minor impurities including broken cells, free starch granules, and cell wall/protein matrix fragments. It appears that intact cells were likely broken by crushing with mortar and pestle and cellular contents were released. Nevertheless, the overall cellular damage was observed to be minimal.

The cell isolation method employed in this study avoids the use of elevated temperatures that could cause irreversible physicochemical changes in cellular components, e.g. cell wall swelling and solubilisation, melting of cell membrane, partial gelatinisation of starch, protein denaturation, etc. Despite the above merits, a disadvantage of this method is the effect of acid and alkali on cells. These substances may modify or remove some components of cell walls, thus altering their structure and porosity. It is therefore sensible to assume that the properties of IC may not be identical to those of cells in native tissues.

3.4.2. Morphological properties

DIC light micrographs of ICC highlight distinctive cellular morphology (Fig. 3.1). Each cell consisted of numerous starch granules that were compactly embedded in a cytoplasmic protein matrix and enclosed within an outer cell wall. The cells exhibited good preservation of structural integrity after isolation. Organelles (e.g. protein bodies) were not clearly visible under the magnification used. The morphological characteristics of ICC varied widely among the four legumes studied with regard to shape and size of starch granules/cells as well as abundance and organisation of granules inside cells. Chickpea cells tended to be elliptical, whereas others were typically spherical in shape. Similar microscopic observations of the cotyledon cell morphology have been previously reported (Dhital *et al.*, 2016). In addition, chickpea and lentil cells appeared to contain a larger number of smaller-sized granules, whereas adzuki and lima bean cells appeared to contain relatively fewer but predominantly larger-sized granules – the number of which inside one cell could easily be counted. Interestingly, adzuki bean cells when viewed under

LM were found to contain granules with noticeably deep fissures (Fig. 3.1A). The formation of fissures that radiate outwards from the granule centre is associated with the tight packing of granules within the protein matrix (Hsieh, Swanson, & Lumpkin, 1999).

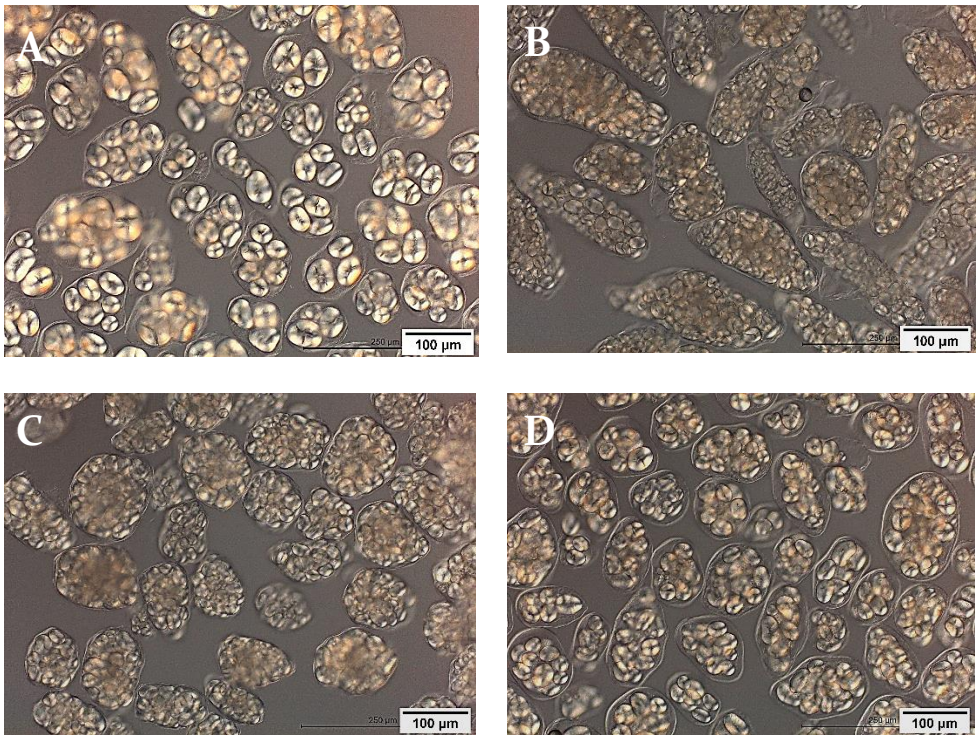

Fig. 3.1. Representative DIC light micrographs of ICC: (A) adzuki bean, (B) chickpea, (C) lentil, and (D) lima bean. Scale bar = 100µm.

All samples exhibited monomodal particle size distributions (Fig. 3.2). As shown in Table 3.1, the mean granule diameter (D50) of ILS differed significantly among the four legumes (adzuki bean > lima bean > lentil > chickpea) and was inversely correlated to the specific surface area. The mean diameter (D50) of ICC ranged from 98.9 to 117.7 µm. Chickpea cells had the widest particle size distribution and the largest mean diameter. Since the cell extract was successively passed through 150 and 53 µm sieves and ICC were collected on the latter sieve, the size distribution of ICC might not be representative of cells in native cotyledon tissues.

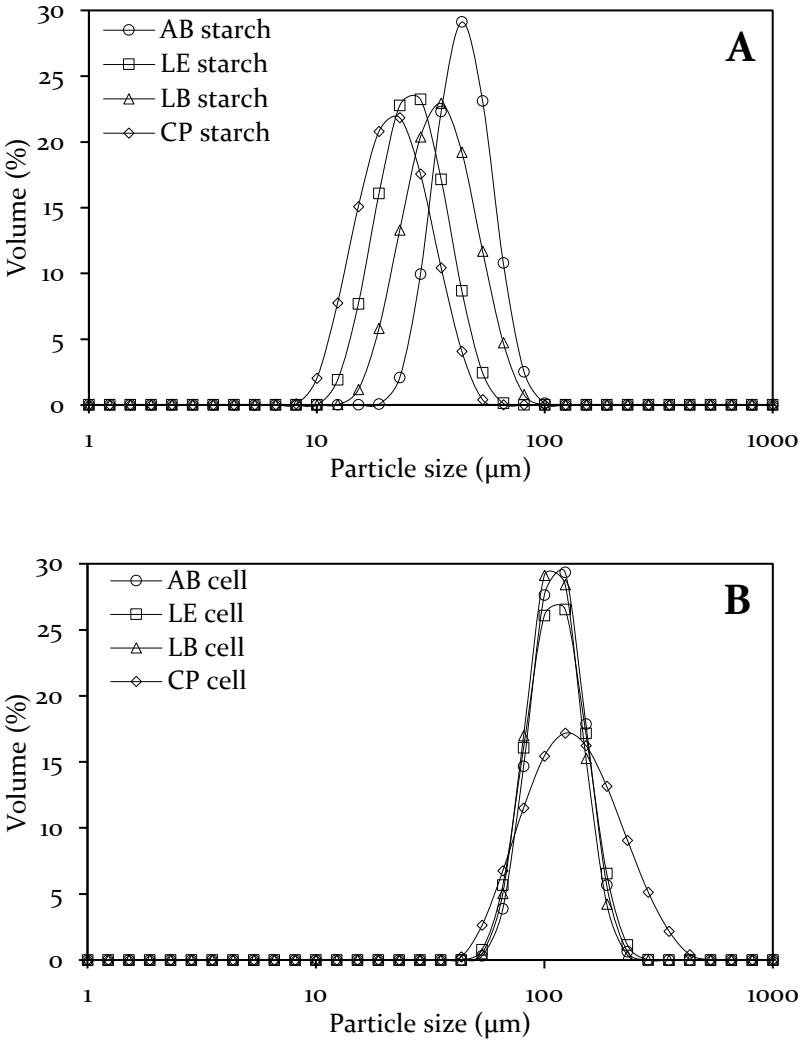

Fig. 3.2. Particle size distribution of (A) ILS and (B) ICC from four legumes: adzuki bean (AB), lentil (LE), lima bean (LB), and chickpea (CP).

Table 3.1. Morphological properties of ILS and ICC from adzuki bean, chickpea, lentil, and lima bean.

Legume type	Starch type	Mean diameter (D50, μm)	Specific surface area (m^2/g)
Adzuki bean	IS	39.3^{e}	0.158^{d}
	IC	102.4^{b}	0.061^{f}
Chickpea	IS	19.5^{h}	0.326^{a}
	IC	117.7^{a}	0.056^{g}
Lentil	IS	23.4^{g}	0.270^{b}
	IC	101.0^{c}	0.062^{ef}
Lima bean	IS	31.0^{f}	0.205^{c}
	IC	98.9^{d}	0.063^{e}

Values with the same subscripts in a column do not differ significantly ($p > 0.05$).

3.4.3. Chemical composition

Total starch content of ILS decreased in the following order: lentil (95.7%) ~ adzuki bean (94.6%) ~ lima bean (93.3%) > chickpea (91.3%), which was similar to the purity level of ~93% reported by Huang *et al.* (2007). Difficulties in isolating pure starch from legumes may be associated with presence in large amounts of insoluble proteins and co-settling of hydrated fine fiber fractions with starch (Schoch & Maywald, 1968). Total amylose content of ILS decreased in the following order: lima bean (34.3%) > lentil (29.0%) > adzuki bean (23.0%) ~ chickpea (22.5%). These values were typical for legume starches (moderate to high amylose) and within range of other published data (Hoover, Hughes, Chung, & Liu, 2010; Hoover & Ratnayake, 2002). Broad variations in amylose content have been found among legume starches, largely due to differences in varieties/cultivars and methods of amylose determination (Hoover *et al.*, 2010).

Proximate analysis showed that the chemical composition of ICC (Table 3.2) differed among the four legumes and was comparable to previous reports (Bhattarai *et al.*, 2017; Fujimura & Kugimiya, 1994). Starch was the most abundant component and comprised between 57.2 and 69.0% of total dry cell mass. Proteins constituted a significant proportion (17.3–20.3%) while lipids were present in minor amounts (0.10–2.46%). Chickpea cells contained markedly more lipid than other legume cells. As a side note, the interactions between starch and proteins/lipids, such as the formation of amylose-lipid complexes, have been known to influence starch digestibility (Singh *et al.*, 2010).

Table 3.2. Chemical composition of ICC (%, w/w, dwb) from adzuki bean, chickpea, lentil, and lima bean.

Legume type	Ash (%)	Protein (%)	Lipid (%)	Carbohydrate (%)	Total starch (%)
Adzuki bean	0.51^{b}	19.8^{a}	0.31^{b}	79.4^{b}	69.0^{a}
Chickpea	0.62^{a}	17.8^{b}	2.46^{a}	79.1^{b}	57.2^{c}
Lentil	0.51^{b}	20.3^{a}	0.31^{b}	78.9^{b}	68.1^{a}
Lima bean	0.62^{a}	17.3^{b}	0.10^{c}	82.0^{a}	63.8^{b}

Values with the same subscripts in a column do not differ significantly ($p > 0.05$).

3.4.4. Swelling power and solubility

As shown in Fig. 3.3, the swelling power and solubility of ILS at 90°C was generally lower than that of cereal or tuber starches reported previously (Singh, Singh, Kaur, Sodhi, & Gill, 2003). One probable explanation for this is that legume starches tend to possess stronger interactions between starch chains (amylose-amylose and/or amylose-amylopectin), leading to more strongly bonded micellar structure and greater granular stability (Hoover *et al.*, 2010; Wani *et al.*, 2016; Joshi *et al.*, 2013). In addition, various degrees of swelling power and solubility were found among the four ILS. Negative correlations have reportedly been found between amylose content and swelling power (Li & Yeh, 2001; Singh *et al.*, 2006); however, such correlations were not observed in our study. Amylopectin chain length distribution, granule organisation, and amylose-lipid complexes may also account for differences in the swelling and solubility behaviour of starch (Singh *et al.*, 2003; Vandeputte, Derycke, Geeroms, & Delcour, 2003). These aspects were not investigated in the present study and could likely be influential factors.

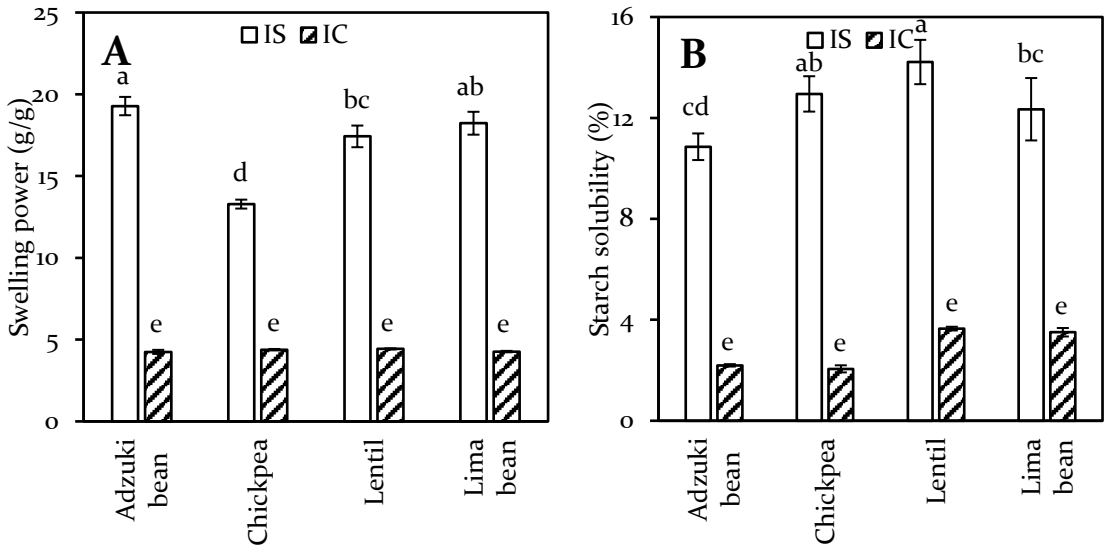

Fig. 3.3. Swelling power (A) and starch solubility (B) of ILS and ICC heated at 90°C for 30 min. Error bars represent the standard deviation.

Starch inside ICC had considerably lower swelling power and solubility compared with ILS (Fig. 3.3). Similar results have been obtained for kidney bean, faba bean, and pea ICC (Fujimura & Kugimiya, 1994; Fujimura *et al.*, 1995, 2007). It is generally believed that native starch granules imbibe water and swell upon heating in excess water. This causes weakening of internal bonds within the granule and leaching of amorphous amylose to the surrounding medium (Wani *et al.*, 2016). It appears that the suppressed swelling and solubility of ICC may be attributed in part to the presence of the cell wall and the protein matrix. Together, they impose restrictions on availability of water and space inside the cell for granule swelling and complete disruption of granular structure, resulting in limited amylose leaching. The cell wall could prevent amylose to further leach out of the cell into the extracellular medium, thus decreasing starch solubility.

3.4.5. Thermal properties

DSC thermograms and thermal characteristics of starch in the four legumes studied are presented in Fig. 3.4 and Table 3.3 respectively. When heated in excess water, ILS displayed a single endotherm with a well-defined sharp peak showing the phase transition in starch known as gelatinisation. The values for T_o, T_p, T_c, and ΔH_{gel} of ILS varied depending on the legume source and were consistent with those reported in literature (Huang *et al.*, 2007; Hoover *et al.*, 2010; Biliaderis, Maurice, & Vose, 1980; Hsieh *et al.*, 1999; Hoover, Rorke, & Martin, 1991). It should be noted that the enthalpy of gelatinisation (ΔH_{gel}) represents loss of molecular (double-helical) order and loss of crystallinity within the starch granule (Cooke & Gidley, 1992). The thermal properties of legume starches have been found to be influenced by differences in the molecular architecture of crystalline regions (i.e. the chain length distribution of amylopectin and the degree of crystalline perfection) rather than the amylose/amylopectin ratio (Wani *et al.*, 2016).

In the present study, higher values for DSC transition temperatures and ΔH_{gel} of lima bean starch may imply higher crystallinity or more ordered crystalline regions, leading to greater granular stability and more energy required for gelatinisation (Barichello, Yada, Coffin, & Stanley, 1990). As a side note, the experimental conditions (e.g. heating rate and water content) and the starch isolation procedure could have a significant impact on the gelatinisation properties studied by DSC (Wootton & Bamunuarachchi, 1979).

Table 3.3. DSC thermal properties of ILS and ICC from adzuki bean, chickpea, lentil, and lima bean.

Legume type	Starch type	T_o (°C)	T_p (°C)	T_c (°C)	ΔH_{gel} (J.g^{-1})
Adzuki bean	ILS	58.8^{b}	66.7^{b}	75.1^{e}	18.02^{a}
	ICC	60.0^{b}	74.7^{a}	104.6^{b}	18.24^{a}
Chickpea	ILS	59.6^{b}	64.5^{bc}	70.5^{ef}	15.27^{b}
	ICC	59.6^{b}	65.9^{b}	95.7^{c}	15.42^{b}
Lentil	ILS	54.4^{c}	59.7^{d}	68.4^{f}	13.49^{c}
	ICC	53.6^{c}	62.7^{c}	98.3^{c}	13.58^{c}
Lima bean	ILS	68.4^{a}	76.5^{a}	85.2^{d}	18.36^{a}
	ICC	69.7^{a}	76.6^{a}	112.6^{a}	17.57^{a}

T_o, onset temperature; T_p, peak temperature; T_c, conclusion temperature; ΔH_{gel}, enthalpy of gelatinisation (J.g^{-1} of starch on dwb). Values with the same subscripts in a column do not differ significantly ($p > 0.05$).

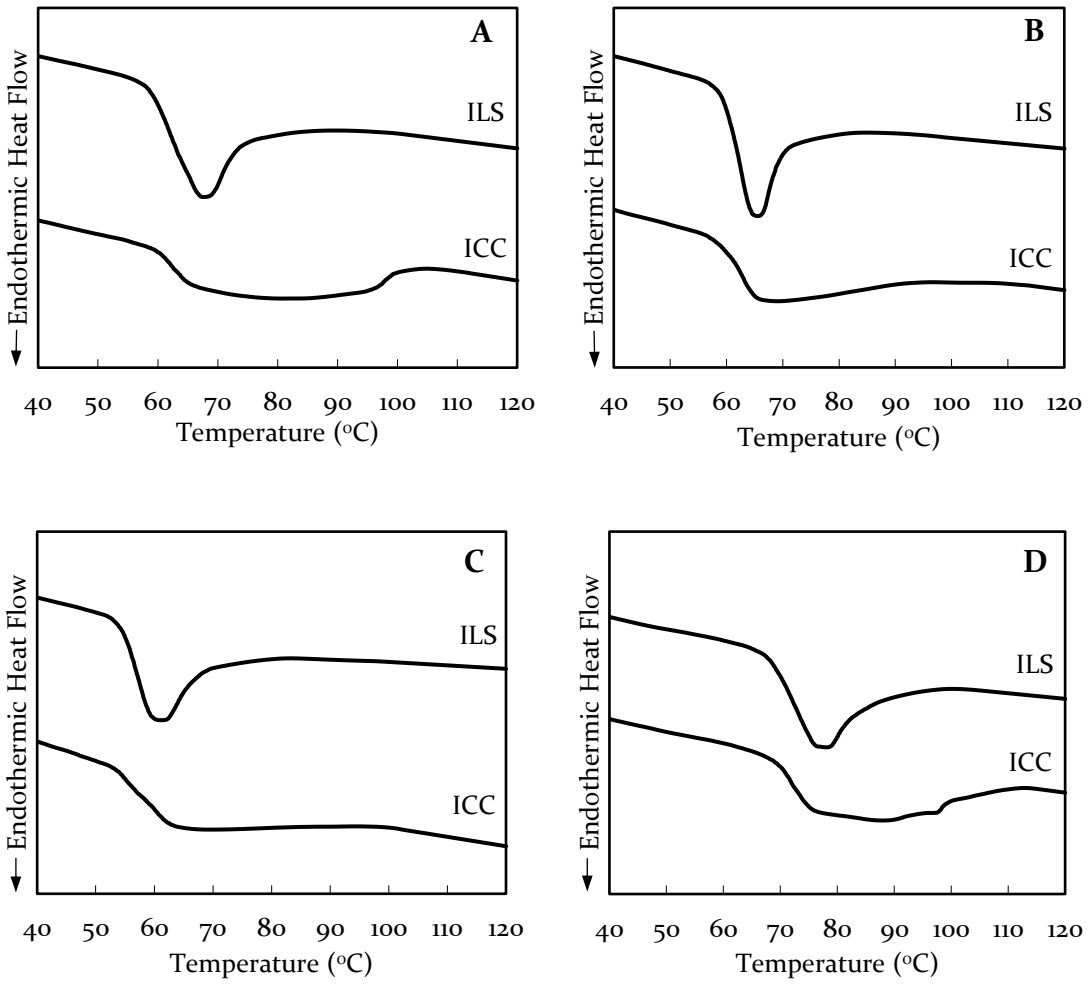

Fig. 3.4. DSC thermograms of ILS and ICC: (A) adzuki bean, (B) chickpea, (C) lentil, and (D) lima bean.

The DSC thermograms of ICC displayed broad endotherms with trailing shoulders from peak temperatures (62.7 – 76.6°C) up to above 95°C. T_o and T_p of ICC were similar or slightly higher while T_c was considerably higher compared to ILS, indicating that starch gelatinisation inside ICC occurred over a wider reaction range. No significant differences in ΔH_{gel} (J.g^{-1} of starch) were found between ILS and ICC, confirming the phase transition characteristics of cells ascribed to those of intracellular starch. This also implies that virtually all starch inside cells may have undergone gelatinisation with nearly complete loss of birefringence. These results are consistent with those of previous studies (Fujimura & Kugimiya, 1993, 1994; Fujimura *et al.*, 1995).

The DSC results suggest limited water supply for starch gelatinisation inside cells leading to a shift in the endotherm of ICC to a wider temperature range. This is in accordance with the mechanism proposed by Donovan (1979) and Biliaderis *et al.* (1980) for starch gelatinisation in water-limited systems. These authors proposed that the phase transition of starch in excess water is governed by cooperative melting of starch crystallites as a result of extensive hydration and swelling of amorphous regions (water uptake), increased motion of polymer chains (heat uptake), and dissociation of semi-crystalline lamella. This phenomenon is characterised by a single endothermic transition over a narrow temperature range. On the other hand, in water-limited environments such that inside cells, the swelling capacity and crystalline disruption of amorphous regions are hampered by insufficient water. Partial melting of crystallites takes place according to the same gelatinisation mechanism described for starch in excess water. This is then followed by direct melting of the remaining crystallites at higher temperatures,

which can give rise to a second higher-temperature endotherm previously observed in the biphasic endothermic transition of starch inside kidney bean ICC (Fujimura & Kugimiya, 1994). It is important to note that, although the DSC results may indicate the melting of crystallites, they do not necessarily reflect whether the gelatinisation of starch inside ICC has completely proceeded from native granules to molecularly dispersed starch (Zhang & Hamaker, 1998).

From these findings, it seems plausible that the cotyledon cell structure is responsible for the delayed starch gelatinisation. The entrapment of starch granules in ICC results in limited water availability inside cells for their hydration and gelatinisation (Edwards *et al.*, 2015; Fujimura & Kugimiya, 1994). The reduced hydration capacity of granules may also be partly attributed to competition for water by non-starch constituents (e.g. proteins and cell wall polysaccharides), thereby delaying breakdown and/or melting of starch ordered structures (Kim & Kim, 2015). These explanations are strongly supported by the previous finding of estimated low content of intracellular water (56 – 61%, w/w) for starch gelatinisation during heating ICC in excess water (85 – 88%, w/w) in sealed DSC pans (Fujimura & Kugimiya, 1995).

3.4.6. Pasting properties

RVA curves and pasting parameters at a starch concentration of 7.4% (w/w) are presented in Fig. 3.5 and Table 3.4 respectively. The pasting profiles of ILS (Fig. 3.5A) showed a high pasting temperature, blurring or absence of peak at maximum viscosity during heating, increasing viscosity during cooling, and a high set-back that were typical for legume starches (Hoover *et al.*, 2010; Huang *et al.*, 2007;

Singh, Sandhu, & Kaur, 2004). However, meaningful comparisons could not be drawn between the RVA pasting measurements in the present study with those in previous reports due to differences in legume cultivar, starch concentration, and method of testing. The pasting properties of ILS differed among the four legumes and could be influenced by amylose content, strong associations between starch chains, and formation of amylose-lipid complexes (Hoover *et al.*, 2010; Wani *et al.*, 2016).

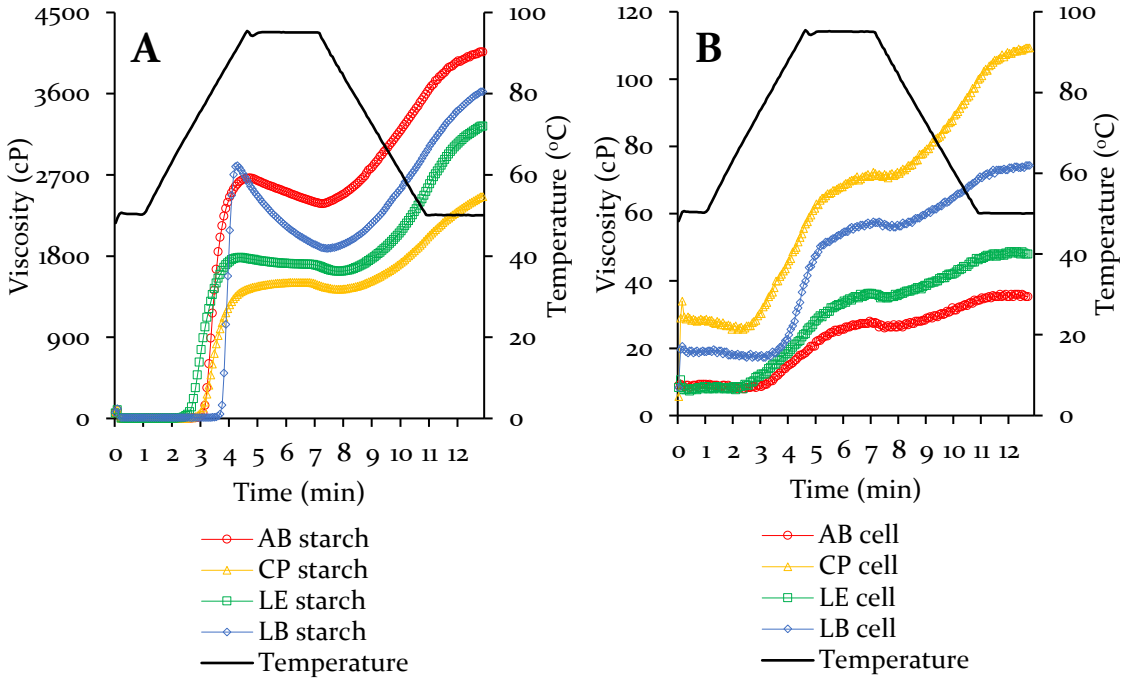

Fig. 3.5. RVA pasting curves of ILS (A) and ICC (B). Abbreviated terms used in the figure are defined as follows: adzuki bean (AB), chickpea (CP), lentil (LE), and lima bean (LB).

Table 3.4. RVA pasting properties of ILS and ICC from adzuki bean, chickpea, lentil, and lima bean.

Legume Type	Starch type	Peak viscosity (cP)	Trough viscosity (cP)	Breakdown viscosity (cP)	Final viscosity (cP)	Setback viscosity (cP)	Pasting temperature (°C)
Adzuki bean	ILS	2665^{b}	2380^{a}	286^{b}	4061^{a}	1682^{ab}	76.0^{e}
	ICC	28^{f}	26^{e}	2^{e}	35^{e}	9^{d}	80.8^{c}
Chickpea	ILS	1508^{d}	1432^{d}	76^{d}	2458^{d}	1026^{c}	73.0^{f}
	ICC	72^{e}	71^{e}	1^{e}	109^{e}	38^{d}	78.2^{d}
Lentil	ILS	1782^{c}	1630^{c}	152^{c}	3239^{c}	1608^{b}	68.7^{g}
	ICC	37^{ef}	35^{e}	2^{e}	48^{e}	13^{d}	74.7^{e}
Lima bean	ILS	2803^{a}	1884^{b}	919^{a}	3621^{b}	1737^{a}	83.4^{b}
	ICC	57^{ef}	56^{e}	1^{e}	74^{e}	18^{d}	87.4^{a}

Values with the same subscripts in a column do not differ significantly ($p > 0.05$).

As shown in Table 3.4, ICC had considerably lower paste viscosities (peak, trough, and final) and significantly higher pasting temperatures than ILS, notwithstanding that all samples contained similar starch concentrations and underwent the same heating and cooling programme under constant shear in RVA. This indicates that starch granules inside ICC are thermally more stable and have higher resistance to swelling and shear-induced rupture. When starch concentration in ICC samples was increased approximately twofold, a marginal increase in paste viscosities was found (data not shown). This is most likely due to the higher concentration of cell materials, rather than due to starch swelling. These findings are corroborated by the results of low swelling power and starch solubility of ICC (Fig. 3.3). It is also interesting to note that RVA pasting temperatures of ILS were higher than DSC gelatinisation onset temperatures (T_o), but relatively similar to conclusion temperatures (T_c) (Table 3.3). This is because the beginning of the breakdown of starch crystalline structure detected by T_o, followed by the complete disintegration of crystalline structure detected by T_c in DSC at which starch polymers leached out

of granules allowing molecular diffusion of starch macromolecules and causing drastic viscosity increase in RVA (Chaiwanichsiri, Ohnishi, Suzuki, Takai, & Miyawaki, 2001).

Heating native starch granules in excess water and under shear in the RVA causes disruption of starch ordered structures and leaching of amylose from granules. The formation of hydrogen bonds between water and amylopectin leads to granule swelling and an increase in hot paste viscosity. Continued heating under shear leads to physical breakdown of swollen granules and a decrease in paste viscosity. Upon cooling, the strong tendency for re-association or retrogradation of leached amylose molecules in the continuous phase of the hot paste causes an increase in cold paste viscosity (Singh *et al.*, 2003). Considering these structural transformations in starch, the lack of viscosity development during pasting of ICC may be due to the presence of cell structural barriers (i.e. the strong cell wall and the protein matrix) hindering granule swelling/disruption as well as retarding amylose leaching from granules and out of cells. This in turn deters the formation of a viscous paste in which remnant granules are interpenetrated within a matrix of leached amylose. During cooling, very limited amylose-amylose interactions in the cell suspension have virtually no viscosity-enhancing effect. On the other hand, the cell structural barriers were completely removed during starch isolation from legumes. As a result, ILS swelled and gelatinised freely during RVA tests, resulting in the observed increase in their paste viscosities.

3.4.7. In vitro *starch digestion*

3.4.7.1. *In vitro* gastro-small intestinal digestion of starch in cooked legume samples

In vitro starch digestion profiles of cooked ILS and ICC under simulated gastric and small intestinal conditions are presented in Fig. 3.6. No starch hydrolysis was detected in the gastric phase due to the absence of starch-degrading enzymes in the SGF. After the SIF containing pancreatic α-amylase was added to the reaction mixture, cooked ILS were rapidly hydrolysed (~75 – 90%) in the first 10 min of the small intestinal phase (I10) and reached a plateau after 30 min. Meanwhile, for all four legumes studied, cooked ICC exhibited a lower rate and extent of starch hydrolysis than cooked ILS. Approximately 23 – 30% starch in cooked ICC was hydrolysed at I10, and the hydrolysis continued slowly until the end point at 120 min of small intestinal digestion (I120). The percentage of starch hydrolysed at I120 was significantly lower for ICC (66.1 – 80.3%) than for ILS (88.0 – 95.0%).

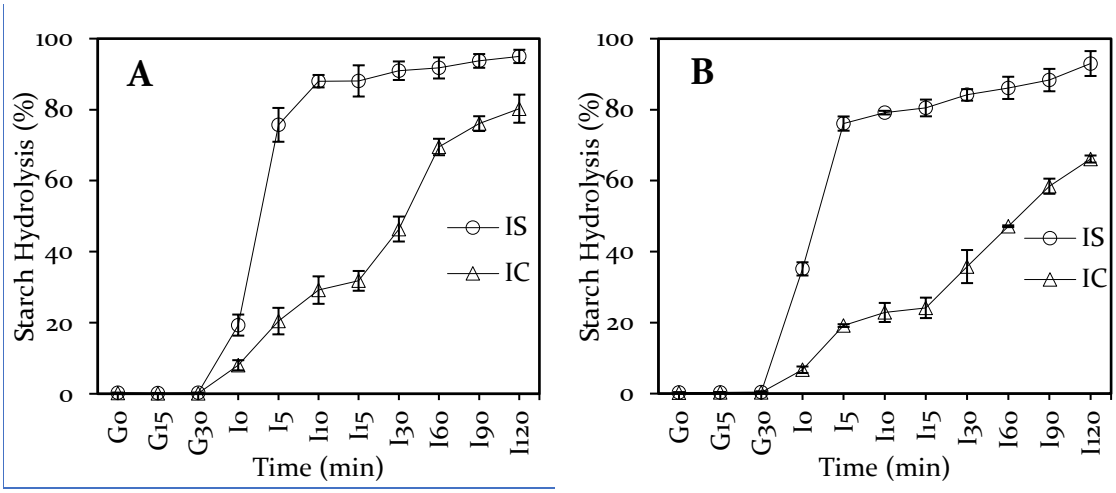

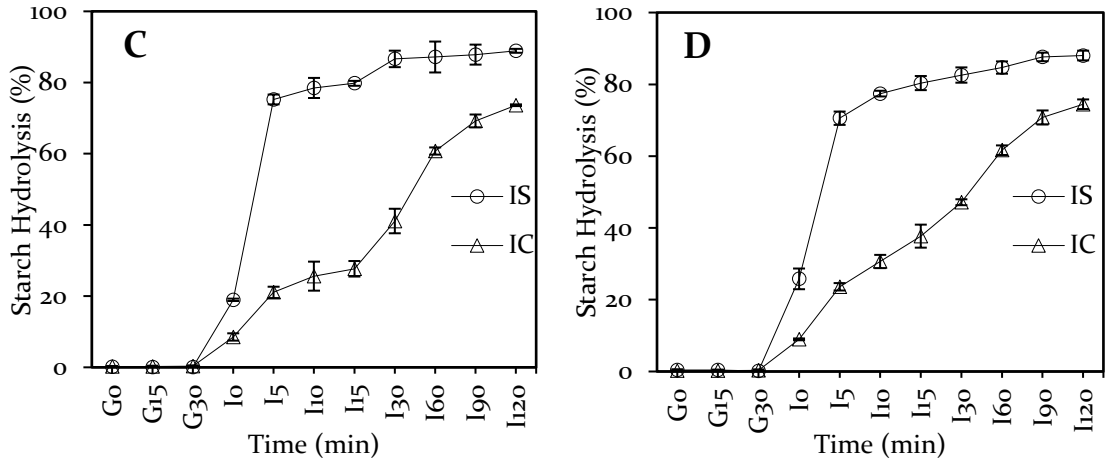

Fig. 3.6. *In vitro* starch hydrolysis curves of cooked ILS and ICC: (A) Adzuki bean, (B) Chickpea, (C) Lentil, and (D) Lima bean during simulated gastric digestion (G, 30 min) followed by small intestinal digestion (I, 2 h). Error bars represent the standard deviation.

These results demonstrate slow starch digestion of ICC, in agreement with Dhital *et al.* (2016) and Rovalino-Córdova *et al.* (2018). The delayed α-amylolysis of ICC could be attributed to a complex interplay of multiple mechanisms. The primary cell wall consisting of a mixture of polysaccharides (i.e. cellulose, hemicellulose, and pectin) is a robust structure. Xyloglucan is believed to interlock cellulose microfibrils, forming a load-bearing framework and conferring structural rigidity to the cell wall (Carpita & Gibeaut, 1993). During cooking, although the cell membrane integrity is lost upon heating above 50-60°C, the cell wall remains mostly intact and becomes the primary barrier protecting the intracellular nutrients from the outside environment (Dhital *et al.*, 2016). The cell wall is also impervious to enzymatic hydrolysis in the human upper GI tract. Due to the resistance towards cooking and subsequent digestion, the cell wall could retard α-amylolysis of ICC by acting as a barrier that limits starch gelatinisation and α-amylase accessibility to starch (Berg *et al.*, 2012; Dhital *et al.*, 2016). Specifically, the ICC samples contained entrapped swollen starch granules that were resistant

to structural disruption and shielded by the cell wall from α-amylase. In contrast, the ILS samples contained swollen granules that were completely disrupted by heat and mechanical agitation during cooking. Thus, the fully gelatinised starch in the ILS samples was more susceptible to α-amylase attack than the partially gelatinised starch in the ICC samples. Furthermore, two other mechanisms have recently been postulated to explain the low amylolytic susceptibility of ICC. Firstly, non-specific binding of α-amylase to cell wall components may inhibit enzyme activity on starch (Bhattarai *et al.*, 2017). Secondly, the densely packed cytoplasmic matrix (starch granule-protein) represents an additional barrier restricting mobility of α-amylase within the cell and reducing starch surface area available for enzyme binding and catalysis (Rovalino-Córdova *et al.*, 2018).

It is also worth mentioning that variation in the extent of starch digestion in ICC existed among the four legumes. Legume cells vary in shape, size, lipid content (see above analysis in section 3.4.2 and 3.4.3) and may vary in starch-protein organisation as well as cell wall composition and structure. We therefore postulate that the morphological and compositional differences between legume ICC may result in the varying extent of *in vitro* starch digestion. As Table 3.1 shows, chickpea ICC have the largest mean diameter and the corresponding smallest surface area for enzyme access to starch. This may explain their lowest percentage of starch hydrolysed (66.1%) and the largest drop in hydrolysis (26.9%) against chickpea ILS (93.0%) at I120. The relationship between the cotyledon cell microstructure and starch digestion remains unclear and warrants further investigation.

3.4.7.2. Microstructural characteristics of cotyledon cells

SEM images of ICC (raw, cooked, G30, I10, and I120) reveal extensive changes in the cellular microstructure throughout cooking and *in vitro* gastro-small intestinal digestion (Fig. 3.7). Raw ICC varied in shape and size. These cells maintained structural integrity but appeared shrunken after isolation, possibly due to water removal during dehydration. It is important to note that dehydrated ICC may be morphologically different to those present in native cotyledon tissues. Cell walls formed thick sheets that wrapped around and encapsulated densely packed native starch granules. Folds and wrinkles were clearly noticeable on cell wall surfaces, particularly on those of lima bean, and these structural artefacts could have formed during the dehydration step.

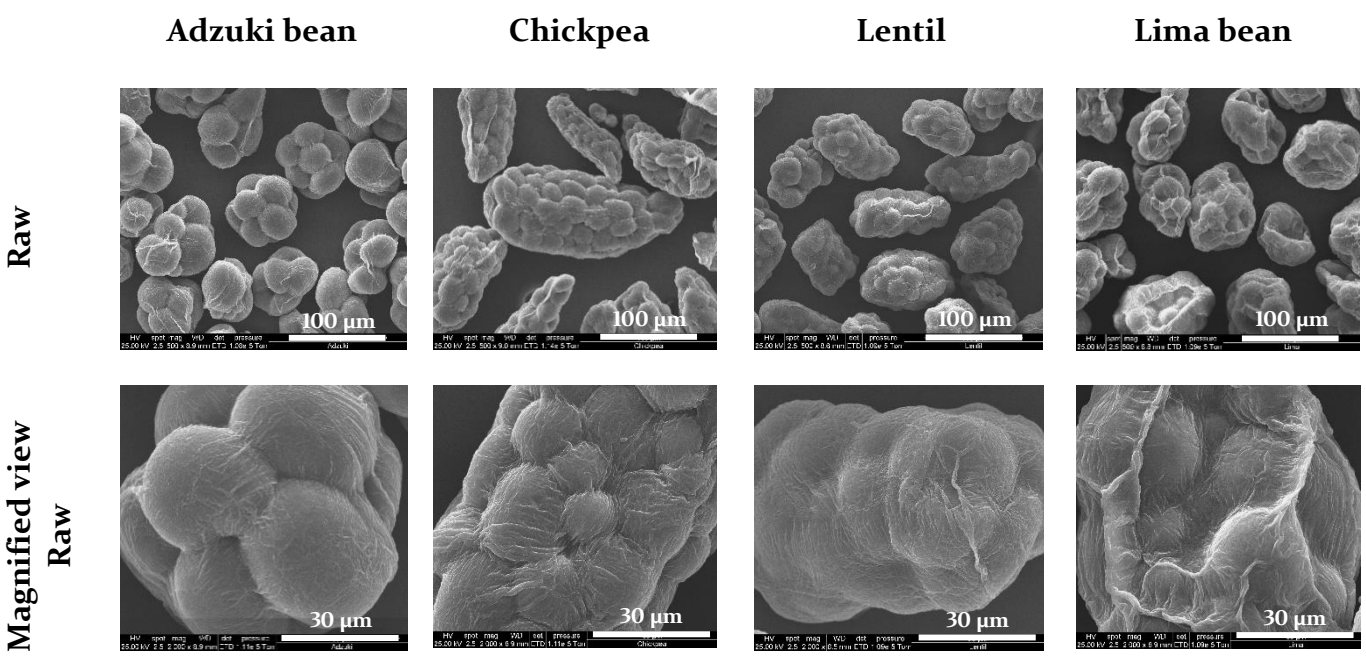

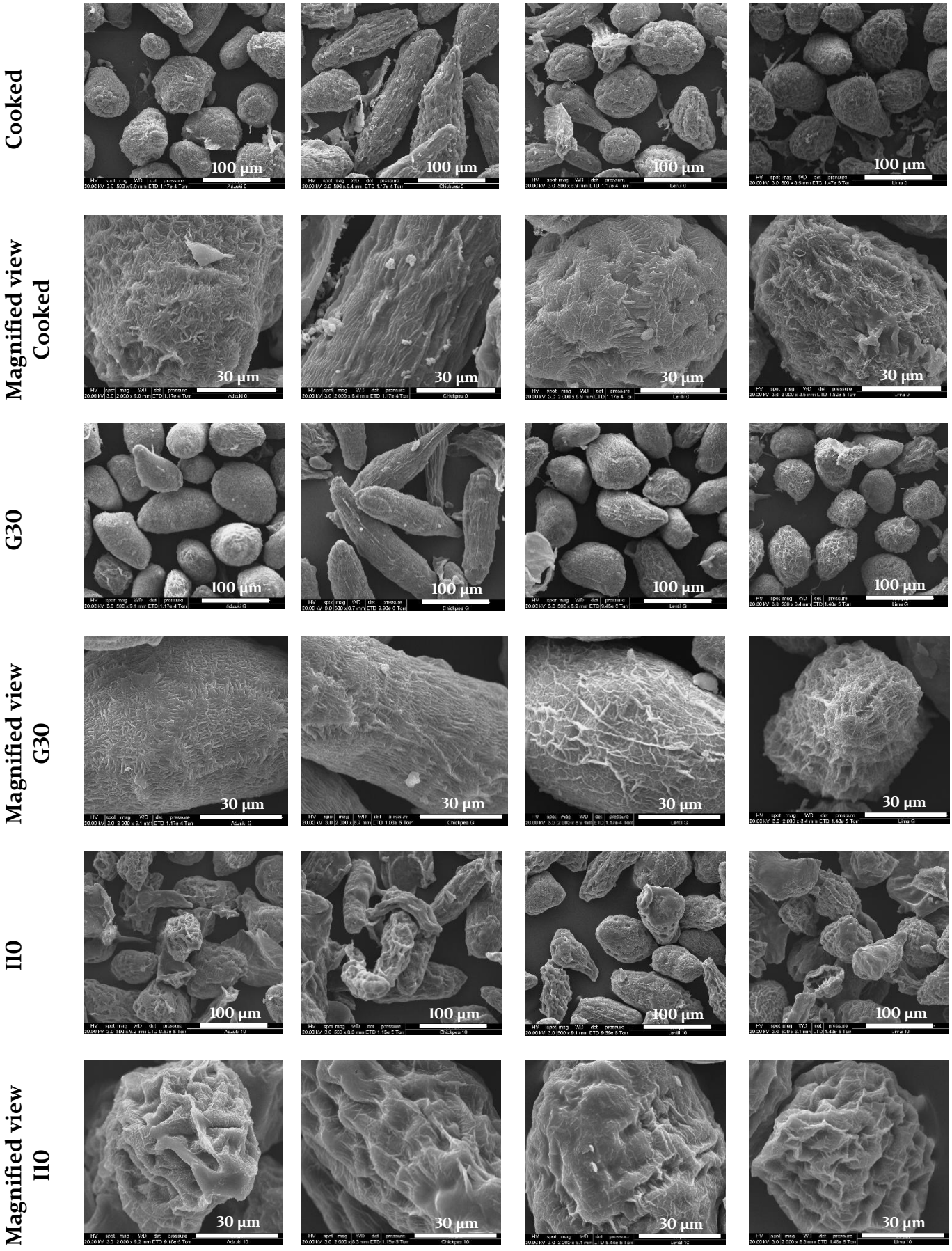
Cooked
Magnified view Cooked
G30
Magnified view G30
I10
Magnified view I10
100 µm
30 µm

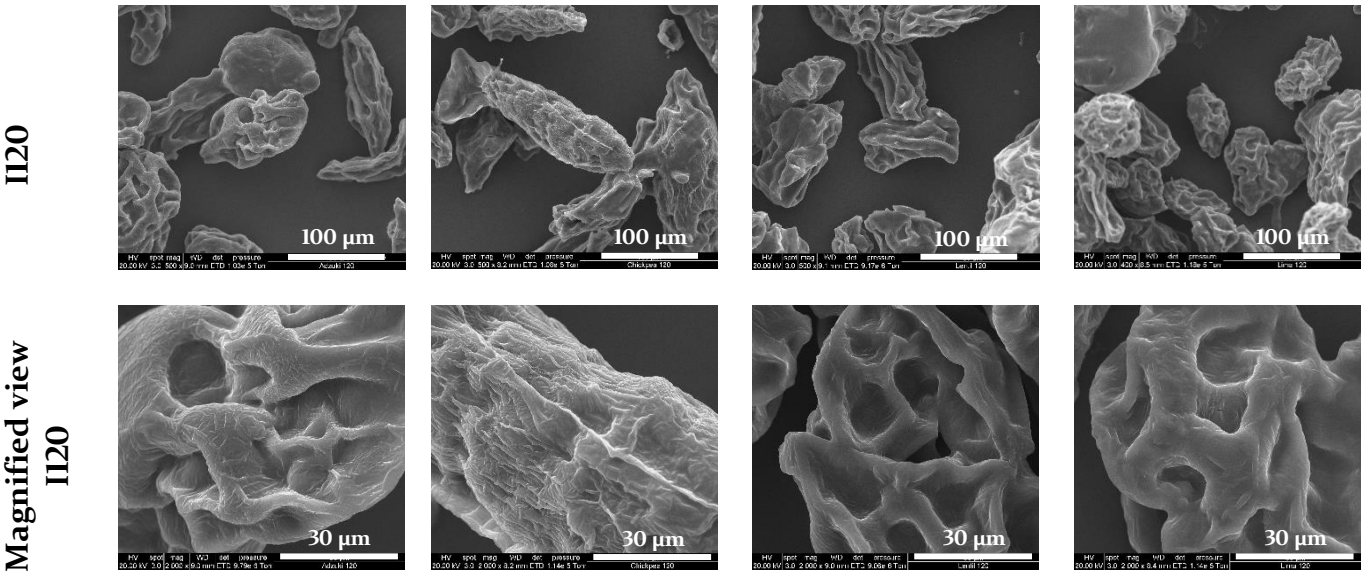

Fig. 3.7. Scanning electron micrographs of representative cells of adzuki bean, chickpea, lentil, and lima bean sampled during cooking followed by *in vitro* gastric and small intestinal digestion.

The presence of heat and water during cooking caused hydration of raw cells and physicochemical changes in intracellular components. Increased water content inside cells along with starch granule swelling could exert pressure that appeared to push against and stretch highly plastic cell walls. Partially gelatinised starch, denatured protein, and leached amylose appeared to have filled the entire cell interior, resulting in swollen and dense structures of cooked cells. Visible strands of dried soluble materials, mainly amylose and non-starch polysaccharides, might have leached out of cells during cooking and adhered onto their surfaces. Similar observations have been noted by other researchers (Berg *et al.*, 2012; Tan, Tan, Tian, Liu, & Shen, 2011). Furthermore, cells remained largely intact but exhibited surface wrinkles and indentations after cooking. In fact, cooking at high temperatures may induce larger-sized pores in the cell wall. Depending on cell wall strength, pore cavities could have also formed due to sublimation of ice crystals during the freeze-drying process of preparing cell samples for SEM examination (Pieniazek & Messina, 2016).

There were no discernible changes in cells after the 30 min gastric digestion. Dramatic changes in the cellular structure occurred during the small intestinal stage. Specifically, digested cells had convoluted sponge-like structures with numerous surface pits and grooves at I10. These surface pits seemed to enlarge as the digestion progressed, resulting in cells with honeycomb-like structures at I120. One possible explanation for the pitted surfaces is that the starch hydrolysis in the small intestine might have left behind empty spaces into which cell walls and undigested materials could have folded during freeze-drying. Similar observations have been reported for digested navy bean cotyledon cells (Berg *et al.*, 2012) and digested potato parenchyma cells (Bordoloi, Singh, & Kaur, 2012b). BF light micrographs of ICC at I120 (Fig. 3.8) confirm the presence of mostly intact cells containing undigested starch residues (stained blue-black by iodine) and internal cavities from which the digested starch had been removed. Fragments of cell walls and cytoplasmic matrix were present in a minor proportion at I120, prompting the suggestion that intact cells could have been broken during isolation or by magnetic stirring in digestion reactors.

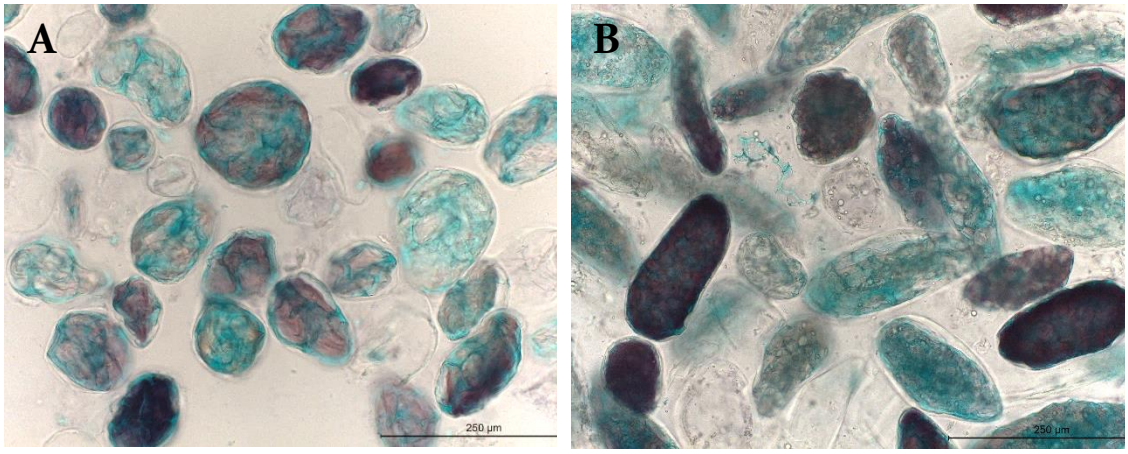

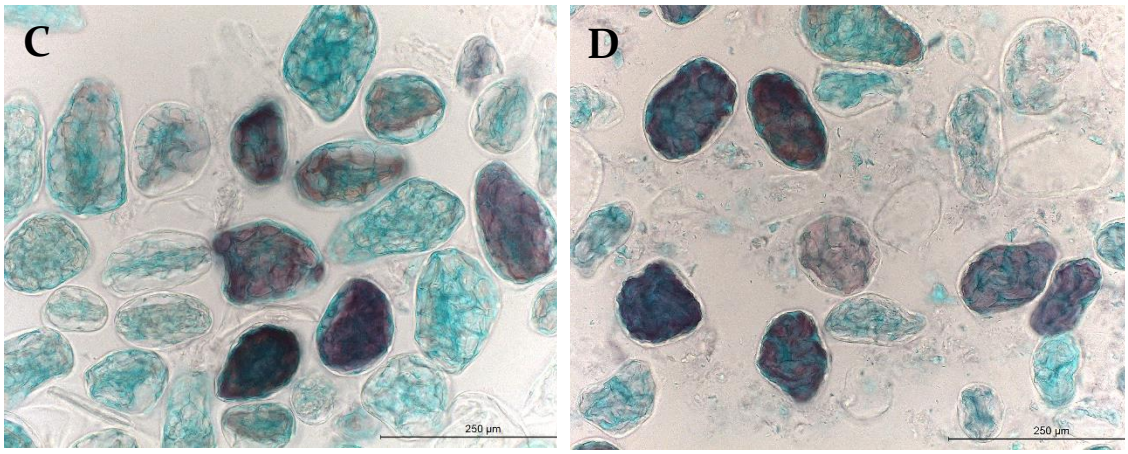

Fig. 3.8. Representative BF light micrographs of ICC after 120 min *in vitro* small intestinal digestion: (A) adzuki bean, (B) chickpea, (C) lentil, and (D) lima bean. Undigested starch residues were stained deep blue-black, and the cytoplasmic matrix was stained green. Scale bar = 250µm.

Magnified view of cells under SEM provides robust evidence for preservation of cell wall integrity. However, despite being chemically and enzymatically stable under simulated cooking and *in vitro* digestion conditions, the plant cell wall may undergo some structural and physicochemical modifications, e.g. hydration and swelling, thermally induced solubilisation of pectins, or acid hydrolysis of glycosidic and ester linkages at very low pH of the stomach. Cell wall permeability may therefore increase with increasing pore size (porosity), facilitating entry of digestive fluids containing enzymes into cells and outflow of intracellular molecules during digestion (Capuano, 2017; Mandalari *et al.*, 2008). Nevertheless, some studies have demonstrated that the chemical composition and structure of the cell wall and its enzyme barrier properties remain largely unaffected during processing and under *in vitro* conditions simulating the human upper GI tract (Carnachan, Bootten, Mishra, Monro, & Sims, 2012; Mandalari *et al.*, 2014). In the present study, since the cell wall remained predominantly intact over the course of digestion and the partially gelatinised starch was apparently of too high molecular mass to escape via cell-wall pores, a majority of starch hydrolysis may

have occurred intracellularly. A possible mechanism underlying this phenomenon is the diffusion of α-amylase through the cell wall and the diffusion of amylolytic products out of the cell; these two events are likely to occur at a slow rate. Grundy *et al.* (2016c) proposed a similar mechanism for the digestion and release of lipids trapped in isolated intact almond cells. Based on these findings, it seems reasonable to conclude that an intact barrier imposed by a single cotyledon cell wall can sufficiently retard the rate and extent of starch digestion *in vitro*.

3.5. Conclusions

Cotyledon cell microstructure consisting of native starch granules trapped within the protein matrix and the intact cell wall exerted modulating effect on *in vitro* digestion of starch in legumes. This unique structure was particularly effective in reducing the rate and extent of α-amylolysis by limiting starch gelatinisation and accessibility of α-amylase to intracellular starch. Based on the evidence presented in this study, we envisage potential incorporation of intact cotyledon cells in starch-based food systems. These cells can be utilised as a novel source of SDS for partial replacement of existing ingredients (e.g. isolated starch and flour) for the development of foods (e.g. baked products) with low glycaemic features. Finally, the cell structural design can serve as a template for the fabrication of BPFs to control GI fate of starch and other nutrients.

CHAPTER FOUR: Effect of parenchyma cell structure on *in vitro* digestion of starch in potatoes

4.1. Abstract

Raw intact parenchyma cells and native starch granules were isolated from Agria and Sunlite potatoes (*Solanum tuberosum* L.) grown in New Zealand. Their morphology, physicochemical properties, and *in vitro* starch digestion were investigated. Parenchyma cells varied in shape, size, and composition. Each cell contained numerous starch granules enveloped by a cell wall. Starch inside Agria cells exhibited higher gelatinisation temperatures than isolated Agria starch. For both cultivars, starch inside cells had higher peak and breakdown paste viscosities than isolated starch. Cooked cells and isolated starch exhibited very similar *in vitro* starch hydrolysis profiles. These results indicate that the entrapment of starch granules in parenchyma cell walls affected starch thermal and pasting properties, but had no effect on starch digestion kinetics *in vitro*. The study provides evidence supporting the use of dehydrated parenchyma cells by the food industry for development of novel potato-based food products with desirable physical properties.

4.2. Introduction

Potatoes (*Solanum tuberosum* L.) are an important source of energy (mainly from carbohydrates) and dietary fiber in the human diet. A potato tuber contains about 20% dry matter by weight and the rest is water. Starch is a principal constituent comprising of approximately 70% of the total dry solids (Singh & Kaur, 2016). The

microstructure of raw and processed potatoes has been extensively studied (Bordoloi, Kaur, & Singh, 2012a; Singh, Kaur, Ezekiel, & Guraya, 2005). Raw potato tissue consists of parenchyma cells bound together by the pectin-rich middle lamella that cements cell walls of adjacent cells together. Each cell contains numerous partially crystalline starch granules with varying degrees of size, shape, composition, and distribution (Troncoso, Zúñiga, Ramírez, Parada, & Germain, 2009).

Hydrothermal processing of potatoes (e.g. boiling) is essential to convert raw indigestible into digestible starch. This is because the gelatinisation of starch during cooking renders it readily accessible to enzymatic attack during GI digestion. The *in vitro* digestibility of potato starch is influenced by various factors, including intrinsic properties of starch (Ek, Wang, Brand-Miller, & Copeland, 2014), food matrix viscosity (Bordoloi *et al.*, 2012b), and cell wall composition and structure (Frost *et al.*, 2016).

Starch granules trapped in parenchyma cells absorb water and undergo gelatinisation upon cooking of potato tissue. Granule swelling pressure during gelatinisation makes cells become round and provides the force to separate them apart. Cooking simultaneously induces loss of turgor pressure and thermal degradation of pectin in the cell wall/middle lamella, leading to weakening of intercellular adhesion. These two concurrent events, independent of each other, facilitate cell separation rather than cell rupture with the latter being identified as the primary mechanism causing cell separation (Jarvis *et al.*, 1992; Ormerod, Ralfs, Jobling, & Gidley, 2002). Since cells of cooked potatoes are easily separated on the

application of mechanical stress during food processing (e.g. mashing) and oral mastication before reaching the GI environment, it becomes relevant to explore the digestive behaviour of micron-scale parenchyma cells.

Intact parenchyma cells isolated from potatoes serve as a model for understanding the effect of cellular structure on gelatinisation and digestion *in vitro* of starch. It has been reported that the cell wall can restrict swelling and delay gelatinisation of entrapped starch granules, but does not limit starch hydrolysis by pancreatic α-amylase (Shin, Baik, & Kim; Kim & Kim, 2015). Furthermore, time-lapse confocal laser scanning microscopy of cooked potato tissue provides evidence indicating that *in vitro* starch hydrolysis may take place intracellularly (Bordoloi *et al.*, 2012b). However, the mechanism of these phenomena remains unclear.

The aim of this study was to gain a better understanding of the effect of parenchyma cell microstructure on starch digestion. Physicochemical properties and *in vitro* starch digestibility of isolated potato cells were investigated. The fate of cells was tracked through each stage of cooking followed by simulated gastric and small intestinal digestion using SEM, allowing visual observations of microstructural changes associated with the digestion process. This could aid in our understanding of the mechanism driving α-amylase digestion of starch trapped inside parenchyma cells.

4.3. Materials and Methods

4.3.1. Materials

Two commercially grown New Zealand potato cultivars, namely Agria and Sunlite, were chosen for the study. One batch of these potatoes was procured from a local grower (Gropack Limited) in Palmerston North. Uniform-sized tubers were selected from each cultivar for isolation of starch and parenchyma cells.

Pepsin (porcine gastric mucosa; ≥ 250 units/mg solid), pancreatin (porcine pancreas; 4x USP), and invertase (from baker's yeast (*S. cerevisiase*), Grade VII, ≥ 300 units/mg solid) were purchased from Sigma – Aldrich Ltd, St Louis, USA. Amyloglucosidase (for Total Dietary Fiber and Starch Assays, 3260U/mL) was purchased from Megazyme International Ireland Ltd., Ireland. All other chemicals and reagents were of analytical grade. Reverse osmosis water was used for all experiments.

4.3.2. Isolation of free starch granules

Isolated potato starch (IPS) was obtained using the method described by Singh *et al.* (2006).

4.3.3. Isolation of raw parenchyma cells

Raw intact parenchyma cells were isolated at room temperature (~ 20°C) following the modified version (Aguilera, Cadoche, López, & Gutierrez, 2001) of the method described by Kugimiya (1990). Fresh potatoes were washed thoroughly in warm water and peeled with all eyes and bruises removed. The peeled potatoes were immediately cut into very thin slices of parenchyma tissue. First, the slices were immersed in a 0.1 M hydrochloric acid solution (pH ~ 1.3) with mild magnetic stirring for 1 h. After rinsing with water to remove the remaining acids, the slices were immersed in a 0.06 M sodium hydroxide solution (pH ~ 12.5) for 1 h with constant magnetic stirring leading to cell separation. The resulting cell suspension was successively passed through 250 and 106 µm standard test sieves by washing with abundant water. Isolated potato parenchyma cells (IPC) were regularly examined under LM for detecting the presence of impurities (e.g. broken cells, cell wall fragments, and free starch granules). The cell extract collected on the 106 µm sieve was dehydrated with a graded ethanol series (25%, 50%, 75%, 95%, 100% for 10 min each) and allowed to air dry in a fume hood overnight at room temperature. The dried powder was bottled and stored at room temperature until further analysis.

4.3.4. Determination of morphological properties

The sample preparation procedure for light microscopy by Bordoloi *et al.* (2012a) was followed. Tissue samples were sectioned from the perimedullary parenchyma of potatoes with a razor blade. Tissue sections were fixed for 2 h at room temperature in a 0.1 M phosphate buffer (pH 7.2) containing 2% (w/v)

formaldehyde and 3% (w/v) glutaraldehyde, washed three times in the same buffer, and post-fixed for 1 h at room temperature in 1% (w/v) osmium tetroxide in the same buffer. Three more buffer washes preceded dehydration in acetone series: 25%, 50%, 75%, 95% for 10 min each, and lastly 100% for 2 h. Dehydrated tissues were embedded in 50% resin (Procure 812) in acetone overnight followed by 100% resin for 8 h, and finally infiltrated with 100% resin and depolymerised at 60°C for 48 h. Ultrathin sections (1 µm thick) were cut from trimmed resin blocks using an ultramicrotome (Leica, Austria). Potato tissue and IPC samples were mounted onto glass microscope slides, stained with 0.05% Toluidine Blue, sealed with cover slips, and viewed under an Axiophot LM (Carl Zeiss, Germany) operating in Brightfield mode using the objective of 20x magnification. Representative micrographs were captured with a Leica DFC320 camera equipped with the Leica software application suite LAS V3.8 (Leica Microsystems).

Particle size distribution was measured with a laser diffraction particle size analyser (Malvern Mastersizer 2000, Malvern Instruments Ltd., UK) according to the method described in section 3.3.4.2.

4.3.5. Determination of chemical composition

Moisture content was determined gravimetrically by drying potato samples in an oven at 105°C to a constant weight. Total starch content was quantified using a total starch assay kit (K-TSTA, Megazyme International Ireland Ltd., Ireland) and following instructions given by the manufacturer. To quantify the starch content of potato tubers, thinly cut potato slices were freeze-dried to a constant weight and ground to fine flour using a coffee grinder (Breville Pty Ltd, Sydney, Australia), and

analysis was immediately performed on this material. Amylose content was determined using an amylose/amylopectin assay kit (K-AMYL, Megazyme International Ireland Ltd., Ireland). Phosphorous content was analysed colorimetrically (AOAC International, method 968.08D). Chemical composition was expressed on a dry weight basis (dwb).

4.3.6. Determination of thermal properties

Thermal properties were analysed using a Differential Scanning Calorimeter (DSC, TA Q100, TA Instruments, Newcastle, DE) according to the method described in section 3.3.7.

4.3.7. Determination of pasting properties

Pasting properties were evaluated using a Rapid Visco Analyser (RVA 4500, Perten Instruments) according to the method described in section 3.3.8.

4.3.8. Static in vitro *starch digestion*

In vitro starch digestion protocol described by Dartois *et al.* (2010) was followed. This employed a two-stage model system simulating the gastric and small intestinal digestion of starch. Aqueous dispersions of samples containing approximately 3% starch (w/w) in 400 mL glass beakers were cooked in a boiling water bath (~95°C) for 20 min. Cooked samples (~ 170 g) were introduced into 500 mL jacketed glass vessels. Temperature was maintained at 37±1°C by circulating water through the vessel jackets. Contents of each reaction vessel were mechanically agitated by a magnetic stirrer bar at 300 rpm throughout digestion. The vessel contents were incubated with pepsin at pH 1.20 for 30 min to simulate

the gastric digestion. After the gastric phase, the pH was adjusted to 6.80, and the vessel contents were incubated with pancreatin, amyloglucosidase, and invertase for 120 min to simulate the small intestinal digestion. Duplicate aliquots (0.5 mL) were withdrawn from each vessel after 1, 15, and 30 min of the gastric digestion, and after 1, 5, 10, 15, 30, 60, 90, and 120 min of the small intestinal digestion. The aliquots were immediately mixed with 2 mL of absolute ethanol in 15 mL centrifuge tubes for stopping enzymatic activities. The resulting mixtures were vortex-mixed and centrifuged at 1800 x *g* for 10 min. Ethanolic supernatants (0.1 mL) were incubated with 0.5 mL amyloglucosidase and invertase in acetate buffer (0.1 mL amyloglucosidase and 3.75 mg invertase per 10 mL acetate buffer) at pH 5.2 and 37°C for 10 min to completely digest soluble dextrins (i.e. produced during enzymatic hydrolysis of starch) to glucose. Quantification of glucose released was carried out using a D-glucose assay kit (GOPOD-FORMAT, K-GLUC, Megazyme International Ireland Ltd., Ireland).

4.3.9. Scanning electron microscopy of parenchyma cells

IPC samples from the two potato cultivars were examined under SEM following the protocol described in section 3.3.9.3.

4.3.10. Statistical analysis

Data were reported as means of triplicate observations ± standard deviations, unless otherwise specified. Tukey's test and analysis of variance (ANOVA) were used to assess the significance of differences ($p \leq 0.05$) between means using Minitab 18 software (Minitab Inc., State College, PA, USA).

4.4. Results and Discussion

4.4.1. Morphological properties

BF light micrographs of stained tissue sections (Figs. 4.1A and B) reveal the microstructural characteristics of raw potato parenchyma tissue. Tissues of both cultivars consisted of irregularly arranged parenchyma cells that were enveloped by polygonal cell walls. Many cells were observed to have lost starch granules due to ultra-thin sectioning of tissue for LM causing cell wall fracture and release of cellular contents. It is evident that the invasive chemical fixation technique used for LM sample preparation greatly altered tissue structures.

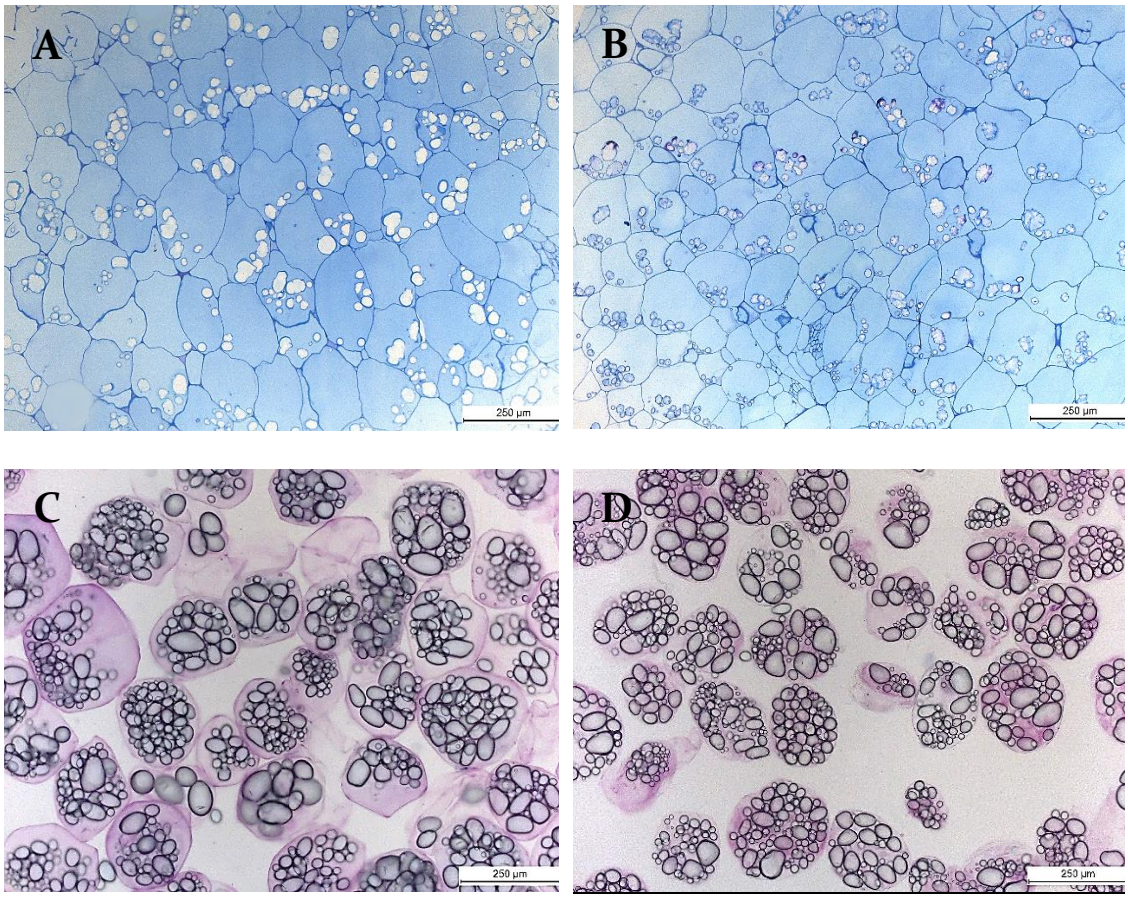

Fig. 4.1. BF light micrographs of parenchyma tissues and IPC from Agria and Sunlite potato cultivars: (A) Agria tissue, (B) Sunlite tissue, (C) Agria IPC, and (D) Sunlite IPC. Scale bar = 250µm.

As shown in Figs. 4.1C and D, raw IPC of both cultivars exhibited good preservation of structural integrity after isolation. Variation in cell shape and size was observed within each cultivar. Agria IPC were round or polygonal, while Sunlite IPC were mostly round or oval. Agria IPC were generally larger in size than their Sunlite counterparts. IPC were filled with numerous native starch granules differing in shape (elliptical or globular) and size. Each cell contained a mixture of large mature granules and many tiny structures or so-called "immature granules". The number and size distribution of granules appeared to vary from cell to cell. These microscopic observations are consistent with previous reports (Bordoloi *et al.*, 2012a; Shin *et al.*, 2015). To characterise the size distribution of cells and starch

granules, particle size was analysed using Mastersizer. As is evident in Fig. 4.2, all samples exhibited monomodal size distributions. Table 4.1 shows that Agria starch had larger mean granule diameter, lower percentages of small and medium granules, and higher percentage of large granules compared to Sunlite starch. Agria cells had larger mean diameter than Sunlite cells.

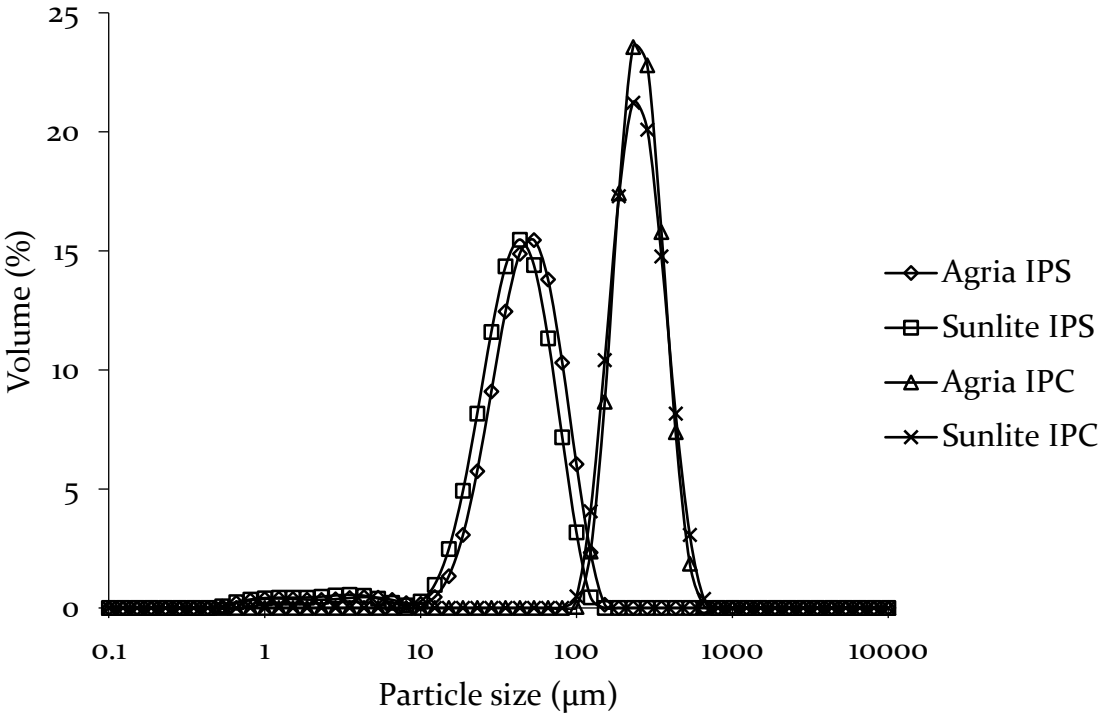

Fig. 4.2. Particle size distribution obtained for IPS and IPC from Agria and Sunlite potato cultivars.

Table 4.1. Properties of IPS and IPC from Agria and Sunlite potato cultivars.

Potato cultivar	Starch type	AM (%)	P (mg/kg)	MPD (D50, µm)	Starch granule size distribution			DSC gelatinisation properties				RVA pasting properties					
					Small 0.1–10 µm (%)	Medium 11–23 µm (%)	Large >23 µm (%)	T_o (°C)	T_p (°C)	T_c (°C)	ΔH_{gel} ($J.g^{-1}$)	PV (cP)	TV (cP)	BV (cP)	FV (cP)	SV (cP)	PT (°C)
Agria	IPS	21.0 ± 0.2[a]	915 ± 7[a]	42.2 ± 0.5[c]	4.8 ± 0.0[b]	10.6 ± 0.4[b]	84.6 ± 0.4[a]	61.0 ± 0.1[b]	63.7 ± 0.1[b]	68.1 ± 0.3[b]	20.4 ± 0.4[bc]	12020 ± 68[a]	2576 ± 64[c]	9444 ± 25[a]	2944 ± 13[c]	368 ± 61[d]	69.3 ± 0.6[ab]
	IPC	21.8 ± 0.5[a]	–	227.0 ± 0.7[a]	–	–	–	61.6 ± 0.0[a]	64.1 ± 0.1[a]	69.6 ± 0.3[a]	19.7 ± 0.3[c]	4209 ± 106[d]	2178 ± 80[d]	2031 ± 56[d]	3524 ± 63[b]	1346 ± 26[b]	68.0 ± 0.5[b]
Sunlite	IPS	21.6 ± 0.9[a]	419 ± 13[b]	36.1 ± 0.3[d]	5.5 ± 0.1[a]	16.5 ± 0.4[a]	78.0 ± 0.4[b]	60.6 ± 0.1[c]	63.6 ± 0.1[bc]	67.9 ± 0.0[b]	21.1 ± 0.1[ab]	5600 ± 19[b]	3015 ± 19[a]	2585 ± 6[b]	3604 ± 38[b]	589 ± 22[c]	70.4 ± 0.0[a]
	IPC	22.5 ± 0.8[a]	–	223.3 ± 0.1[b]	–	–	–	60.6 ± 0.1[c]	63.4 ± 0.2[c]	67.5 ± 0.3[b]	21.3 ± 0.2[a]	5063 ± 63[c]	2777 ± 33[b]	2286 ± 82[c]	4498 ± 65[a]	1721 ± 56[a]	69.0 ± 0.6[ab]

[a, b, c, d] Values with the same subscripts in a column do not differ significantly ($p > 0.05$).

Abbreviations: AM, amylose content; P, phosphorous content; MPD, mean particle diameter; T_o, onset temperature; T_p, peak temperature; T_c, conclusion temperature; ΔH_{gel}, enthalpy of gelatinization ($J.g^{-1}$ of dry starch); PV, peak viscosity; TV, trough viscosity; BV, breakdown viscosity; FV, final viscosity; SV, setback viscosity; PT, pasting temperature.

The staining of IPC with Toluidine Blue enabled direct visualisation of cell wall intactness (see Figs. 4.1C and D). The majority of IPC were observed to be intact with no signs of disruption to the cell wall and cytoplasm. However, we noted the presence of minor impurities, i.e. empty ruptured cells, free starch granules, and multi-cell aggregates. It appears that some cells may have been broken/damaged under constant magnetic stirring during isolation and starch granules were subsequently released from the cell interior. It is worth noting that the acid-alkali treatment of potato tissues resulted in effective separation of intact cells without gelatinising starch and minimal damage to the cellular integrity. However, the acid and alkali could modify some components of the cell walls, altering their structure and porosity. Therefore, IPC may be morphologically different to those present in native tissues.

4.4.2. Chemical composition

Agria and Sunlite potatoes contained 76.3 g moisture & 17.4 g starch and 81.0 g moisture & 13.1 g starch per 100g fresh weight respectively. As shown in Table 4.1, the starch content of Agria and Sunlite IPC was 87.4 ± 0.9 and 82.0% ± 0.3 (w/w, dwb), respectively. The amylose content ranged between 21.0 and 21.6%, and no significant differences were found among all samples ($p > 0.05$). Agria IPS (915 ± 7 mg/kg) contained more than twice as phosphorous as Sunlite IPS (419 ± 13 mg/kg). Variations in amylose and phosphorous content of potato starches have been found among different cultivars (Singh *et al.*, 2006).

4.4.3. Thermal properties

Fig. 4.3 shows representative DSC thermograms obtained for IPS and IPC from the two potato cultivars. All samples displayed single sharp endothermic peaks corresponding to the phase transition of potato starch in excess water known as gelatinisation. Gelatinisation parameters are presented in Table 4.1. The gelatinisation onset temperature (T_o) of IPS was slightly higher for Agria (61.0 ± 0.1°C) than for Sunlite (60.6 ± 0.1°C), whereas none of the values obtained for T_p, T_c, and ΔH_{gel} were significantly different between these two starches ($p > 0.05$). These values were within range of those reported in literature (Singh *et al.*, 2006; Ek *et al.*, 2014; Kim & Kim, 2015). Singh *et al.* (2006) found a negative correlation between phosphorous content of potato starches and DSC gelatinisation temperatures; nevertheless, such correlation was not observed in the present study. There was also no apparent effect of amylose content on starch gelatinisation.

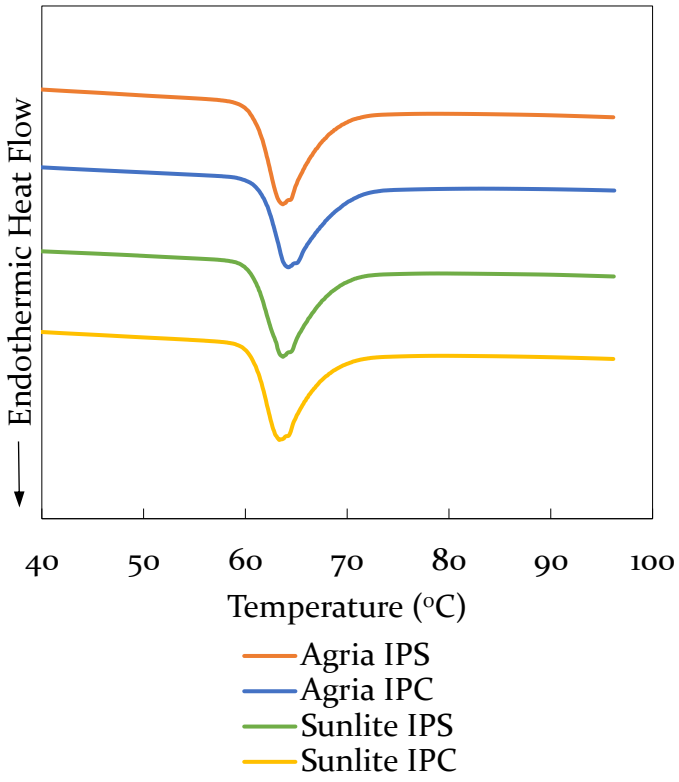

Fig. 4.3. Representative DSC thermograms obtained for IPS and IPC from Agria and Sunlite potato cultivars.

Agria IPC exhibited higher gelatinisation temperatures (T_o, T_p, and T_c) than Agria IPS, whereas this trend was not observed in the Sunlite cultivar. A possible explanation for this is limited water supply for starch hydration inside Agria cells, causing restricted breakdown of starch ordered structures and delay in gelatinisation. The lack of intracellular water may result from competition for water with starch by non-starch constituents such as proteins and cell wall polysaccharides (Shin *et al.*, 2015; Kim & Kim, 2015). It must also be noted that although statistically significant difference was found in gelatinisation temperatures between IPC and IPS in Agria cultivar ($p < 0.05$), the difference was only minor (0.4 – 1.5°C). Moreover, there were no significant differences in gelatinisation enthalpy (ΔH_{gel}) between IPS and IPC within each cultivar ($p > 0.05$).

This suggests that the phase transition characteristics of IPC were ascribed to those of intracellular starch. This also further implies that all starch inside cells may have fully gelatinised after heating in the DSC.

These findings suggest that the entrapment of starch in IPC appeared to have little or no effect on the DSC gelatinisation properties. This suggestion is supported by previous evidence of sufficient water within a potato cell (~ 4 g water per g starch or ~ 80%, w/w) to allow for complete starch gelatinisation, resulting in a single endothermic peak over a narrow temperature range in DSC (Jarvis *et al.*, 1992). In contrast, Fujimura and Kugimiya (1995) reported a low content of intracellular water (~ 56–61%, w/w) for starch gelatinisation in legume ICC, resulting in a broad endothermic peak with a trailing shoulder in DSC. The formation of a second higher-temperature peak was also observed in some cases. The evidence presented here supports the role of water availability in determining the mechanism of starch gelatinisation studied by DSC reported previously (Donovan, 1979). It appears that microstructural differences between potato and legume cells may account for differences in their starch gelatinisation behaviours. Specifically, legume ICC contain starch granules that are embedded in a compact protein matrix (Berg *et al.*, 2012). Unlike ICC, very little protein is present in potato cells (Shin *et al.*, 2015). This may result in quantities of water and free space inside IPC large enough so that gelatinisation proceeds in a similar manner to that observed in IPS.

4.4.4. Pasting properties

Fig. 4.4 shows RVA pasting curves of starch (7.4%, w/w). Pasting profiles of IPS resembled those of native potato starches (Singh *et al.*, 2006). As shown in Table

4.1, Agria IPS had a considerably higher peak paste viscosity than Sunlite IPS ($p \leq 0.05$). It has been reported that the physicochemical characteristics of potato starches, including phosphorous content and granule size distribution, affect their pasting properties (Singh *et al.*, 2006). The higher peak viscosity of Agria IPS may result from its higher phosphorous content (see Table 4.1). This is because the repulsion between negatively charged phosphate groups on adjacent chains of amylopectin weakens the strong bonding within crystalline domains in starch granules, and thus increases granule hydration and swelling (Singh & Singh, 2001). It is also possible that the presence of a relatively higher percentage of large granules in Agria IPS (see Table 4.1) contributes towards its higher peak viscosity.

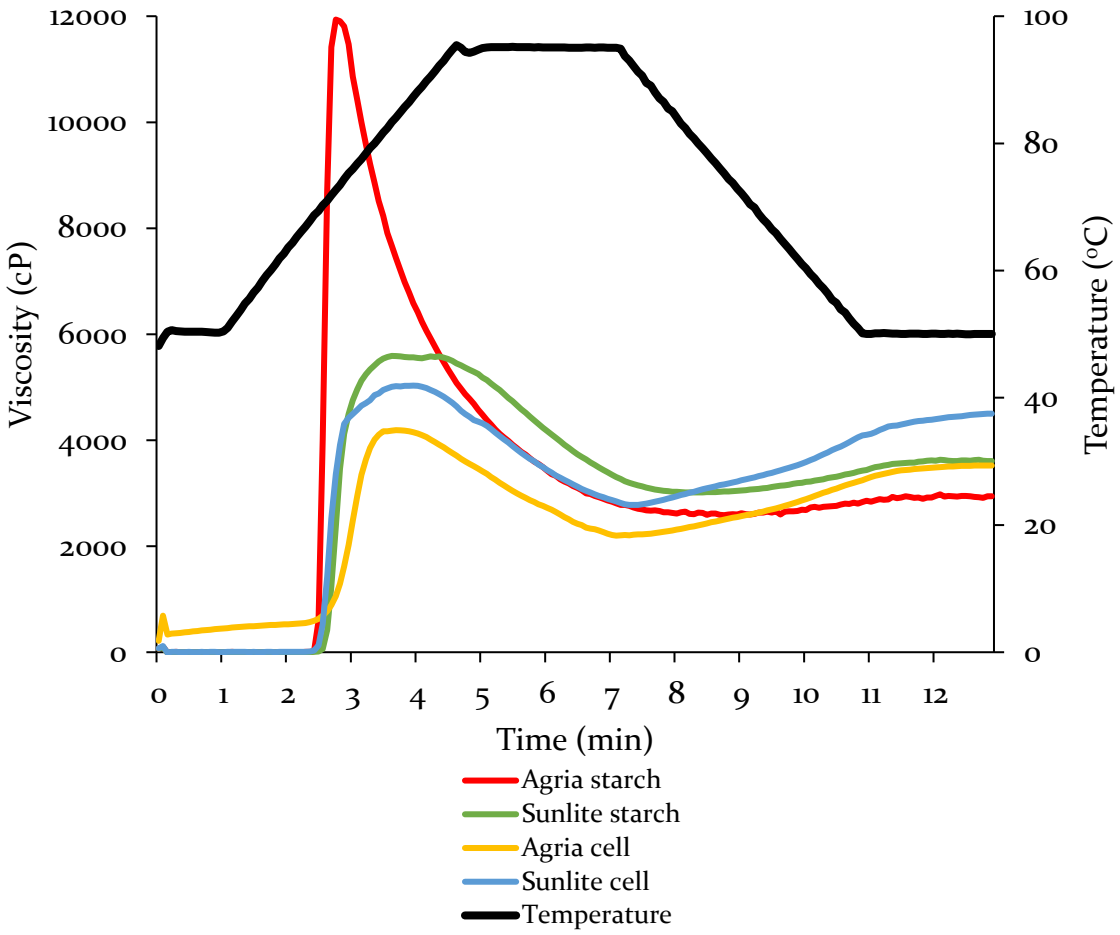

Fig. 4.4. RVA pasting curves of IPS and IPC from Agria and Sunlite potato cultivars.

Comparison between the pasting profiles of IPS and IPC allowed us to assess whether the entrapment of starch granules in the parenchyma cell affects pasting behaviours. Within each cultivar, pasting temperatures ranged between 68.0 and 70.4°C and did not differ significantly between IPS and IPC ($p > 0.05$). Peak, trough, and breakdown viscosities for IPS were higher than for IPC ($p \leq 0.05$). This observed difference in paste viscosities may be attributed to the parenchyma cell structure. Specifically, the cell wall restricts starch granule swelling and shear-induced rupture of the swollen granules during heating as well as prevents leaching of amylose from the granules and out of the cells. It is also noteworthy that the effect of the parenchyma cell wall on hindering peak viscosity development was more pronounced in Agria than in Sunlite, suggesting that the cell wall is capable of suppressing swelling of intracellular starches differing in swelling capacities.

Upon cooling, IPC displayed higher final and setback paste viscosities than IPS. A possible explanation for this is that IPC could be broken under constant shear in the RVA and gelatinised starch was released from the cell interior. This may lead to subsequent increases in relative concentration of cellular materials (i.e. starch molecules and cell wall fragments) and reassociation of leached amylose within starch paste, resulting in a marked increase in cold paste viscosity (Shin *et al.*, 2015).

4.4.5. Static in vitro *starch digestion*

Cooked samples of IPS and IPC showed a similar *in vitro* starch hydrolysis pattern (Fig 4.5). There was virtually no starch hydrolysed during 30 min of gastric digestion due to the absence of starch-degrading enzymes. During small intestinal

digestion in the presence of pancreatic α-amylase, hydrolysis of cooked starch paste was rapid within the first 10 min (~90%) before reaching a plateau after 30 min, and nearly all the starch had been hydrolysed after 120 min of digestion.

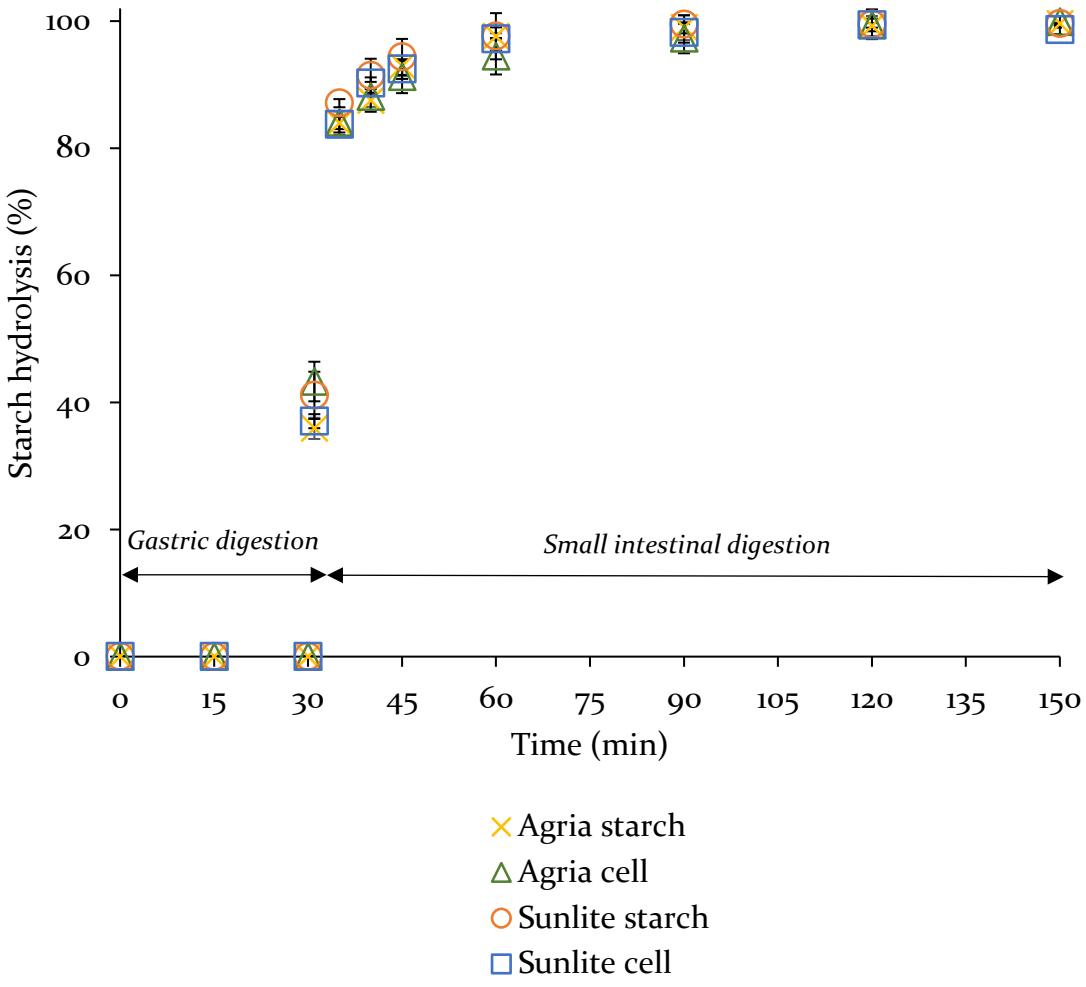

Fig. 4.5. *In vitro* starch hydrolysis curves of IPS and IPC from Agria and Sunlite potato cultivars during simulated gastric digestion (30 min) followed by small intestinal digestion (2 h).

There were no apparent differences in IPS digestion between the two cultivars despite the observed differences in intrinsic starch characteristics (e.g. phosphorous content). Within each cultivar, there were also no significant differences in the rate and extent of amylolysis between IPS and IPC, indicating that the parenchyma cell wall has no inhibitory effect on α-amylase digestion of

entrapped starch and confirming previous results (Shin *et al.*, 2015). It is likely that starch swelling during gelatinisation exerts strong pressure on the cell wall, which can cause cell rupture followed by discharge of intracellular starch. In addition, cooking can cause partial disintegration of the cell wall (e.g. loosening of cellulose microfibrils and pectin solubilisation), leading to increased wall permeability (Bordoloi *et al.*, 2012; Van Marle *et al.*, 1997). Therefore, the rapid starch hydrolysis of IPC may be due to cell wall breakdown and extensive leakage of soluble starch through the cell wall during cooking (Shomer, 1995), making the starch substrate more accessible for amylolysis.

To provide further evidence for these findings, microstructural changes in the parenchyma cell associated with cooking and *in vitro* digestion were visualised under SEM. As clearly seen in Fig 4.6, potato cells of both cultivars exhibited similar morphological characteristics. Each raw cell consisted of visible starch granules loosely trapped in a thin sheet-like cell wall. It is apparent that the dehydration process removed aqueous cellular contents leaving transparent cell structures. This is consistent with previous SEM observations of the morphology of air-dried isolated potato cells (Aguilera *et al.*, 2001). Starch granules inside raw cells had a smooth surface, whereas cell walls had an irregular wrinkled surface possibly due to their shrinkage and folding during dehydration.

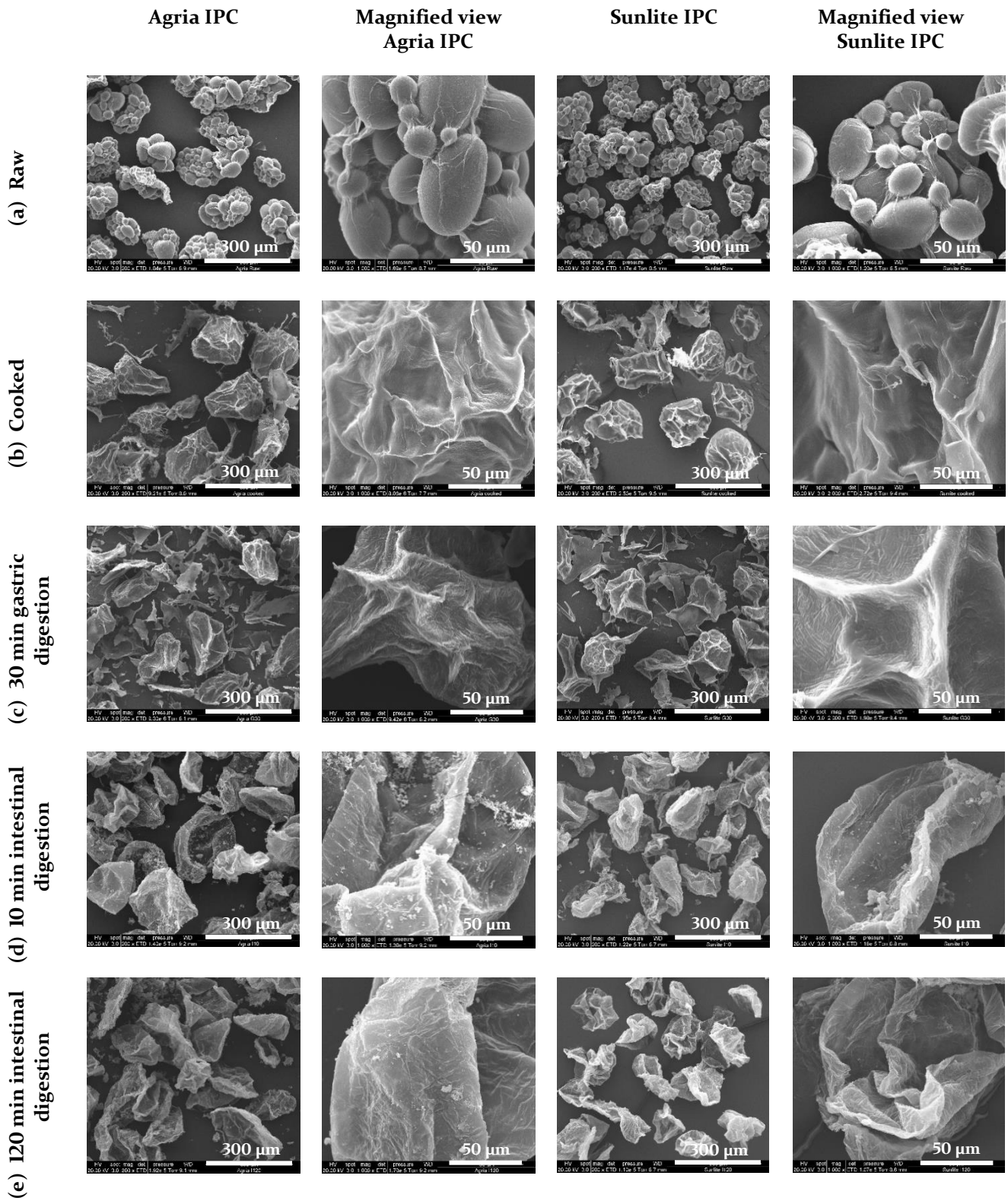

Fig. 4.6. Representative scanning electron micrographs of parenchyma cells from Agria and Sunlite potato cultivars sampled at different time points: (a) raw, (b) after cooking, (c) 30 min gastric digestion, (d) 10 min and (e) 120 min small intestinal digestion. Images were acquired with accelerating voltage of 20 kV.

After cooking, cells were no longer transparent and appeared very dense. This is because cooking caused starch granules to swell and gelatinise, resulting in the formation of a compact gelled mass filling the entire cell interior. The large-concentration high-density of the starchy mass could exert strong pressure against cell walls and inflate cells (Shomer, 1995). These results support previous findings that the high swelling capacity of potato starch granules results in dense packing of starch in cooked cells that is analogous to concentrated heated potato starch dispersions (Sjoo, Eliasson, & Autio, 2009). Closer examination of cell surface revealed visible strands of dried material (e.g. amylose) that were adherent to highly wrinkled, convoluted cell walls. No evidence for cell wall breakage caused by cooking was detected. The integrity of cell walls and the presence of cell surface-attached material may be suggestive of leakage of soluble starch, confirming previous findings that the potato cell remains mostly intact during cooking and starch molecules smaller than cell-wall pores diffuse out through the porous lattice of the cell wall (Shomer, 1995).

Cells remained dense and intact after 30 min of gastric digestion (G30). Dried fragments of cellular materials were detected outside cells. These could be leached soluble starch and/or remnants of ruptured cells, suggesting that some intact cells could have been broken under magnetic stirring in the digestion reactor and their contents were released. During simulated small intestinal digestion, the majority of cells exhibited no visual evidence of cellular disruption. This is in line with the microscopic observation by Bordoloi *et al.* (2012b) that the potato cell walls remain mostly intact throughout simulated gastro-small intestinal digestion. As the digestion advanced, cells became progressively emptier after 10 min (I10) and

appeared completely empty after 120 min (I120). Furthermore, empty cells after I120 collapsed into convoluted sheet-like structures. This can be explained by the formation of empty intracellular space from which hydrolysed starch and water had been removed, causing extensive folding of cell walls during freeze-drying (Bordoloi *et al.*, 2012b). These SEM findings imply that the enzymatic starch hydrolysis of cooked IPC is facilitated most likely by diffusion of α-amylase through the intact cell wall, rather than by cell wall disruption.

4.5. Conclusions

The physical entrapment of native starch granules in parenchyma cells of potatoes resulted in slightly higher DSC gelatinisation temperatures in Agria cultivar and significantly lower RVA peak and breakdown paste viscosities in both cultivars, but did not slow down starch digestion *in vitro*. It was suggested that the parenchyma cell wall could restrict granule swelling. Nevertheless, thermally induced disintegration of the thin cell wall during cooking could facilitate easy access of α-amylase to starch. The results obtained from this study demonstrate the encapsulation of starch granules in micron-capsules, such that in plant cells, as a potential strategy for manipulating the physicochemical properties of entrapped starch. A compact, low-porosity encapsulation matrix is necessary to prevent α-amylase diffusion for effective protection of starch against amylolytic degradation, which can lead to slow starch digestion and absorption.

CHAPTER FIVE: The role of protein matrix in modulating *in vitro* digestion of starch inside cotyledon cells of navy beans

5.1. Abstract

Starch granules are encapsulated within the inner protein matrix and the outer cell wall of the cotyledon cell in legumes. Thus, we propose that the cell wall and protein matrix may have a potentially synergistic barrier effect on enzymatic digestion of starch. Despite detailed knowledge regarding the role of the former in controlling starch digestion, the latter has received little attention. In this study, isolated cotyledon cells of navy beans were used for experiments to assess the effect of the protein matrix on *in vitro* starch digestion. Cells were treated with pepsin for 1, 4, or 24 h in order to hydrolyse the protein matrix to different degrees prior to *in vitro* digestion. Results showed that longer pepsin treatment time was associated with lower protein content of cells and higher initial rate and extent of starch hydrolysis. It was therefore suggested that the protein matrix provides a secondary barrier in addition to the cell wall restricting accessibility of α-amylase to starch. The study also demonstrated clearly that efficient protein hydrolysis prior to or during simulated GI digestion is necessary for improving starch digestibility.

5.2. Introduction

Epidemiologic evidence supports the association between consumption of legumes and decreased risk of incident type 2 diabetes and improved glycaemic control in diabetic individuals (Becerra-Tomás *et al.*, 2018; Villegas *et al.*, 2008; Sievenpiper

et al., 2009). In fact, starchy legumes (e.g. beans, peas, chickpeas, and lentils) contain a substantial proportion of SDS that can slow down the rate of glucose release upon consumption and lower the postprandial glycaemic response (Jenkins *et al.*, 1982; Tovar, 1996). An earlier study (Berg *et al.*, 2012) suggested that the physical entrapment of multiple starch granules in cotyledon cells limits *in vitro* starch hydrolysis in cooked whole navy beans. This is because the cell wall remains mostly intact throughout cooking and digestion, and thus acts as a physical barrier restricting α-amylase accessibility to intracellular starch. Recent studies have used intact micron-scale cotyledon cells isolated from legumes as a food model for mechanistic understanding of the role of cellular structure in limiting *in vitro* starch digestion (Xiong *et al.*, 2018; Dhital *et al.*, 2016). Bhattarai *et al.* (2017) proposed three mechanisms to explain this phenomenon in legume cells. First, cell wall intactness prevents starch-amylase interactions during simulated digestion. Second, swelling and gelatinisation of entrapped starch granules is restricted during cooking, resulting in retention of enzyme-resistant crystalline starch structure. Third, non-catalytic binding of α-amylase to cell wall components inhibits enzyme activity on starch. Furthermore, new evidence has emerged suggesting that cell-wall porosity controls the extent of diffusion of digestive enzymes through intact cell walls, which can affect the hydrolysis of starch inside cells (Li, Gidley, & Dhital, 2019). Various combinations of food processing parameters (i.e. temperature, pressure, time) can induce changes in cell wall porosity/permeability and produce cotyledon cell microstructures with different *in vitro* starch digestion profiles (Pallares *et al.*, 2018a, 2018b).

The aforementioned studies have largely emphasised the role of cell wall encapsulation in limiting starch digestion. Despite the fact that protein co-exists and naturally encapsulates starch inside cotyledon cells (Berg *et al.*, 2012), the relative contribution of the protein matrix in modulating starch digestion has received inadequate consideration. Rovalino-Córdova *et al.* (2018) proposed that the protein matrix represents a structural barrier hindering mobility of α-amylase within the cell and reducing starch surface area available for enzyme binding and catalysis. In the present study, raw isolated cotyledon cells from navy beans were pre-treated with pepsin at various incubation times to generate different protein matrix microstructures while retaining intact cell walls. Digestive behaviour of entrapped starch was studied using a static *in vitro* digestion model. It was postulated that enzymatic modification of the protein matrix can be used to manipulate the kinetics of starch hydrolysis.

5.3. Materials and Methods

5.3.1. Materials

One batch of whole dried navy beans (*Phaseolus vulgaris*) was procured from a local store in Palmerston North, New Zealand. Pepsin (porcine gastric mucosa, ≥ 250 units/mg protein), pancreatin (porcine pancreas, 4x USP), invertase (from baker's yeast (*S. cerevisiae*), Grade VII, ≥ 300 units/mg solid), α-amylase (porcine pancreas, type VI-B), soluble potato starch (S-2630), and maltose (S-5885) were purchased from Sigma – Aldrich Ltd, St Louis, USA. Amyloglucosidase (for Total Dietary Fiber and Starch Assays, 3260U/mL) was purchased from Megazyme

International Ireland Ltd., Ireland. All other chemicals and reagents were of analytical grade. Reverse osmosis (RO) water was used for all experiments.

5.3.2. Preparation of navy bean materials

5.3.2.1. Isolation of raw cotyledon cells

Raw intact cotyledon cells were isolated without gelatinising starch by successive treatments of navy beans with acid and then alkali according to the method described in section 3.3.2, the only difference being that the cell extract collected on the 53 µm sieve was dehydrated in three changes of absolute ethanol for 5 min each. The cells were then spread onto clean glass plates and air-dried in a fume hood overnight at room temperature. The dried powder was bottled and stored at room temperature until further analysis.

5.3.2.2. Isolation of free starch granules

Free starch granules were isolated from navy beans according to the method described by Berg *et al.* (2012).

5.3.2.3. Modification of intracellular protein matrix

Modification of intracellular protein matrix was performed by treating cotyledon cells with pepsin. The cell extracts (~20 g) were collected on the 53 µm sieve (as described in section 3.2.2) and were mixed with pepsin solution (3.2 g pepsin in 400 mL of 0.034 M sodium chloride buffer, pH 2.0) in 1L Schott bottles. These bottles were incubated in a shaking incubator at 37°C and 100 rpm for 1, 4, or 24 h. The pH of the cell slurries was occasionally checked and, if necessary, adjusted

to 2.0 with 1.0 M HCl. After the pepsin digestion, the cell slurries were transferred to 50 mL centrifuge tubes and centrifuged at 1500 *x g* for 10 min to recover the solids. This solid material was reslurried and washed with water before being recovered by centrifugation at 1500 *x g* for 10 min. The washing and centrifugation procedure was repeated five times to remove the acids and protein digests. The pepsin-treated cells were dehydrated in three changes of absolute ethanol for 5 min each. The cells were then spread onto clean glass plates and air-dried in a fume hood overnight at room temperature. The dried powder was bottled and stored at room temperature until further analysis. Cells treated with pepsin for 1, 4, and 24 h were denoted as INC-1h, INC-4h, and INC-24h respectively. A control sample (INC-Native) was prepared by treating the cell extract only with 0.034 M sodium chloride buffer solution in the shaking incubator at 100 rpm, pH 2.0 and 37^{o}C for 24 h.

5.3.3. Microscopy analysis

For LM, samples of cotyledon cells were mounted onto glass microscope slides, suspended in water, sealed with cover slips, and then viewed under an Axiophot light microscope (Carl Zeiss, Germany) operating in Brightfield mode using the objective of 20x magnification. Representative light micrographs of cell samples were captured using a Leica DFC320 camera equipped with the Leica software application suite LAS V3.8 (Leica Microsystems).

For SEM, dried powder samples of cotyledon cells were directly mounted on double-sided adhesive tapes on aluminium stubs, sputter coated with gold (SCD 050, Balzers, Liechtenstein), and viewed under a scanning electron microscope

(FEI Quanta 200 FEI Electron Optics, Eindhoven, the Netherlands). Representative electron micrographs of cell samples were captured with accelerating voltage of 25 kV and using the xT microscope software version 3.0.7 (FEI Quanta, Eindhoven, the Netherlands).

5.3.4. Determination of physicochemical properties

Moisture content was determined gravimetrically by drying samples in an oven at 105°C to a constant weight. Crude protein was analysed using the Dumas method (AOAC 968.06) and a conversion factor of 6.25 from nitrogen to protein.

Total starch content was quantified using a total starch assay kit (K-TSTA). Total amylose content in starch was analysed using an amylose/amylopectin assay kit (K-AMYL). Both the starch kits were obtained from Megazyme International Ireland Ltd., Ireland, and the analysis was carried out according to the instructions given by the manufacturer. Chemical composition was expressed on dwb.

Swelling power and solubility of starches were determined after heating aqueous dispersions of starch (2%, w/w) at 90°C for 30 min according to the method of Leach, McCowen, & Schoch (1959).

5.3.5. Determination of α-amylase activity

Alpha-amylase activities of pancreatin and α-amylase (from porcine pancreas, type VI-B) were measured using the α-amylase assay procedure described by Bernfeld (1955). Enzyme solutions were prepared by dissolving enzyme powders in distilled water at concentrations of approximately 1 unit/mL of α-amylase. One-millilitre aliquots of enzyme solution were added to 1 mL aliquots of soluble potato starch

(1%, w/v) in 20 mM sodium phosphate buffer pH 6.9 in 15 mL Kimax screw-capped glass tubes. The capped tubes were mixed by swirling and incubated in a water bath at 20°C. After 3 min, the reaction was stopped by adding 1 mL of colour reagent solution (prepared by adding 8 mL of 5.3 M sodium potassium tartrate solution in 2 M NaOH and 20 mL of 96 mM 3.5-dinitrosalicylic acid in 12 mL of distilled water) to each tube. The tubes were capped, mixed by swirling, and immediately placed in a boiling water bath for 15 min. The tubes were then cooled on ice to room temperature, and 9 mL of distilled water was added to each tube. The tube contents were mixed by inversion, and the absorbance of the resulting coloured solutions was measured spectrophotometrically at 540 nm. Blank assays were prepared by addition of 1 mL of enzyme solution only after adding the colour reagent and placing the tubes in the boiling water bath. A standard calibration curve was prepared from a series of aqueous maltose solutions ($5x10^{-3}$ – 0.2%, w/v) and run parallel with the samples. The α-amylase activity was calculated and expressed in units of α-amylase per milligram of enzyme powder. One unit (U) of amylase was defined as the amount of enzyme that liberates 1.0 mg of maltose from starch in 3 min at pH 6.9 and 37°C.

5.3.6. In vitro *starch digestion*

5.3.6.1. Static *in vitro* starch digestion procedure

The static *in vitro* gastric and small intestinal digestion protocol (Dartois *et al.*, 2010) described in section 3.3.9 was followed.

The initial rate of starch hydrolysis for the first 10 min of reaction (R_{10}) was calculated using the following formula:

$$R_{10} = \frac{m}{Vxt} \quad (5.1)$$

where m is the amount of starch hydrolysed (mg), V is the volume of reaction mixture (mL) at 10 min of small intestinal digestion, and t is the reaction time (t = 10 min) (Ezeogu *et al.*, 2005).

Cell samples taken after 0 and 120 min of small intestinal digestion were stained with 2% (w/v) Lugol's iodine solution and visualised under LM for detecting the presence of starch.

5.3.6.2. Effect of digestive proteases on in vitro *starch digestion*

A set of four different experiments was designed to evaluate the effect of digestive proteases on *in vitro* digestion of starch in cooked samples of native cotyledon cells, as illustrated in Fig 5.1. The *in vitro* digestion protocol described by Dartois *et al.* (2010) was followed for all experiments, using enzyme concentrations specified in this protocol, but with different combinations of digestive enzymes. All enzyme solutions were prepared freshly prior to analysis. Four experiments were conducted: (Exp 1) a control digestion with pepsin in the gastric juice and with pancreatin, amyloglucosidase (AMG) and invertase (IVT) in the small intestinal juice; (Exp 2) a digestion with only pancreatin proteases (PP); (Exp 3) a digestion with only gastric pepsin (GP); (Exp 4) a digestion without digestive proteases (GP and PP). For Exps (3) and (4), porcine pancreatin was replaced by porcine pancreatic α-amylase (PPA) having the same α-amylase unit of activity per mL of

final digestion mixture (U/mL) to that of pancreatin. The α-amylase activities (U/mg solid) of enzymes were determined using Bernfeld (1955)'s method (described in section 5.3.5). The pancreatin and PPA (type VI-B) used in this study were found to have 92.2 ± 1.0 and 45.4 ± 1.4 U/mg solid of α-amylase activity, respectively.

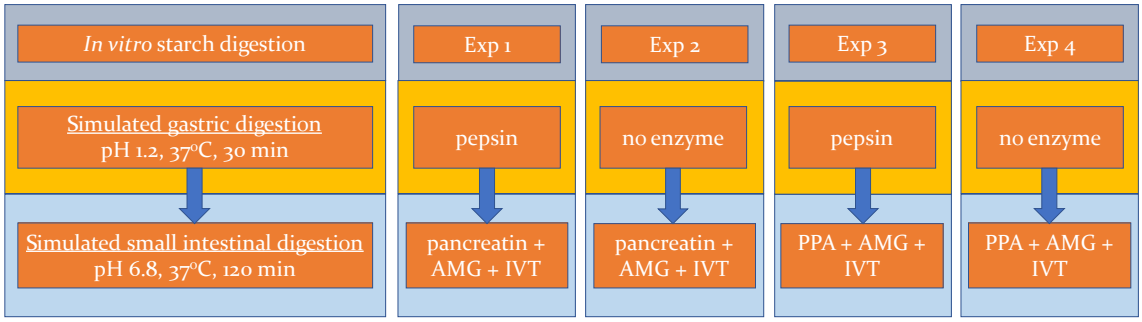

Fig. 5.1. Schematic diagram of four different experiments for evaluating the effect of digestive proteases on *in vitro* starch digestion of cotyledon cells. Abbreviations: AMG, amyloglucosidase; IVT, invertase; PPA: porcine pancreatic α-amylase.

5.4. Results and Discussion

5.4.1. Effect of protein matrix modification on cotyledon cell microstructure

Raw intact cotyledon cells were obtained from navy beans using a modified version of the sequential acid-alkali isolation method (Kugimiya, 1990). This method enabled easy separation of intact cells without disrupting cell wall integrity and gelatinising starch. Representative light micrographs of isolated navy bean cotyledon cells (INC) confirmed structural intactness as shown in Figs 5.2.A – D. Cell samples contained minor impurities (i.e. broken cells, free starch granules, and cell wall fragments), which could have resulted from breakage of intact cells by pestle crushing followed by release of cellular contents during isolation.

Samples of isolated navy bean starch (INS) were observed to be largely free of impurities (Fig 5.2E).

Native INC (Fig. 5.2A) consisted of multiple starch granules that were compactly embedded in dark layers of the cytoplasmic protein matrix and encased by intact cell walls. Cells and starch granules generally had oval or round shapes. Similar microstructural observations of INC have been reported previously (Do *et al.*, 2019). The treatment of INC with pepsin at pH 2 resulted in proteolysis of the protein matrix and corresponding visual disappearance of the dark-coloured substance (protein) surrounding granules when viewed under LM. The protein matrix appeared progressively fainter under LM as the pepsin incubation time increased from 1 to 24 h (Figs. 5.2B–D). It was observed to be no longer visually perceptible after 24 h incubation with pepsin (Fig 5.2D).

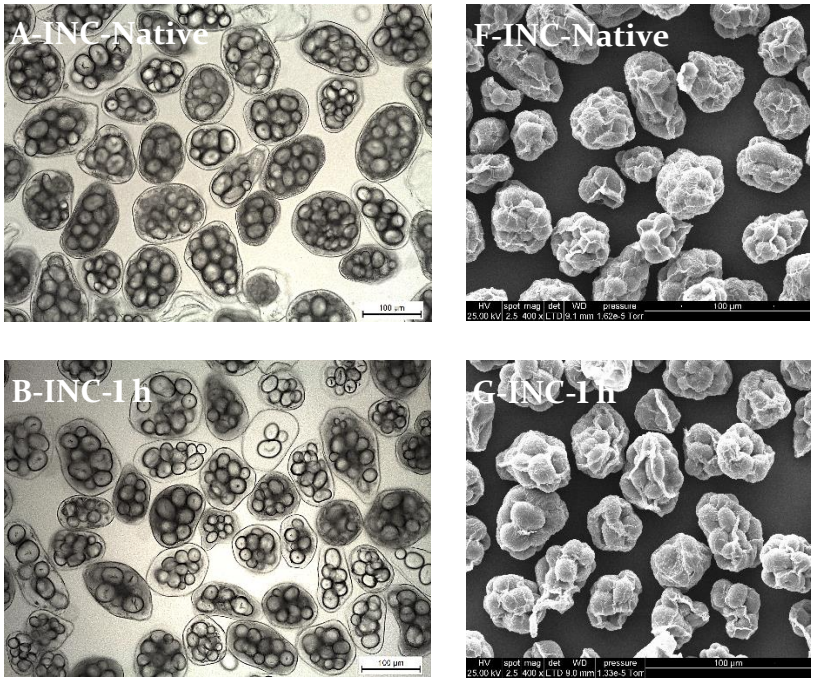

Fig. 5.2. Representative Brightfield light micrographs (A-E) and scanning electron micrographs (F-J) of INS, native INC, and INC after treatment with pepsin for 1, 4, or 24 h at pH 2. Scale bar = 100µm.

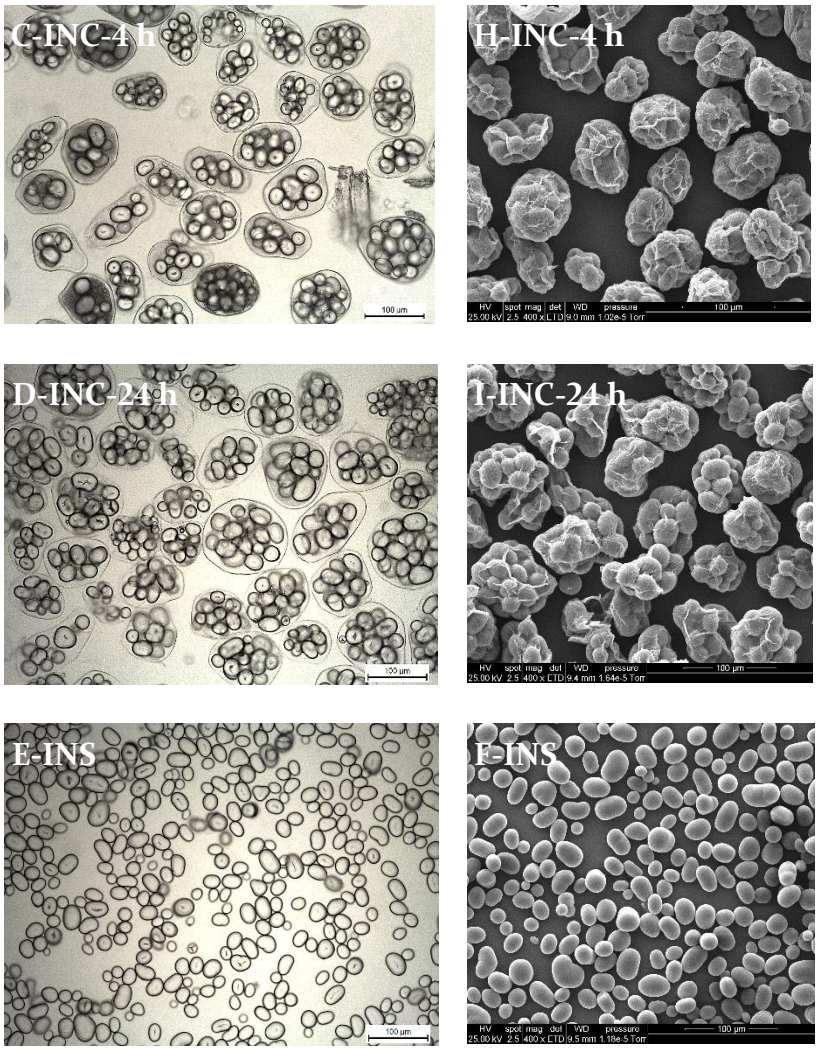

SEM images (Figs. 5.2F–H) show INC having highly wrinkled surfaces due to extensive shrinkage and folding of cell walls during the ethanol dehydration and air-drying process, whereas INS displayed a smooth surface. Native starch granules were packaged into cells and wrapped around by sheet-like cell walls while the protein matrix was not visible under SEM. These SEM observations agree well with those of previous reports (Do *et al.*, 2019; Xiong *et al.*, 2018). It appears that the cell structure became progressively transparent as the pepsin incubation time increased, leading to increased visual clarity of native granules inside cells. It is possible that the protein matrix was partially removed from the cytoplasm due to

hydrolysis by pepsin, leaving transparent cell structures with noticeable granules enclosed in loose cell walls.

5.4.2. Effect of protein matrix modification on physicochemical properties of intracellular starch

The physicochemical properties of INC (native and pepsin-treated) and INS are presented in Table 5.1. Native INC contained 64.3% starch and 17.6% protein (w/w, dwb). These values are within range of previously published data (Do *et al.*, 2019) showing that starch and protein are the two major components of legume cotyledon cells. They constitute 57.2–69.0% and 17.3–20.3% of total dry cell mass, respectively. In addition, it is evident from Table 5.1 that the pepsin treatment reduced the protein content, while simultaneously increasing the total starch content of INC. Specifically, cells with longer incubation times (1, 4, and 24 h) had corresponding higher total starch contents (70.5, 73.4, and 80.2%) and lower protein contents (11.4, 9.2, and 2.7%). Changes in the protein and starch contents were found to be statistically significant ($p \leq 0.05$). These quantitative results support earlier LM observations of the visual disappearance of proteins in cells after pepsin treatment. Furthermore, INS contained 91.9 and 0.3% of starch and residual protein respectively. The amylose content was similar (~ 28%) across all samples ($p > 0.05$), indicating that the cell isolation and subsequent pepsin treatment used in this study had virtually no effect on the amylose content.

Table 5.1. Physicochemical properties of INS, native INC, and INC after treatment with pepsin for 1, 4, or 24 h.

Navy bean materials	AM (%)	TS (% dwb)	P (% dwb)	SP (g/g)	SS (%)
INC-Native	28.8 ± 0.0^{a}	64.3 ± 0.5^{e}	17.6 ± 0.7^{a}	5.2 ± 0.1^{d}	5.5 ± 0.0^{c}
INC-1h	28.6 ± 0.2^{a}	70.5 ± 0.4^{d}	11.4 ± 0.3^{b}	5.4 ± 0.1^{cd}	5.5 ± 0.0^{c}
INC-4h	27.8 ± 0.3^{a}	73.4 ± 0.2^{c}	9.2 ± 0.3^{c}	5.6 ± 0.0^{c}	6.1 ± 0.1^{c}
INC-24h	29.0 ± 0.0^{a}	80.2 ± 0.5^{b}	2.7 ± 0.2^{d}	7.4 ± 0.2^{b}	8.3 ± 0.3^{b}
INS	28.0 ± 0.7^{a}	91.9 ± 0.9^{a}	0.3 ± 0.2^{e}	12.6 ± 0.1^{a}	16.9 ± 0.2^{a}

$^{a\ b\ c\ d\ e}$ Values are means ± standard deviations of three determinations. Values with the same subscripts in a column do not differ significantly ($p > 0.05$). Abbreviations: AM, amylose content; TS, total starch content; P, protein content; SP, swelling power; SS, starch solubility.

Table 5.1 shows that the swelling power (SP) and starch solubility (SS) of native INC did not differ significantly from that of INC-1h or INC-4h ($p > 0.05$). Only prolonged incubation with pepsin up to 24 h could result in INC with a higher degree of SP and SS. It has been suggested that the suppressed swelling and gelatinisation of starch trapped in legume ICC is attributed to limited water availability and spatial constraints inside cells (Fujimura & Kugimiya, 1994, 1995). This is due to the physical confinement of starch granules in the cell wall/protein matrix and the competition for water and space with starch by non-starch constituents such as proteins (Do *et al.*, 2019). Therefore as the pepsin hydrolysis progresses, it frees up intracellular space that has been occupied by proteins. This may allow more water and free space to be made available for granule swelling and disruption/dissolution upon heating, resulting in greater leaching of solubles (mainly amylose) from the granules into solution. It is also worth noting that, despite the extensive degradation of protein, INC-24h exhibited a much lower degree of SP and SS than INS. This suggests that the remaining protein and cell wall together prevent complete starch gelatinisation. From these findings, it

appears that the limited SP and SS of starch inside INC is linked to the barrier effects of the cell wall and protein matrix that combine to inhibit starch swelling and gelatinisation.

5.4.3. Effect of protein matrix on in vitro *starch digestion*

Cooked samples of native and pepsin-treated INC differing in protein content were subjected to *in vitro* gastric and small intestinal digestion, and starch hydrolysis curves are shown in Fig 5.3. As clearly seen in this figure, virtually no hydrolysis occurred during 30 min of gastric digestion with pepsin due to the absence of starch-hydrolysing enzymes. Starch was hydrolysed by pancreatic α-amylase during 120 min of small intestinal digestion. All samples generally exhibited increased percentage of hydrolysis before reaching a plateau towards the end of digestion. However, as shown in Table 5.2, statistically significant differences in digestion kinetic parameters were found among samples ($p \leq 0.05$). The extent of starch hydrolysis after 120 min of small intestinal digestion (H_{120}, %) decreased in the following order: INS (85.1±0.4) > INC-24h (80.6±1.6) > INC-4h (77.6±0.6) > INC-1h (73.2±0.3) > INC-Native (70.6±0.6). In a somewhat similar pattern to that observed for H_{120}, the initial rate of starch hydrolysis (R_{10}, mg/mL/min), calculated for the first 10 min of reaction when the hydrolysis rate was highest, decreased in the following order: INS (2.76±0.13) > INC-24h (2.11±0.13) ~ INC-4h (2.07±0.13) > INC-1h (1.50±0.03) ~ INC-Native (1.40±0.11). It is evident from these results that both R_{10} and H_{120} progressively increased as the pepsin treatment time increased from 1 to 24 h.

Table 5.2. Kinetic parameters of *in vitro* starch digestion of INS, native INC, and INC after treatment with pepsin for 1, 4, or 24 h.

Navy bean materials	R_{10} (mg/mL/min)[f]	H_{120} (%)[g]
INC-Native	1.40 ± 0.11[c]	70.6 ± 0.6[e]
INC-1h	1.50 ± 0.03[c]	73.2 ± 0.3[d]
INC-4h	2.07 ± 0.13[b]	77.6 ± 0.6[c]
INC-24h	2.11 ± 0.13[b]	80.6 ± 1.6[b]
INS	2.76 ± 0.13[a]	85.1 ± 0.4[a]

[a b c d e] Values are means ± standard deviations of three determinations. Values with the same subscripts in a column do not differ significantly ($p > 0.05$).

[f] R_{10} : initial rate of starch hydrolysis calculated for the first 10 min of reaction.

[g] H_{120} : *in vitro* values of starch digestion extent determined experimentally after 120 min of small intestinal digestion.

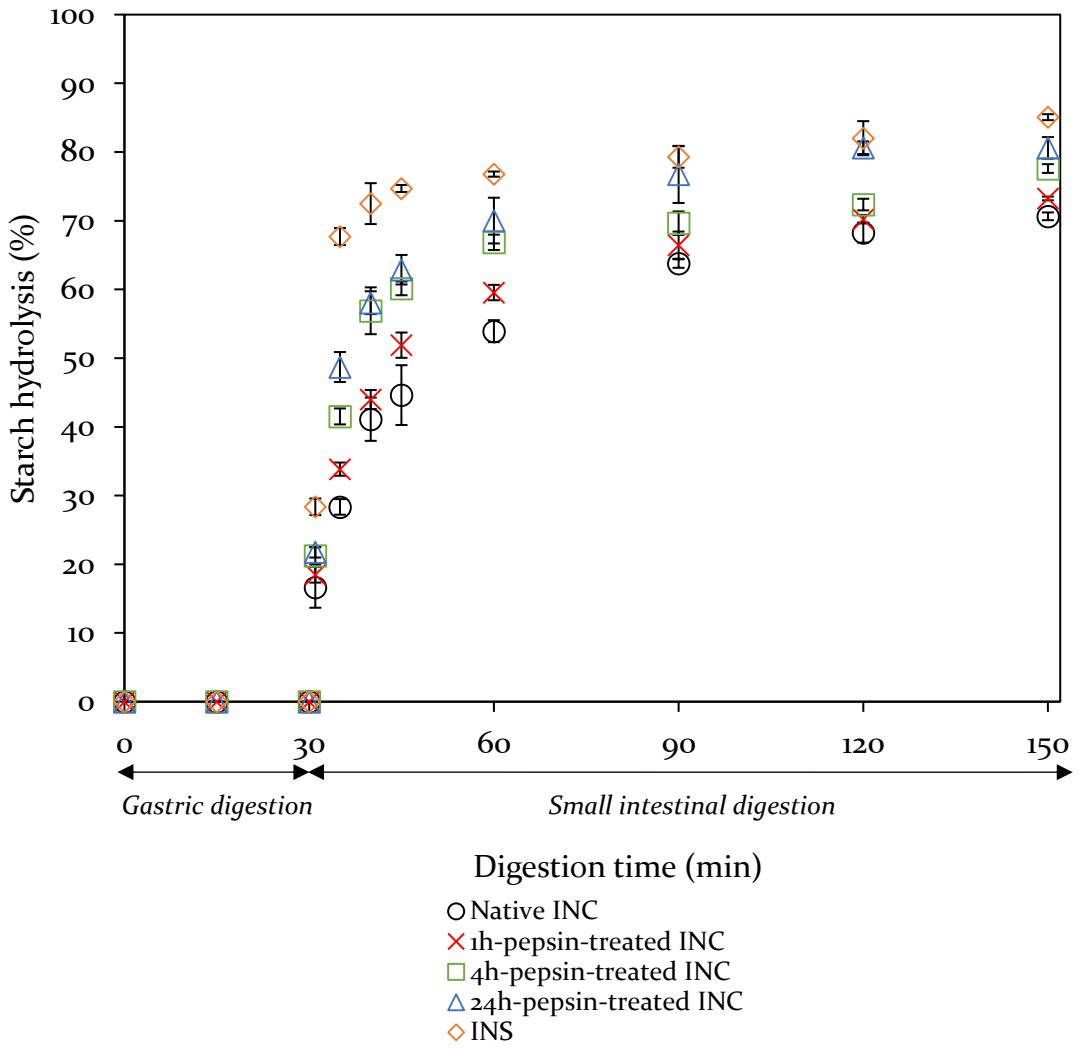

Fig. 5.3. *In vitro* starch hydrolysis curves of native INC (○) and INC after treatment with pepsin for 1 (×), 4 (□), or 24 (△) h. A sample of INS (◇) was included as a control. Errors bars represent the standard deviation.

Fig. 5.4 shows representative light micrographs of cotyledon cells before and after the simulated small intestinal digestion. Cells maintained structural integrity under magnetic stirring throughout *in vitro* digestion. Only a minor portion of cells was observed to have been broken and cellular contents were released. A general trend was observed in all samples that cells became "emptier" after 120 min. Empty gap spaces were formed between cellular contents and peripheral cell walls in most cells as a result of starch hydrolysis by α-amylase from the periphery towards the centre of the cells.

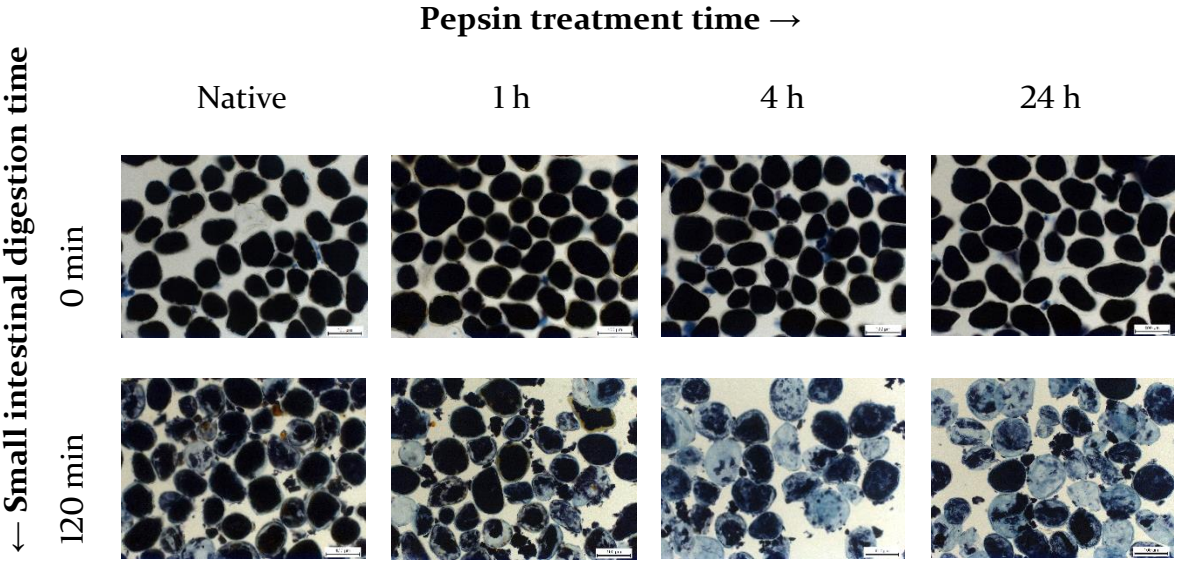

Fig. 5.4. Representative Brightfield light micrographs of INC obtained before (Native) and after pepsin treatment (1, 4, or 24 h) and taken at 0 and 120 min of small intestinal digestion. Cells were stained with iodine solution for detecting the presence of starch. Scale bar = 100μm.

Staining of cotyledon cells with iodine enabled visualisation of changes in the starch content. The blue-black colour intensity of amylose-iodine complexes is proportional to the amount of starch present in cells, thus providing qualitative information on the extent of starch hydrolysis at specific digestion times. Emptying of cellular contents and decrease in iodine staining intensity were noticeable after 120 min in all samples, and occurred to a much greater extent in those with longer

pepsin treatment. This observation is consistent with quantitative results for H_{120} and in agreement with previous reports (Do, Singh, Oey, Singh, Yada, & Frostad, 2020; Rovalino-Córdova *et al.*, 2018; Pallares *et al.*, 2018a).

It is also interesting to note that the pepsin treatment of native INC resulted in only partial protein hydrolysis. After 24 h, approximately 85% of protein digestion was achieved as calculated from Table 5.2. Despite the removal of most proteins, INC-24h had significantly lower values for R_{10} and S_{120} than INS (deprived entirely of cell structural barriers). This is mostly due to retention of intact cell walls in pepsin-treated INC, providing a diffusion barrier to the passage of α-amylase. This evidence suggests the occlusive effects of the cytoplasmic protein matrix and cell wall that combine to inhibit *in vitro* starch digestion.

In an attempt to separate the net contribution of the protein matrix from that of the cell wall, Rovalino-Córdova, Fogliano, & Capuano (2019) incubated kidney bean ICC with proteases for 20 h in order to completely hydrolyse proteins prior to *in vitro* starch digestion with α-amylase. Contrary to expectations, it was found that only 50% protein digestion was achieved despite prolonged protease treatment. However, protease-treated ICC showed a higher starch hydrolysis rate at early digestion times compared to control ICC. These results are consistent with our findings showing the protein matrix as an additional barrier to starch digestion aside from the cell wall, but its net contribution could not be quantitatively determined due to the incomplete protein digestion.

Starch-protein matrix consists of a compact continuous protein matrix entrapping starch granules and is a distinctive microstructural feature of some natural and

processed foods. Starch-protein interactions and characteristics of the protein matrix (e.g. gluten network in pasta, disulphide-bonded kafirin network in sorghum, etc.) may play an important role in retarding α-amylase digestion of starch, resulting in foods with slow starch digestion properties and low glycaemic responses (Kim *et al.*, 2008; Ezeogu *et al.*, 2008). However due to the low content of sulphur amino acids in bean proteins, the slow starch digestion of INC is primarily attributed to the microstructural organisation of starch granules and proteins in the cell cytoplasm rather than the disulphide bond formation in proteins (Rovalino-Córdova *et al.*, 2019). In fact, INC can be represented as an encapsulation system with double layer structure. The protein matrix acts as an inner layer for coating starch granules, while the cell wall acts as an outer layer for coating starch granule-protein. These dual encapsulation layers provide double protection for starch from amylolytic degradation by hindering α-amylase access/binding to starch. Therefore, disruption of either the cell wall or the protein barrier can lead to a substantial increase in the rate and extent of starch hydrolysis as has been demonstrated in this and other studies (Rovalino-Córdova *et al.*, 2018; Pallares *et al.*, 2018a).

5.4.4. Effect of digestive proteases on in vitro *starch digestion*

As demonstrated above, the protein matrix plays a role in limiting *in vitro* digestion of starch in INC. Since proteins are susceptible to proteolysis by GP in the gastric fluid followed by PP in the small intestinal fluid, it is worthwhile to explore the effect of digestive proteases on starch digestion. Fig. 5.5 shows *in vitro* starch digestion curves of cooked INC for four experiments with different protease

combinations, i.e. digestion in the presence of GP alone (Exp2) or PP alone (Exp3) and in the presence (Exp1) or absence (Exp4) of all digestive proteases. As evident in this figure, all samples exhibited a similar digestion pattern. Specifically, virtually no starch hydrolysis was observed during 30 min of gastric digestion. This was followed by a gradual increase in percentage of hydrolysis during 120 min of small intestinal digestion. As shown in Table 5.3, the extent of starch hydrolysis (H_{120}, %) decreased in the following order: Exp1 (70.6±0.6) ~ Exp2 (70.8±0.9) ~ Exp3 (69.9±0.7) > Exp4 (65.8±1.6). The initial rate of starch hydrolysis (R_{10}, mg/mL/min) decreased in the following order: Exp1 (1.40±0.11) ~ Exp3 (1.41±0.07) > Exp2 (0.97±0.04) ~ Exp4 (1.04±0.04).

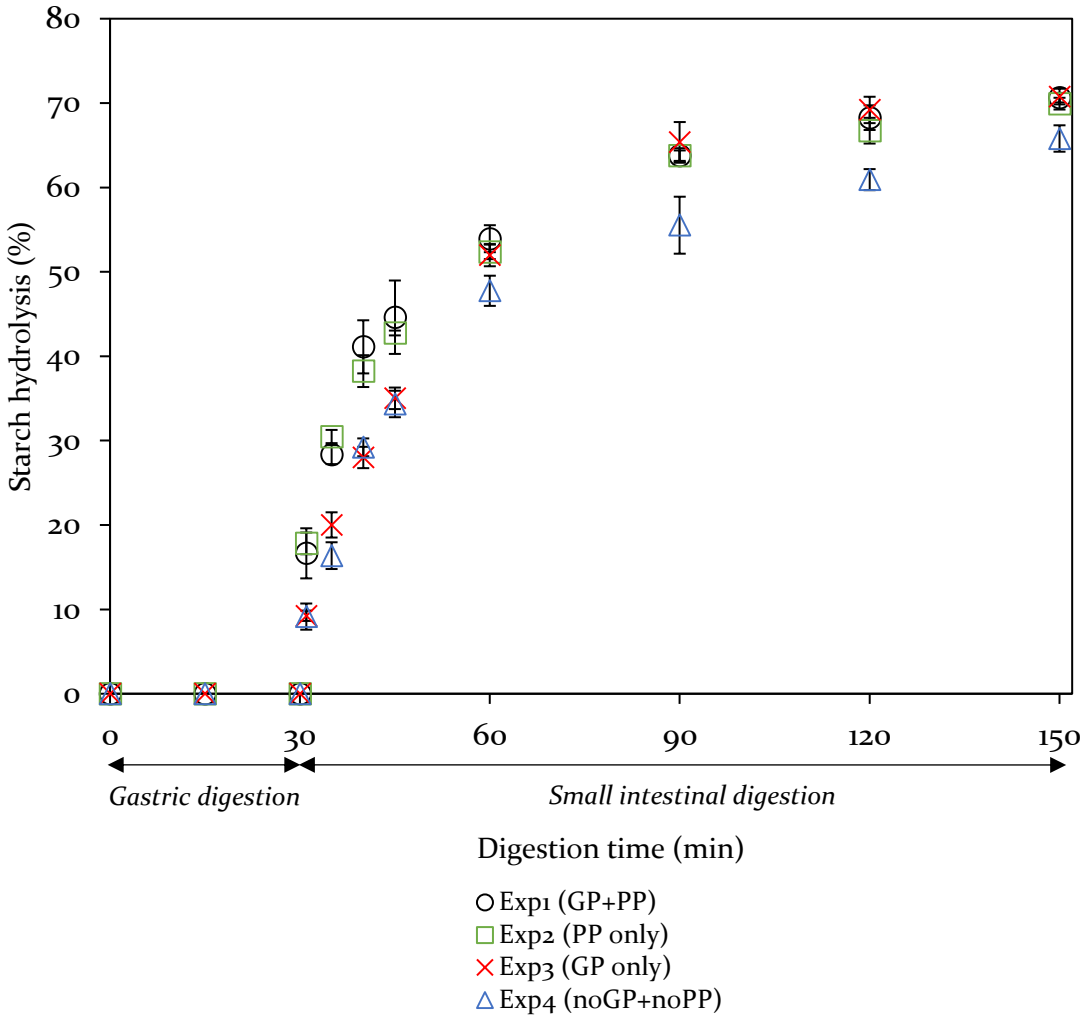

Fig. 5.5. *In vitro* starch hydrolysis curves of native INC with different protease combinations. Symbols (○, □, ×, △) are results of four different experiments (see Experimental Procedures 5.2.6.2). Errors bars represent standard deviations. Abbreviations: GP, gastric pepsin; PP, pancreatin proteases.

Table 5.3. Kinetic parameters of *in vitro* starch digestion of native INC for four experiments with different protease combinations.

Experiments	R_{10} (mg/mL/min)[c]	H_{120} (%)[d]
Exp1 (GP+PP)	1.40 ± 0.11[a]	70.6 ± 0.6[a]
Exp2 (PP only)	1.41 ± 0.07[a]	69.9 ± 0.7[a]
Exp3 (GP only)	0.97 ± 0.04[b]	70.8 ± 0.9[a]
Exp4 (noGP+noPP)	1.04 ± 0.04[b]	65.8 ± 1.6[b]

[a] [b] Values are means ± standard deviations of three determinations. Values with the same subscripts in a column do not differ significantly ($p > 0.05$).

[c] R_{10} : initial rate of starch hydrolysis calculated for the first 10 min of reaction.

[d] H_{120} : *in vitro* values of starch digestion extent determined experimentally after 120 min of small intestinal digestion.

The above results clearly show that both R_{10} and H_{120} values were significantly reduced when cooked INC were digested in the absence of all proteases. This is in agreement with previous work by Rovalino-Córdova *et al.* (2018) and Rovalino-Córdova *et al.* (2019), who both found a significant decrease in the rate and extent of α-amylase digestion of starch when kidney bean ICC were digested with exclusion of all proteolytic enzymes (i.e. pepsin in the gastric fluid and trypsin & chymotrypsin in the small intestinal fluid). Wang, Li, Zhang, Wang, and Copeland (2017) also found that the greatest starch digestibility of cooked rice by PPA and AMG was achieved in the presence of a combination of all proteolytic enzymes, whereas their total exclusion resulted in the lowest starch digestibility. These findings demonstrate that efficient protein hydrolysis by digestive proteases is necessary for efficient starch hydrolysis, which has previously been described as a cooperative process (Rovalino-Córdova *et al.*, 2018). In addition, digestion with only PP resulted in a higher R_{10} value but a similar H_{120} value compared to digestion with only GP, which may be suggestive of the effectiveness of different proteolytic enzymes in degrading the protein matrix. This is supported by the previous suggestion that PP are more efficient in hydrolysing dietary proteins than GP (Rovalino-Córdova *et al.*, 2019).

The results in this study provide strong evidence that the presence of digestive proteases in both the stomach and the small intestine found in the human GI tract is necessary for *in vitro* digestion of starch in INC. Specifically, GP is likely to play a role in loosening the compact cytoplasmic matrix. Extensive protein degradation by PP during small intestinal digestion may facilitate enzyme mobility within the cell cytoplasm and enhance starch-amylase interactions. Considering the

facilitating effect of digestive proteases on starch digestion, the encapsulation of starch granules in double-layered INC with the protein matrix (inner layer) being surrounded by the cell wall (outer layer) seems to be advantageous in the sense that the protein matrix is shielded from digestive proteases, making it less susceptible to proteolysis while providing extra protection for starch.

5.5. Conclusions

The results of the present study provide new insight into the role of the protein matrix in modulating the *in vitro* digestion of starch in cotyledon cells. We have shown that the entanglement of starch granules in the protein matrix may restrict granule swelling and gelatinisation. In addition to the cell wall, the protein matrix provides a secondary physical barrier restricting access/binding of α-amylase to starch. Proteolytic degradation of the protein matrix removes these restrictions, rendering starch more susceptible to α-amylolysis. Therefore, efficient protein hydrolysis prior to or during simulated GI digestion is necessary for improving starch digestibility. Finally, the unique cotyledon cell structure may serve as inspiration and a template for designing biomimetic materials. Encapsulation of starch granules within a protein core and a polysaccharide shell to form a double-layer structure is a novel strategy for fabricating food-grade particles for reduced glycaemic impact.

CHAPTER SIX: A novel apparatus for time-lapse optical microscopy of gelatinisation and digestion of starch inside plant cells

6.1. Abstract

A new instrument was developed for time-lapse optical microscopy of a cohort of individual food particles, which is denoted as ParCS (**Par**ticle **C**ohort **S**tudy). The cohort can be observed through each stage of simulated hydrothermal processing, followed by *in vitro* gastrointestinal digestion. Instrument capabilities include the quantification of cooking and digestion dynamics of starch trapped inside isolated cotyledon cells from navy beans. The cells, contained within a flow-through chamber, were cooked at 90°C and subsequently subjected to simulated gastric digestion and simulated small intestinal digestion. Little or no cell expansion was observed, and the cells remained intact, i.e., the cell walls showed no signs of rupture throughout the entire process. In contrast, intracellular starch granules partially swelled and gelatinised with a maximum relative granule area of approximately 2.4 at the end of cooking. During the small intestinal digestion, cellular contents were observed to visually "shrink" radially inwards towards the centre of the cells, implying that starch hydrolysis by pancreatic α-amylase had occurred inside the cells. Kinetic modelling of this shrinking process showed that the cells underwent amylolysis of cellular contents at different rates. This latter finding demonstrates that our new technique allows quantitative characterisation of starch gelatinisation and digestion inside cotyledon cells at the single-particle scale and may be used to test mechanistic hypotheses.

6.2. Introduction

The modulating effect of plant food microstructure on the digestibility and bioaccessibility of nutrients (e.g. starch, proteins, and lipids) along with its nutritional and health implications has recently become the subject of intensive research (Do *et al.*, 2018; Ogawa *et al.*, 2018; Berg *et al.*, 2012). Intact cotyledon cells isolated from starchy legumes serve as a food model for understanding the effect of plant cellular structure on the starch gelatinisation process and starch digestion *in vitro* (Fujimura & Kugimiya, 1994; Do *et al.*, 2019). Starch is naturally present inside cotyledon cells in legumes. Within each cell, tightly packed starch granules are embedded in a compact protein matrix, all enclosed within a thick, robust cell wall (Do & Singh, 2018). Physicochemical characterisation and *in vitro* digestion of starch inside isolated cells have been investigated by a number of researchers. It has been reported that when intact cells are heated in water, intracellular starch displays restricted swelling and gelatinisation due to limited water availability and constrained space inside cells (Do *et al.*, 2019; Fujimura & Kugimiya, 1994). During small intestinal digestion *in vitro*, starch trapped in the intact cells exhibits a slower rate and a lower extent of hydrolysis compared to that in non-encapsulated form (isolated starch) or inside cells devoid of intact structures (broken/damaged cells) (Dhital *et al.*, 2016; Do *et al.*, 2019). Multiple mechanisms have been proposed to explain the slow starch digestion property of cotyledon cells. Xiong *et al.* (2018) suggested that the cellular structure (e.g. cell wall, protein matrix) plays a predominant role in limiting starch digestion, rather than starch structural features. The intact and resilient cell walls present a primary

physical barrier restricting intracellular starch gelatinisation during cooking and the accessibility of amylolytic enzymes during digestion (Dhital *et al.*, 2016; Do *et al.*, 2019).

Various microscopy techniques, including LM, SEM, and confocal laser scanning microscopy (CLSM), have been employed to observe the microstructural and temporal changes of cotyledon cells associated with cooking and starch digestion *in vitro* (Do *et al.*, 2019; Rovalino-Córdova *et al.*, 2018; Pallares *et al.*, 2018a). Each type of microscopy provides distinct microstructural data regarding the cells and the intracellular starch. CLSM and LM further reveal unique information that can assist in understanding possible mechanisms for the slow starch digestion, e.g. binding of fluorescent-labelled α-amylase to cell wall components that can inhibit enzyme activity for hydrolysing starch (Bhattarai *et al.*, 2017), and gradual progression of starch hydrolysis from the periphery towards the core of the cell (Rovalino-Córdova *et al.*, 2018). However, the microscopic examination of cells involving those techniques in previous studies has suffered from several limitations. First, static images are captured for representative cells sampled at specific time points during experiments, but provide limited information on digestion *dynamics*. Second, sampling different aliquots over time makes it impossible to monitor the progress of the same cells. Third, sample collection and preparation techniques (e.g. snap freezing and freeze-drying of cells for SEM) may alter the cellular structure and integrity, and sample artefacts could lead to misinterpretation of cell data.

These limitations have motivated the development of an apparatus for studying a cross-section of the population of cotyledon cells from within a batch of navy beans in a cohort study. For those unfamiliar with the term, a cohort study is a type of longitudinal study in which a sampling of individual members within a population are observed to see how they change as a function of time (Grimes & Schulz, 2002). We therefore refer to this technique as a "Particle Cohort Study" or "ParCS", and the instrument as a ParCS apparatus. In this case, the ParCS apparatus consists of a flow-through chamber with temperature control and time-lapse light microscopy for cooking and *in vitro* digestion of cotyledon cells. A similar approach has previously been used to directly observe microstructural changes in isolated potato cells and starch granules heated in oil (simulated frying) (Aguilera *et al.*, 2001). Time-lapse microscopy studies of starch digestion in parenchyma cells of cooked potatoes (Bordoloi *et al.*, 2012b) and lipolysis of fat droplets (Patton *et al.*, 1985) have also been reported in literature. Unfortunately, these studies only attempt to simulate a single process of either cooking or small intestinal digestion. Using our new ParCS system, one can visually observe individual cells and their fates in real-time under conditions that chronologically simulate those during cooking, followed by various stages of digestion in one continuous sequence.

ParCS with optical microscopy for imaging of cells in a flow-through chamber is not a new concept. This technique has been used extensively for decades in cell biology for live cell imaging, i.e. visualisation of cell responses upon exposure to controlled extracellular conditions, such as under shear stress (Ulker *et al.*, 2011), or at high temperatures and pressures (Deguchi & Tsujii, 2002). However, its application in studying simulated enzymatic digestion of plant cells is rather

underexploited. An advantageous aspect of this technique is that it provides an opportunity to probe the digestive behaviour of a single cell. This differs from the utilisation of population averaging assays (e.g. *in vitro* static digestion models) for a mixed population of cells, which generates statistical metrics of digestion, but provides limited mechanistic understanding. Furthermore, microscopy that traditionally places emphasis on producing qualitative data has evolved into a powerful, quantitative technique due mainly to the advances in digital camera technology (Nature Methods, 2012). In combination with image analysis, meaningful quantitative data can be extracted from images that could not be obtained with conventional *in vitro* digestion methods to aid in understanding of the underlying mechanisms and modelling of food digestion. Our simple, low-cost ParCS apparatus was designed for time-lapse imaging of physicochemical phenomena encountered in foods under simulated processing and digestion conditions. In this study, we demonstrated the capabilities of this apparatus by quantifying the cooking and digestion dynamics of starch trapped in legume cotyledon cells.

6.3. Instrument

6.3.1. Description of flow-through chamber

A rectangular chamber was custom-designed by the authors and constructed in the Physics Machine Shop at the University of British Columbia. As shown in Fig. 6.1, the chamber body is machined from a block of aluminium with the outer dimensions of 51 mm (length) x 25 mm (width) x 9 mm (height). The chamber has an upper and lower window (fashioned from a microscope slide) for optical

transparency and viewing through a microscope. Both windows are fitted into recesses such that the surface of the glass is nearly flush with the edges of the inlet and outlet flow channels. The lower window is glued in place, and the upper window is removable for cleaning. The upper window is sealed by sandwiching a 1 mm thick silicone rubber gasket between it and the sample chamber.

When fully assembled (with both windows in place), the viewable section is approximately 18.6 mm x 6 mm x 2.4 mm for the sample chamber for a volume of ~ 0.26 mL. Four holes are bored into the sides of the chamber body for inlet and outlet flow, as well as for the insertion of a 1/16" diameter, 7" length thermocouple probe (Type J, McMaster-Carr, USA 39095K95) and a 1/4" diameter, 1.25" length cartridge heater (McMaster-Carr, USA 8376T22). Inlet and outlet flow tubes are connected with push-to-connect adapters (McMaster-Carr, USA 5111K462) to short aluminium tubes (ID = 1/16 in, OD = 1/8 in) that are glued into the chamber and align with the flow channels.

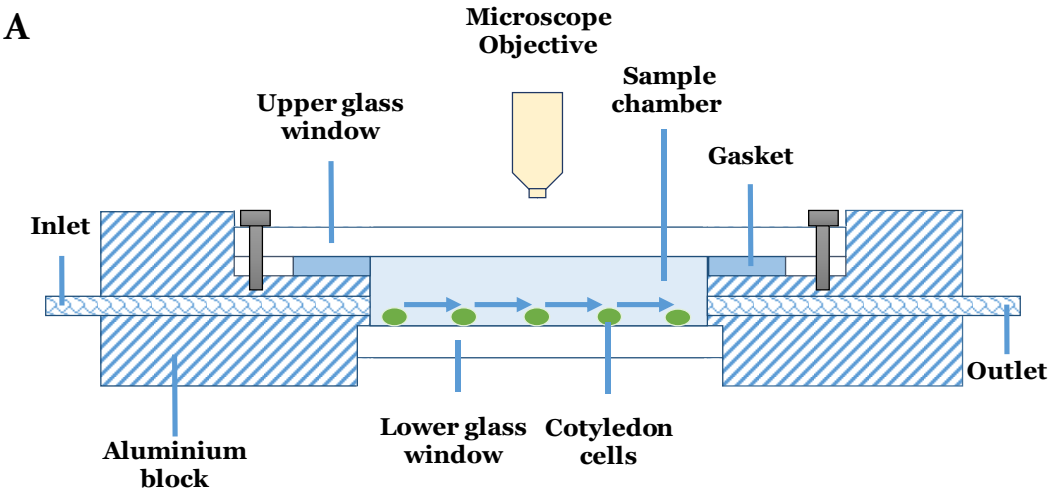

B

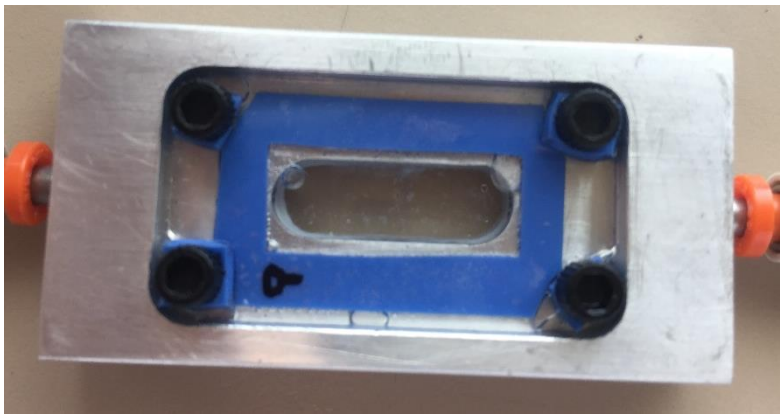

Fig. 6.1. (A) Schematic layout of the flow-through chamber. Arrows indicate the direction of flow. (B) Photograph of chamber (top view) used for experiments.

6.3.2. Description of ParCS apparatus

The ParCS apparatus consists of several components as shown in Fig. 6.2. A 50 mL volumetric flask containing water (for cooking) or digestive mixtures (for digestion) is immersed in a temperature-controlled water bath (Grant Instruments Cambridge Ltd., Barrington, England) and serves as a reservoir to supply liquids and/or heat to the flow loop. The apparatus has a closed liquid circulation system wherein liquids from the flask are pumped by a peristaltic pump at ~1.9 mL/min (120S/DM2, Watson-Marlow 120 Series, Thermo Fisher Scientific, Canada) into the chamber via the inlet, and then from the outlet back to the flask. It can also be operated in an open-loop fashion. The desired volumetric flow rates can be achieved by adjusting the pump motor speed. Separate pieces of 1/8" OD, 1/16" ID clear polyurethane tubing (McMaster-Carr, USA 5648K67) are used to connect the reservoir flask, the chamber, and the pump together. Plastic push-to-connect adapters are used to securely connect the tubing to the chamber inlet and outlet. The peristaltic pump has a marprene double-segment manifold tubing piece that is joined to the system tubing via barbed adapters.

For cooking, the cartridge heater is used as the sole heat source, and no flow is applied. For digestion, the water bath is used to heat the flask to 37°C and the cartridge heater in the chamber is used to make up heat losses (around 7°C) while flowing through the tubes. The heat input from the cartridge heater in the chamber is controlled by changing the voltage applied to the heater using a variable transformer or variac (3PN1010, Staco Energy Products Co., Ohio, USA). The actual temperature inside the sample chamber is monitored by the thermocouple probe connected to a digital display temperature controller (Watlow Series CV, McMaster-Carr, USA). To minimize heat losses to the ambient environment between the water bath and the chamber, several system features were optimised: (i) tubing length was minimized, (ii) the chamber was placed directly after the water bath in the flow loop (flask–chamber–pump–flask), (iii) all tubings were wrapped with one-inch thick sheets of fiberglass insulation , (iv) the 50 mL volumetric flask was used to provide a sufficient thermal mass while avoiding overly large liquid volumes.

The chamber is mounted by gluing atop a 75 mm x 25 mm microscope slide that is fitted into a slide holder on the stage of a light microscope (Carl Zeiss, Germany), allowing the chamber position to be adjusted in both X– and Y–directions. An objective lens of 10X magnification with long working distance is used for this system. Microscopic images are recorded using a machine vision camera (UI-3880LE-C-HQ from IDS Imaging) fitted to the microscope, and digitally transferred to a computer via USB for image and video processing.

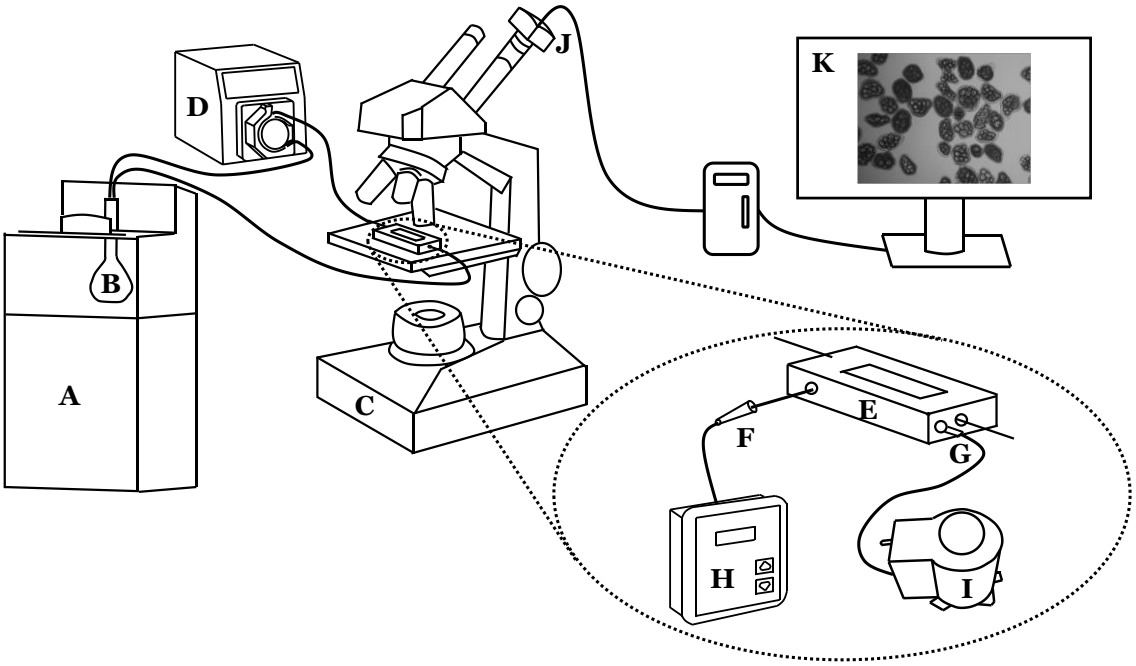

Fig. 6.2. The ParCS apparatus used for time-lapse optical imaging of isolated navy bean cotyledon cells under simulated cooking and digestion conditions: (A) temperature-controlled water bath; (B) 50 mL volumetric flask; (C) upright microscope; (D) peristaltic pump; (E) flow-through chamber; (F) temperature probe; (G) cartridge heater; (H) digital temperature display; (I) variable transformer; (J) video camera; (K) Raspberry Pi computer.

6.4. Instrument Operation

6.4.1. Materials

Raw navy beans (*Phaseolus vulgaris*) were purchased from a local store in Vancouver, British Columbia, Canada. Pepsin (porcine gastric mucosa; lyophilized powder; ≥ 2500 units/mg protein) and pancreatin (porcine pancreas; 4 x USP) were purchased from Sigma – Aldrich Ltd, St Louis, USA. All other chemicals and reagents were of analytical grade. Distilled water was used for all experiments.

Raw, intact cotyledon cells were isolated without gelatinising starch according to the method described by Kugimiya (1990) with some modifications. Dry, raw navy beans were soaked in a 0.1 M hydrochloric acid (HCl) solution (pH ~ 1.3) at room

temperature (~20°C) for 24 h. The hydrated beans were manually dehulled, split into cotyledons, and rinsed with distilled water to remove the remaining acids. The cotyledons were then soaked in a 0.06 M sodium hydroxide (NaOH) solution (pH ~ 12.5) in a 500 mL Schott bottle. This bottle was placed in a shaking incubator at 20°C and shaken at 150 rpm for 24 h. The softened, alkali-treated cotyledons were gently mashed by a pestle and mortar to a consistent paste. The resultant paste was successively passed through 125 µm (No. 120) and 63 µm (No. 230) standard stainless-steel testing sieves (Cole-Palmer, Canada) by extensive washing with water. The cell extract collected on the 63 µm sieve was dehydrated by rinsing in two changes of absolute ethanol (1 g of extract per 5 mL of ethanol) for 5 min each at room temperature, and recovered by centrifugation at 1800 x *g* for 20 min. The cells were allowed to air-dry in a fume hood overnight at room temperature. The dried powder was stored at room temperature in a sealed centrifuge tube for later use.

6.4.2. Simulated static cooking of cotyledon cells

Isolated cotyledon cells were suspended in distilled water and introduced into the ParCS chamber by slowly pumping through the flow loop. Once loaded, the cells were left to settle to the lower glass window of the chamber. The residual cells were flushed out of the tubing by disconnecting the tubing pieces and rinsing them with distilled water. This step was necessary to prevent the uncooked residual cells in the upstream tubing from re-entering into the sample chamber during subsequent digestion. The flow loop was then re-assembled and ready for experimentation.

The 50 mL volumetric flask was filled with 40 mL distilled water. The tubing was inserted into the flask and secured in place with the flask in the water bath. The flow loop was then replenished with water. The chamber was tilted and tapped gently to evenly spread the cells throughout the lower window as well as to remove any air bubbles.

Cooking of cotyledon cells was performed under static conditions (no flow). The cooking time and temperature suggested by Do *et al.* (2019) was used. The variable transformer was set to reach a steady-state of 90°C, which was achieved in approximately 10 minutes, and held at 90°C for 10 additional minutes for a total cooking time of ~20 min. The heating profile was documented by manually recording the time at 1°C increments. Following cooking, the chamber was left at room temperature to cool down passively until reaching 37°C prior to *in vitro* digestion.

6.4.3. Simulated in vitro *gastric and small intestinal digestion of cotyledon cells*

The static *in vitro* digestion protocol described by Dartois *et al.* (2010) was followed, but with enzyme concentrations suggested by Minekus *et al.* (2014). This employed a two-stage method to simulate the gastric and small intestinal conditions for starch digestion. The simulated gastric and intestinal fluids (SGF and SIF) were prepared according to the US Pharmacopeia (Pharmacopeia, 2000).

The water bath was maintained at 37°C and the pump was run throughout digestion. The constant flow was designed to facilitate mass transport of digestive

fluids and hydrolysis products without disturbing the location of the cells, thereby allowing the same cells to be tracked over time. Next, the pump was stopped, and the pH of the flask contents was initially adjusted to 2.0 by the addition of 0.05 mL of 3 M HCl. The SGF (4 mL) containing pepsin (2000 units per mL of final digestion mixture) was added to the flask, and the final pH was adjusted to 1.2 by the addition of 0.25 mL of 3 M HCl and 0.2 mL of 0.5 M HCl. The flask was shaken gently by hand after each addition of fluid. The flask was then left to sit for 3–5 min before running the pump for 30 minutes to complete the gastric digestion step.

After the gastric phase, the pump was stopped, and the pH was adjusted to ~6.8 by the addition of 0.42 mL of 3 M NaOH. Subsequently, the SIF (5.17 mL) containing pancreatin (based on pancreatic amylase activity at 200 units per mL of final digestion mixture) was added to the flask, and the pH was adjusted to 6.8 by the addition of 0.05 mL of 0.5 M NaOH. The flask was shaken and left to sit for 3–5 min before restarting the pump in order to complete the 120 min small intestinal digestion step.

6.4.4. Image acquisition

Micrographs were acquired using an upright microscope and a video camera. Prior to the experiment, a desired field of view containing at least 20 cotyledon cells was selected. Time-lapse experiments were carried out using a custom script written in Python on a Raspberry Pi computer. Images were taken every second during static cooking and every 10 and 12 seconds during gastric and small intestinal digestion respectively (see supplementary video accompanied with this thesis).

6.4.5. Image processing

Digital image analysis was conducted using ImageJ/Fiji software. Outer boundaries of objects were outlined manually using a polygon selection tool. Projected surface area (measured based on pixel counting) and circularity of the defined objects were then automatically computed by the software. The estimation of the number of starch granules within each cell was conducted through manually counting the discernible granules. The discernibility was hampered at times in larger cells by the three-dimensional arrangement of the starch granules causing some granules to be out of focus or obscured by multiple layers, though in most cases this was not a major issue. Data from these measurements was curated and processed using Microsoft Excel. Tukey's test and analysis of variance (ANOVA) were used to analyse the significance of differences ($p \leq 0.05$) between means using Minitab 18 software.

The relative area (RA) and circularity (C) of cells and starch granules were calculated using the following formulae:

$$RA = \frac{A}{A_0} \tag{6.1}$$

$$C = \frac{4\pi A}{P^2} \tag{6.2}$$

where A is the projected area at a given time, A_0 is the initial projected area, and P is the perimeter.

A total of 148 raw cotyledon cells were randomly selected for analysis. Frequency distribution histograms of projected surface area, circularity, and estimated number of starch granules per cell are shown in Fig. 6.3. Cell area ranged between

0.002 and 0.015 mm^2 (Fig. 6.3A). The histogram for circularity (Fig. 6.3B) displayed a right-skewed distribution with a peak value in the range of 0.9–0.92, suggesting that most cells were reasonably circular. The estimated number of discernible starch granules in each cell was between 5 and 20 (Fig. 6.3C). To demonstrate how the physical parameters of cells were analysed using ImageJ, three representative cells with their respective measurements of projected surface area (mm^2) and circularity are shown in Fig. 6.3D.

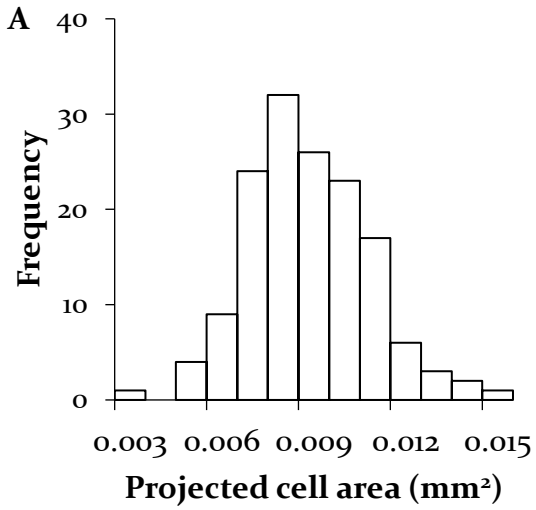

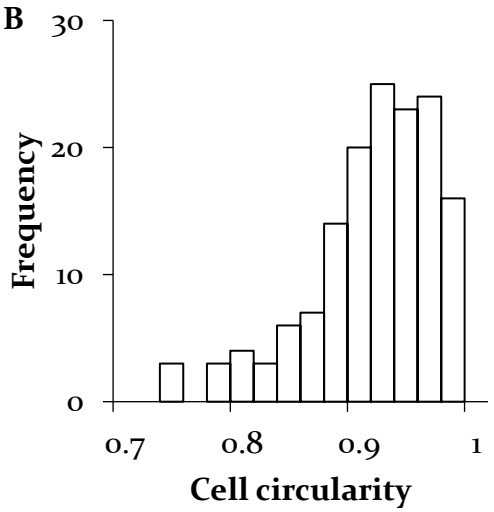

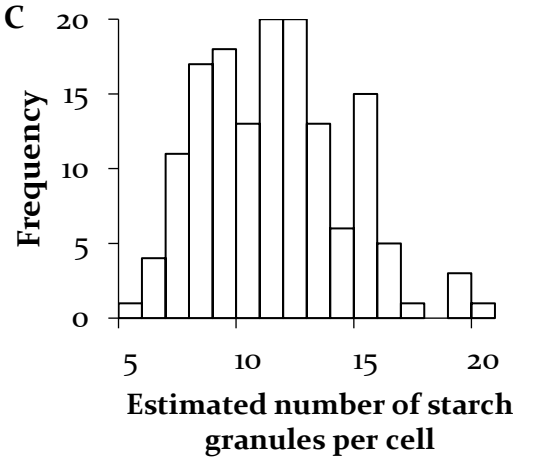

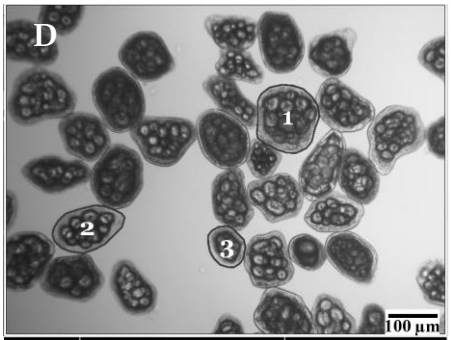

Cell	Projected surface area (mm²)	Circularity
1	0.014	0.963
2	0.010	0.886
3	0.005	0.972

Fig. 6.3. Frequency distribution histograms showing variations in microstructural characteristics of 148 raw cotyledon cells: (A) projected surface area (mm^2); (B) circularity; (C) estimated number of starch granules per cell; (D) sample image in ImageJ of three representative cells labelled 1, 2, and 3 with their respective measurements of projected surface area (mm^2) and circularity.

6.5. Instrument Capabilities

The ParCS apparatus is capable of performing quantitative time-lapse optical microscopy for examining the dynamics of individual, microscopic food particles under simulated conditions of hydrothermal processing and enzymatic digestion. This apparatus can potentially be used to study a wide range of food materials, such as plant cells, starch granules, lipid droplets, emulsions, and capsules – to name a few. In this study, a microscopic quantification of the cooking and digestion dynamics of starch inside cotyledon cells is demonstrated as an example of the instrument capabilities. To the best of our knowledge, the time-lapse microscopy of food digestion *in vitro* demonstrated here has not been previously performed on a flow-through chamber device.

6.5.1. Simulated cooking of cotyledon cells

Fig. 6.4 displays a sequence of representative images at increasing cooking temperatures (see video). Fig. 6.4A of raw cotyledon cells shows a good preservation of cellular integrity after the acid-alkali isolation procedure. Also revealed in this figure is the cell microstructure that consists of multiple native starch granules (globular or elliptical) embedded in thick dark layers of cellular matrix and encapsulated within intact cell walls. The matrix substance is thought to be mainly comprised of proteins as previously reported by Berg *et al.* (2012). Also visible is a noticeable “gap space” where the granules are not in contact with the cell wall.

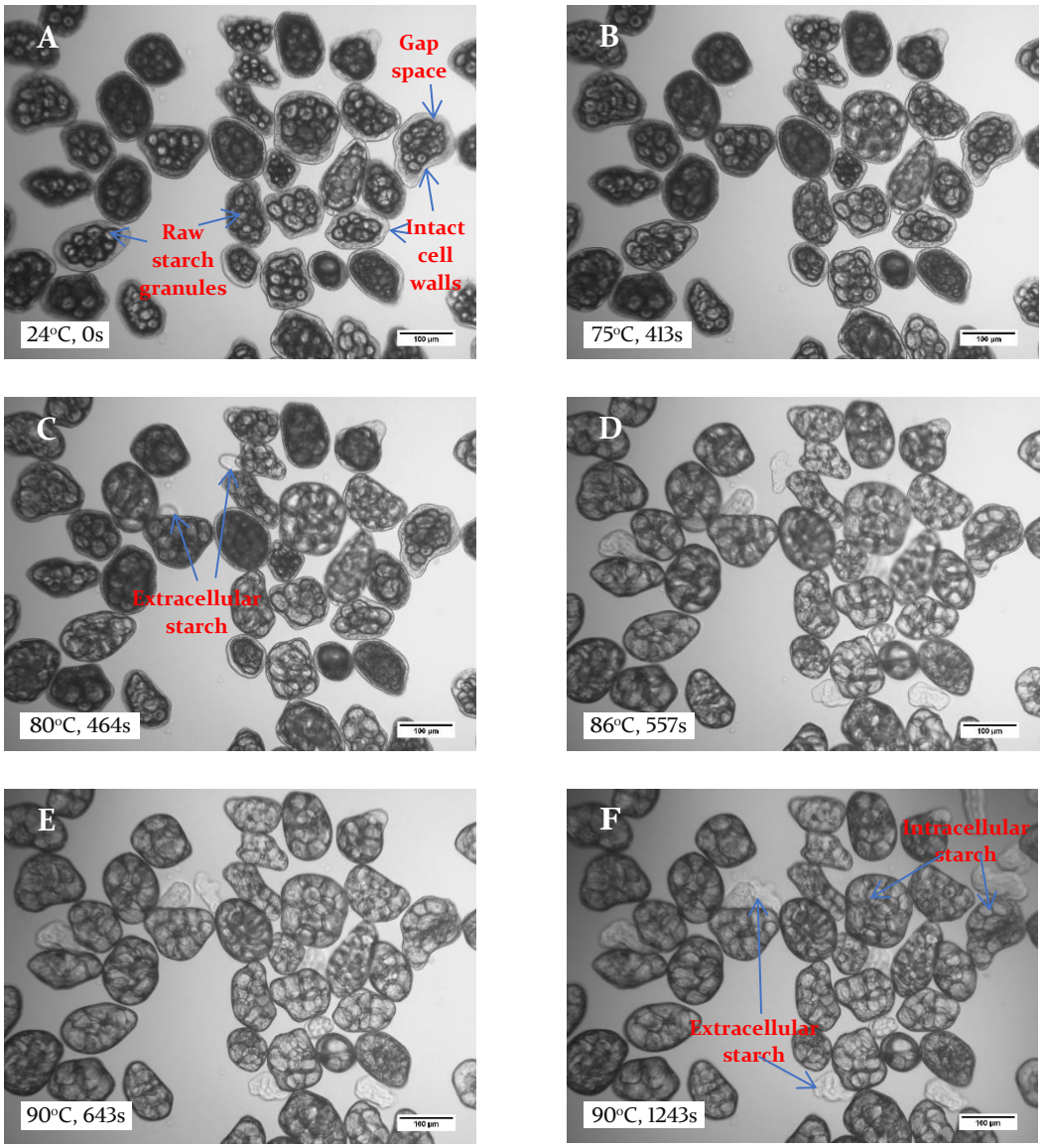

Fig. 6.4. Representative light photomicrographs of intact navy bean cotyledon cells at different temperatures, taken from a time-lapse imaging sequence of the cooking experiment during which cells were heated from 24 to 90°C (heating rate ~ 6.2 °C/min) and held for additional 10 min at 90°C: (A) Raw cotyledon cells at room temperature (24°C); (B) Initial swelling of starch granules inside cells (75°C); (C) Extensive swelling (80°C) and (D) end of swelling (86°C) of starch granules inside cells; (E) Cells at the end of the heating period (90°C); (F) Cells at the end of cooking.

During the cooking process, there were no apparent morphological changes in the cells and starch granules at recorded temperatures up to about 65°C (00:05:15 in part 1 of video). Rapid granule swelling in most cells was observed above 80°C (Fig. 6.4C and 00:07:45 in video), and swelling had mostly ceased by the time the temperature reached 90°C about 6 minutes later (Fig. 6.4E and 00:11:35 in video).

At the same time, the cells expanded very little and retained their original shape. Further cooking for 10 min (Fig. 6.4F) resulted in imperceptible changes in the cells and starch.

It is noteworthy that the initiation of swelling of individual starch granules was observed to occur over a range of temperatures. This suggests the existence of a distribution of gelatinisation temperatures (T_{gel}) among individual granules rather than a single T_{gel} for all granules, which is supported by Rockland, Jones, and Hahn's (1977) observation that the susceptibility of individual lima bean starch granules to deformation and gelatinisation varies both with temperature and granule size.

During cooking the appearance of starches outside of the cells was also noted and marked in Fig. 6.4C. It was inferred that these were released from broken cells and were not separated out by sieving during cell isolation. These are termed "extracellular starches" (ES) to distinguish them from starches inside cells or "intracellular starches" (IS). Upon cooking in excess water, IS expanded and occupied the available intracellular space including the "gap space" (marked in Fig. 6.4A) noted earlier. Nevertheless, IS maintained their granular form while remaining trapped by cell walls and separate from each other despite significant deformation in their shape. In contrast, ES freely swelled and gelatinised, resulting in the formation of highly swollen, hydrated structures commonly known as "granule ghosts" (Fig. 6.4F) (Zhang, Dhital, Flanagan, & Gidley, 2014). ES also lost their original granule appearance, and exhibited faint outlines at the conclusion of

the cooking period. Leakage of solubilised starch polymers (e.g. amylose) out of the cells is possible, but was not visible in this setup.

Taking advantage of quantitative post-processing of the image data, RA and C of cells (n=11 randomly selected cells) were plotted against the logarithm of the time, and temperature during the cooking experiment (Fig. 6.5). No significant changes ($p > 0.05$) in these cell parameters were detected throughout cooking, which is in line with our visual observations of little or no swelling of cells and the maintenance of cell shape. Unlike cells, individual IS granules swelled, which is reflected by a parallel increase in their RA (n=9 randomly selected granules from different cells) over time with increasing cooking temperatures (Fig. 6.6). At the end of the cooking period (Fig. 6.4F), IS had grown by approximately 2.4 times their original area, and this change was found to be statistically significant ($p \leq 0.05$). Another interesting finding is that starch RA differed among individual IS granules at maximum swelling (data not shown). This difference could be due to variations in starch granule size and intracellular volume that is available for swelling.

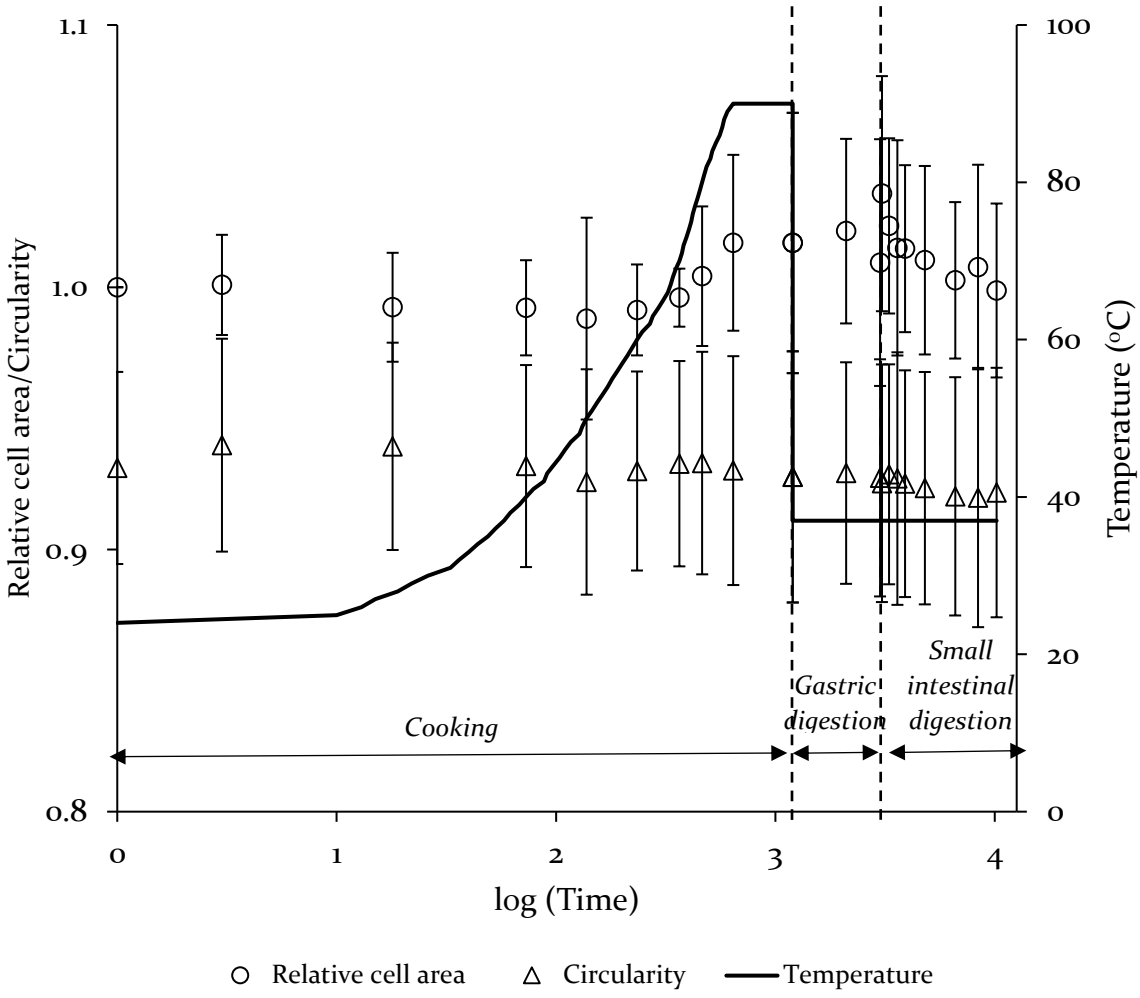

Fig. 6.5. The change in relative area and circularity of cotyledon cells (n=11) during three sequential stages of cooking, gastric digestion, and small intestinal digestion. Time is plotted on a logarithmic scale. Error bars represent the standard deviation.

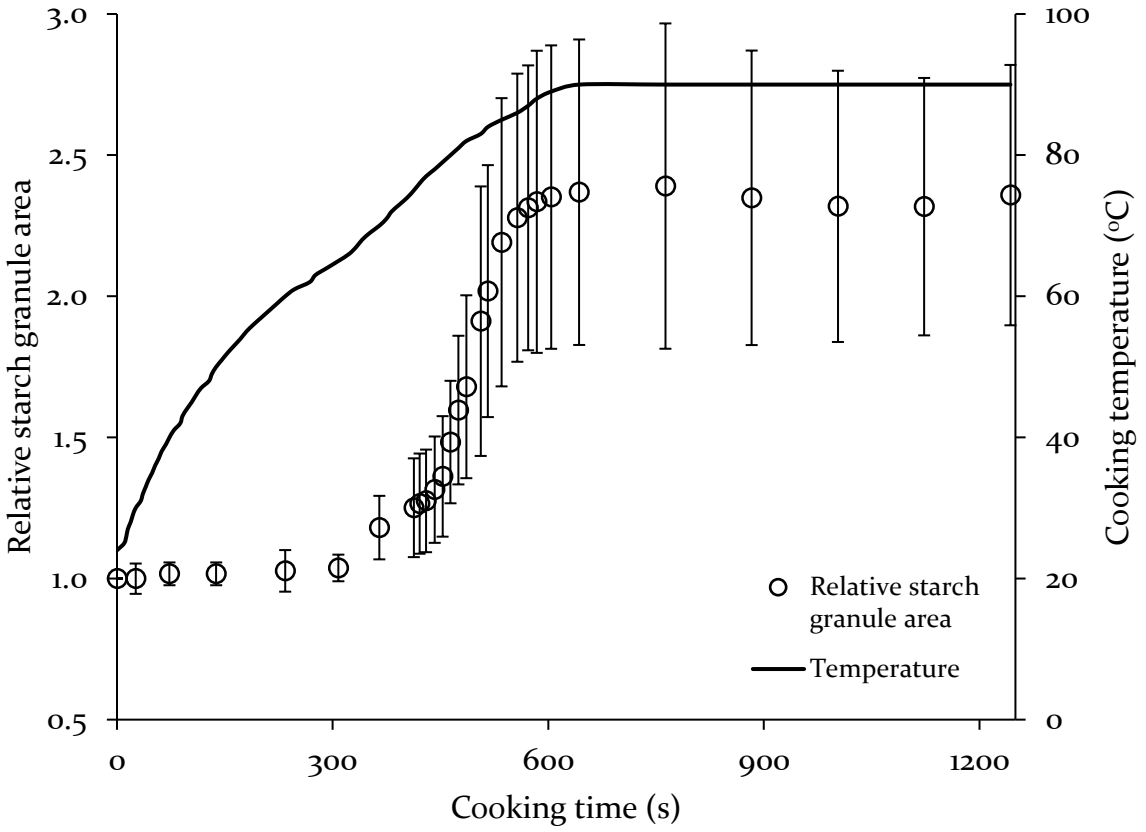

Fig. 6.6. The change in relative area of starch granules (n=9) inside cotyledon cells during cooking. Error bars represent the standard deviation.

The microscopic examination in conjunction with image analysis provides evidence for the maintenance of cellular integrity throughout cooking at 90°C. Furthermore, time-lapse visualisation of IS and ES during cooking supports previous suggestions that the swelling and gelatinisation in the presence of excess water is suppressed in IS, but not in ES (Do *et al.*, 2019; Fujimura & Kugimiya, 1994). In fact, the physical encapsulation of multiple starch granules by the intact cell wall and protein matrix may restrict water availability and free space volume inside the cell that are necessary conditions for granule hydration and swelling, resulting in only partial gelatinisation of IS. As a side note, the distorted "buckle-saddle" granule shape observed here is a distinctive feature in starch trapped inside

cells of legume tissues that undergo hydrothermal processing (Edwards *et al.*, 2015; Hahn *et al.*, 1977).

6.5.2. Simulated gastric digestion of cotyledon cells

The cotyledon cells, immediately following cooking, were subjected to simulated gastric digestion. Fig. 6.7 shows a sequence of representative images at various digestion times (see also supplementary video). As can be clearly seen, the cells did not shift during the transition from cooking (Fig. 6.4) to and throughout gastric digestion (Fig. 6.7), which shows that the flow was slow enough to prevent undesirable cell movement that could interfere with imaging.

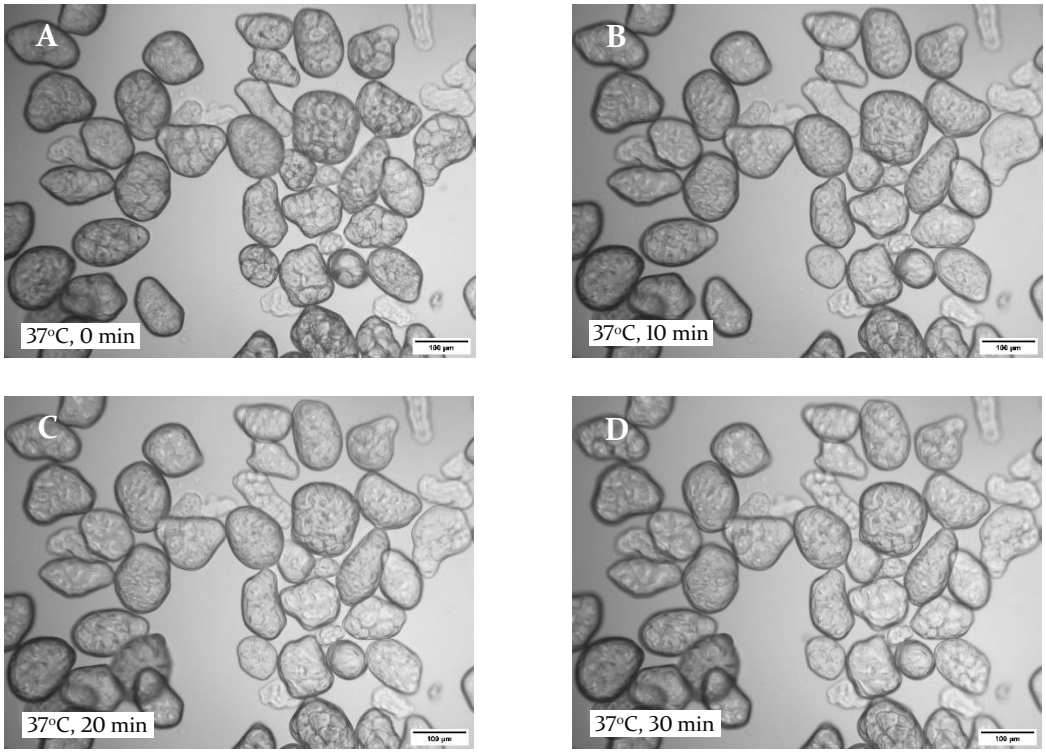

Fig. 6.7. Representative light photomicrographs of navy bean cotyledon cells, taken from a time-lapse imaging sequence of the gastric digestion by pepsin at 37°C and pH ~1.2 for 30 min: (A) 0 min; (B) 10 min; (C) 20 min; (D) 30 min.

During the 30 min of the gastric digestion, no apparent changes in the gelatinised starch were observed (Fig. 6.7). This was expected because of the absence of starch-

hydrolysing enzymes in the gastric fluid, meaning that both IS and ES remained virtually unaffected in the gastric environment (Do *et al.*, 2019). On the other hand, the cells became noticeably more translucent during the first several minutes of this phase of digestion. This can be explained by recalling that protein coexists with starch inside the cells and is susceptible to proteolysis by gastric pepsin. It has also been hypothesized that the acidic environment in the stomach can induce structural and physicochemical changes in the cell wall, e.g., cell wall swelling and the acid hydrolysis of glycosidic or ester linkages; the possible consequence being an increase in cell wall permeability (Capuano, 2017). However, the resolution of the microscopy employed in this work was insufficient to visualise such changes.

6.5.3. Simulated small intestinal digestion of cotyledon cells

Following gastric digestion, small intestinal digestion of the cells was simulated. A time series of representative images are presented in Fig. 6.8 (see also supplementary video).

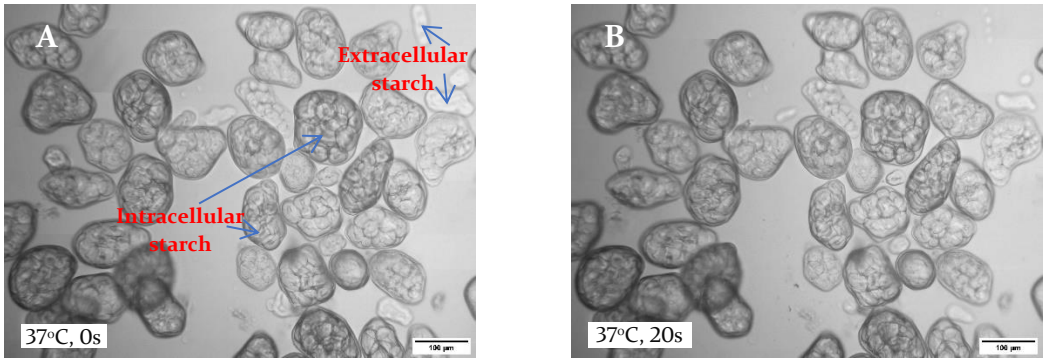

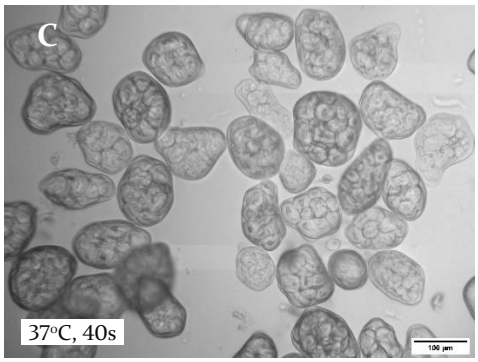
C
37°C, 40s

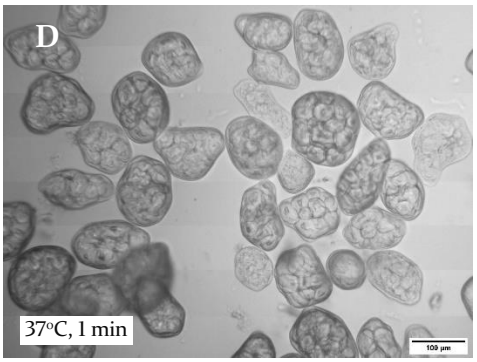
D
37°C, 1 min

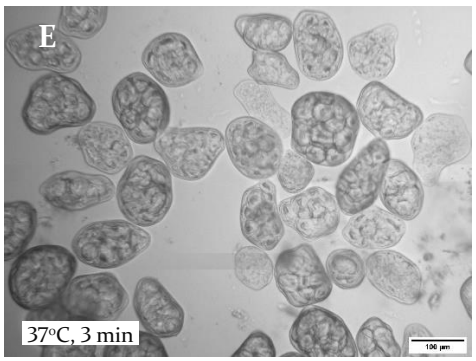
E
37°C, 3 min

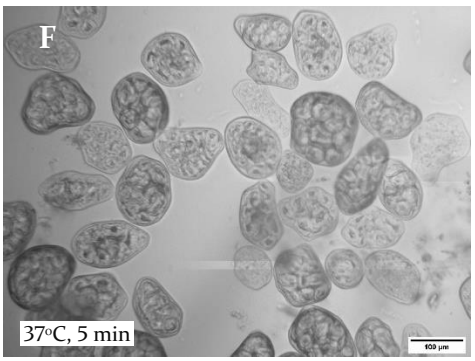
F
37°C, 5 min

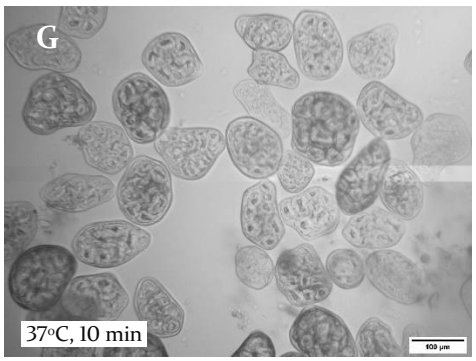
G
37°C, 10 min

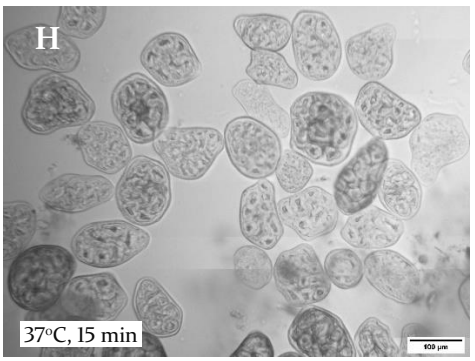
H
37°C, 15 min

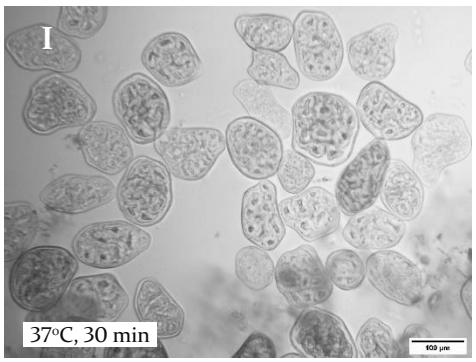
I
37°C, 30 min

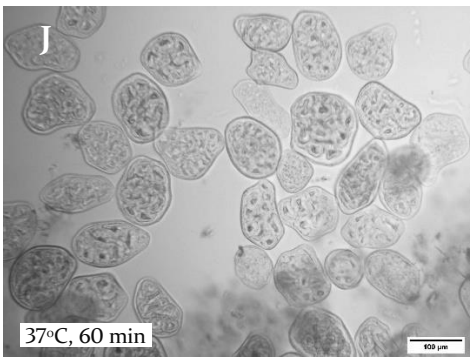
J
37°C, 60 min

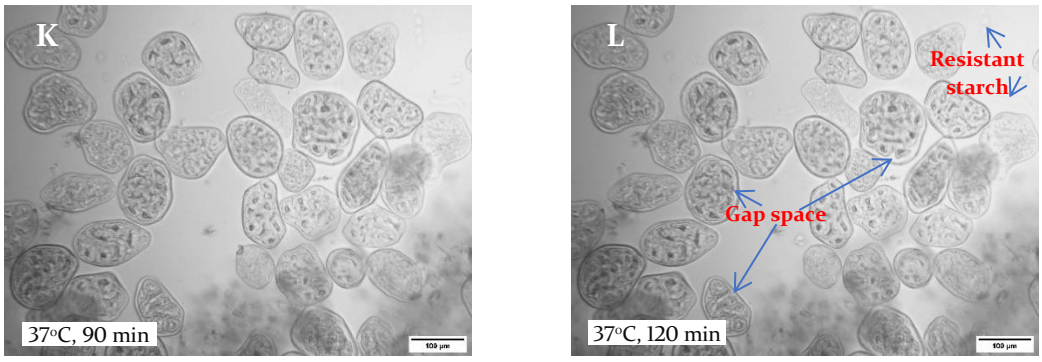

Fig. 6.8. Representative light photomicrographs of navy bean cotyledon cells, taken from a time-lapse imaging sequence of the small intestinal digestion by pancreatin at 37°C and pH ~ 6.8 for 120 min: (A) 0s; (B) 20s; (C) 40s; (D) 1 min; (E) 3 min; (F) 5 min; (G) 10 min; (H) 15 min; (I) 30 min; (J) 60 min; (K) 90 min; (L) 120 min.

The cells exhibited no visual evidence of cellular disruption (rupture/disintegration) for the entire duration of the small intestinal digestion (Fig. 6.8), which is consistent with the data in Fig. 6.5. In contrast, distinct visual changes in ES and IS were observed. Specifically, ES granule ghosts began to immediately "shrink" in size (Fig. 6.8B) and largely disappeared after 40 seconds (Fig. 6.8C). Complete disappearance of these ghosts with only traces of starch remnants was observed after 1 min (Fig. 6.8D). These remnants of starch (marked in Fig. 6.8L) persisted until the end of 120 min digestion and may be classified as "resistant starch" as defined by Englyst, Kingman, and Cummings (1992). The disappearance of starch indicates starch hydrolysis by pancreatic α-amylase and can be used to quantify the kinetics of this process. Further, because we are tracking individual cells and ghost particles, the kinetic parameters of starch digestion can be quantified on the single particle scale.

Similar to ES, IS was also observed to visually "shrink" inside the cells; however, in this case the process was radially inward towards the centre of each cell rather than towards the centre of each granule ghost. Virtually all the ES ghost particles had

disappeared before the start of IS digestions in most cells (Figs. 6.8A–C), which shows that ES is generally digested more rapidly than IS and supports the findings of Do *et al.* (2019). As the digestion advanced, the cells became progressively emptier over time (Figs. 6.8D–L) with the reappearance of an empty "gap space" (marked in Fig. 6.8L) between the cellular contents and the peripheral cell walls. This proves that the majority of starch digestion occurs inside the cells confirming previous observations pertaining to the intracellular starch hydrolysis of cotyledon cells (Do *et al.*, 2019; Rovalino-Córdova *et al.*, 2018; Pallares *et al.*, 2018a).

For the analysis, several cells from two different experiments were randomly selected for monitoring the "shrinkage" of their contents over time. The outlines of the cellular contents were manually traced using the ImageJ polygonal selection tool and the projected area (A) was converted to an equivalent spherical radius ($R = \sqrt{A/\pi}$) with the resulting data shown in Figs. 6.9 A–D.

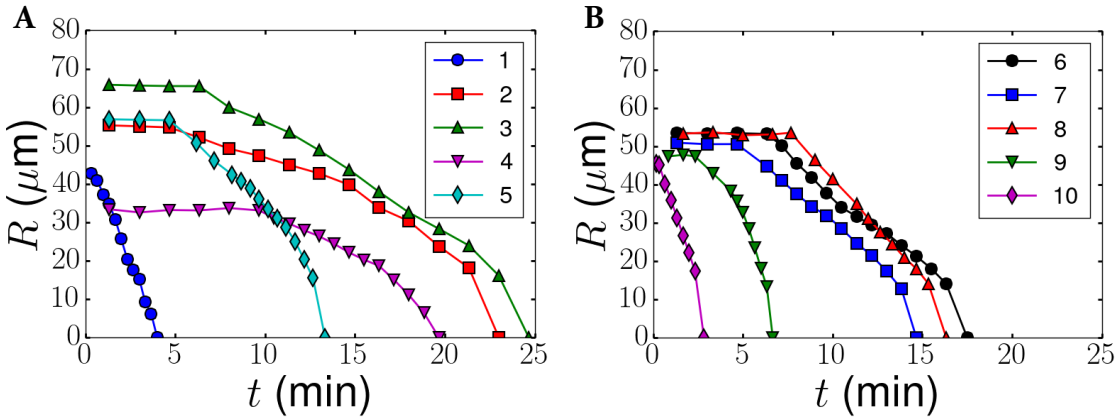

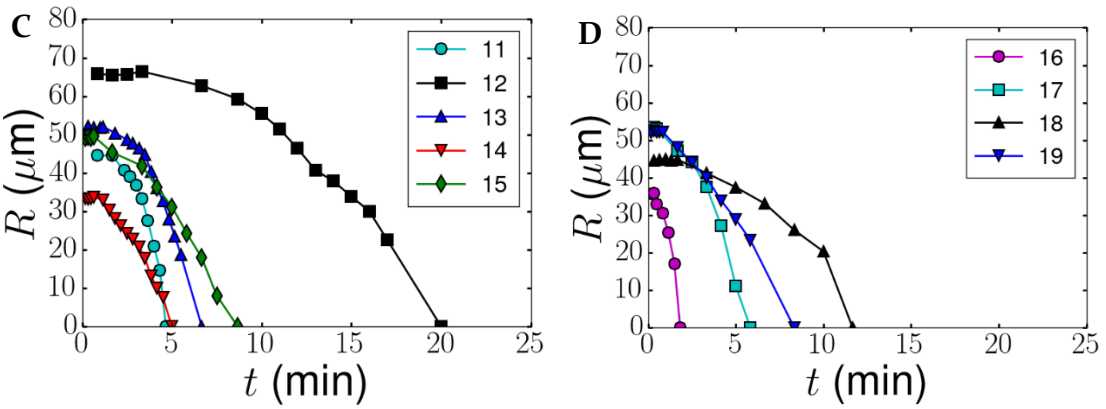

Fig. 6.9. The change in equivalent spherical radius of cellular contents in cotyledon cells (n = 19) during the small intestinal digestion by pancreatin at pH 6.8 and 37°C: (A) Cells #1–5; (B) Cells #6–10; (C) Cells #11–15; (D) Cells #16–19. The lines connecting the symbols are meant to guide the eye.

The observed radial inward progression of the "shrinking core" can be mathematically modelled by the convection-diffusion equation for mass transport in which enzyme is convected in the fluid flowing through the ParCS chamber to the cell wall where it diffuses through the cell wall to digest the starch. Following this, lower-molecular-weight digestion products (e.g., dextrins) diffuse out of the cell and are convected away in the flow. Therefore, by employing this model to fit the data, we can quantify the physical parameters of the material. The development of this model is presented as follows. First, we write a mass balance for the starch assuming a spherical particle (as in the well-known "shrinking core" model):

$$\frac{d}{dt}\left(\rho\phi\frac{4\pi}{3}R^3\right) = -4\pi R^2 v \tag{6.3}$$

where R is the starch core radius, ρ is the density of the starch, ϕ is the volume fraction of the starch within the core (assumed homogeneously distributed), and v is the reaction rate for starch digestion. After rearrangement this reduces to:

$$\frac{dR}{dt} = -\frac{v}{\rho\phi} \tag{6.4}$$

Next, we assume a Michaelis-Menten reaction rate for an enzyme with a single substrate and a single rate-limiting step which gives us:

$$v = k_c E(t) \frac{S(t)}{k_M + S(t)} \tag{6.5}$$

where k_c is the reaction rate constant, $E(t)$ is the time-dependent enzyme concentration at the surface of the starch core, $S(t)$ is the starch concentration at the surface of the core (where the reaction is taking place), and k_M is the starch concentration at which the reaction rate is half of the maximum rate. Assuming that the enzyme concentration at the surface is initially zero and increasing with time according to the convection-diffusion equation, we propose the following model for the enzyme concentration:

$$E(t) = E_0 \left(1 - \exp\left[-\frac{t}{t_c} \right] \right) \tag{6.6}$$

where E_0 is the enzyme concentration in the well-mixed solution outside the cell, t_c is the time constant associated with diffusion through the cell wall and is related to the diffusion length l_c and diffusivity D by $t_c = l_c^2/D$. This equation represents the first term in the infinite series that is the exact solution of the convection-diffusion equation in spherical coordinates. It can be found in standard textbooks on mass transport that this equation is accurate for $t > 0.2t_c$ and that the constants C_1 and C_2 depend only on the geometry (Bergman, Lavine, Incropera, & DeWitt, 2017). In this case, we assume that $C_1 = C_2 = 1$. Assuming that $C_2 = 1$ is consistent with treating the cell wall as a thin shell such that the local curvature of the cell wall is negligible and assuming a large Biot number. Assuming that $C_1 = 1$ is more ad hoc in nature, but is required to preserve the correct initial condition for the

enzyme concentration and avoid non-physical values at early times (where additional terms in the infinite series are normally required). Nevertheless, since the cell is not a completely homogeneous material and may have different rates of diffusion through the cell wall and intracellular matrix, we have chosen to make this convenient simplifying assumption for this initial analysis. Note that while we assume that Biot number is large in this case (diffusive resistance inside the cell, rather than convective resistance outside the cell, is the rate-limiting step), the functional form of equation 6.6 would not change for other values of the Biot number; only the values of C_1 and C_2 would change (Bergman *et al.*, 2017).

Because of the high concentration of starch in the cell we can assume that $k_M << S(t)$ and then combine the previous three equations to give:

$$\frac{dR}{dt} = -K\left(1 - \exp\left[-\frac{t}{t_c}\right]\right); \qquad K = \frac{k_c E_0}{\rho\phi} \tag{6.7}$$

which can be integrated using the initial condition $R(0) = R_0$ to give:

$$R(t) = R_0 + Kt_c\left(1 - \exp\left[-\frac{t}{t_c}\right]\right) - Kt \tag{6.8}$$

This model has three parameters R_0, K, and t_c (each of which has a specific physical meaning) that can either be estimated from other data or determined by fitting them to our digestion data. However, before fitting the data there are some important considerations when using this model that are revealed by non-dimensionalizing the equation as follows:

$$\rho(\tau) = 1 + \frac{Kt_c}{R_0}(1 - \exp[-\tau] - \tau); \qquad \rho = \frac{R}{R_0}; \qquad \tau = \frac{t}{t_c} \tag{6.9}$$

Using this form, we can consider the two limiting cases where $\tau \ll 1$ and $\tau \gg 1$, which will occur when the total time for digestion of the cellular contents to be completed is either much smaller or much larger than the time scale for diffusion.

For this we have:

$$\rho \approx 1 - \frac{Kt_c}{R_0}\tau; \qquad \tau \gg 1 \tag{6.10}$$

$$\rho \approx 1 - \frac{Kt_c}{2R_0}\tau^2; \qquad \tau \ll 1 \tag{6.11}$$

which can then be transformed back into dimensional form:

$$R \approx R_0 - Kt; \qquad \tau \gg 1 \tag{6.12}$$

$$R \approx R_0 - \frac{K}{2t_c}t^2; \qquad \tau \ll 1 \tag{6.13}$$

In both cases the result is a reduction in the number of independent parameters in the model. Therefore, when fitting the data it will only be possible to determine all three parameters separately when $\tau = O(1)$ for the majority of the experiment. In the former case, we cannot determine the time scale for diffusion, which makes sense because diffusion is so fast that we would not observe its effects and the radius of the particle will decrease linearly. In the latter case, we can only determine the ratio between the reaction rate parameter and the diffusion time constant. This also makes sense when one considers that no reaction takes place until at least some enzyme has diffused into the cell and then the rate will speed up in proportion to how fast the reaction occurs relative to how fast more enzyme diffuses in.

In our data we observed all three regimes, though most of the data falls into the category where diffusion is slow ($\tau \ll 1$). To illustrate this, Fig. 6.10 shows data for three representative cells each fit to all three versions of the model. Best model fits for all of the cells can be found in the Appendix A1. For cell #1 the fit using the linear model is the best, while the quadratic model fits poorly. This suggests that diffusion of enzyme into the cell was very rapid, which may be due to the presence of a rupture in the cell wall or a high degree of cell wall permeability. For cell #19 the quadratic model fits quite well, while the linear model fits poorly, suggesting that diffusion is quite slow for this cell. For cell #12 neither of the models for the limiting cases fits the data well, but the complete model using all three parameters produces a good fit. It is worth noting that while the complete model also visually produces a good fit for cells #1 and #19, the numerical values of the diffusion time constant and reaction rate parameter in this case will not be physically meaningful because the values are no longer independent (and will not result in unique values of parameters). The quality of the fits shown in Fig. 6.10 are representative of the fits for the remaining cells and the resulting values of the fitted parameters are reported in Table 6.1. It is important to note that the calculated values for digestion rate constants in previous studies (Pallares *et al.*, 2018a; Dhital *et al.*, 2016) were reported for a mixed cell population and assuming an empirical model, whereas the present results are based on a model derived from first principles and can be directly related to standard material parameters. The fitted parameters for individual cells can then be used to compute statistics for the distribution of rate constants for a particular system.

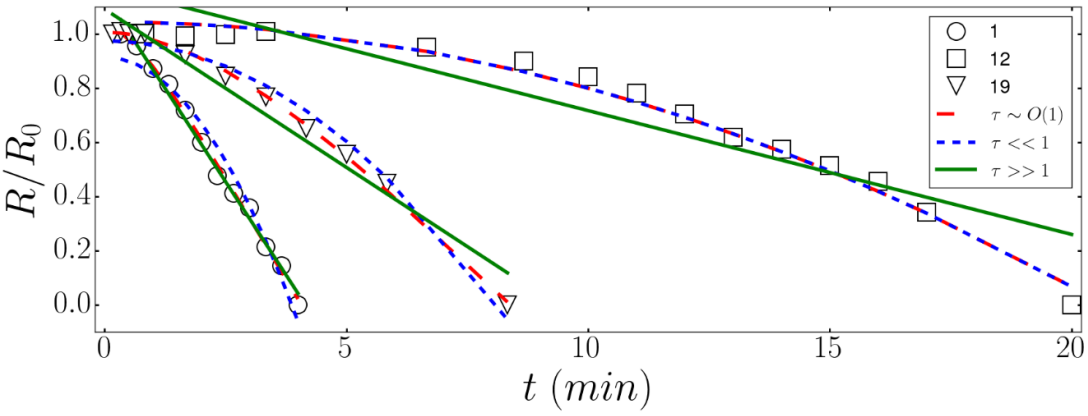

Fig. 6.10. Kinetic fits of "shrinking core" data to three versions ($\tau << 1$, $\tau >> 1$, and $\tau \sim O(1)$) of the digestion rate model for three representative cotyledon cells (#1, 12 and 19).

Table 6.1. Kinetic parameters of the "shrinking" of cellular contents inside cotyledon cells (n = 19) estimated from the digestion rate model.

Cell #	$t_{experiment}$ (min)	R_0 (um)	K (um/min)	t_c (min)	K/t_c (um/min^2)	Best model
1	4.00	49	11.8	-	-	$\tau >> 1$
2	23.00	57	-	-	0.18	$\tau << 1$
3	24.67	67	-	-	0.21	$\tau << 1$
4	19.67	38	-	-	0.16	$\tau << 1$
5	13.33	62	-	-	0.58	$\tau << 1$
6	17.50	56	-	-	0.34	$\tau << 1$
7	14.67	53	-	-	0.45	$\tau << 1$
8	16.33	60	-	-	0.40	$\tau << 1$
9	6.67	53	-	-	1.98	$\tau << 1$
10	2.83	44	33.9	2.2	-	$\tau \sim O(1)$
11	4.67	52	-	-	4.04	$\tau << 1$
12	20.00	69	-	-	0.32	$\tau << 1$
13	6.67	55	-	-	2.35	$\tau << 1$
14	5.00	34	56.0	19.5	-	$\tau \sim O(1)$
15	8.67	49	17.4	9.8	-	$\tau \sim O(1)$
16	1.83	37	-	-	20.43	$\tau << 1$
17	5.83	53	-	-	3.18	$\tau << 1$
18	11.67	45	-	-	0.60	$\tau << 1$
19	8.33	52	9.6	3.2	-	$\tau \sim O(1)$

The remaining material inside the cells after the cores have stopped shrinking (Fig. 6.8L) is likely to consist of undigested residues of RS and/or protein. However, it is not possible to verify the composition or precisely quantify the amount of the remaining material by simple image analysis. Selective staining of cells with iodine could be employed to detect IS because the blue-black colour intensity of the amylose-iodine complex is proportional to the amount of starch present in the cell. This could provide an alternative way to quantitatively measure the percentage of starch hydrolysis at any given time. Initial testing of this technique was performed, but will require additional work to refine the technique and produce quantitative results. For example, the thermal instability of the complex due to the dissociation of iodine from the amylose helix at the temperature above 15°C (Fonslick & Khan, 1989) poses a significant challenge for adopting this method for quantification of amylolysis.

Overall, we have shown that the digestion rates of IS vary among individual cells. Inadequate mixing inside the chamber could cause differing amounts of pancreatic α-amylase to diffuse into different cells. However, the flow circulation employed here is expected to minimize these effects and overcome the limitations of mixing methods used by other researchers (Bordoloi *et al.*, 2012b; Patton *et al.*, 1985), which involved manually placing drops of digestive fluids on microscopic slides and vigorously mixing them with samples using a pipette. This leads us to hypothesize that the different rates of amylolysis could be attributed to microstructural and compositional differences among cells within the cohort.

Cells vary in shape, size, and number of starch granules (see above analysis in section 6.4.5). Larger-sized cells contain more starch, which generally takes longer time to digest. In addition, different cells appear to contain varying amounts of available water and intracellular space, which are required for granule swelling and gelatinisation inside cells. As a consequence, starch granules inside different cells may undergo gelatinisation to different extents during cooking. According to Holm, Lundquist, Björck, Eliasson, and Asp (1988), the rate of *in vitro* starch digestion by α-amylase is positively correlated to the degree of starch gelatinisation. Therefore, starches inside cells with a greater degree of gelatinisation tend to be more susceptible to α-amylase attack and degraded more rapidly and/or to a larger extent. Furthermore, differences in permeability characteristics of the cell wall and intracellular matrix may result in the three different observed regimes of enzyme diffusion into the cell (Fig. 6.10 and Table 6.1), leading to the variation in amylolysis rates among individual cells.

It is worth noting that the enzyme/substrate (starch) ratio could play a role in influencing the susceptibility of starch towards hydrolysis by pancreatic α-amylase. Due to a very small sample size, the ratio employed in the present study was much higher compared to those used in previous reports (Do *et al.*, 2019, Rovalino-Córdova *et al.*, 2018) for *in vitro* starch digestion. This higher ratio could have resulted in a higher amount of α-amylase to diffuse into the cells, therefore leading to increased susceptibility of starch to amylolytic attack as well as higher amylolysis rate.

6.5.4. Significance of findings

The results of the present study have led to new insights into the role of cell wall encapsulation in regulating starch digestion *in vitro*. The absence of cell wall degrading enzymes secreted into the human upper GI tract results in cell wall stability, thereby providing protection for entrapped nutrients such as starch from enzymatic degradation in the gut environment (Do *et al.*, 2018). The cell wall acts as a physical barrier hindering starch granule swelling, gelatinisation during cooking and retarding the accessibility of α-amylase to IS during the small intestinal digestion. Therefore, incompletely-gelatinised, encapsulated starches (IS) become less physically accessible to α-amylase and more resistant to amylolysis compared to fully-gelatinised, non-encapsulated starches (ES).

Our results also support the mechanism driving α-amylase digestion of starch in cotyledon cells previously proposed by Do *et al.* (2019) and Pallares *et al.* (2018a). Specifically, it was proposed that amylolysis is a slow process that occurs intracellularly and can involve several events, including diffusion of α-amylase into the cell interior through the cell wall, amylase binding to starch, amylase-catalysed starch hydrolysis from the periphery towards the centre of the cell, and outflow of digestion products.

Finally, we have developed a mathematical model for kinetics of starch hydrolysis in cotyledon cells and quantitatively demonstrated for the first time that the rate of amylolysis varies on a single-cell basis. In fact, previous studies (Dhital *et al.*, 2016; Do *et al.*, 2019) have solely focused on the group (cell population) effects on the starch gelatinisation and digestion properties, and in doing so, disregard the

within-group (individual cells) effects. In this study, tracking of single cells enables researchers to observe them as separate entities independently of each other, as well as to assess the heterogeneity of their digestion characteristics as it pertains to the cell population.

6.6. Conclusions

This study has introduced a microscopic imaging technique for real-time visualisation of the dynamic behaviour of trapped starch granules in a cohort of legume cotyledon cells under cooking and *in vitro* digestion conditions that can be simulated in one continuous process. Using the ParCS apparatus, various extracellular factors can be controlled, including time, temperature, pH, enzyme concentration, and volume of digestive fluids. The results in the present study confirm and complement those of previous studies, and open an avenue for new insights into the limited gelatinisation and digestion of starch inside plant cells.

A novel aspect of this technique is the generation of data and information at the single-cell scale, which would not otherwise be obtained using conventional *in vitro* digestion models, to aid mechanistic understanding and kinetic modelling of the starch digestion process. For example, transient intermediate stages of cooking (swelling of starch granules) and digestion ("shrinkage" of starch core) were directly captured with video imaging. We were then able to use the "shrinking core" data to develop and validate a first-principles model that describes the starch digestion for individual cells. Further, the technique provides an orthogonal method for studying food digestion that can be compared to existing *in vitro* and *in vivo* methods, hence enabling development and validation of digestion models.

Finally, the development of a more sophisticated version of the ParCS apparatus is currently underway. Future research opportunities in this area could expand to the use of CLSM and fluorescence labelling of α-amylase for tracking the location of the enzyme relative to starch/cells throughout the course of digestion or the utilisation of polarised light microscopy for monitoring the disappearance of starch granule birefringence during cooking.

CHAPTER SEVEN: Designing starch-entrapped food particles for reduced glycaemic impact

7.1. Abstract

Previous research has revealed that the entrapment of starch granules in legume cotyledon cells slows down the rate and extent of starch digestion. In the present study, we explored the biomimetic design of starch-entrapped particles inspired by the natural cotyledon cell structure for reduced glycaemic impact. Beads were formed by ionotropic gelation of pectin via calcium cross-linking in the presence of native corn starch. Dried beads were milled to obtain a range of particle size fractions. Results showed that starch encapsulated in the pectin matrix exhibited significantly higher gelatinisation transition temperatures and lower peak paste viscosities compared with non-encapsulated starch. Particle size did not affect DSC gelatinisation behaviours, but affected RVA pasting properties and *in vitro* digestion kinetics. The digestion rate and extent of entrapped starch was reduced with increasing particle size due to hindering effect of the pectin matrix on α-amylase access. It is expected that this work will help inform the design of novel food ingredients containing SDS and/or RS that can provide beneficial health benefits.

7.2. Introduction

The global epidemic of diabetes continues to grow and presents a substantial economic and health-care burden to society. The prevention and management of diabetes can be achieved through nutritional interventions designed to improve

glycaemic control (Ley, Hamdy, Mohan, & Hu, 2014). For this reason, reducing overall glycaemic impact of the diet has become the priority for the food industry. One approach to this is the design of novel foods for slowing down digestion of starch – a major source of glycaemic carbohydrate in the human diet.

Mimicking natural food structures is a novel strategy for rational food design that is worth exploring. Nature with its remarkable diversity never ceases to amaze scientists. Diverse structures and functions found in nature provide seemingly endless ideas for biomimetic design. A great deal of attention in the last three years has been drawn towards the behaviours of starch granules trapped in legume cotyledon cells during cooking and *in vitro* digestion, and the role of the cell structure in modulating starch digestion. Recent studies have provided convincing evidence for the barrier properties of intact cell walls in limiting access of α-amylase to entrapped starch, thus slowing down the rate and extent of glucose release during amylolysis (Do *et al.*, 2019; Dhital *et al.*, 2016). Such findings present an opportunity for the biomimetic design of starch-entrapped particles inspired by cotyledon cells for reduced glycaemic impact.

Previous studies have shown that the entrapment of native starch granules within calcium-cross-linked alginate matrix results in particles with slow starch digestion profile and reduced postprandial glycaemic response in healthy humans (Venkatachalam *et al.*, 2009; Luo & Zhang, 2018). In addition, starch-entrapped particles may be capable of delivering slowly fermentable carbohydrate to the colon with potentially beneficial influence on the gut microbiota (Rose *et al.*, 2009). Further, *in vivo* studies have shown that these particles can decrease gastric

emptying rate in humans when ingested before meals (Cisse *et al.*, 2017), and exhibit an anti-obesity effect on body weight gain of obese mice when incorporated into high-fat diet (Luo, Wang, & Zhang, 2018).

In the present study, we apply the principle of plant cell wall entrapment of starch granules to the design of starch-entrapped particles. To mimic the cellular structure, pectin – a major component and a complex polysaccharide in the plant cell wall – was used due to its ability to form stable gels in the presence of divalent cations (e.g. Ca^{2+}). Calcium pectinate gel beads have been successfully used for controlled release drug delivery (Sriamornsak & Nunthanid, 1998; Wong, Colombo, & Sonvico, 2011). However, very little is known about the pectin entrapment of starch for controlled release of glucose. It is possible that pectin particles could slow down starch digestion *in vitro* in a similar manner to alginate particles (Venkatachalam *et al.*, 2009). Effect of particle size on kinetics of starch digestion was also investigated. The findings from this study will provide critical information for design optimisation of pectin particles.

7.3. Materials and Methods

7.3.1. Materials

Unmodified regular starch from corn (S-4126) was purchased from Sigma – Aldrich Ltd, St Louis, USA. Corn starch (CS) contains approximately 73% amylopectin and 27% amylose according to manufacturer's specifications. Amidated apple pectin (Amid AF 005-A, Degree of Esterification (DE) 32-38%, Degree of Amidation (DA) 8-12%) was kindly supplied free of charge by Hawkins Watts, Auckland, New

Zealand. *Alpha*-amylase (porcine pancreas, type VI-B) and invertase (from baker's yeast (*S. cerevisiae*), Grade VII, ≥ 300 units/mg solid) were purchased from Sigma – Aldrich Ltd, St Louis, USA. All other chemicals and reagents were of analytical grade. Reverse osmosis (RO) water was used for all experiments.

7.3.2. Preparation of starch-entrapped particles

Pectin solution (3%, w/v) was prepared by dissolving pectin (15 g) in RO water (500 mL) at 70°C for 1 h under continuous magnetic stirring and subsequently cooled to room temperature. Raw CS (45 g) was uniformly dispersed in the pectin solution under constant stirring using a stirrer (IKA overhead digital stirrer, Germany) at 1000 rpm for 5 min. The resultant dispersion was extruded drop-wise through a 1.2-mm diameter needle into a bath of calcium chloride ($CaCl_2$) solution (2%, w/v) at room temperature under gentle magnetic stirring. The beads formed were kept in the $CaCl_2$ solution for 2 h and then collected by filtration. The beads were washed several times with RO water and dried in a hot-air oven at 45°C for 12 h.

The dried beads were milled using a coffee grinder and the milled materials were segregated by size using vertical multiple sieving under gravity with mechanical agitation using an Electrolab electromagnetic sieve shaker. Three sieve sizes (1, 0.5, and 0.25 mm) were selected to give a broad spectrum of particle size fractions ranging from 1 mm to 0.25 mm that represent those present in the bolus post-mastication of edible plant tissues (Edwards, Maillot, Parker, & Warren, 2018). These particle sizes were also chosen to be reasonably small for practical incorporation into foods.

7.3.3. Determination of moisture and total starch contents

Moisture content was determined gravimetrically by drying the samples in an oven at 105°C to a constant weight. Total starch content was analysed using Total Starch Assay (K-TSTA, Megazyme International Ireland Ltd., Ireland) using the method for cereal products not containing RS, D-glucose and/or maltodextrins (all incubations at pH 5.0) and following the instructions given by the manufacturer.

7.3.4. Determination of thermal properties

Thermal properties were analysed using a Differential Scanning Calorimeter (DSC, TA Q100, TA Instruments, Newcastle, DE) according to the method described in section 3.3.7, but with a starch:water ratio of 1:3 (w/w) to ensure excess water for starch gelatinisation and a heating rate of 5 °C/min.

7.3.5. Determination of pasting properties

Pasting properties were evaluated using a Rapid Visco Analyser (RVA 4500, Perten Instruments) according to the method described in section 3.3.8.

7.3.6. In vitro *starch digestion*

7.3.6.1. Static starch digestion protocol

Starch digestibility was determined based on a modified version of the *in vitro* starch digestion protocol described by Ezeogu *et al.* (2005). Samples equivalent to 100 mg starch (dwb) were accurately weighed and transferred into capped glass bottles. The samples were suspended in 5 mL distilled water and cooked in a water

bath at 90°C for 30 min with intermittent mixing by vigorously shaking the bottles by hand, thus facilitating complete dispersion and gelatinisation of starch granules. Following cooking the samples were allowed to equilibrate at 37°C in a water bath. Contents of each bottle were then combined with 5 mL porcine pancreatic α-amylase in 0.05M Tris-maleate buffer (50 *mM* maleic acid, 50 *mM* Tris-(hydroxymethyl)aminomethane, pH 6.9, pre-warmed to 37°C) to achieve a final enzyme concentration of 2 U/mL of digestion mixture. One unit of α-amylase activity (1 U) is defined as the amount of enzyme required to liberate 1 mg maltose from starch in 3 min at pH 6.9 and 37°C (Edwards *et al.*, 2018). The bottles were mixed vigorously before being placed in a water bath and horizontally shaken at 120 strokes/min and 37°C for 120 min.

7.3.6.2. Glucose measurement

Duplicate samples (0.1 mL) were withdrawn at 1, 3, 5, 8, 10, 15, 30, 45, 60, 90, and 120 min and immediately mixed in 0.4 mL of absolute ethanol to inactivate the enzyme. The resulting mixtures were vortex-mixed and centrifuged at 1800 *x g* for 10 min. Ethanolic supernatants (0.1 mL) were incubated with 0.5 mL amyloglucosidase and invertase in acetate buffer (0.1 mL amyloglucosidase and 3.75 mg invertase per 10 mL acetate buffer) at pH 5.2 and 37°C for 10 min to completely digest soluble dextrins (i.e. produced during enzymatic hydrolysis of starch) in the supernatant to glucose. The concentration of glucose was then quantified using a D-glucose assay kit (GOPOD-FORMAT, K-GLUC, Megazyme International Ireland Ltd., Ireland).

7.3.6.3. Modelling starch digestograms

Kinetics of starch digestion can be described by the non-linear model according to Goñi, Garcia-Alonso, and Saura-Calixto (1997). Starch hydrolysis data can be fitted to a first-order equation (Eq. (7.1)):

$$C_t = C_\infty(1 - e^{-kt}) \tag{7.1}$$

where C_t is the percentage of starch hydrolysed at a given time (t), C_∞ is the percentage of starch hydrolysed at the end of the reaction (after 120 min), k is the pseudo-first order rate constant of digestion (min^{-1}), and t is the time (min).

For ease of plotting, this equation can be expressed in logarithmic form (Eq. (7.2)):

$$ln\left[\frac{(C_\infty - C_t)}{C_\infty}\right] = -kt \tag{7.2}$$

This gives a linear plot of $\ln[(C_\infty - C_t)/C_\infty]$ against t, and the rate constant is calculated from the slope ($-k$).

7.4. Results and Discussion

7.4.1. Material characteristics

The total starch content of native CS and milled fractions of CS-entrapped particles was 92.2 ± 1.0 and 67.4 ± 0.9 (w/w, dwb), respectively. The moisture content of these two materials was 8.5 ± 1.5 and 11.1 ± 0.1 (w/w), respectively.

7.4.2. Thermal properties

Fig. 7.1 shows representative DSC thermograms for native CS and different size fractions of CS-entrapped particles. All samples exhibited single endothermic

transitions related to gelatinisation during heating in excess water. Gelatinisation parameters are shown in Table 7.1. CS showed a single, narrow endotherm with an onset temperature of 64.6°C, a peak at 68.9°C, a conclusion temperature of 72.9°C, and a gelatinisation enthalpy of 15.4 ± 0.1 $J.g^{-1}$ dry starch. These results are consistent with those of previous reports (Sandhu & Singh, 2007; Singh *et al.*, 2003). On the other hand, CS trapped inside the pectin matrix showed a broader endotherm and significantly higher values for T_o, T_p, and T_c than those of native CS. A possible reason for the observed delay in gelatinisation is the physical encapsulation of multiple CS by pectin. This may impose restrictions on water availability and free space within the pectin matrix, thus resulting in limited starch-water interactions and delayed breakdown of starch ordered structures. This is similar to the previously reported delay in gelatinisation caused by the plant cell wall entrapment of starch (Do *et al.*, 2019; Fujimura & Kugimiya, 1993, 1994; Fujimura *et al.*, 1995).

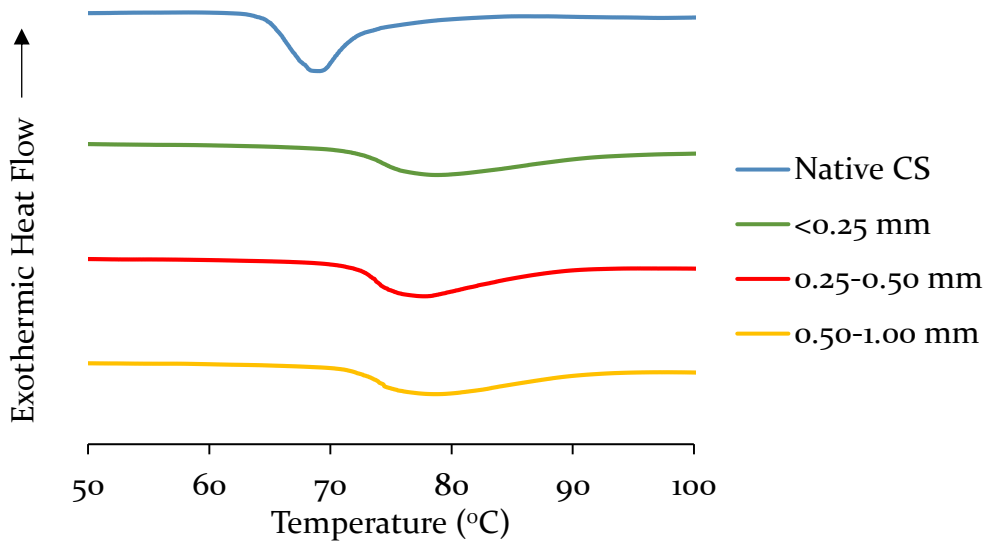

Fig. 7.1. Representative DSC thermograms obtained for native CS and different size fractions of CS-entrapped particles.

Table 7.1. DSC gelatinisation parameters of native CS and different size fractions of CS-entrapped particles.

Samples	T_o (°C)	T_p (°C)	T_c (°C)	ΔH_{gel} (J.g^{-1})
Native CS	64.6 ± 0.1^b	68.9 ± 0.2^b	72.9 ± 0.1^c	15.4 ± 0.1^a
<0.25 mm	71.7 ± 0.2^a	78.2 ± 0.2^a	93.1 ± 0.3^a	15.3 ± 0.5^a
0.25-0.50 mm	71.9 ± 0.2^a	77.3 ± 0.3^a	88.0 ± 1.2^b	15.3 ± 0.3^a
0.50-1.00 mm	72.0 ± 0.0^a	78.5 ± 0.7^a	91.8 ± 1.3^a	15.1 ± 0.2^a

T_o, onset temperature; T_p, peak temperature; T_c, conclusion temperature; ΔH_{gel}, enthalpy of gelatinization (J.g^{-1} of starch on dwb). Values with the same subscripts in a column do not differ significantly ($p > 0.05$).

Particle size did not appear to affect the starch gelatinisation behaviour of different milled fractions of CS-entrapped particles. Mahasukhonthachat, Sopade, and Gidley (2010) reported a similar finding that there is no evident effect of particle size on gelatinisation temperatures of different size fractions of milled sorghum grains. In addition, no significant differences in ΔH_{gel} were observed among all samples, indicating that neither the pectin matrix nor particle size seemed to inhibit the extent of starch gelatinisation. This is supported by a previous study on the encapsulation of native potato starch granules in whey protein by cold gelation (Lavoisier & Aguilera, 2019). It was found in this study that ΔH_{gel} was not modified by the presence of the protein network, regardless of the protein concentration.

7.4.3. Pasting properties

Fig. 7.2 shows pasting profiles of native CS and CS-entrapped particles of different size fractions. There were clearly defined peaks and troughs in RVA viscograms of native CS and particles < 0.25 mm. Particles < 0.25 mm exhibited lower peak, trough and final viscosities as well as lower breakdown and setback viscosities

compared with native CS, suggesting a decrease in starch granule swelling/ solubility due to the entrapment of CS within the pectin matrix. This finding is confirmed by a previous study (Xu & Zhang, 2014) showing a similar effect that the encapsulation of corn starch granules in a hydrophobic zein matrix had on starch pasting behaviours.

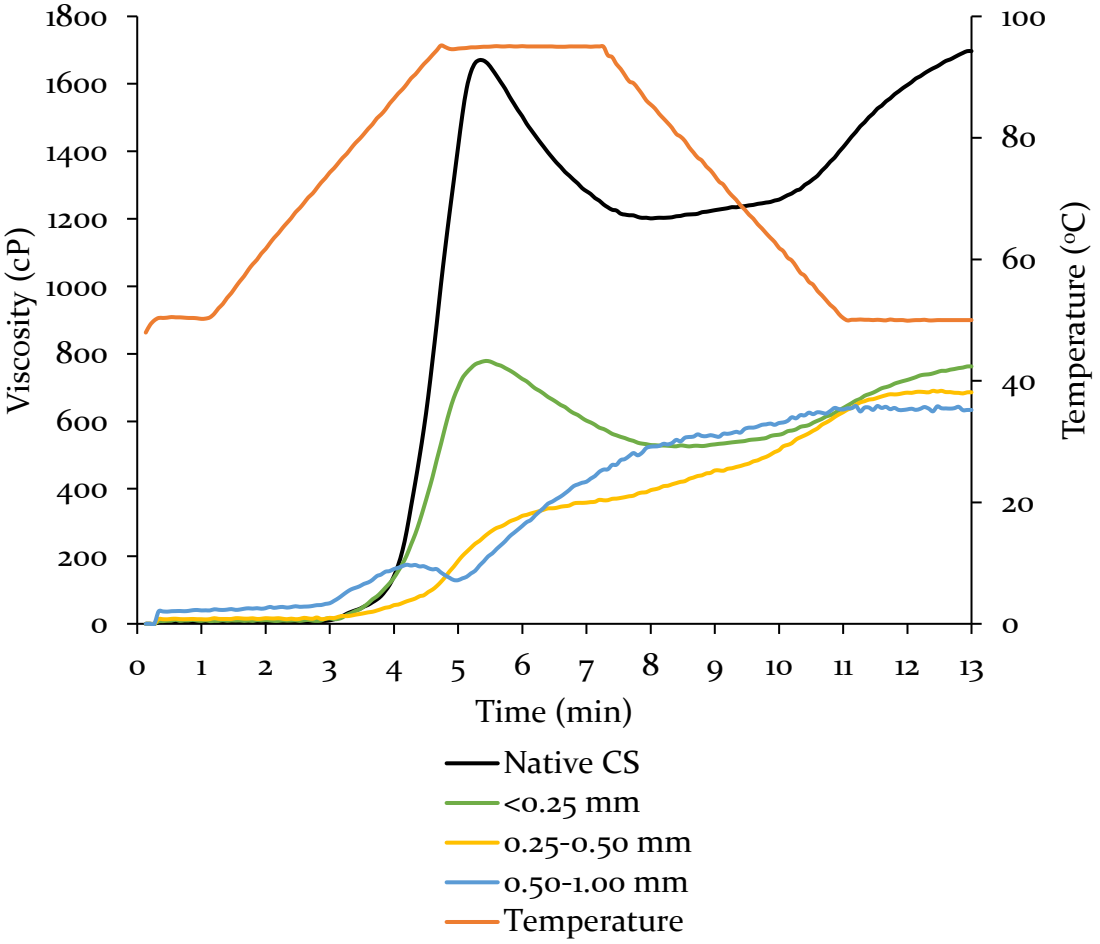

Fig. 7.2. RVA pasting curves of native CS and different size fractions of CS-entrapped particles.

For particles > 0.25 mm, RVA viscograms showed no well-defined peaks and troughs as well as shear-thickening behaviours during the holding period at 95°C and the cooling phase. Their peak viscosities were markedly lower compared with those of particles < 0.25 mm, suggesting that particle size influenced peak pasting

viscosity. Larger particle size fractions appeared to impose greater restrictions on the degree of granule swelling. These results are suggestive of a delay in swelling and gelatinisation of entrapped CS during the heating period and high resistance of swollen CS to breakdown during the holding period at 95°C as a consequence of pectin encapsulation. Similar results have previously been reported for pasting behaviours of starch in milled sorghum grains of different particle sizes (Mahasukhonthachat *et al.*, 2010).

7.4.4. Static in vitro *starch digestion*

Starch hydrolysis curves are shown for cooked samples of native CS and CS-entrapped particles of different size fractions in Fig. 7.3. Native CS was rapidly digested and had the highest digestibility. The rate of digestion was generally lower for CS trapped inside pectin particles, and was significantly reduced with increase in particle size and degree of pectin encapsulation. The extent of digestion followed a similar trend to that observed for the digestion rate although the <0.25 mm and 0.25-0.50 mm fractions had similar starch digestibility. Cooked whole intact beads (~2.00-3.50 mm) showed very low rate and extent of starch digestion. The maximum starch hydrolysis was reached after 60 min of small intestinal digestion for all samples except for the whole beads.

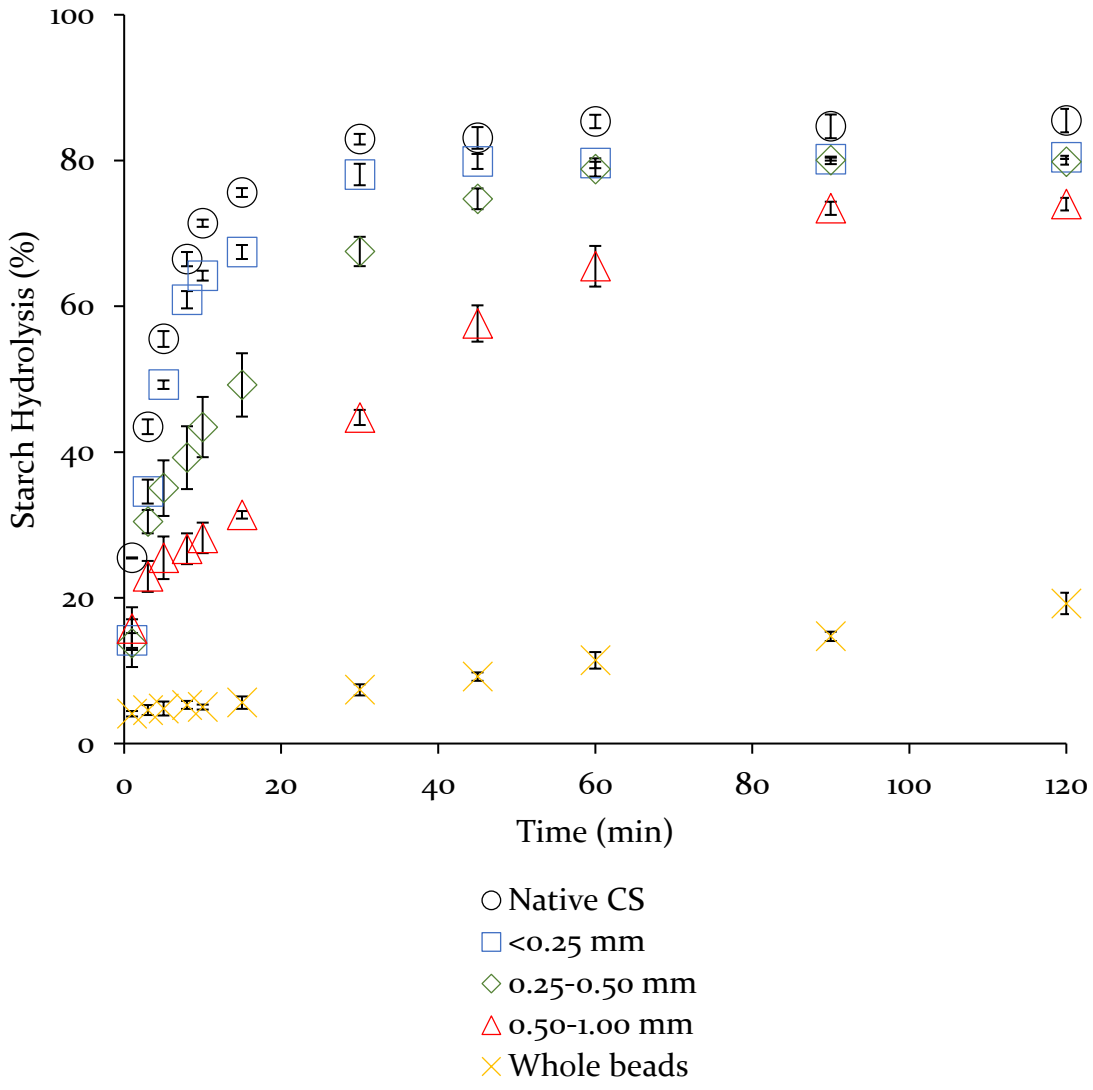

Fig. 7.3. Hydrolysis curves obtained for *in vitro* digestion by porcine pancreatic α-amylase of cooked samples of native CS and CS-entrapped particles of different size fractions.

Starch hydrolysis data was fitted to the first-order kinetic model by Goñi *et al.* (1997) (Fig. 7.4). The first-order rate constant (k, min^{-1}) and the total starch digested at the end of the reaction (C_∞, %) were then estimated as shown in Table 7.2. All Goñi plots revealed a single linear phase of starch amylolysis characterised by a single rate constant. High R^2 values (> 0.90) indicated a good fit of the kinetic model to the experimental data. The rate constant (k) and the total starch digested (C_∞) were higher for the native CS than for any of the milled fractions of CS-entrapped particles. These also appeared to decrease with increasing particle size.

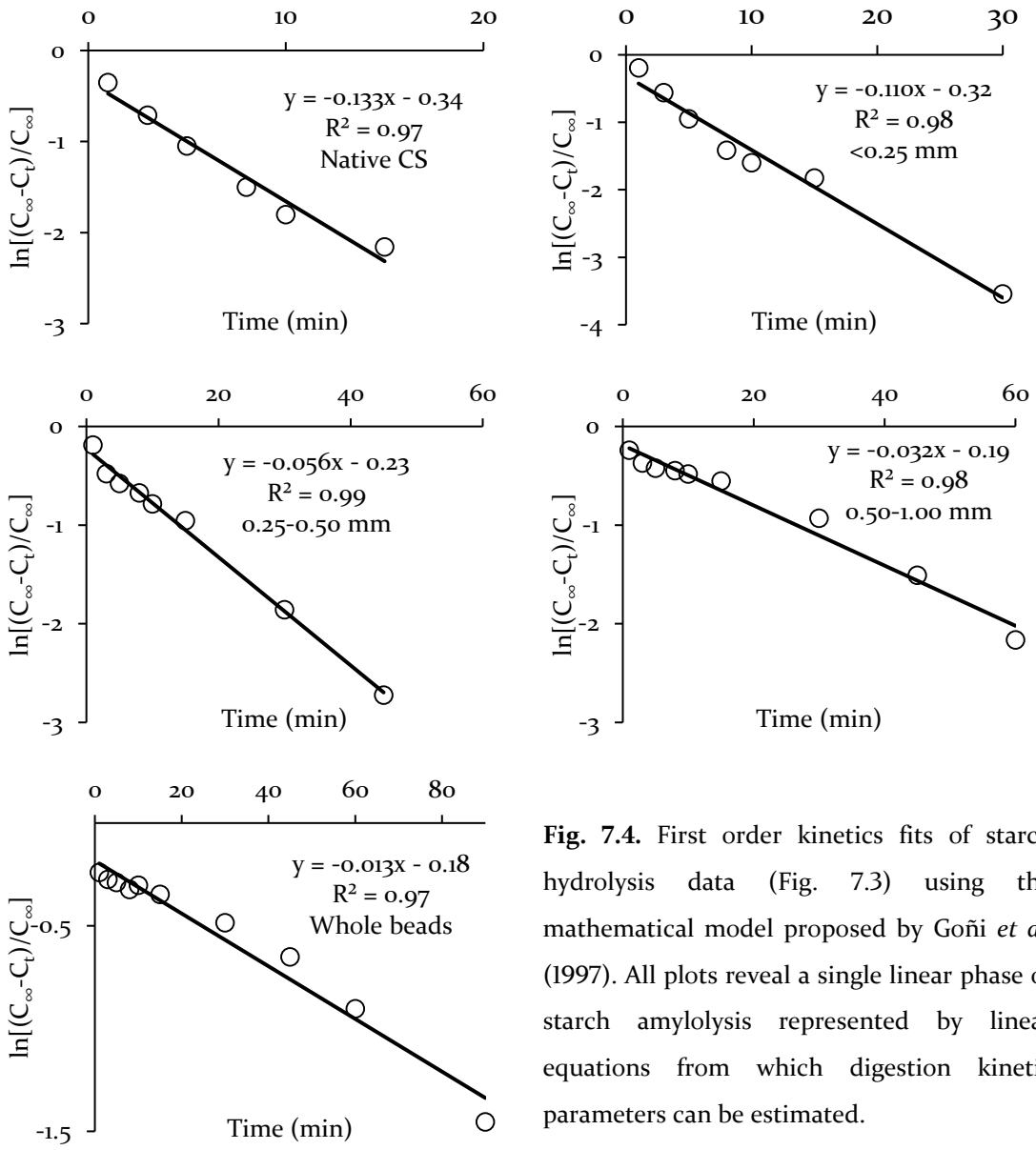

Fig. 7.4. First order kinetics fits of starch hydrolysis data (Fig. 7.3) using the mathematical model proposed by Goñi *et al.* (1997). All plots reveal a single linear phase of starch amylolysis represented by linear equations from which digestion kinetic parameters can be estimated.

Table 7.2. First-order kinetic parameters of starch amylolysis estimated from the Goñi mathematical digestion model.

Samples	k (min^{-1})	C_∞ (% total starch digested)
Native CS	0.133 ± 0.015^{a}	85.5 ± 1.6^{a}
<0.25 mm	0.110 ± 0.016^{a}	80.4 ± 0.2^{b}
0.25-0.50 mm	0.056 ± 0.005^{b}	79.8 ± 0.4^{b}
0.50-1.00 mm	0.032 ± 0.005^{bc}	74.0 ± 0.9^{c}
Whole beads	0.013 ± 0.003^{c}	19.2 ± 1.5^{d}

$^{a\ b\ c\ d}$ Values are means ± standard deviations of three determinations.

Values with the same subscripts in a column do not differ significantly ($p > 0.05$).

The starch hydrolysis curves and digestion kinetic analysis clearly demonstrated the effect of pectin encapsulation on reducing the rate and extent of starch digestion *in vitro*. This finding is consistent with Venkatachalam *et al.* (2009) showing that the alginate matrix hinders the accessibility of α-amylase to entrapped CS, thus delaying starch hydrolysis and resulting in slow and gradual release of glucose. Luo and Zhang (2018) also showed that CS embedded in the cell wall-like β-glucan-alginate gel matrix exhibits slow starch digestion due to the hindering effect of the polysaccharide matrix on starch-amylase interactions. In this study, the pectin matrix provides an efficient barrier against α-amylase access for hydrolysis of encapsulated starch substrate in a similar manner to the legume cotyledon cell wall (Dhital *et al.*, 2016; Do *et al.*, 2019). In addition, it appears that α-amylase diffuses through the pectin matrix and digests starch inwardly towards the particle core. This suggestion is based on previous observations of layer-by-layer inward progression of starch digestion towards the centre of the cotyledon cell (Chapter 6) and the alginate microsphere (Venkatachalam *et al.*, 2009).

Further, it is possible that the pectin matrix may play a role in limiting starch gelatinisation during cooking, thus reducing starch susceptibility to amylolysis. However, we can rule out this possibility, because the DSC analysis indicated that the extent of starch gelatinisation was independent of the presence of the pectin matrix. It is important to note that the gelatinisation of CS inside the pectin matrix may not proceed completely from native granules to molecularly dispersed starch, which could impede starch hydrolysis. Moreover, the presence of calcium ions may have led to a slight increase in enzyme activity because they are essential for the activity of α-amylase and provide structural integrity for the enzyme (Buisson,

Duee, Haser, & Payan, 1987). However, starch is trapped in the dense pectin matrix such that the slight increase in amylase activity would be unlikely to overcome the effect of pectin inhibition on starch digestion.

Another interesting finding from the present study is that the rate and extent of starch digestion was inversely correlated with particle size and therefore degree of pectin encapsulation. This finding is consistent with Venkatachalam *et al.* (2009) that increasing particle size of starch-entrapped alginate microspheres significantly increases RS content while decreasing RDS and SDS contents. Mahasukhonthachat *et al.* (2010), Al-Rabadi *et al.* (2009), and Edwards *et al.* (2018) also reported this inverse correlation between particle size and kinetics of starch digestion in milled legumes and cereal grains. They found that digestion of starch trapped within plant tissues is a diffusion-controlled process and cell wall encapsulation is a rate-liming factor controlling the digestion. Indeed, higher degree of cell wall encapsulation/intactness can impose greater restriction on diffusion of α-amylase in the tissue matrix. Therefore, particle size is an important factor to consider in designing particles for efficiently delaying starch digestion. In this study, whole beads had the lowest rate and extent of starch digestion, probably because of their largest size and therefore highest degree of pectin encapsulation. Also, these beads are intact and possibly have a lower amount of peripheral damaged starch and a smaller surface area for amylase binding compared with milled particles (Roman *et al.*, 2017).

On a side note, another factor worth considering when designing starch-entrapped particles is the matrix microstructure that has been shown to be determined by

matrix polymer concentration. Venkatachalam *et al.* (2009) and Lavoisier and Aguilera (2019) found that digestibility of starch trapped inside protein/alginate gels cross-linked with $CaCl_2$ is significantly reduced with increasing protein/alginate concentration. It is likely that larger polymer concentration may result in more dense, compact gel network structure with smaller pores that provide a more effective barrier to enzyme diffusion. This has not been explored in this study and warrants further investigation.

7.5. Conclusions

Starch-entrapped pectin particles exhibited slow starch digestion, and the rate and extent of amylolysis was inversely correlated with particle size. It is suggested that the pectin matrix hinders the accessibility of α-amylase to entrapped starch and therefore slows down starch digestion *in vitro* in a similar manner to the legume cotyledon cell wall. The findings from this study provide new insights into digestive behaviours of encapsulated starch and aid in the design of food-grade particles for reduced glycaemic impact. Apart from particle size, other design considerations that warrant further investigation include particle microstructure (e.g. compactness and porosity), particle composition (e.g. ratio of starch to pectin), and polymer matrix composition (e.g. incorporation of xyloglucan and microcrystalline cellulose into pectin-based formulations).

CHAPTER EIGHT: Protein limits *in vitro* digestion of starch in sorghum flour: new opportunities for development of low-glycaemic-index biomimetic flour

8.1. Abstract

Sorghum is a drought-resistant cereal crop that is widely cultivated in many parts of Asia and Africa. Despite being an essential food source for millions of the world's poorest people, sorghum has poor nutritional value due to its generally low starch and protein digestibility. In this study, the effects of protein on physicochemical properties and *in vitro* digestion of starch were investigated using two model systems: (i) whole grain sorghum flour (WGF) and (ii) binary blends consisting of sorghum starch and kafirin protein isolate (KPI) (0, 5, 10, 15, or 20% KPI, w/w). The results show that proteins in the WGF could cause delay in starch gelatinisation and reduction in peak paste viscosity. On the other hand, KPI in the blends had no significant influence in gelatinisation and pasting properties of starch regardless of the protein blend ratio. The rate and extent of amylolysis was low in cooked samples of both the WGF and blends, possibly due to the disulfide-bonded protein network hindering access of α-amylase to starch.

8.2. Introduction

Sorghum (*Sorghum bicolour* (L.) Moench) is a drought-resistant cereal crop that thrives in dry tropical climates of Africa and Asia. In these regions of the world, sorghum has the distinction of being a vital staple food for the poor (Rooney, 1996). Whole grain sorghum provides a great source of starch and protein; however, the

digestibility of these two constituents is generally low, leading to poor nutritional value (Duodu *et al.*, 2003; Rooney & Pflugfelder, 1986). The starch digestibility of sorghum is generally considered to be the lowest among the cereals and is influenced by plant species, type of starch, and inhibitors (e.g. tannins) (Rooney & Pflugfelder, 1986). Several *in vitro* studies have reached a consensus that the starch-protein interaction plays a critical role in the low α-amylase digestibility of starch in cooked sorghum flour. These studies have pointed out the extensive formation of disulfide cross-linked protein polymers upon wet cooking of flour. The protein matrix appears to slow down starch digestion by restricting starch gelatinisation and impeding α-amylase access to starch. The degree of protein polymerisation is higher in vitreous endosperm flour, resulting in lower starch digestibility when compared with floury endosperm flour. Reducing agents (e.g. 2-mercaptoethanol) mitigate the low starch digestibility by breaking disulfide bonds in the protein matrix, thus rendering starch more susceptible to amylolysis (Ezeogu *et al.*, 2005, 2008; Zhang & Hamaker, 1998; Wong *et al.*, 2009).

Starch-protein interactions occurring in natural food systems is an area of growing interest for its promising application in designing novel starch-based foods with low or slow glycaemic features. Recent studies have shown that exogenous proteins can slow down *in vitro* digestion of starch in binary blends, possibly due to the formation during processing of a protein network that envelops starch granules and acts as a physical barrier to α-amylase access (Yang, Zhong, Goff, & Li, 2019; López-Barón, Gu, Vasanthan, & Hoover, 2017; López-Barón *et al.*, 2018). Kafirins are the prolamin storage protein of sorghum, accounting for 70 – 80% of the proteins in whole grain flour (Hamaker, Mohamed, Habben, Huang, & Larkins,

1995). Kafirin cross-linking via inter- and intra-molecular disulfide bonds upon wet heating has been shown to occur in isolated kafirin (Byaruhanga *et al.*, 2006) and in sorghum flour (Ezeogu *et al.*, 2008), the latter in turn has a negative impact on *in vitro* starch digestion (Ezeogu *et al.*, 2005). Therefore, adding kafirin isolate to delay starch digestion is a potential strategy for the development of low-glycaemic-index sorghum-based foods. Most studies have focused on the starch-protein interactions occurring in natural whole sorghum flour, but research is scant regarding the effect of exogenous kafirin protein on starch digestibility.

The objectives of this study were to investigate the effect of protein on physicochemical properties and *in vitro* digestion of starch in natural sorghum flour matrix and in a simple biomimetic flour system consisting of sorghum starch and kafirin protein isolate. The results from this study are expected to provide a basis for understanding starch-protein interactions in complex food systems and for utilisation of sorghum protein in gluten-free biomimetic flour formulations.

8.3. Materials and Methods

8.3.1. Materials

Grains of two different cultivars (NGT17N216 and NGT17N217) of white, non-waxy sorghum hybrids (*Sorghum bicolor*) were grown in the 2017/18 season and kindly donated by the Summer Crop Breeding Program of Nuseed Pty. Ltd. based in Toowoomba, Queensland, Australia. The grains selected for the study represented sorghum cultivars differing in protein content. The grains were carefully cleaned from impurities and stored in sacks at 4°C throughout the course of the study. Whole grain flours (WGFs) were prepared by dry milling the grains using a coffee grinder (Breville Pty Ltd, Sydney, Australia) to pass through a 180µm standard test sieve. The purpose of sieving was to remove the coarse fraction so as to eliminate any effect of differing grain particle size on kinetics of starch digestion (Mahasukhonthachat *et al.*, 2010; Ezeogu *et al.*, 2008). In addition, the sorghums selected in this study were white, non-tannin varieties genetically bred to contain very low phenolic contents that would be likely to have minimal inhibitory effects on starch digestion.

8.3.2. Sorghum sample preparation

8.3.2.1. Starch isolation

Starch was isolated following the method described by Beta, Corke, Rooney, and Taylor (2001). Dry sorghum grains were steeped in sodium hydroxide (0.25%, w/v) at ratio 1:2 (w/v) for 24 h at 4°C. After the soaking medium was discarded, the steeped grains were washed and wet ground with an equal volume of water using

a laboratory blender (Breville Pty Ltd, Sydney, Australia) for 5 min at full speed. The resulting milky slurry was filtered through a 75 µm standard test sieve. The remaining residue on the sieve was washed with water. Repeated grinding and filtering were carried out on this material until virtually no more starch passing through. The filtrate was allowed to stand for 1 h in a beaker and centrifuged at 760 x *g* for 10 min. The supernatant was then decanted, and the grey-coloured, protein-rich top layer was scraped off using a spatula. The starch deposit was resuspended in excess water and centrifuged again. The starch was obtained by repeated washing with water and resettling by centrifugation several times until the top starch layer became white. The isolated starch was regularly examined under a light microscope for the presence of impurities (e.g. cell wall fragments). The starch cake was dried at 40°C for 24 h. Isolated starches and WGFs prepared from the two sorghum cultivars (NGT17N216 and NGT17N217) are denoted as S216, F216 and S217, F217 respectively.

8.3.2.2. Kafirin isolation

The kafirin isolation method described by Wang, Tilley, Bean, Sun, and Wang (2009) was followed, but with extractant composition suggested by Espinosa-Ramírez and Serna-Saldívar (2016). Freshly ground F216 was mixed with 70% (v/v) aqueous ethanol containing 0.03% (w/v) sodium metabisulfite at ratio 1:10 (w/v) flour to extractant in 1 L Schott bottles. These bottles were secured horizontally in a shaking water bath at 70°C and stirred vigorously for 1 h with continuous shaking (120 strokes/min). The extracts were separated from insoluble matter by centrifugation at 3500 x *g* for 15 min. The extracts were pooled, and the ethanol

content was diluted to 40% (v/v). The suspension was then kept in a freezer at -20°C overnight to promote protein precipitation. The protein pellet was recovered by centrifugation at 3500 x *g* for 15 min and dried in an oven at 40°C overnight. The protein was ground to very fine powder and defatted three times for 1 h each with hexane (5 mL hexane/g powder) in a shaking incubator with continuous shaking at 120 rpm and room temperature. The defatted kafirin protein isolate (KPI) was air-dried in a fume hood overnight to evaporate the solvent.

8.3.2.3. Binary blends of starch and kafirin protein isolate

Following Lu, Donner, Yada, and Liu (2016), binary blends of sorghum starch and native KPI were prepared by stepwise addition of starch to protein in zip lock plastic bags. The composite mixtures were thoroughly whisked for 5 min during the addition until achieving homogeneity. Blends with a range of protein ratio of 5, 10, 15, and 20% (w/w) were prepared by combining 5, 10, 15, and 20 g KPI, respectively, with 100 g starch (dwb). To ensure correct mixing proportion and blend uniformity, total starch content of blend samples taken from the top, centre, and bottom of the bags were analysed and verified against the theoretical value.

8.3.2.4. Pepsin treatment of whole flours

WGF samples (1.5 g) were combined with 50 mL pepsin solution (250 mg enzyme in 0.01 M HCl solution, pH 2.0, pre-warmed to 37°C) in 100 mL Schott glass bottles. These bottles were horizontally secured in a shaking water bath and shaken at 120 strokes/min and 37°C. After an incubation of 4 h, the flour mixtures were transferred into 50 mL polypropylene centrifuge tubes and centrifuged at

1800 *x g* for 10 min. The supernatants were discarded, and the residues were washed several times with distilled water and recovered by centrifugation at 1800 *x g* for 10 min. The residues were freeze-dried and ground to fine powder to pass through the 180 µm sieve.

8.3.3. Analytical methods

Moisture content was determined gravimetrically by drying the sorghum samples in an oven at 105°C to a constant weight. Protein content was estimated using the Dumas method (AOAC 968.06) with a conversion factor of 6.25 from nitrogen to protein. Total starch and amylose contents were analysed using Total Starch Assay (K-TSTA with KOH method) and Amylose/Amylopectin Assay (K-AMYL) kits, respectively, from Megazyme International Ireland Ltd., Ireland, following the instructions given by the manufacturer.

Total phenolic content was determined using the modified Folin-Ciocalteau assay following a combination of the methods described by Dicko *et al.* (2002) and Dykes, Rooney, Waniska, and Rooney (2005). Approximately 0.5 g of freshly prepared ground flour was extracted in 15 mL of 75% (v/v) aqueous acetone in a shaking incubator with continuous shaking at 150 rpm and 25°C for 20 min. The extract was collected by decanting the supernatant following centrifugation at 3500 x *g* for 10 min. The residue was re-extracted with acetone following the same procedure as described above. The two extracts were pooled, and analysis of total phenols was performed immediately. An aliquot of the extract (0.1 mL) was mixed and allowed to react with 0.25 mL of Folin-Ciocalteau reagent (1 N) for 5 min at room temperature. Sodium carbonate solution (20%, w/v, 0.25 mL) and water

were then added to a final volume of 2 mL. The mixture was shaken vigorously and allowed to stand for 30 min at room temperature, and the absorbance was measured at 760 nm. A blank was prepared by replacing Folin-Ciocalteau reagent with water. A standard calibration curve was prepared from a series of aqueous gallic acid solutions (0 – 250 µg/mL) and run in parallel with the samples. The total phenolic content was calculated and expressed as mg of gallic acid equivalent (GAE) per 100 g of dry flour.

8.3.4. Determination of thermal properties

Thermal properties were analysed using a Differential Scanning Calorimeter (DSC, TA Q100, TA Instruments, Newcastle, DE) according to the method described by Lu *et al.* (2016). Sorghum sample equivalent to ~2 mg of starch (dwb) was directly weighed into a 40 µL aluminium pan. A pre-determined amount of water was then added to the pan using a Hamilton micro-syringe to achieve 30% (w/w) dry starch equivalent and 70% water. This ratio of starch to water was chosen to ensure excess water available for starch gelatinisation. The moisture of the sample was determined and included in the total amount of water added. The pan was hermetically sealed and allowed to equilibrate overnight at room temperature prior to heating scan in the DSC. The sample pan was heated from 20 to 120°C at a rate of 10°C/min with an empty pan included as the reference. The sealed pan was weighed before and after scanning and checked against the initial weight to ensure that no leakage had taken place. Onset temperature (T_o), peak temperature (T_p), conclusion temperature (T_c), and enthalpy of gelatinization (ΔH_{gel}) were calculated using Universal Analysis Software (version 4.5A, TA Instruments).

Gelatinisation enthalpies were normalized by subtracting protein denaturation enthalpy from total enthalpies obtained from DSC thermograms.

8.3.5. Determination of pasting properties

Pasting properties were evaluated using a Rapid Visco Analyser (RVA 4500, Perten Instruments) according to the method described by Beta *et al.* (2001). For RVA analysis, WGFs were prepared by dry milling the grains to pass through a 500µm standard test sieve. WGF (equivalent to ~2 g of dry starch) or isolated starch/binary blend (equivalent to ~3 g of dry starch) was accurately weighed and mixed with 25 g of water in an aluminium canister. The moisture of the sample was determined and included in the total amount of water added. The starch slurry was subjected to a programmed heating and cooling regime, where the slurry was equilibrated at 50°C for 1 min, heated to 95°C at the rate of 6°C/min, held at 95°C for 5 min, cooled to 50°C at the rate of 6°C/min, and held at 50°C for 1 min. The entire procedure took a total of 21 min to complete. The rotating speed of the paddle was 960 rpm for the first 10 seconds for sample dispersion, and then maintained at constant 160 rpm throughout the analysis. Peak, trough, and breakdown viscosities were calculated and reported in centipoise (cP). The effect of reducing agent on the flour pasting property was evaluated by combining dithiothreitol (DDT) or sodium metabisulfite ($Na_2S_2O_5$) at a 100 mM concentration with the flour slurry in the canister without pre-incubation prior to RVA analysis (Zhang & Hamaker, 2005).

8.3.6. In vitro *starch digestion*

8.3.6.1. Static starch digestion protocol

Starch digestibility was determined based on a modified version of the *in vitro* starch digestion protocol (Ezeogu *et al.*, 2005) described in Section 7.3.6.1 & 2. To account for natural sugars present in WGFs, the amount of glucose released from starch hydrolysis was corrected for blanks from which enzyme was omitted. To evaluate the effect of protein on starch digestibility, WGFs were treated with pepsin (described in Section 8.3.2.4) to remove some proteins prior to starch digestibility determination.

8.3.6.2. Modelling starch digestograms

Kinetics of starch digestion can be described by the non-linear model proposed by Goñi *et al.* (1997) and described in Section 7.3.6.3.

8.3.7. Statistical analysis

Data was reported as mean of triplicate observations ± standard deviation, unless otherwise specified. Tukey's test and analysis of variance (ANOVA) were used to assess the significance of differences ($p \leq 0.05$) between means using the Minitab 19 software (Minitab Inc., Pennsylvania, USA). Linear regression analysis was performed using Microsoft Excel.

8.4. Results and Discussion

8.4.1. Sorghum material composition

The total starch content of S216 and S217 was 90.1 ± 0.9 and 91.3 ± 1.0 (w/w, dwb), respectively. The amylose content (%) of S216 (22.6 ± 0.1) was significantly lower than that of S217 (24.2 ± 0.7) ($p \leq 0.05$). F216 contained 67.3 ± 0.5 g starch, 11.7 ±

0.6 g protein, and 75.6 ± 2.1 mg GAE phenolics, per 100 g flour (dwb). F217 contained 69.9 ± 0.8 g starch, 9.6 ± 0.4 g protein, and 87.0 ± 0.9 mg GAE phenolics, per 100 g flour (dwb). These values were close to those reported previously for white sorghum (Srichuwong *et al.*, 2017). Pepsin pre-treatment markedly increased the starch content of WGFs ($p \leq 0.05$) due to protein removal, i.e. pepsin treated F216 and F217 contained 75.3 ± 1.1 g and 79.6 ± 0.7 g starch per 100 g flour (dwb), respectively. Additionally, the protein isolation process yielded high-purity KPI (91.6%, w/w, dwb).

8.4.2. Thermal properties

Fig. 8.1A shows representative DSC thermograms obtained for isolated starches and WGFs (< 180 μm) of two sorghum cultivars. Gelatinisation parameters are presented in Table 8.1. Two sorghum starches (S216 and S217) exhibited identical DSC thermograms. No significant differences in gelatinisation temperature and enthalpy were found between these two starches. Gelatinisation occurred between 67 to 75°C with an endothermic peak at ~ 71.0°C and an enthalpy of 16.6 ± 0.2 $J.g^{-1}$. The gelatinisation temperature range found in this study was similar to that reported for sorghum grown in Algeria (Boudries *et al.*, 2009), but was lower than that obtained for sorghum grown in India (Akingbala, Gomez, Rooney, & Sweat, 1988). This is indicative of differences in variety and growing location that may affect gelatinisation properties of sorghum starch studied by DSC.

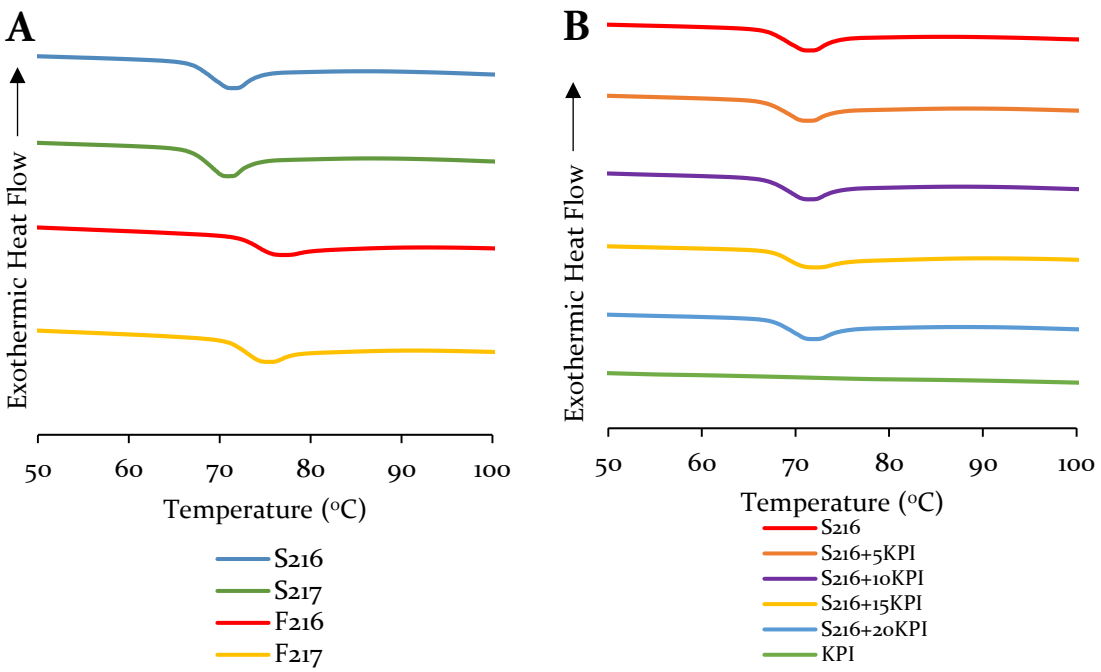

Fig. 8.1. Representative DSC thermograms obtained for (A) isolated starches and WGFs (< 180 µm) and (B) S216/KPI blends.

Table 8.1. DSC gelatinisation parameters of isolated starches, WGFs (< 180 µm), and S216/KPI blends prepared from sorghum.

Sorghum samples	T_o (°C)	T_p (°C)	T_c (°C)	ΔH_{gel} (J.g^{-1})
S216	66.9 ± 0.0^{c}	71.0 ± 0.0^{c}	75.0 ± 0.0^{c}	16.6 ± 0.2^{a}
S217	67.0 ± 0.1^{c}	70.6 ± 0.2^{c}	74.6 ± 0.3^{c}	16.6 ± 0.2^{a}
F216 (< 180 µm)	71.9 ± 0.6^{a}	75.9 ± 0.7^{a}	84.6 ± 2.2^{a}	13.7 ± 0.7^{c}
F217 (< 180 µm)	70.4 ± 0.6^{b}	74.4 ± 0.7^{b}	79.9 ± 0.3^{b}	15.7 ± 0.1^{b}
S216+5KPI	67.0 ± 0.2^{c}	71.0 ± 0.2^{c}	75.6 ± 0.4^{c}	16.5 ± 0.1^{ab}
S216+10KPI	66.9 ± 0.1^{c}	71.0 ± 0.1^{c}	75.6 ± 0.2^{c}	16.7 ± 0.2^{a}
S216+15KPI	67.3 ± 0.1^{c}	71.2 ± 0.1^{c}	76.2 ± 0.1^{c}	16.4 ± 0.2^{ab}
S216+20KPI	67.5 ± 0.3^{c}	71.4 ± 0.2^{c}	76.5 ± 0.3^{c}	16.8 ± 0.1^{a}
KPI	_	_	_	_

T_o, onset temperature; T_p, peak temperature; T_c, conclusion temperature; ΔH_{gel}, enthalpy of gelatinization (J.g^{-1} of starch on dwb). Values with the same subscripts in a column do not differ significantly ($p > 0.05$).

"_", kafirin protein isolate (KPI) exhibited no endothermic peak.

In WGF (< 180μm) of both sorghum cultivars, gelatinisation occurred at significantly higher temperatures (T_o, T_p, and T_c) with a T_p ~ 4 – 5°C higher than that of isolated starch. These findings are consistent with previous research (Srichuwong *et al.*, 2017) showing that gelatinisation of whole sorghum flour shifted to a higher temperature range compared with that of isolated sorghum starch. One possible explanation for this is the competition of protein with starch for available water. This may lead to water re-distribution between these two polymers (i.e. separation of water into a protein aggregate phase and a starch phase), thus limiting starch-water interactions and delaying starch gelatinisation (Evans & Haisman, 1982; Eliasson, 1983). Apart from protein, dietary fibers may also compete for water with starch and consequently restrict granule hydration/swelling (Srichuwong *et al.*, 2017). It must also be noted that the conditions used for DSC study (i.e. excess water and overnight soaking) were favourable for complete starch gelatinisation. However, heterogeneity of the flour materials could cause uneven water distribution and/or inefficient heat transfer across individual flour particles, which could impede the starch gelatinisation process (Edwards *et al.*, 2015). In addition, gelatinisation enthalpy (ΔH_{gel}) of WGF was significantly lower than that of isolated starch. This could be explained due to a partial loss of starch crystallinity during mechanical grinding of grains (Srichuwong *et al.*, 2017).

The effect of KPI on the thermal properties of S216 was studied by DSC (Fig. 8.1B). KPI showed no denaturation peak, suggesting that endothermic transitions observed in S216/KPI blends were primarily attributed to starch gelatinisation. All the blends exhibited similar DSC thermograms. The values for T_o, T_p, T_c, and ΔH_{gel}

were not modified by increasing protein blend ratio (Table 8.1), indicating that the presence of native KPI had no significant effect on the gelatinisation behaviour of sorghum starch. These results are consistent with previous work that the addition of purified native plant proteins did not affect wheat starch gelatinisation (López-Barón *et al.*, 2017). However, these results contradict earlier reports (Lu *et al.*, 2016; Yang *et al.*, 2019) that increasing ratio of native protein in starch/protein blends shifted endothermic gelatinisation peak for starch to a higher temperature, possibly due to competition for available water between these two polymers.

8.4.3. Pasting properties

Figs. 8.2A and B display RVA pasting curves of starch (7%, w/w) in WGFs (< 500 μm) prepared from the two sorghum cultivars. Their pasting profiles were typical of freshly ground sorghum flour with the presence of a single starch gelatinisation peak. This is followed by a breakdown of viscosity under constant shear during the 95°C holding period, and a noticeable increase in setback viscosity upon cooling due mainly to the strong tendency for reassociation of amylose molecules (Zhang & Hamaker, 2005).

During wet cooking of sorghum flour, Chandrashekar and Kirleis (1988) identified the formation of a disulfide cross-linked protein matrix interwoven with starch granules that can act as an effective barrier to inhibit starch gelatinisation. On the other hand, the cleavage of disulfide bonds by reducing agents (e.g. 2-mercaptoethanol) causes disruption of the protein matrix, thus allowing the granules to swell more freely. To investigate this, the WGFs were cooked in the presence of dithiothreitol (DDT) or sodium metabisulfite ($Na_2S_2O_5$).

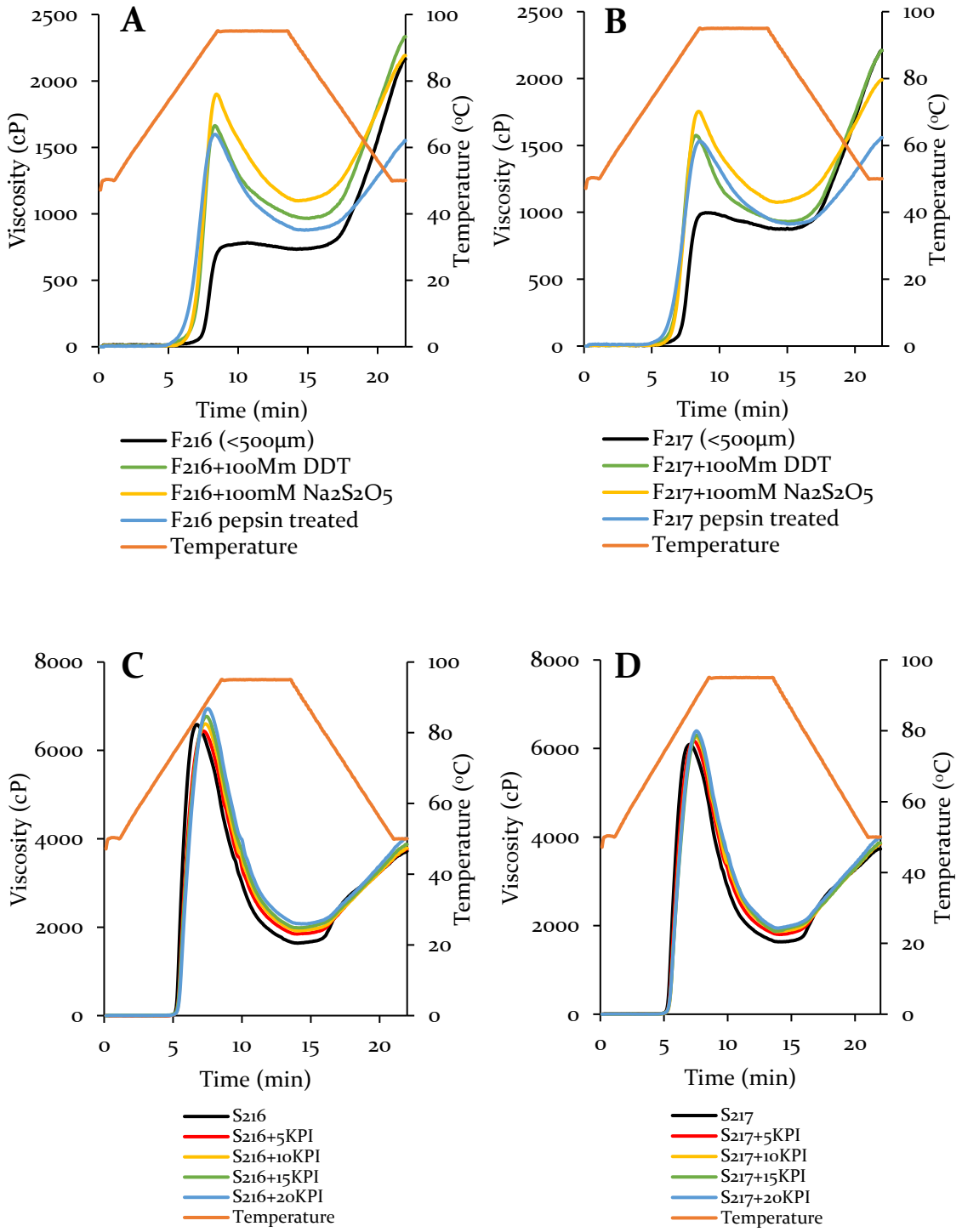

Fig. 8.2. (A) (B) Effect of protein on RVA pasting profiles of starch (7%, w/w) in WGFs (< 500 μm). Legends are defined as follows: F+100mM DDT, flours cooked in the presence of 100 mM dithiothreitol; F+100mM $Na_2S_2O_5$, flours cooked in the presence of 100 mM sodium metabisulfite; F pepsin treated, flours treated with pepsin for 4 h prior to cooking. (C) (D) Effect of KPI on RVA pasting profiles of starch (10%, w/w) in sorghum starch/KPI blends. Legends are defined as follows: 5, 10, 15, and 20KPI represent the blend ratios of protein 5, 10, 15, and 20 (%, w/w), respectively.

These reducing agents are known to cleave inter- and intra-molecular disulfide bonds. As evident in Figs. 8.2A & B and Table 8.2, the addition of these agents markedly increased the peak and breakdown viscosities as well as the pasting temperature of the WGFs from both sorghum cultivars. This is in line with the results from earlier studies (Zhang & Hamaker, 2005; Srichuwong *et al.*, 2017). Furthermore, the pre-incubation of the WGFs with pepsin for removing some proteins prior to cooking in the RVA resulted in the lowest pasting temperature among all the flour treatments, while also significantly increasing the peak and breakdown viscosities (Table 8.2). This finding confirms the role of proteins present in sorghum flour in inhibition of the degree of starch swelling and gelatinisation (Chandrashekar & Kirleis, 1988).

Table 8.2. Effect of protein on RVA pasting parameters of starch (7%, w/w) in WGFs (< 500 μm).

Sorghum samples	Peak viscosity (cP)*	Trough viscosity (cP)*	Breakdown viscosity (cP)*	Pasting temperature (°C)*
F216 (< 500 μm)	786 ± 11^{g}	733 ± 6^{e}	53 ± 7^{f}	88.8 ± 0.4^{a}
F216+100mM DDT [1]	1663 ± 7^{c}	965 ± 11^{b}	698 ± 8^{b}	83.9 ± 0.0^{c}
F216+100mM $Na_2S_2O_5$ [2]	1901 ± 6^{a}	1096± 21^{a}	805 ± 19^{a}	82.7 ± 0.5^{d}
F216 pepsin treated [3]	1598 ± 26^{d}	876 ± 5^{d}	723 ± 29^{b}	80.2 ± 0.3^{e}
F217 (< 500 μm)	999 ± 8^{f}	870 ± 4^{d}	128 ± 11^{e}	86.7 ± 0.3^{b}
F217+100mM DDT [1]	1575 ± 13de	928 ± 6^{c}	647 ± 7^{cd}	82.3 ± 0.0^{d}
F217+100 mM $Na_2S_2O_5$ [2]	1754 ± 25^{b}	1074 ± 8^{a}	680 ± 23^{bc}	82.4 ± 0.3^{d}
F217 pepsin treated [3]	1532 ± 20^{e}	911 ± 7^{c}	621 ± 14^{d}	80.8 ± 0.0^{e}

* Values with the same subscripts in a column do not differ significantly ($p > 0.05$). [1] WGFs cooked in the presence of 100 mM dithiothreitol (DDT). [2] WGFs cooked in the presence of 100 mM sodium metabisulfite ($Na_2S_2O_5$). [3] WGFs treated with pepsin for 4 h prior to cooking.

To further explore the effect of sorghum protein on starch gelatinisation, binary blends consisting of sorghum starch and KPI were studied using the RVA. Figs. 8.2C and D show RVA pasting curves of starch (10%, w/w) with and without added KPI. As shown in Table 8.3, S216 displayed substantially higher peak and breakdown viscosities than S217. It is well known that amylose forms complexes with lipids, leading to suppressed swelling of starch granules. The extent of this complex formation during pasting could influence the granule resistance to swelling and breakdown under heat and shear force (Srichuwong *et al.*, 2017). As such, the higher amylose content found in S217 may be associated with greater restriction on granule swelling and thus lower peak and breakdown viscosities.

Contrary to expectations, the addition of KPI did not seem to decrease the peak and breakdown viscosities nor increase the pasting temperature in both S216 and S217. Within each cultivar, the RVA pasting curves of the isolated starch and the blends followed a similar pattern (Figs. 8.2C & D). Although ANOVA detected some statistically significant differences in pasting parameters among these materials (Table 8.3), it is apparent that KPI had no measurable impact on the pasting behaviour of starch and the observed slight increase in viscosities with increasing blend ratio of KPI was mostly attributed to the increase in total solids concentration of solution. This seems to contradict earlier findings that the naturally occurring proteins in WGF inhibit the peak viscosity of starch paste. In this case, it could be argued that the starch/KPI model used in the present study may not be representative of the structural complexity of the natural sorghum flour matrix.

Table 8.3. Effect of KPI on RVA pasting parameters of starch (10%, w/w) in sorghum starch/KPI blends.

Sorghum samples**	Peak viscosity (cP)*	Trough viscosity (cP)*	Breakdown viscosity (cP)*	Pasting temperature (°C)*
S216	6589 ± 69^{cd}	1639 ± 11^{e}	4950 ± 75^{a}	74.5 ± 0.3^{b}
S216+5KPI	6439 ± 36^{cde}	1843 ± 32^{cd}	4596 ± 48^{cd}	75.1 ± 0.4^{ab}
S216+10KPI	6602 ± 74^{bc}	1918 ± 43^{bc}	4684 ± 82^{bc}	75.3 ± 0.3^{a}
S216+15KPI	6769 ± 50^{b}	1984 ± 42^{ab}	4785 ± 8^{ab}	75.0 ± 0.2^{ab}
S216+20KPI	6947 ± 63^{a}	2072 ± 47^{a}	4875 ± 45^{a}	75.4 ± 0.3^{a}
S217	6091 ± 21^{g}	1632 ± 16^{e}	4459 ± 34^{de}	74.8 ± 0.0^{ab}
S217+5KPI	6168 ± 24^{fg}	1800 ± 28^{d}	4368 ± 53^{e}	75.4 ± 0.3^{a}
S217+10KPI	6264 ± 21^{efg}	1861 ± 86^{bcd}	4403 ± 107^{de}	75.3 ± 0.3^{a}
S217+15KPI	6301 ± 91^{ef}	1876 ± 23^{bcd}	4425 ± 68^{de}	75.1 ± 0.0^{ab}
S217+20KPI	6402 ± 95^{de}	1942 ± 41^{bc}	4460 ± 54^{de}	75.1 ± 0.0^{ab}

* Values with the same subscripts in a column do not differ significantly ($p > 0.05$).

** The blend ratios of protein 5, 10, 15, and 20 (%, w/w) are denoted as 5, 10, 15, and 20KPI, respectively.

8.4.4. Static in vitro *starch digestion*

Figs. 8.3A and B show *in vitro* starch hydrolysis curves for cooked samples of isolated starches, WGFs (< 180 μm), and pepsin-treated WGFs from two sorghum cultivars. As can be clearly seen, starch digestibility in S216 (72.3%) was ~ 8% higher than that observed in S217 (64.4%). It has been reported that intrinsic characteristics of starches of different botanical source influence starch digestibility (Singh *et al.*, 2010). In this case, S217 had a lower digestibility possibly due to its higher amylose content (24.2%) as compared with that of S216 (22.6%). The starch digestibility in WGF was found to be ~ 12 – 20% lower than that in isolated starch. This is suggestive of the interactions between starch and other flour constituents (e.g. protein, lipid, fiber, and phenolic compounds) that can reduce

the extent of starch hydrolysis (Bhattarai, Dhital, & Gidley, 2016; Barros, Awika, & Rooney, 2012). Interestingly, despite S216 being much more digestible than S217, their flours had similar starch digestibility. This provides further evidence that the flour digestibility may be determined by extrinsic factors such as starch-protein interactions. Considering an approximately 1.9 g (per 100 g dry flour) difference in protein content between F216 and F217, it seems likely that starch digestibility is influenced by the level of protein present in the flour. Pre-treatment of the flours with pepsin for removing some native proteins prior to cooking improved starch digestibility by ~ 10 – 15%. Starch digestibility in pepsin treated F217 was similar to that in S217. These results are consistent with previous findings (Zhang & Hamaker, 1998) and confirm the influence of protein on starch digestibility in cooked sorghum flour.

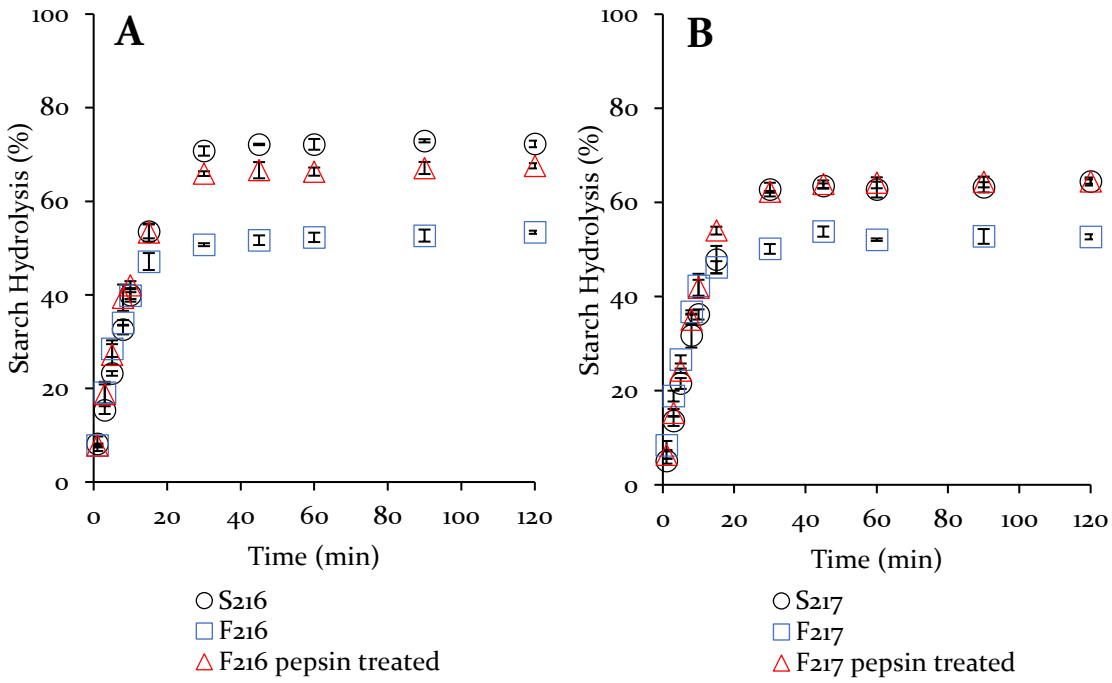

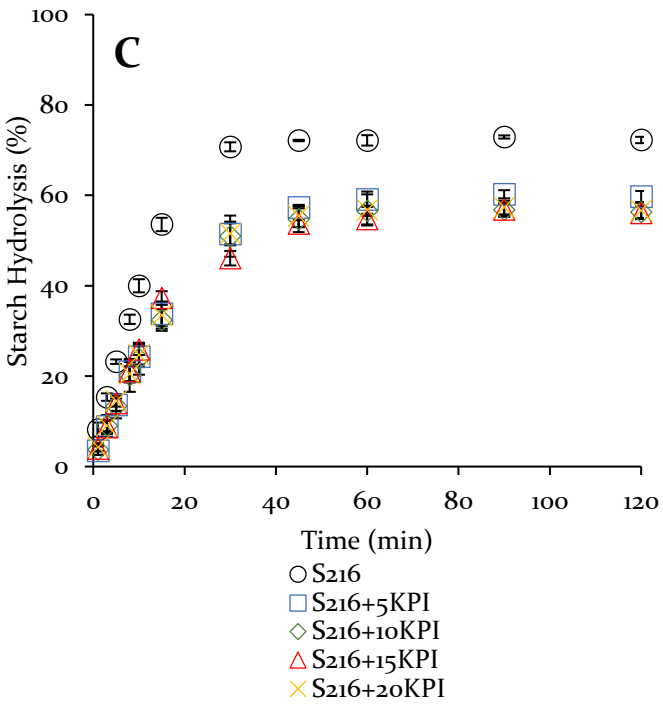

Fig. 8.3. Hydrolysis curves obtained for *in vitro* digestion by porcine pancreatic α-amylase of cooked samples of isolated starches, WGFs (< 180 μm), and pepsin–treated WGFs: (A) NGT17N216 and (B) NGT17N217 sorghum cultivars. (C) Hydrolysis curves obtained for *in vitro* digestion by porcine pancreatic α-amylase of 100 mg cooked S216 in the presence of 5, 10, 15, and 20 mg of KPI. Error bars represent standard deviations of triplicate measurements.

To better understand kinetics of the starch digestion process, starch hydrolysis data was fitted to the Goñi first-order kinetic model (Fig. 8.4), hence enabling the estimation of pseudo-first order rate constant (k, min^{-1}) and total starch digested at the end of the reaction (C_∞, %) as shown in Table 8.4. All plots obtained for isolated starches and flours revealed a single linear phase of starch amylolysis characterised by a single rate constant. High R^2 values (> 0.90) indicated a good fit of the kinetic models to the experimental data.

Table 8.4. First-order kinetic parameters of starch amylolysis estimated from Goñi model.

Sorghum samples	k (min^{-1})	C_∞ (% total starch digested)
S216	0.130 ± 0.017^{a}	72.3 ± 0.7^{a}
F216 (< 180 μm)	0.100 ± 0.003^{bc}	53.4 ± 0.3^{fg}
F216 pepsin treated	0.124 ± 0.006^{ab}	67.6 ± 0.6^{b}
S217	0.128 ± 0.012^{a}	64.4 ± 0.3^{c}
F217 (< 180 μm)	0.094 ± 0.003^{c}	52.7 ± 0.5^{g}
F217 pepsin treated	0.117 ± 0.013^{abc}	64.5 ± 0.9^{c}
S216+5KPI	0.066 ± 0.005^{d}	59.7 ± 1.2^{d}
S216+10KPI	0.056 ± 0.005^{d}	56.3 ± 1.3^{e}
S216+15KPI	0.059 ± 0.005^{d}	56.1 ± 0.9^{ef}
S216+20KPI	0.058 ± 0.007^{d}	56.6 ± 1.7^{e}

[a b c d e f g] Values are means ± standard deviations of three determinations.
Values with the same subscripts in a column do not differ significantly ($p > 0.05$).

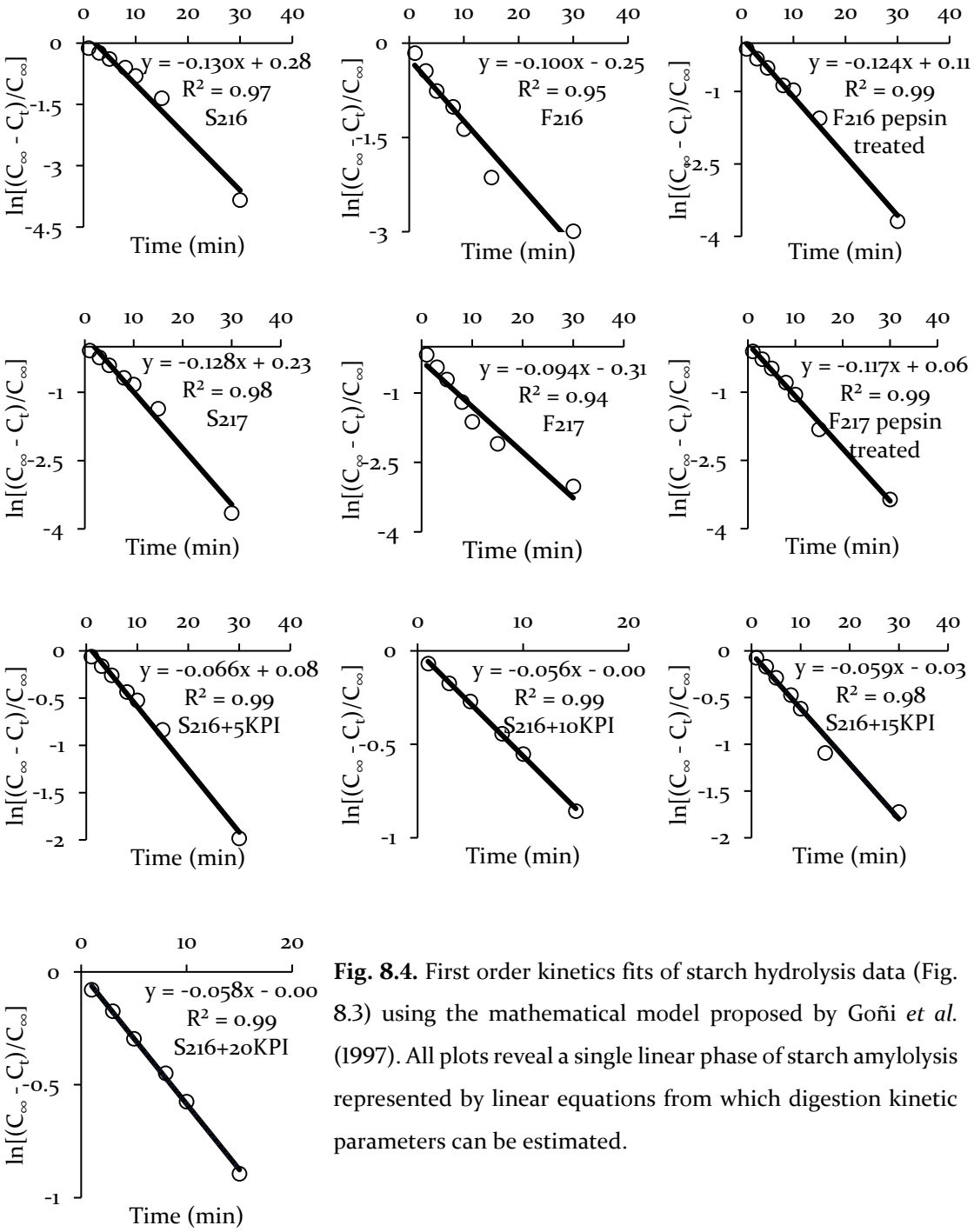

Fig. 8.4. First order kinetics fits of starch hydrolysis data (Fig. 8.3) using the mathematical model proposed by Goñi *et al.* (1997). All plots reveal a single linear phase of starch amylolysis represented by linear equations from which digestion kinetic parameters can be estimated.

It was noted that while the rate constant for S216 and S217 appeared to be relatively similar, S216 was digested to a much greater extent (i.e. higher C_∞ value). Since the rate constant (k) is an indicator of the inherent susceptibility of starch to α-amylase (Goñi *et al.*, 1997), the difference in the hydrolysis extent between these two starches may reflect different proportion of starch that could be digested at the

same rate (Edwards *et al.*, 2018). For each sorghum cultivar, the values of k and C_∞ for WGF were generally lower than those for isolated starch or pepsin-treated flour. This again confirms the role of protein in hindering starch hydrolysis in cooked sorghum flour.

To gain insight into the effect of protein on the kinetics of *in vitro* starch digestion while separating the contribution from other non-starch flour constituents (e.g. lipid and fiber), the α-amylase digestion of S216/KPI blends was investigated using *in vitro* assays. As can be clearly seen in Fig. 8.3, S216 digestibility was markedly reduced by ~ 13 – 16% upon the addition of KPI. Increasing the protein blend ratio did not seem to influence the kinetics of starch digestion. Goñi plots of all the blends revealed a single linear phase of amylolysis represented by a single rate constant. Values for k and C_∞ were much lower for all the blends than for S216, but did not seem to vary among the different blends. It is likely that the protein blend ratio could have reached optimum threshold (5 g KPI per 100 g starch) above which adding more protein did not seem to have any effect on starch digestion.

Based on these results, it is proposed that the starch-protein interactions occurring either in the natural WGF or binary mixtures may be responsible for attenuating the rate and extent of amylase digestion of sorghum starch. Indeed, the extensive disulfide cross-linking of kafirin upon wet cooking of WGF leads to the formation of high-molecular-weight protein polymers and oligomers (Ezeogu *et al.*, 2005; Duodu *et al.*, 2002). This complex protein network may impede starch gelatinisation and retard α-amylase access to the starch substrate, thus lowering *in vitro* starch digestibility (Ezeogu *et al.*, 2005, 2008).

The results in this study also indicated that KPI effectively limits the rate and extent of amylase hydrolysis of cooked sorghum starch in the binary mixtures. Heating wet KPI may induce changes in protein structure with an increase in disulfide bonds and kafirin oligomers (Byaruhanga *et al.*, 2006). Moreover, DSC and RVA analysis showed little or no inhibitory effect of KPI on starch gelatinisation. Hence, it is likely that the formation upon wet cooking of disulfide cross-linked protein barrier restricting α-amylase access is the main limiting factor for *in vitro* amylolysis of the starch/KPI blends. These results are consistent with previous research showing a pronounced reduction in the RDS content of wheat starch when cooked in the presence of hydrolysed or denatured plant proteins. Protein was observed to form a coating around cooked starch, which could obstruct α-amylase access during digestion (López-Barón *et al.*, 2017).

8.5. Conclusions

DSC analysis showed that proteins in sorghum WGF could delay starch gelatinisation. RVA analysis showed that sorghum proteins were responsible for suppressed paste peak viscosity and increased pasting temperature of starch in WGF. In contrast, no such inhibitory effect of protein on gelatinisation and pasting properties of starch was found in sorghum starch/KPI blends. Proteins greatly decreased *in vitro* rate and extent of amylolysis in both WGF and binary blends. This could be explained by the formation of disulfide-bonded protein matrix limiting α-amylase access to starch. These results show a great potential for the development of low-glycaemic-index biomimetic flour containing sorghum proteins.

CHAPTER NINE: General discussion, conclusions, and recommendations

9.1. Summary and Discussion

Nature provides a vast array of fascinating structures that have a wide range of functions with optimal efficiency at minimal costs. Critical understanding of the structure-function relationship – one of the fundamental design principles in nature – is the key for biomimetic design (Cohen, Reich, & Greenberg, 2014). Adopting a biomimetic approach to the design of nutritious and healthy foods is a novel idea. In addition, decades of research, especially this decade, have established links between structures and health-related functional properties of starch-based plant foods (Do *et al.*, 2018; Ogawa *et al.*, 2018). The aim of this thesis was (1) to delve into the relationship between edible plant microstructure and starch digestion *in vitro*, (2) to contemplate the possibility of designing BPFs for reduced glycaemic impact.

Starch granules are physically trapped inside the cellular matrix of plant-based foods such as legumes and potatoes. Intact plant cells serve as a model to study the effect of cell structure on gelatinisation and digestion of enclosed starch. Two types of cells isolated from legume cotyledons and potato parenchyma were studied (Chapter 3 and 4). Several published methods were attempted in order to establish optimal conditions for isolating intact cells. The sequential acid/alkali method (Kugimiya, 1990) was found to result in effective separation of cells without

disrupting cell wall integrity and gelatinising starch. For this reason, this method was used for cell preparation in subsequent studies.

Firstly, microstructural and physicochemical properties of isolated cells and purified starches were studied to gain a clear understanding of the gelatinisation behaviour of starch inside cells. Microscopic analysis revealed that both ICC and IPC contained many native starch granules trapped in intact cell walls. Starch was embedded in a cytoplasmic protein matrix inside ICC, whereas no such matrix was present in IPC. In addition, DSC thermal analysis showed that starch inside ICC underwent gelatinisation over a wider temperature range and at much higher T_c than ILS. This gave rise to a broad endotherm with a trailing shoulder in ICC as opposed to a narrow endotherm with a well-defined, sharp peak in ILS. The delayed gelatinisation in ICC could be attributed to limited amounts of available water and free space inside cells due to the confinement of starch granules within the cell wall. This confinement, on the other hand, had little or no apparent effect on gelatinisation of starch inside IPC. Considering the microstructural differences between ICC and IPC, it seems possible that the absence of intracellular protein matrix entrapping starch could lead to quantities of water and space inside IPC large enough to allow for complete gelatinisation. Furthermore, RVA analysis clearly demonstrated the role of the cell wall in suppressing granule swelling and preventing subsequent shear-induced rupture of swollen granules. This led to lower peak and breakdown paste viscosities of both IPC and ICC compared with those of isolated starch.

Next, *in vitro* digestion following the established protocol described by Dartois *et al.* (2010) was carried out to evaluate hydrolysis kinetics by α-amylase of starch trapped inside cells. Cooked ICC was found to have a lower rate and extent of α-amylolysis than cooked ILS. SEM examination of ICC showed cell wall intactness throughout simulated cooking and digestion. Based on these results, it was apparent that the cotyledon cell structure is responsible for the lower susceptibility of starch to amylolysis. Specifically, the strong cell wall is highly effective in restricting water ingress and intracellular space for starch gelatinisation. Moreover, the intact cell wall and protein matrix can act as physical barriers against α-amylase access to starch substrate.

Contrary to what was observed in ICC, no significant differences in the rate and extent of starch digestion were found between cooked IPC and cooked IPS. SEM examination of IPC revealed cell wall intactness throughout cooking and digestion. These results indicated that, despite the intact cell wall barrier, the IPC structure had no apparent effect on slowing down starch digestion. It was speculated that partial breakdown of the cell wall during cooking may lead to increase in wall permeability and facilitate starch-amylase interactions.

The studies of starch-entrapped plant cells yielded some interesting results and provided important insights into the effect of cellular structure on starch digestion. Evidently, ICC structure was more effective in slowing down starch digestion than IPC structure. A likely explanation for this is the microstructural differences between these two cell types, e.g. the presence of protein matrix, cell wall structure and composition, etc. Given the fact that previous studies have mainly focused on

the cell wall as the primary barrier to starch digestion (Dhital *et al.*, 2016; Do *et al.*, 2019), this finding raised the interesting possibility that the protein matrix present in ICC also plays a role in limiting starch digestion as explored in Chapter 5.

To investigate this, native INC were pre-treated with pepsin for 1, 4, or 24 h to generate cell samples with different degrees of protein hydrolysis prior to *in vitro* gastro-small intestinal digestion. Results showed that the protein content of cells declined, whereas the rate and extent of starch hydrolysis generally increased as the treatment time progressively increased from 1 to 24 h. Further, the 24 h treatment with pepsin achieved the highest percentage of protein hydrolysis (~85%) and yielded cells with a higher degree of starch swelling and solubility compared to that of native cells. Based on these results, it was thought that the cleavage of intracellular proteins surrounding starch granules may leave behind more water and free space for granules to swell and dissolve, while exposing greater starch surface area for possible interactions with enzymes. As such, the starch substrate becomes more accessible to amylolytic attack. It would therefore be reasonable to conclude that, aside from the cell wall, the protein matrix acts as an additional barrier for protecting starch against amylolytic degradation.

SEM analysis of ICC and IPC (Chapter 3 & 4) provided convincing although indirect evidence for cell wall intactness throughout simulated cooking and *in vitro* digestion. This is suggestive of a starch digestion process in which α-amylase diffuses through the cell wall and digestive products diffuse out. In fact, the microscopic examination of cells in these studies involved the capture of static images of representative cells sampled at specific time points during experiments.

This in turn provided very limited information on dynamics and mechanism of the slow starch digestion inside cells. This limitation motivated the development of a novel microscope chamber for direct observations and tracking of individual plant cells in real-time through each stage of simulated cooking followed by GI digestion *in vitro* (Chapter 6).

Time-lapse optical imaging of a cohort of INC, which were contained within the chamber and gradually heated from 24 to 90°C in water, revealed that individual starch granules rapidly swelled between 80 and 86°C. These swollen granules completely filled the entire intracellular space after ~20 min of cooking. No apparent visual changes in cells were observed during 30 min gastric digestion with pepsin at pH 1.2 and 37°C. During 120 min small intestinal digestion with pancreatin at pH 6.8 and 37°C, starch was observed to "shrink" radially inwards towards the centre of each cell, implying that starch hydrolysis by pancreatic α-amylase had occurred inside cells. The cells showed no visual evidence of disruption during the entire process of cooking and digestion. These results provide direct evidence for the cell wall intactness and strongly support the proposed mechanism of starch digestion inside ICC reported in previous studies (Berg *et al.*, 2012; Do *et al.*, 2019).

For data analysis, the "shrinkage" of cellular contents was manually traced over time using ImageJ to generate data for quantitatively characterising the starch digestion process. A first principle-based mathematical model was then constructed to describe the kinetics of this process, which accounted for enzyme diffusion through the cell wall (diffusion-limited mass transfer), for enzyme-

catalysed starch hydrolysis (Michaelis-Menten model), and for radially inward "shrinking" of starch core ("shrinking core" model). Fitting this model to the experimental data allowed calculation of different rates of starch hydrolysis for different cells. The variation in the rate of α-amylolysis could be due to microstructural and compositional differences among cells within the cohort. This important finding highlights the capability of the novel apparatus for aiding the mechanistic understanding and quantitative characterisation of starch digestion process at the single-cell scale.

Taking inspiration from the fundamental understanding of the role of the cotyledon cell wall and protein in inhibition of starch digestion gained from previous research chapters, the fabrication of starch-entrapped particles was explored in Chapter 7. These particles were prepared by entrapping native CS within pectin matrix and were formed by ionotropic gelation of pectin via calcium cross-linking. These particles exhibited a delay in starch gelatinisation and a reduction in the rate and extent of starch digestion *in vitro* compared with non-trapped CS. In general, kinetics of starch digestion was found to vary inversely with particle size. These results lead to the suggestion that the pectin matrix, in a similar manner to the cotyledon cell wall, acts as a physical barrier against α-amylase access to entrapped starch. Further, several factors should be taken into consideration when designing starch-entrapped particles, such as particle size, particle microstructure and composition, and polymer matrix composition.

It is well established that the formation of disulphide cross-linked protein network in sorghum and maize flours upon wet cooking limits starch digestion *in vitro*

(Ezeogu *et al.*, 2005, 2008). In an additional study, we investigated the effect of protein on physicochemical properties and *in vitro* digestion of starch in two flour model systems: (i) WGF and (ii) binary blends consisting of sorghum starch and KPI. The results showed that protein in WGF could delay the gelatinisation process by competing with starch granules for water. The protein in WGF could also hinder initial granule swelling, resulting in reduced peak paste viscosity during the RVA heating phase. Conversely, we found no apparent effect of KPI in the blends on gelatinisation and pasting properties of starch. Following cooking, both the WGF and blends showed a lower rate and extent of *in vitro* amylolysis compared with isolated starch. It was suggested that the formation of disulphide-bonded kafirin matrix under wet-heating conditions could hamper α-amylase access to starch. This has potential implications for biomimetic food design, i.e. the possibility to formulate low-glycaemic-index biomimetic flour by combining starch granules, KPI, and other food-grade ingredients.

9.2. Conclusions and Recommendations for Future Research

This dissertation explores the natural and biomimetic design of starch-entrapped structures (illustrated in Fig. 9.1) and the critical role of these structures in modulating starch digestion *in vitro*. One of the most important findings presented in this dissertation is that the encapsulation of native starch granules within protein matrix and/or cell-wall-polymer network is capable of slowing down starch digestion *in vitro* via two possible mechanisms: (i) restricting water availability and free space for granule swelling and gelatinisation and thus reducing starch susceptibility to amylolytic attack, and (ii) restricting free diffusion of enzymes

through the protein/cell wall barrier and thus reducing enzyme accessibility to entrapped starch. Another key finding is that IPC, unlike ICC, is not capable of limiting starch digestion despite possessing starch-entrapped structure. This is possibly due to microstructural differences between these two cell types. It has been speculated that the presence of a compact protein matrix in ICC but not in IPC provides an additional protective barrier against α-amylase for efficiently slowing down starch digestion. These findings provide crucial information to aid in the biomimetic design of starch-entrapped particles. Some essential design lessons learned from nature are related to the desired properties of the encapsulation matrix for starch granules as shown below.

(i) Robustness and high resistance to enzymatic degradation, e.g. cotyledon cell walls are not digestible by enzymes and remain intact in the upper GI tract.

(ii) Hydrophobicity, e.g. disulphide cross-linked kafirin network is highly hydrophobic and may restrict water ingress for granule swelling.

(iii) Compactness, e.g. tight packing of starch granules in the dense protein matrix of cotyledon cells may limit starch surface area accessible for enzyme binding/catalysis.

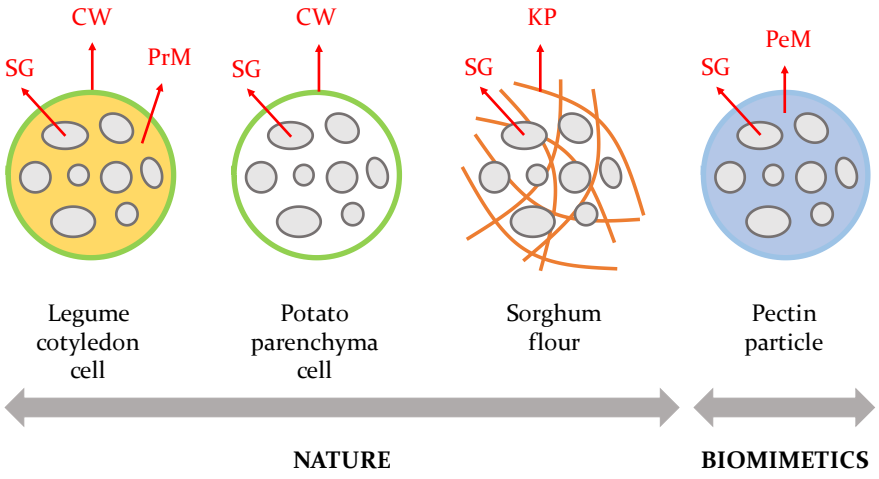

Fig. 9.1. Schematic illustrations of natural and biomimetic design of starch-entrapped structures. Abbreviations used in this figure: SG, starch granule; CW, cell wall; PrM, protein matrix; PeM, pectin matrix; KP, kafirin protein.

The emerging area of BPFs offers a plethora of opportunities for further research work. The findings from this dissertation lay a strong foundation for future studies that are briefly discussed below.

(i) The ParCS apparatus for time-lapse optical microscopy of a cohort of individual INC provided a new tool to probe gelatinisation and digestive behaviours of entrapped starch at the single-cell scale. Future research is needed to investigate the use of this novel technique to study different plant cell types, such as IPC and chickpea ICC. This technique can also be used to examine the effect of the intracellular protein matrix on starch digestion, which can provide both qualitative and quantitative evidence to support the findings presented in Chapter 6.

(ii) The attempt to fabricate biomimetic starch-entrapped pectin particles with slow starch digestion property showed promising potential for

incorporation of this type of structure into food systems. Several critical design factors should be carefully considered for achieving desired starch digestion profiles, including size, microstructure, and composition of particles. Xyloglucan and cellulose, two other major components in dicotyledonous plant cell walls, can be incorporated into pectin-based formulations in order to mimic the cell wall composition. Future work will aim to explore these possibilities.

(iii) The protein matrix is an integral component of legume ICC and has been shown to have enzyme barrier properties (Chapter 5). The intact cell wall and protein matrix provide double protection for entrapped starch against α-amylolysis. Double encapsulation of starch granules within a protein core and a polysaccharide shell could be a novel strategy worth exploring for designing biomimetic cotyledon cells.

(iv) In Chapter 8, sorghum kafirin has been shown to impede *in vitro* starch digestion, possibly due to its propensity to form disulphide-bonded network entrapping starch upon wet cooking. Encapsulation of starch granules by kafirin protein using low-temperature spray drying to mimic the natural starch-protein matrix in sorghum grains, similar to that reported for zein protein (Xu & Zhang, 2014), can produce starch-entrapped particles for slowing down starch digestion.

Bibliography

Aguilera, J. M., & Stanley, D. W. (1999). *Microstructural Principles of Food Processing and Engineering* (2nd ed.). Maryland: Aspen Publishers Inc.

Aguilera, J. M., Cadoche, L., López, C., & Gutierrez, G. (2001). Microstructural changes of potato cells and starch granules heated in oil. *Food Research International*, *34*(10), 939-947.

Akingbala, J. O., Gomez, M. H., Rooney, L. W., & Sweat, V. E. (1988). Thermal properties of sorghum starch. *Starch-Stärke*, *40*(10), 375-378.

Alminger, M. L., Eklund-Jonsson, C., Kidman, S., & Langton, M. (2012). Starch microstructure and starch hydrolysis in barley and oat tempe during *in vitro* digestion. *Food Digestion*, *3*(1-3), 53-62.

Al-Rabadi, G. J., Gilbert, R. G., & Gidley, M. J. (2009). Effect of particle size on kinetics of starch digestion in milled barley and sorghum grains by porcine alpha-amylase. *Journal of Cereal Science*, *50*(2), 198-204.

Barichello, V., Yada, R. Y., Coffin, R. H., & Stanley, D. W. (1990). Low temperature sweetening in susceptible and resistant potatoes: starch structure and composition. *Journal of Food Science, 55*(4), 1054-1059.

Barros, F., Awika, J. M., & Rooney, L. W. (2012). Interaction of tannins and other sorghum phenolic compounds with starch and effects on *in vitro* starch digestibility. *Journal of Agricultural and Food Chemistry*, *60*(46), 11609-11617.

Becerra-Tomás, N., Díaz-López, A., Rosique-Esteban, N., Ros, E., Buil-Cosiales, P., Corella, D., ... & Lamuela-Raventós, R. M. (2018). Legume consumption is inversely associated with type 2 diabetes incidence in adults: A prospective assessment from the PREDIMED study. *Clinical Nutrition*, *37*(3), 906-913.

Beisson, F., Ferté, N., Bruley, S., Voultoury, R., Verger, R., & Arondel, V. (2001). Oil-bodies as substrates for lipolytic enzymes. *Biochimica et Biophysica Acta (BBA)-Molecular and Cell Biology of Lipids*, *1531*(1), 47-58.

Bengtsson, A., Brackmann, C., Enejder, A., Alminger, M. L., & Svanberg, U. (2010). Effects of thermal processing on the *in vitro* bioaccessibility and microstructure of β-carotene in orange-fleshed sweet potato. *Journal of Agricultural and Food Chemistry*, *58*(20), 11090-11096.

Berg, T., Singh, J., Hardacre, A., & Boland, M. J. (2012). The role of cotyledon cell structure during *in vitro* digestion of starch in navy beans. *Carbohydrate Polymers*, *87*(2), 1678-1688.

Bergman, T. L., Lavine, A. S., Incropera, F. P., & DeWitt, D. P. (2017). *Fundamentals of Heat and Mass Transfer* (8th ed.). Hoboken, NJ: Wiley.

Bernfeld, P. (1955). Amylases, α and β. *Methods Enzymol*, *1*, 149-158.

Berry, S. E., Tydeman, E. A., Lewis, H. B., Phalora, R., Rosborough, J., Picout, D. R., & Ellis, P. R. (2008). Manipulation of lipid bioaccessibility of almond seeds influences postprandial lipemia in healthy human subjects. *The American Journal of Clinical Nutrition*, *88*(4), 922-929.

Beta, T., Corke, H., Rooney, L. W., & Taylor, J. R. N. (2001). Starch properties as affected by sorghum grain chemistry. *Journal of the Science of Food and Agriculture*, *81*(2), 245-251.

Bhattarai, R. R., Dhital, S., & Gidley, M. J. (2016). Interactions among macronutrients in wheat flour determine their enzymic susceptibility. *Food Hydrocolloids*, *61*, 415-425.

Bhattarai, R. R., Dhital, S., Mense, A., Gidley, M. J., & Shi, Y. C. (2018). Intact cellular structure in cereal endosperm limits starch digestion in vitro. *Food Hydrocolloids*, *81*, 139-148.

Bhattarai, R. R., Dhital, S., Wu, P., Chen, X. D., & Gidley, M. J. (2017). Digestion of isolated legume cells in a stomach-duodenum model: three mechanisms limit starch and protein hydrolysis. *Food & Function*, *8*(7), 2573-2582.

Bhushan, B. (2009). Biomimetics: lessons from nature – an overview. *Philosophical Transactions of the Royal Society, 367*, 1445–86.

Biliaderis, C. G., Maurice, T. J., & Vose, J. R. (1980). Starch gelatinization phenomena studied by differential scanning calorimetry. *Journal of Food Science*, *45*(6), 1669-1674.

Black, J. L. (2001, September). Quality feed grains—research highlights and opportunities. In *Proceedings of the 10th Australian barley technical symposium, http://www. regional. org. au/au/abts/2001/m3/black.*

Bordoloi, A., Kaur, L., & Singh, J. (2012a). Parenchyma cell microstructure and textural characteristics of raw and cooked potatoes. *Food Chemistry*, *133*(4), 1092-1100.

Bordoloi, A., Singh, J., & Kaur, L. (2012b). In vitro digestibility of starch in cooked potatoes as affected by guar gum: Microstructural and rheological characteristics. *Food Chemistry*, *133*(4), 1206-1213.

Bornhorst, G. M., & Singh, R. P. (2014). Gastric digestion *in vivo* and *in vitro*: how the structural aspects of food influence the digestion process. *Annual Review of Food Science and Technology*, *5*, 111-132.

Bornhorst, G. M., Chang, L. Q., Rutherfurd, S. M., Moughan, P. J., & Singh, R. P. (2013). Gastric emptying rate and chyme characteristics for cooked brown and white rice meals *in vivo*. *Journal of the Science of Food and Agriculture*, *93*(12), 2900-2908.

Boudries, N., Belhaneche, N., Nadjemi, B., Deroanne, C., Mathlouthi, M., Roger, B., & Sindic, M. (2009). Physicochemical and functional properties of starches from sorghum cultivated in the Sahara of Algeria. *Carbohydrate Polymers*, *78*(3), 475-480.

Brooker, R. J., Widmaier, E. P., Graham, L. E., & Stiling, P. D. (2017). *Biology* (4th ed.). New York: *McGraw-Hill Education*.

Brummer, Y., Kaviani, M., & Tosh, S. M. (2015). Structural and functional characteristics of dietary fibre in beans, lentils, peas and chickpeas. *Food Research International*, *67*, 117-125.

Buisson, G., Duee, E., Haser, R., & Payan, F. (1987). Three dimensional structure of porcine pancreatic alpha-amylase at 2.9 A resolution. Role of calcium in structure and activity. *The EMBO Journal*, *6*(13), 3909-3916.

Burton, R. A., Gidley, M. J., & Fincher, G. B. (2010). Heterogeneity in the chemistry, structure and function of plant cell walls. *Nature Chemical Biology*, *6*(10), 724-732.

Byaruhanga, Y. B., Emmambux, M. N., Belton, P. S., Wellner, N., Ng, K. G., & Taylor, J. R. N. (2006). Alteration of kafirin and kafirin film structure by heating with microwave energy and tannin complexation. *Journal of Agricultural and Food Chemistry*, *54*(12), 4198-4207.

Capuano, E. (2017). The behaviour of dietary fiber in the gastrointestinal tract determines its physiological effect. *Critical Reviews in Food Science and Nutrition*, *57*(16), 3543-3564.

Capuano, E., & Pellegrini, N. (2019). An integrated look at the effect of structure on nutrient bioavailability in plant foods. *Journal of the Science of Food and Agriculture*, *99*(2), 493-498.

Carnachan, S. M., Bootten, T. J., Mishra, S., Monro, J. A., & Sims, I. M. (2012). Effects of simulated digestion *in vitro* on cell wall polysaccharides from kiwifruit (Actinidia spp.). *Food Chemistry*, *133*(1), 132-139.

Carpita, N. C., & Gibeaut, D. M. (1993). Structural models of primary cell walls in flowering plants: consistency of molecular structure with the physical properties of the walls during growth. *The Plant Journal*, *3*(1), 1-30.

Chaiwanichsiri, S., Ohnishi, S., Suzuki, T., Takai, R., & Miyawaki, O. (2001). Measurement of electrical conductivity, differential scanning calorimetry and viscosity of starch and flour suspensions during gelatinisation process. *Journal of the Science of Food and Agriculture*, *81*(15), 1586-1591.

Chandrashekar, A., & Kirleis, A. W. (1988). Influence of protein on starch gelatinization in sorghum. *Cereal Chemistry*, *65*(6), 457-462.

Chen, M. C., Chyan, C. L., Lee, T. T., Huang, S. H., & Tzen, J. T. (2004). Constitution of stable artificial oil bodies with triacylglycerol, phospholipid, and caleosin. *Journal of Agricultural and Food Chemistry*, *52*(12), 3982-3987.

Choct, M., Bird, S. H., Littlefield, P., Balogun, R., & Rowe, J. B. (2001). Microstructure of grains as an indicator of nutritive value. *Recent Advanced Animal Nutrition Australia*, *13*, 223–228.

Cisse, F., Pletsch, E. A., Erickson, D. P., Chegeni, M., Hayes, A. M., & Hamaker, B. R. (2017). Preload of slowly digestible carbohydrate microspheres decreases gastric emptying rate of subsequent meal in humans. *Nutrition Research*, *45*, 46-51.

Clemente, A., Vioque, J., Sánchez-Vioque, R., Pedroche, J., Bautista, J., & Millán, F. (2000). Factors affecting the *in vitro* protein digestibility of chickpea albumins. *Journal of the Science of Food and Agriculture*, *80*(1), 79-84.

Cohen, Y. H., Reich, Y., & Greenberg, S. (2014). Biomimetics: structure–function patterns approach. *Journal of Mechanical Design*, *136*(11), 111108.

Cooke, D., & Gidley, M. J. (1992). Loss of crystalline and molecular order during starch gelatinisation: origin of the enthalpic transition. *Carbohydrate Research*, *227*, 103-112.

Cosgrove, D. J. (1997). Assembly and enlargement of the primary cell wall in plants. *Annual Review of Cell and Developmental Biology*, *13*(1), 171-201.

Cybulska, J., Vanstreels, E., Ho, Q. T., Courtin, C. M., Van Craeyveld, V., Nicolaï, B., Zduneck, A., & Konstankiewicz, K. (2010). Mechanical characteristics of artificial cell walls. *Journal of Food Engineering*, *96*(2), 287-294.

Dartois, A., Singh, J., Kaur, L., & Singh, H. (2010). Influence of guar gum on the in vitro starch digestibility—rheological and microstructural characteristics. *Food Biophysics*, *5*(3), 149-160.

Deguchi, S., & Tsujii, K. (2002). Flow cell for in situ optical microscopy in water at high temperatures and pressures up to supercritical state. *Review of Scientific Instruments*, *73*(11), 3938-3941.

Dhital, S., Bhattarai, R. R., Gorham, J., & Gidley, M. J. (2016). Intactness of cell wall structure controls the *in vitro* digestion of starch in legumes. *Food & Function*, *7*(3), 1367-1379.

Dhital, S., Gidley, M. J., & Warren, F. J. (2015). Inhibition of α-amylase activity by cellulose: Kinetic analysis and nutritional implications. *Carbohydrate Polymers*, *123*, 305-312.

Dicko, M. H., Hilhorst, R., Gruppen, H., Traoré, A. S., Laane, C., van Berkel, W. J., & Voragen, A. G. (2002). Comparison of content in phenolic compounds, polyphenol oxidase, and peroxidase in grains of fifty sorghum varieties from Burkina Faso. *Journal of Agricultural and Food Chemistry*, *50*(13), 3780-3788.

Do, D. T., & Singh, J. (2018). Legume Microstructure. In *Reference Module in Food Science*. https://doi.org/10.1016/B978-0-08-100596-5.21683-1

Do, D. T., Singh, J., Oey, I., & Singh, H. (2018). Biomimetic Plant Foods: Structural design and functionality. *Trends in Food Science & Technology*, *82*, 46-59.

Do, D. T., Singh, J., Oey, I., & Singh, H. (2019). Modulating effect of cotyledon cell microstructure on *in vitro* digestion of starch in legumes. *Food Hydrocolloids*, *96*, 112-122.

Do, D. T., Singh, J., Oey, I., Singh, H., Yada, R.Y., & Frostad, J. (2020). A novel apparatus for time-lapse optical microscopy of gelatinisation and digestion of starch inside plant cells. *Food Hydrocolloids*, *104*.

Dona, A. C., Pages, G., Gilbert, R. G., & Kuchel, P. W. (2010). Digestion of starch: *In vivo* and *in vitro* kinetic models used to characterise oligosaccharide or glucose release. *Carbohydrate Polymers*, *80*(3), 599-617.

Donovan, J. W. (1979). Phase transitions of the starch–water system. *Biopolymers*, *18*(2), 263-275.

Duodu, K. G., Nunes, A., Delgadillo, I., Parker, M. L., Mills, E. N. C., Belton, P. S., & Taylor, J. R. N. (2002). Effect of grain structure and cooking on sorghum and maize *in vitro* protein digestibility. *Journal of Cereal Science*, *35*(2), 161-174.

Duodu, K. G., Taylor, J. R. N., Belton, P. S., & Hamaker, B. R. (2003). Factors affecting sorghum protein digestibility. *Journal of Cereal Science*, *38*(2), 117-131.

Dykes, L., Rooney, L. W., Waniska, R. D., & Rooney, W. L. (2005). Phenolic compounds and antioxidant activity of sorghum grains of varying genotypes. *Journal of Agricultural and Food Chemistry*, *53*(17), 6813-6818.

Edwards, C. H., Maillot, M., Parker, R., & Warren, F. J. (2018). A comparison of the kinetics of in vitro starch digestion in smooth and wrinkled peas by porcine pancreatic alpha-amylase. *Food Chemistry*, *244*, 386-393.

Edwards, C. H., Warren, F. J., Campbell, G. M., Gaisford, S., Royall, P. G., Butterworth, P. J., & Ellis, P. R. (2015). A study of starch gelatinisation behaviour in hydrothermally-processed plant food tissues and implications for *in vitro* digestibility. *Food & Function*, *6*(12), 3634-3641.

Ek, K. L., Wang, S., Brand-Miller, J., & Copeland, L. (2014). Properties of starch from potatoes differing in glycemic index. *Food & Function*, *5*(10), 2509-2515.

Eliasson, A. C. (1983). Differential scanning calorimetry studies on wheat starch—gluten mixtures: I. Effect of gluten on the gelatinization of wheat starch. *Journal of Cereal Science*, *1*(3), 199-205.

Ellis, P. R., Kendall, C. W., Ren, Y., Parker, C., Pacy, J. F., Waldron, K. W., & Jenkins, D. J. (2004). Role of cell walls in the bioaccessibility of lipids in almond seeds. *The American Journal of Clinical Nutrition*, *80*(3), 604-613.

Englyst, H. N., Kingman, S. M., & Cummings, J. H. (1992). Classification and measurement of nutritionally important starch fractions. *European Journal of Clinical Nutrition*, *46*, S33-50.

Espinosa-Ramírez, J., & Serna-Saldívar, S. O. (2016). Functionality and characterization of kafirin-rich protein extracts from different whole and decorticated sorghum genotypes. *Journal of Cereal Science*, *70*, 57-65.

Evans, I. D., & Haisman, D. R. (1982). The effect of solutes on the gelatinization temperature range of potato starch. *Starch-Stärke*, *34*(7), 224-231.

Ezeogu, L. I., Duodu, K. G., & Taylor, J. R. N. (2005). Effects of endosperm texture and cooking conditions on the in vitro starch digestibility of sorghum and maize flours. *Journal of Cereal Science*, *42*(1), 33-44.

Ezeogu, L. I., Duodu, K. G., Emmambux, M. N., & Taylor, J. R. (2008). Influence of cooking conditions on the protein matrix of sorghum and maize endosperm flours. *Cereal Chemistry*, *85*(3), 397-402.

Fardet, A. (2015). A shift toward a new holistic paradigm will help to preserve and better process grain products' food structure for improving their health effects. *Food & Function*, *6*(2), 363-382.

Fonslick, J., & Khan, A. (1989). Thermal stability and composition of the amylose–iodine complex. *Journal of Polymer Science Part A: Polymer Chemistry*, *27*(12), 4161-4167.

Fratzl, P. (2007). Biomimetic materials research: what can we really learn from nature's structural materials?. *Journal of the Royal Society Interface*, *4*(15), 637-642.

Frost, J. K., Flanagan, B. M., Brummell, D. A., O'Donoghue, E. M., Mishra, S., Gidley, M. J., & Monro, J. A. (2016). Composition and structure of tuber cell walls affect *in vitro* digestibility of potato (Solanum tuberosum L.). *Food & Function*, *7*(10), 4202-4212.

Fujimura, T., & Kugimiya, M. (1993). Gelatinization of starches inside cotyledon cells of adzuki bean studied by differential scanning calorimetry. *Nippon Shokuhin Kogyo Gakkaishi*, *40*(10), 702-707.

Fujimura, T., & Kugimiya, M. (1994). Gelatinization of starches inside cotyledon cells of kidney beans. *Starch-Stärke*, *46*(10), 374-378.

Fujimura, T., & Kugimiya, M. (1995). Estimation of Intracellular Water Content during Gelatinization of Starches inside Cotyledon Cells of Legumes. *Journal of Applied Glycoscience*, *42*(1), 7-13.

Fujimura, T., Liu, X. Y., & Kugimiya, M. (1995). Gelatinization of starches inside cotyledon cells separated from faba beans. *Nippon Shokuhin Kogaku Kogaku Kaishi*, *42*(3), 190-195.

Fujimura, T., Tanaka, Y., Narita, M., & Isobe, Y. (2007). Gelatinization of starches inside cotyledon cells separated from Tutankhamen's pea [Pisum sativum]. *Nippon Shokuhin Kogaku Kogaku Kaishi*, *54*(11), 463-467.

Gallier, S., & Singh, H. (2012a). Behavior of almond oil bodies during *in vitro* gastric and intestinal digestion. *Food & Function*, *3*(5), 547-555.

Gallier, S., & Singh, H. (2012b). The physical and chemical structure of lipids in relation to digestion and absorption. *Lipid Technology*, *24*(12), 271-273.

Gibson, L. J. (2012). The hierarchical structure and mechanics of plant materials. *Journal of the Royal Society Interface*, *9,* 2749-2766.

Gibson, L. J., Ashby, M. F. & Harley, B. A. (2010). *Cellular Materials in Nature and Medicine*. Cambridge, UK: Cambridge University Press.

Glahn, R. P., Tako, E., Cichy, K., & Wiesinger, J. (2016). The cotyledon cell wall and intracellular matrix are factors that limit iron bioavailability of the common bean (Phaseolus vulgaris). *Food & Function*, *7*(7), 3193-3200.

Golding, M., & Wooster, T. J. (2010). The influence of emulsion structure and stability on lipid digestion. *Current Opinion in Colloid & Interface Science*, *15*(1), 90-101.

Goñi, I., Garcia-Alonso, A., & Saura-Calixto, F. (1997). A starch hydrolysis procedure to estimate glycemic index. *Nutrition Research*, *17*(3), 427-437.

Grimes, D. A., & Schulz, K. F. (2002). Cohort studies: marching towards outcomes. *The Lancet*, *359*(9303), 341-345.

Grundy, M. M. L., Edwards, C. H., Mackie, A. R., Gidley, M. J., Butterworth, P. J., & Ellis, P. R. (2016a). Re-evaluation of the mechanisms of dietary fibre and implications for macronutrient bioaccessibility, digestion and postprandial metabolism. *British Journal of Nutrition*, *116*(05), 816-833.

Grundy, M. M. L., Lapsley, K., & Ellis, P. R. (2016b). A review of the impact of processing on nutrient bioaccessibility and digestion of almonds. *International Journal of Food Science & Technology*, *51*(9), 1937-1946.

Grundy, M. M., Carrière, F., Mackie, A. R., Gray, D. A., Butterworth, P. J., & Ellis, P. R. (2016c). The role of plant cell wall encapsulation and porosity in regulating lipolysis during the digestion of almond seeds. *Food & Function*, *7*(1), 69-78.

Grundy, M. M., Wilde, P. J., Butterworth, P. J., Gray, R., & Ellis, P. R. (2015). Impact of cell wall encapsulation of almonds on *in vitro* duodenal lipolysis. *Food Chemistry*, *185*, 405-412.

Gu, J., & Catchmark, J. M. (2012). Impact of hemicelluloses and pectin on sphere-like bacterial cellulose assembly. *Carbohydrate Polymers*, *88*(2), 547-557.

Guerra, A., Etienne-Mesmin, L., Livrelli, V., Denis, S., Blanquet-Diot, S., & Alric, M. (2012). Relevance and challenges in modeling human gastric and small intestinal digestion. *Trends in Biotechnology*, *30*(11), 591-600.

Hahn, D. M., Jones, F. T., Akha Van, I., & Rockland, L. B. (1977). Light and scanning electron microscope studies on dry beans: intracellular gelatinization of starch in cotyledons of large lima beans (Phaseolus lunatus). *Journal of Food Science*, *42*(5), 1208-1212.

Hamaker, B. R., & Bugusu, B. A. (2003). *Overview: sorghum proteins and food quality*. Pretoria, South Africa: Paper presented at the Workshop on the proteins of sorghum and millets: enhancing nutritional and functional properties for Africa [CD].

Hamaker, B. R., Mohamed, A. A., Habben, J. E., Huang, C. P., & Larkins, B. A. (1995). Efficient procedure for extracting maize and sorghum kernel proteins reveals higher prolamin contents than the conventional method. *Cereal Chemistry*, 72, 583-588.

Hayashi, T., Marsden, M. P., & Delmer, D. P. (1987). Pea xyloglucan and cellulose: VI. Xyloglucan-cellulose interactions in vitro and in vivo. *Plant Physiology*, *83*(2), 384-389.

Holm, J., Lundquist, I., Björck, I., Eliasson, A. C., & Asp, N. G. (1988). Degree of starch gelatinization, digestion rate of starch in vitro, and metabolic response in rats. *The American Journal of Clinical Nutrition*, *47*(6), 1010-1016.

Hoover, R., & Ratnayake, W. S. (2002). Starch characteristics of black bean, chick pea, lentil, navy bean and pinto bean cultivars grown in Canada. *Food Chemistry*, *78*(4), 489-498.

Hoover, R., Hughes, T., Chung, H. J., & Liu, Q. (2010). Composition, molecular structure, properties, and modification of pulse starches: A review. *Food Research International*, *43*(2), 399-413.

Hoover, R., Rorke, S. C., & Martin, A. M. (1991). Isolation and characterization of lima bean (Phaseolus lunatus) starch. *Journal of Food Biochemistry*, *15*(2), 117-136.

Hsieh, H. M., Swanson, B. G., & Lumpkin, T. A. (1999). Starch gelatinization and microstructure of azuki an granules prepared from whole, abraded, or ground beans. *LWT-Food Science and Technology*, *32*(8), 469-480.

Huang, J., Schols, H. A., van Soest, J. J., Jin, Z., Sulmann, E., & Voragen, A. G. (2007). Physicochemical properties and amylopectin chain profiles of cowpea, chickpea and yellow pea starches. *Food Chemistry*, *101*(4), 1338-1345.

Jarvis, M. C. (2011). Plant cell walls: supramolecular assemblies. *Food Hydrocolloids*, *25*(2), 257-262.

Jarvis, M. C., Briggs, S. P. H., & Knox, J. P. (2003). Intercellular adhesion and cell separation in plants. *Plant, Cell & Environment*, *26*(7), 977-989.

Jarvis, M. C., Mackenzie, E., & Duncan, H. J. (1992). The textural analysis of cooked potato. 2. Swelling pressure of starch during gelatinisation. *Potato Research*, *35*(1), 93-102.

Jenkins, D. J. A., Ghafari, H., Wolever, T. M. S., Taylor, R. H., Jenkins, A. L., Barker, H. M., ... & Bowling, A. C. (1982). Relationship between rate of digestion of foods and post-prandial glycaemia. *Diabetologia*, *22*(6), 450-455.

Joshi, M., Aldred, P., McKnight, S., Panozzo, J. F., Kasapis, S., Adhikari, R., & Adhikari, B. (2013). Physicochemical and functional characteristics of lentil starch. *Carbohydrate Polymers*, *92*(2), 1484-1496.

Kamal-Eldin, A., Lærke, H. N., Knudsen, K. E. B., Lampi, A. M., Piironen, V., Adlercreutz, H., ... & Åman, P. (2009). Physical, microscopic and chemical characterisation of industrial rye and wheat brans from the Nordic countries. *Food & Nutrition Research*, *53*(1), 1912.

Khorasani, A. C., & Shojaosadati, S. A. (2016). Bacterial nanocellulose-pectin bionanocomposites as prebiotics against drying and gastrointestinal condition. *International Journal of Biological Macromolecules*, *83*, 9-18.

Kim, E. H. J., Petrie, J. R., Motoi, L., Morgenstern, M. P., Sutton, K. H., Mishra, S., & Simmons, L. D. (2008). Effect of structural and physicochemical characteristics of the protein matrix in pasta on in vitro starch digestibility. *Food Biophysics*, *3*(2), 229-234.

Kim, E. J., & Kim, H. S. (2015). Physicochemical properties of dehydrated potato parenchyma cells with ungelatinized and gelatinized starches. *Carbohydrate Polymers*, *117*, 845-852.

Kong, F., & Singh, R. P. (2009a). Digestion of raw and roasted almonds in simulated gastric environment. *Food Biophysics*, *4*(4), 365-377.

Kong, F., & Singh, R. P. (2009b). Modes of disintegration of solid foods in simulated gastric environment. *Food Biophysics*, *4*(3), 180-190.

Kugimiya, M. (1990). Separation of cotyledon cells of legumes by successive treatments with acid and alkali. *Nippon Shokuhin Kogyo Gakkaishi*, *37*(11), 867-871.

Lavoisier, A., & Aguilera, J. M. (2019). Effect of a Whey Protein Network Formed by Cold Gelation on Starch Digestibility. *Food Biophysics*, *14*(2), 214-224.

Leach, H. W., McCowen, D. L., & Schoch, T. J. (1959). Swelling and solubility patterns of various starches, structure of starch granules. *Cereal Chemistry*, *36*, 534-544.

Lending, C. R., Kriz, A. L., Larkins, B. A., & Bracker, C. E. (1988). Structure of maize protein bodies and immunocytochemical localization of zeins. *Protoplasma*, *143*(1), 51-62.

Lesmes, U., & McClements, D. J. (2009). Structure–function relationships to guide rational design and fabrication of particulate food delivery systems. *Trends in Food Science & Technology*, *20*(10), 448-457.

Ley, S. H., Hamdy, O., Mohan, V., & Hu, F. B. (2014). Prevention and management of type 2 diabetes: dietary components and nutritional strategies. *The Lancet*, *383*(9933), 1999-2007.

Li, H., Gidley, M. J., & Dhital, S. (2019). Wall porosity in isolated cells from food plants: Implications for nutritional functionality. *Food Chemistry*, *279*, 416-425.

Li, J. Y., & Yeh, A. I. (2001). Relationships between thermal, rheological characteristics and swelling power for various starches. *Journal of Food Engineering*, *50*(3), 141-148.

Liu, Q., Donner, E., Yin, Y., Huang, R. L., & Fan, M. Z. (2006). The physicochemical properties and *in vitro* digestibility of selected cereals, tubers and legumes grown in China. *Food Chemistry*, *99*(3), 470-477.

López-Barón, N., Gu, Y., Vasanthan, T., & Hoover, R. (2017). Plant proteins mitigate *in vitro* wheat starch digestibility. *Food Hydrocolloids*, *69*, 19-27.

López-Barón, N., Sagnelli, D., Blennow, A., Holse, M., Gao, J., Saaby, L., ... & Vasanthan, T. (2018). Hydrolysed pea proteins mitigate *in vitro* wheat starch digestibility. *Food Hydrocolloids*, *79*, 117-126.

Lu, Z. H., Donner, E., Yada, R. Y., & Liu, Q. (2016). Physicochemical properties and *in vitro* starch digestibility of potato starch/protein blends. *Carbohydrate Polymers*, *154*, 214-222.

Luo, K., & Zhang, G. (2018). Nutritional property of starch in a whole-grain-like structural form. *Journal of Cereal Science*, *79*, 113-117.

Luo, K., Wang, X., & Zhang, G. (2018). The anti-obesity effect of starch in a whole grain-like structural form. *Food & Function*, *9*(7), 3755-3763.

Macfarlane, G. T., & Macfarlane, S. (2012). Bacteria, colonic fermentation, and gastrointestinal health. *Journal of AOAC International*, *95*(1), 50-60.

Mahasukhonthachat, K., Sopade, P. A., & Gidley, M. J. (2010). Kinetics of starch digestion in sorghum as affected by particle size. *Journal of Food Engineering*, *96*(1), 18-28.

Mandalari, G., Faulks, R. M., Rich, G. T., Lo Turco, V., Picout, D. R., Lo Curto, R. B., ... & Ellis, P. R. (2008). Release of protein, lipid, and vitamin E from almond seeds during digestion. *Journal of Agricultural and Food Chemistry*, *56*(9), 3409-3416.

Mandalari, G., Grundy, M. M. L., Grassby, T., Parker, M. L., Cross, K. L., Chessa, S., ... & Butterworth, P. J. (2014). The effects of processing and mastication on almond lipid bioaccessibility using novel methods of *in vitro* digestion modelling and micro-structural analysis. *British Journal of Nutrition*, *112*(09), 1521-1529.

Maurer, S., Waschatko, G., Schach, D., Zielbauer, B. I., Dahl, J., Weidner, T., Bonn, M., & Vilgis, T. A. (2013). The role of intact oleosin for stabilization and function of oleosomes. *The Journal of Physical Chemistry B*, *117*(44), 13872-13883.

McClements, D. J., Decker, E. A., & Park, Y. (2008). Controlling lipid bioavailability through physicochemical and structural approaches. *Critical Reviews in Food Science and Nutrition*, *49*(1), 48-67.

McClements, D. J., Decker, E. A., Park, Y., & Weiss, J. (2009). Structural design principles for delivery of bioactive components in nutraceuticals and functional foods. *Critical Reviews in Food Science and Nutrition*, *49*(6), 577-606.

Melito, C., & Tovar, J. (1995). Cell walls limit *in vitro* protein digestibility in processed legume seeds. *Food Chemistry*, *53*(3), 305-307.

Mesa-Stonestreet, D., Jhoe, N., Alavi, S., & Bean, S. R. (2010). Sorghum proteins: the concentration, isolation, modification, and food applications of kafirins. *Journal of Food Science*, *75*(5), 90-104.

Messina, M. J. (1999). Legumes and soybeans: overview of their nutritional profiles and health effects. *The American Journal of Clinical Nutrition*, *70*(3), 439-450.

Minekus, M., Alminger, M., Alvito, P., Ballance, S., Bohn, T. O. R. S. T. E. N., Bourlieu, C., ... & Dufour, C. (2014). A standardised static in vitro digestion method suitable for food–an international consensus. *Food & Function*, *5*(6), 1113-1124.

Nature Methods (2012). The quest for quantitative microscopy. *Nature Methods: Editorial*, *9*(7), 627. http://dx.doi.org/10.1038/nmeth.2102.

Nestle, M. (1999). Animal v. plant foods in human diets and health: is the historical record unequivocal?. *Proceedings of the Nutrition Society*, *58*(2), 211-218.

Noah, L., Guillon, F., Bouchet, B., Buleon, A., Molis, C., Gratas, M., & Champ, M. (1998). Digestion of carbohydrate from white beans (Phaseolus vulgaris L.) in healthy humans. *The Journal of Nutrition*, *128*(6), 977-985.

Ogawa, Y., Donlao, N., Thuengtung, S., Tian, J., Cai, Y., Reginio, F. C., ... & Tamura, M. (2018). Impact of food structure and cell matrix on digestibility of plant-based food. *Current Opinion in Food Science*, *19*, 36-41.

Oria, M. P., Hamaker, B. R., & Shull, J. M. (1995). Resistance of Sorghum α-, β-, and γ-Kafirins to Pepsin Digestion. *Journal of Agricultural and Food Chemistry*, *43*(8), 2148-2153.

Ormerod, A., Ralfs, J., Jobling, S., & Gidley, M. (2002). The influence of starch swelling on the material properties of cooked potatoes. *Journal of Materials Science*, *37*(8), 1667-1673.

Padayachee, A., Day, L., Howell, K., & Gidley, M. J. (2017). Complexity and health functionality of plant cell wall fibers from fruits and vegetables. *Critical Reviews in Food Science and Nutrition*, *57*(1), 59-81.

Pallares, A. P., Miranda, B. A., Truong, N. Q. A., Kyomugasho, C., Chigwedere, C. M., Hendrickx, M., & Grauwet, T. (2018a). Process-induced cell wall permeability modulates the in vitro starch digestion kinetics of common bean cotyledon cells. *Food & Function*, *9*(12), 6544-6554.

Pallares, A. P., Rousseau, S., Chigwedere, C. M., Kyomugasho, C., Hendrickx, M., & Grauwet, T. (2018b). Temperature-pressure-time combinations for the generation of common bean microstructures with different starch susceptibilities to hydrolysis. *Food Research International*, *106*, 105-115.

Parada, J., & Aguilera, J. M. (2007). Food microstructure affects the bioavailability of several nutrients. *Journal of Food Science*, *72*(2), 21-32.

Parker, C. C., Parker, M. L., Smith, A. C., & Waldron, K. W. (2001). Pectin distribution at the surface of potato parenchyma cells in relation to cell– cell adhesion. *Journal of Agricultural and Food Chemistry*, *49*(9), 4364-4371.

Patton, J. S., Vetter, R. D., Hamosh, M., Borgstrom, B., Lindstrom, M., & Carey, M. C. (1985). The light microscopy of triglyceride digestion. *Food Structure*, *4*(1), 5.

Peng, C. C., Lin, I. P., Lin, C. K., & Tzen, J. T. (2003). Size and stability of reconstituted sesame oil bodies. *Biotechnology Progress*, *19*(5), 1623-1626.

Pharmacopeia, U. S. pharmacopeia, simulated gastric fluid, TS, simulated intestinal fluid, TS, United States Pharmacopeial Convention, vol. 24, The national formulary 9 (U.S. Pharmacopeia Board of Trustees), Rockville, MD, USA, p 2235 (2000).

Pieniazek, F., & Messina, V. (2016). Scanning electron microscopy combined with image processing technique: Microstructure and texture analysis of legumes and vegetables for instant meal. *Microscopy Research and Technique*, *79*(4), 267-275.

Rasmussen, H. E., Hamaker, B., Rajan, K. B., Mutlu, E., Green, S. J., Brown, M., ... & Keshavarzian, A. (2017). Starch-entrapped microsphere fibers improve bowel habit but do not exhibit prebiotic capacity in those with unsatisfactory bowel habits: a Phase I, randomized, double-blind, controlled human trial. *Nutrition Research*, *44*, 27-37.

Rizkalla, S. W., Bellisle, F., & Slama, G. (2002). Health benefits of low glycaemic index foods, such as pulses, in diabetic patients and healthy individuals. *British Journal of Nutrition*, *88*(3), 255-262.

Rockland, L. B., Jones, F. T., & Hahn, D. M. (1977). Light and scanning electron microscope studies on dry beans: extracellular gelatinization of lima bean starch in water and a mixed salt solution. *Journal of Food Science*, *42*(5), 1204-1207.

Roman, L., Gomez, M., Li, C., Hamaker, B. R., & Martinez, M. M. (2017). Biophysical features of cereal endosperm that decrease starch digestibility. *Carbohydrate Polymers*, *165*, 180-188.

Rooney, L. W. (1996). Sorghum and millets. In *Cereal Grain Quality* (pp. 153-177). Springer, Dordrecht.

Rooney, L. W., & Pflugfelder, R. L. (1986). Factors affecting starch digestibility with special emphasis on sorghum and corn. *Journal of Animal Science*, *63*(5), 1607-1623.

Rose, D. J., Keshavarzian, A., Patterson, J. A., Venkatachalam, M., Gillevet, P., & Hamaker, B. R. (2009). Starch-entrapped microspheres extend in vitro fecal fermentation, increase butyrate production, and influence microbiota pattern. *Molecular Nutrition & Food Research*, *53*(S1), S121-S130.

Rovalino-Córdova, A. M., Fogliano, V., & Capuano, E. (2018). A closer look to cell structural barriers affecting starch digestibility in beans. *Carbohydrate Polymers*, *181*, 994-1002.

Rovalino-Córdova, A. M., Fogliano, V., & Capuano, E. (2019). The effect of cell wall encapsulation on macronutrients digestion: A case study in kidney beans. *Food Chemistry*, *286*, 557-566.

Sandhu, K. S., & Singh, N. (2007). Some properties of corn starches II: Physicochemical, gelatinization, retrogradation, pasting and gel textural properties. *Food Chemistry*, *101*(4), 1499-1507.

Schoch, T. J., & Maywald, E. C. (1968). Preparation and properties of various legume starches. *Cereal Chemistry*, *45*(6), 564-573.

Scholten, E., Moschakis, T., & Biliaderis, C. G. (2014). Biopolymer composites for engineering food structures to control product functionality. *Food Structure*, *1*(1), 39-54.

Shahidi, F., & Han, X. Q. (1993). Encapsulation of food ingredients. *Critical Reviews in Food Science & Nutrition*, *33*(6), 501-547.

Shin, E. H., Baik, M. Y., & Kim, H. S. (2015). Comparison of physicochemical properties of starches and parenchyma cells isolated from potatoes cultivated in Korea. *Food Science and Biotechnology*, *24*(3), 955-963.

Shomer, I. (1995). Swelling behaviour of cell wall and starch in potato (Solanum tuberosum L.) tuber cells—I. Starch leakage and structure of single cells. *Carbohydrate Polymers*, *26*(1), 47-54.

Sievenpiper, J. L., Kendall, C. W. C., Esfahani, A., Wong, J. M. W., Carleton, A. J., Jiang, H. Y., ... & Jenkins, D. J. A. (2009). Effect of non-oil-seed pulses on glycaemic control: a systematic review and meta-analysis of randomised controlled experimental trials in people with and without diabetes. *Diabetologia*, *52*, 1479-1495.

Singh, J., & Kaur, L. (Eds.). (2016). *Advances in Potato Chemistry and Technology* (2nd ed.). Oxford, UK: Academic Press, Elsevier.

Singh, J., & Singh, N. (2001). Studies on the morphological, thermal and rheological properties of starch separated from some Indian potato cultivars. *Food Chemistry*, *75*(1), 67-77.

Singh, J., Dartois, A., & Kaur, L. (2010). Starch digestibility in food matrix: a review. *Trends in Food Science & Technology*, *21*(4), 168-180.

Singh, J., McCarthy, O. J., & Singh, H. (2006). Physico-chemical and morphological characteristics of New Zealand Taewa (Maori potato) starches. *Carbohydrate Polymers*, *64*(4), 569-581.

Singh, N., Kaur, L., Ezekiel, R., & Guraya, H. S. (2005). Microstructural, cooking and textural characteristics of potato (Solanum tuberosum L) tubers in relation to physicochemical and functional properties of their flours. *Journal of the Science of Food and Agriculture, 85*(8), 1275-1284.

Singh, N., Sandhu, K. S., & Kaur, M. (2004). Characterization of starches separated from Indian chickpea (Cicer arietinum L.) cultivars. *Journal of Food Engineering*, *63*(4), 441-449.

Singh, N., Singh, J., Kaur, L., Sodhi, N. S., & Gill, B. S. (2003). Morphological, thermal and rheological properties of starches from different botanical sources. *Food Chemistry*, *81*(2), 219-231.

Sjoo, M. E., Eliasson, A. C., & Autio, K. (2009). Comparison of different microscopic methods for the study of starch and other components within potato cells. *Food*, *3*(special issue 1), 39-44.

Sriamornsak, P., & Nunthanid, J. (1998). Calcium pectinate gel beads for controlled release drug delivery: I. Preparation and in vitro release studies. *International Journal of Pharmaceutics*, *160*(2), 207-212.

Srichuwong, S., Curti, D., Austin, S., King, R., Lamothe, L., & Gloria-Hernandez, H. (2017). Physicochemical properties and starch digestibility of whole grain sorghums, millet, quinoa and amaranth flours, as affected by starch and non-starch constituents. *Food Chemistry*, *233*, 1-10.

Sticklen, M. B. (2008). Plant genetic engineering for biofuel production: towards affordable cellulosic ethanol. *Nature Reviews Genetics*, *9*(6), 433-443.

Tamura, M., Singh, J., Kaur, L., & Ogawa, Y. (2016). Impact of structural characteristics on starch digestibility of cooked rice. *Food Chemistry*, *191*, 91-97.

Tan, B., Tan, H. Z., Tian, X. H., Liu, M., & Shen, Q. (2011). Eight underexploited broad beans from China:(II) Effects of steaming methods on their quality and microstructure. *Journal of Food Processing and Preservation*, *35*(1), 20-45.

Teuber, S. S. (2002). Hypothesis: the protein body effect and other aspects of food matrix effects. *Annuals of the New York Academy of Sciences*, *964*(1), 111-116.

Thompson, L. U., Button, C. L., & Jenkins, D. J. (1987). Phytic acid and calcium affect the *in vitro* rate of navy bean starch digestion and blood glucose response in humans. *The American Journal of Clinical Nutrition*, *46*(3), 467-473.

Thorne, M. J., Thompson, L. U., & Jenkins, D. J. (1983). Factors affecting starch digestibility and the glycemic response with special reference to legumes. *The American Journal of Clinical Nutrition*, *38*(3), 481-488.

Tosh, S. M. (2013). Review of human studies investigating the post-prandial blood-glucose lowering ability of oat and barley food products. *European Journal of Clinical Nutrition*, *67*(4), 310.

Tovar, J. (1996). Bioavailability of carbohydrates in legumes: digestible and indigestible fractions. *Archivos latinoamericanos de Nutrición*, *44*, 36-40.

Troncoso, E., Zúñiga, R., Ramírez, C., Parada, J., & Germain, J. C. (2009). Microstructure of Potato Products: Effect on Physico-Chemical Properties and Nutrient Bioavailability. *Food, 3*(2), 41-54.

Tydeman, E. A., Parker, M. L., Wickham, M. S., Rich, G. T., Faulks, R. M., Gidley, M. J., Fillery-Travis, A, & Waldron, K. W. (2010a). Effect of carrot (Daucus carota) microstructure on carotene bioaccessibilty in the upper gastrointestinal tract. 1. *In vitro* simulations of carrot digestion. *Journal of Agricultural and Food Chemistry*, *58*(17), 9847-9854.

Tydeman, E. A., Parker, M. L., Faulks, R. M., Cross, K. L., Fillery-Travis, A., Gidley, M. J., Rich, G. T., & Waldron, K. W. (2010b). Effect of carrot (Daucus carota) microstructure on carotene bioaccessibility in the upper gastrointestinal tract. 2. *in vivo* digestions. *Journal of Agricultural and Food Chemistry*, *58*(17), 9855-9860.

Tzen, J. T. C. (2012). Integral proteins in plant oil bodies. *International Scholarly Research Network Botany*. doi:10.5402/2012/173954

Ubbink, J., Burbidge, A., & Mezzenga, R. (2008). Food structure and functionality: a soft matter perspective. *Soft Matter*, *4*(8), 1569-1581.

Ulker, P., Yaras, N., Yalcin, O., Celik-Ozenci, C., Johnson, P. C., Meiselman, H. J., & Baskurt, O. K. (2011). Shear stress activation of nitric oxide synthase and increased nitric oxide levels in human red blood cells. *Nitric Oxide*, *24*(4), 184-191.

Van Marle, J. T., Stolle-Smits, T., Donkers, J., van Dijk, C., Voragen, A. G., & Recourt, K. (1997). Chemical and microscopic characterization of potato (Solanum tuberosum L.) cell walls during cooking. *Journal of Agricultural and Food Chemistry*, *45*(1), 50-58.

Vandeputte, G. E., Derycke, V., Geeroms, J., & Delcour, J. A. (2003). Rice starches. II. Structural aspects provide insight into swelling and pasting properties. *Journal of Cereal Science*, *38*(1), 53-59.

Venkatachalam, M., Kushnick, M. R., Zhang, G., & Hamaker, B. R. (2009). Starch-entrapped biopolymer microspheres as a novel approach to vary blood glucose profiles. *Journal of the American College of Nutrition*, *28*(5), 583-590.

Villegas, R., Gao, Y. T., Yang, G., Li, H. L., Elasy, T. A., Zheng, W., & Shu, X. O. (2008). Legume and soy food intake and the incidence of type 2 diabetes in the Shanghai Women's Health Study. *The American Journal of Clinical Nutrition*, *87*(1), 162-167.

Wahlqvist, M. L. (2016). Food structure is critical for optimal health. *Food & Function*, *7*(3), 1245-1250.

Waldron, K. W., Parker, M. L., & Smith, A. C. (2003). Plant cell walls and food quality. *Comprehensive Reviews in Food Science and Food Safety*, *2*(4), 128-146.

Wang, S., Li, P., Zhang, T., Wang, S., & Copeland, L. (2017). Trypsin and chymotrypsin are necessary for in vitro enzymatic digestion of rice starch. *RSC Advances*, *7*(7), 3660-3666.

Wang, Y., Tilley, M., Bean, S., Sun, X. S., & Wang, D. (2009). Comparison of methods for extracting kafirin proteins from sorghum distillers dried grains with solubles. *Journal of Agricultural and Food Chemistry*, *57*(18), 8366-8372.

Wani, I. A., Sogi, D. S., Hamdani, A. M., Gani, A., Bhat, N. A., & Shah, A. (2016). Isolation, composition, and physicochemical properties of starch from legumes: A review. *Starch-Stärke*, *68*(9-10), 834-845.

Weber, E., & Neumann, D. (1980). Protein bodies, storage organelles in plant seeds. *Biochemie und Physiologie der Pflanzen*, *175*(4), 279-306.

White, D. A., Fisk, I. D., Makkhun, S., & Gray, D. A. (2009). *In vitro* assessment of the bioaccessibility of tocopherol and fatty acids from sunflower seed oil bodies. *Journal of Agricultural and Food Chemistry*, *57*(13), 5720-5726.

Whitney, S. E., Brigham, J. E., Darke, A. H., Reid, J. S., & Gidley, M. J. (1995). *In vitro* assembly of cellulose/xyloglucan networks: ultrastructural and molecular aspects. *The Plant Journal*, *8*(4), 491-504.

Wijesundera, C., & Shen, Z. (2014). Mimicking natural oil bodies for stabilising oil-in-water food emulsions. *Lipid Technology*, *26*(7), 151-153.

Wijesundera, C., Boiteau, T., Xu, X., Shen, Z., Watkins, P., & Logan, A. (2013). Stabilization of Fish Oil-in-Water Emulsions with Oleosin Extracted from Canola Meal. *Journal of Food Science*, *78*(9), C1340-C1347.

Wong, J. H., Lau, T., Cai, N., Singh, J., Pedersen, J. F., Vensel, W. H., ... & Buchanan, B. B. (2009). Digestibility of protein and starch from sorghum (Sorghum bicolor) is linked to biochemical and structural features of grain endosperm. *Journal of Cereal Science*, *49*(1), 73-82.

Wong, T. W., Colombo, G., & Sonvico, F. (2011). Pectin matrix as oral drug delivery vehicle for colon cancer treatment. *Aaps PharmSciTech*, *12*(1), 201-214.

Wootton, M., & Bamunuarachchi, A. (1979). Application of differential scanning calorimetry to starch gelatinization. II. Effect of heating rate and moisture level. *Starch-Stärke*, *31*(8), 262-264.

Würsch, P., Del Vedovo, S., & Koellreutter, B. (1986). Cell structure and starch nature as key determinants of the digestion rate of starch in legume. *The American Journal of Clinical Nutrition*, *43*(1), 25-29.

Xiong, W., Zhang, B., Huang, Q., Li, C., Pletsch, E. A., & Fu, X. (2018). Variation in the rate and extent of starch digestion is not determined by the starch structural features of cooked whole pulses. *Food Hydrocolloids*, *83*, 340-347.

Xu, H., & Zhang, G. (2014). Slow digestion property of microencapsulated normal corn starch. *Journal of Cereal Science*, *60*(1), 99-104.

Yang, C., Zhong, F., Goff, H. D., & Li, Y. (2019). Study on starch-protein interactions and their effects on physicochemical and digestible properties of the blends. *Food Chemistry*, *280*, 51-58.

Yu, W., Tan, X., Zou, W., Hu, Z., Fox, G. P., Gidley, M. J., & Gilbert, R. G. (2017). Relationships between protein content, starch molecular structure and grain size in barley. *Carbohydrate Polymers*, *155*, 271-279.

Zhang, B., Dhital, S., Flanagan, B. M., & Gidley, M. J. (2014). Mechanism for starch granule ghost formation deduced from structural and enzyme digestion properties. *Journal of Agricultural and Food Chemistry*, *62*(3), 760-771.

Zhang, G., & Hamaker, B. R. (1998). Low α-amylase starch digestibility of cooked sorghum flours and the effect of protein. *Cereal Chemistry*, *75*(5), 710-713.

Zhang, G., & Hamaker, B. R. (2005). Sorghum (Sorghum bicolor L. Moench) flour pasting properties influenced by free fatty acids and protein. *Cereal Chemistry*, *82*(5), 534-540

Appendix

A1. Best model fits for the "shrinking" of cellular contents in intact cotyledon cells

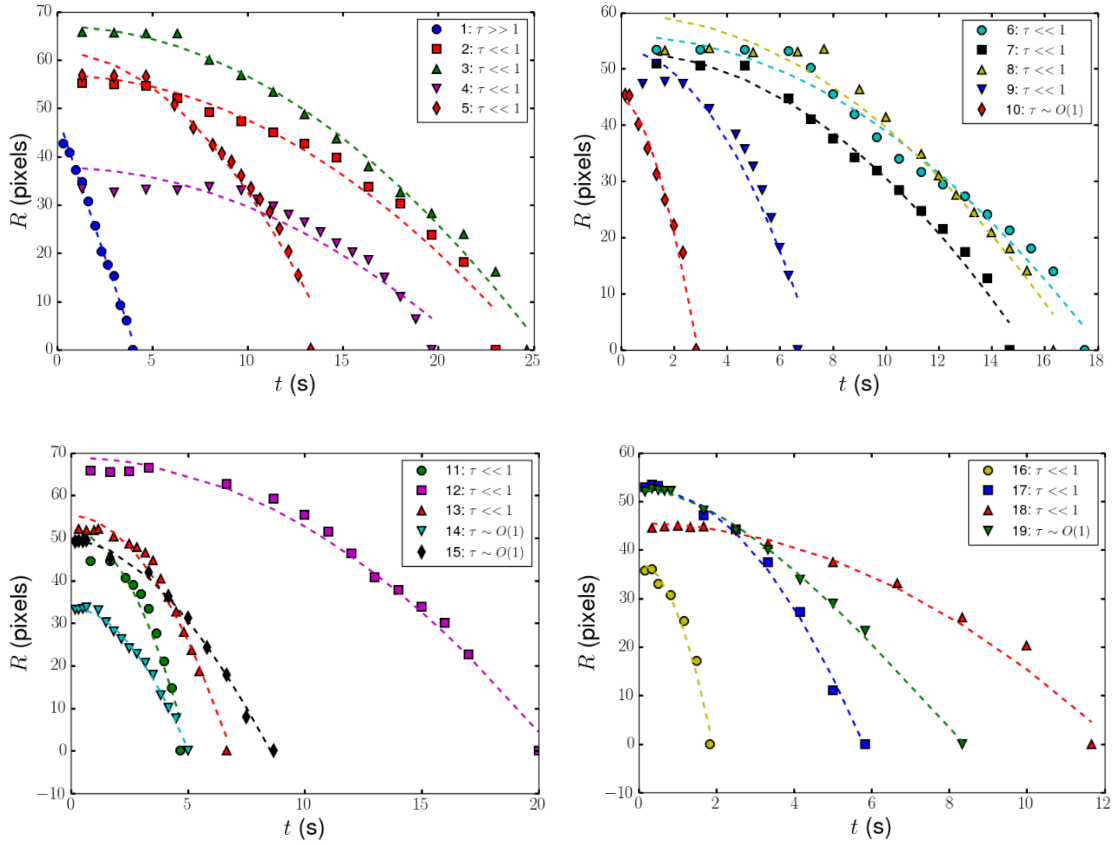

Fig. A1. Best fits of "shrinking core" data to the digestion rate model for cotyledon cells #1–19.

A2. Statement of Contribution for Doctorate with Publications/Manuscripts

DRC 16

MASSEY UNIVERSITY
GRADUATE RESEARCH SCHOOL

STATEMENT OF CONTRIBUTION
DOCTORATE WITH PUBLICATIONS/MANUSCRIPTS

We, the candidate and the candidate's Primary Supervisor, certify that all co-authors have consented to their work being included in the thesis and they have accepted the candidate's contribution as indicated below in the *Statement of Originality*.

Name of candidate:	Duc Toan Do
Name/title of Primary Supervisor:	Jaspreet Singh / Senior Research Officer
Name of Research Output and full reference: Do, D. T., Singh, J., Oey, I., & Singh, H. (2018). Biomimetic Plant Foods: Structural design and functionality. Trends in Food Science & Technology, 82, 46-59.	
In which Chapter is the Manuscript /Published work:	Chapter 2
Please indicate:	
• The percentage of the manuscript/Published Work that was contributed by the candidate:	90%
and	
• Describe the contribution that the candidate has made to the Manuscript/Published Work:	
The candidate carried out 90% of the preparation of the published work.	
For manuscripts intended for publication please indicate target journal:	
Candidate's Signature:	
Date:	18/10/2019
Primary Supervisor's Signature:	
Date:	18/10/2019

(This form should appear at the end of each thesis chapter/section/appendix submitted as a manuscript/ publication or collected as an appendix at the end of the thesis)

DRC 16

MASSEY UNIVERSITY
GRADUATE RESEARCH SCHOOL

STATEMENT OF CONTRIBUTION
DOCTORATE WITH PUBLICATIONS/MANUSCRIPTS

We, the candidate and the candidate's Primary Supervisor, certify that all co-authors have consented to their work being included in the thesis and they have accepted the candidate's contribution as indicated below in the *Statement of Originality*.

Name of candidate:	Duc Toan Do
Name/title of Primary Supervisor:	Jaspreet Singh / Senior Research Officer
Name of Research Output and full reference: Do, D. T., Singh, J., Oey, I., & Singh, H. (2019). Modulating effect of cotyledon cell microstructure on in vitro digestion of starch in legumes. Food Hydrocolloids, 96, 112-122.	
In which Chapter is the Manuscript /Published work:	Chapter 3
Please indicate:	
• The percentage of the manuscript/Published Work that was contributed by the candidate:	90%
and	
• Describe the contribution that the candidate has made to the Manuscript/Published Work:	
The candidate carried out all the experiments and data analysis as well as 90% of the preparation of the published work.	
For manuscripts intended for publication please indicate target journal:	
Candidate's Signature:	
Date:	18/10/2019
Primary Supervisor's Signature:	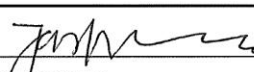
Date:	18/10/2019

(This form should appear at the end of each thesis chapter/section/appendix submitted as a manuscript/ publication or collected as an appendix at the end of the thesis)

DRC 16

MASSEY UNIVERSITY
GRADUATE RESEARCH SCHOOL

STATEMENT OF CONTRIBUTION
DOCTORATE WITH PUBLICATIONS/MANUSCRIPTS

We, the candidate and the candidate's Primary Supervisor, certify that all co-authors have consented to their work being included in the thesis and they have accepted the candidate's contribution as indicated below in the *Statement of Originality*.

Name of candidate:	Duc Toan Do
Name/title of Primary Supervisor:	Jaspreet Singh / Senior Research Officer
Name of Research Output and full reference: Do, D. T., Singh, J., Oey, I., Singh, H., Yada, R. Y., & Frostad, J. (2019). A novel apparatus for time-lapse optical microscopy of gelatinisation and digestion of starch inside plant cells. Palmerston North, New Zealand: Riddet Institute, Massey University. Submitted manuscript.	
In which Chapter is the Manuscript /Published work:	Chapter 6
Please indicate:	
• The percentage of the manuscript/Published Work that was contributed by the candidate:	80%
and	
• Describe the contribution that the candidate has made to the Manuscript/Published Work:	
The candidate carried out all the experiments, 80% data analysis as well as 80% of the preparation of the manuscript.	
For manuscripts intended for publication please indicate target journal:	
Journal of Food Hydrocolloids	
Candidate's Signature:	
Date:	18/10/2019
Primary Supervisor's Signature:	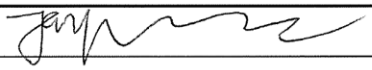
Date:	18/10/2019

(This form should appear at the end of each thesis chapter/section/appendix submitted as a manuscript/ publication or collected as an appendix at the end of the thesis)

DRC 16

MASSEY UNIVERSITY
GRADUATE RESEARCH SCHOOL

STATEMENT OF CONTRIBUTION
DOCTORATE WITH PUBLICATIONS/MANUSCRIPTS

We, the candidate and the candidate's Primary Supervisor, certify that all co-authors have consented to their work being included in the thesis and they have accepted the candidate's contribution as indicated below in the *Statement of Originality*.

Name of candidate:	Duc Toan Do
Name/title of Primary Supervisor:	Jaspreet Singh / Senior Research Officer
Name of Research Output and full reference: Do, D. T., Singh, J., Oey, I., & Singh, H. Effect of parenchyma cell structure on in vitro digestion of starch in potato cultivars grown in New Zealand. Palmerston North, New Zealand: Riddet Institute, Massey University. Manuscript in preparation.	
In which Chapter is the Manuscript /Published work:	Chapter 4
Please indicate:	
• The percentage of the manuscript/Published Work that was contributed by the candidate:	90%
and	
• Describe the contribution that the candidate has made to the Manuscript/Published Work:	
The candidate carried out all the experiments and data analysis as well as 90% of the preparation of the manuscript.	
For manuscripts intended for publication please indicate target journal:	
Carbohydrate Polymers	
Candidate's Signature:	
Date:	18/10/2019
Primary Supervisor's Signature:	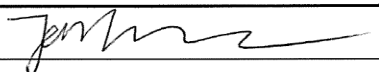
Date:	18/10/2019

(This form should appear at the end of each thesis chapter/section/appendix submitted as a manuscript/ publication or collected as an appendix at the end of the thesis)

DRC 16

MASSEY UNIVERSITY
GRADUATE RESEARCH SCHOOL

STATEMENT OF CONTRIBUTION
DOCTORATE WITH PUBLICATIONS/MANUSCRIPTS

We, the candidate and the candidate's Primary Supervisor, certify that all co-authors have consented to their work being included in the thesis and they have accepted the candidate's contribution as indicated below in the *Statement of Originality*.

Name of candidate:	Duc Toan Do
Name/title of Primary Supervisor:	Jaspreet Singh / Senior Research Officer
Name of Research Output and full reference: Do, D. T., & Singh, J. (2018). Legume Microstructure. In Reference Module in Food Science. https://doi.org/10.1016/B978-0-08-100596-5.21683-1	
In which Chapter is the Manuscript /Published work:	Appendix
Please indicate:	
• The percentage of the manuscript/Published Work that was contributed by the candidate:	90%
and	
• Describe the contribution that the candidate has made to the Manuscript/Published Work:	
The candidate carried out 90% of the preparation of the published work.	
For manuscripts intended for publication please indicate target journal:	
Candidate's Signature:	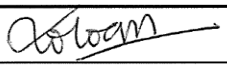
Date:	18/10/2019
Primary Supervisor's Signature:	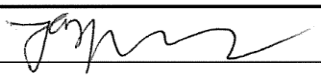
Date:	18/10/2019

(This form should appear at the end of each thesis chapter/section/appendix submitted as a manuscript/ publication or collected as an appendix at the end of the thesis)